ENANTIOCONVERGENT SYNTHESIS OF DIARYLMETHANES VIA ASYMMETRIC MIGRATORY TSUJI–WACKER OXIDATIONS

Dissertation

zur Erlangung des Doktorgrades der Naturwissenschaften

(Dr. rer. nat.)

an der Fakultät für Chemie und Pharmazie

der Universität Regensburg

vorgelegt von

EDUARD FRANK

aus Sulzbach-Rosenberg

Dezember 2025

Der experimentelle Teil dieser Arbeit wurde unter der Aufsicht von Prof. Dr. Alexander Breder im Zeitraum von November 2021 bis August 2025 an der Fakultät für Chemie und Pharmazie der Universität Regensburg durchgeführt.

Promotionsgesuch eingereicht am:	16.12.2025
Promotionskolloquium am:	20.02.2026

Prüfungsausschuss:

Vorsitzender:	Prof. Dr. Steffen Pockes
1. Gutachter:	Prof. Dr. Alexander Breder
2. Gutachterin:	Prof. Dr. Julia Rehbein
3. Prüfer:	Prof. Dr. Patrick Nürnberger

"Hard work is worthless for those that don't believe in themselves."

Might Guy

Translated into English from

Naruto, Episode 49, Studio Pierrot/TV Tokyo, 2003

Table of Content

Abbreviations and Symbols

	generic substituents
	photocatalyst
	chiral catalyst
δ	chemical shift
3CzClIPN	2,4,6-tri(9*H*-carbazol-9-yl)-5-chloroisophthalonitrile
Ac	acetyl
acac	acetylacetonate
anisyl	4-methoxybenzyl
APCI	atmospheric pressure chemical ionization
aq.	aqueous
Ar*	chiral arene backbone
ATR	attenuated total reflexion
BET	back electron-transfer
BINAP	2,2'-bis(diphenylphosphino)-1,1'-binaphthyl
calcd.	calculated
CBS	COREY–BAKSHI–SHIBATA
cCB	chiral counter-base
ci	constitutional isomer
CG	coordinative group
cod	1,5-cyclooctadiene
conv.	conversion
CPA	chiral phosphoric acid
dba	dibenzylideneacetone
DCE	1,2-dichloroethane
DCM	dichloromethane
DKR	dynamic kinetic resolution
DMRB	dimethylated Rose Bengal
DyKAT	dynamic kinetic asymmetric transformation
e.g.	for example
EA	ethyl acetate
EDG	electron-donating group
ee	enantiomeric excess
EI	electron impact
ent	enantiomer (of)
eq	equilibrium
equiv.	equivalent(s)
ESI	electron spray ionization
et al.	and others (co-authors)
etc.	et cetera/and so on
EWG	electron-withdrawing group
hν	photon energy
HAT	hydrogen-atom transfer
HFIP	1,1,1,3,3,3-hexafluoro-2-propanol
HMPA	hexamethylphosphoramide
HOMO	highest occupied molecular orbital
HPLC	high performance liquid chromatography
HRMS	high-resolution mass spectrometry
i.e.	id est/that is
IR	infrared
J	spectroscopic coupling constant
KIE	kinetic isotope effect
KR	kinetic resolution
LDA	lithium diisopropylamide
LED	light emitting diode
M	molar (mole(s) per liter)
m.p.	melting point
m/z	mass-to-charge ratio
*m*CPBA	*meta*-chloroperbenzoic acid

Mes	mesityl (1,3,5-trimethyl phenyl)	PT	proton transfer
mol%	mole per cent	*rac*	racemic/racemate
Ms	mesyl	rc	recrystallization/recrystallized
MS	molecular sieves	R_f	retardation factor
MTW	migratory TSUJI–WACKER	ri	regioisomer
n-BuLi	*n*-butyllithium	sat.	saturated
NCI	non-covalent interactions	SCE	standard calomel electrode
NMR	nuclear magnetic resonance	SET	single-electron transfer
NOESY	Nuclear OVERHAUSER Effect spectroscopy	SM	starting material
NPA	natural population analysis	TAPT	2,4,6-tris(4-methoxyphenyl)-pyrylium tetrafluoroborate
P	product	TFA	trifluoroacetic acid
PCET	proton-coupled electron-transfer	TFE	1,1,1-trifluoroethanol
PET	photoinduced electron-transfer	TLC	thin-layer chromatography
PhMe	toluene	TS / ‡	transition state
PHMS	polymethylhydrosiloxane	Ts	tosyl
pin	2,3-dimethyl-2,3-butandiol	vs.	versus
ppm	parts per million		

Stereochemistry is indicated as following:

 = relative stereochemistry

 = absolute stereochemistry

1 Introduction

1.1 Concepts in Stereoinformation Transfer

1.1.1 Origins of Enantioselectivity

The control of stereoselectivity remains a central challenge in modern synthetic chemistry. Classical strategies for the generation of enantiomerically enriched compounds typically rely on asymmetric induction, wherein a chiral catalyst, auxiliary, or reagent biases the formation of one enantiomer over the other during a bond-forming event in a prochiral motif.[1] Under such conditions, enantiomeric excess (ee) arises kinetically:[a] the transition state leading to one enantiomer is lower in energy than that leading to its mirror image, resulting in a product mixture enriched in one of two absolute configurations (Scheme 1a).[2] Despite the undeniable success of asymmetric synthesis, the number of readily accessible prochiral functional groups is finite. Given the abundance of racemic feedstocks, a complementary approach to generate material of high ee is to selectively eliminate pre-existing stereochemical information from a chiral, racemic mixture. In this scenario, stereoinformation is *not* constructed de novo but rather destroyed (or "ablated") from part or all of the chiral substrate.[3] The resulting stereoablative reactions, a term introduced by STOLTZ and co-workers, expand the scope of enantioselective catalysis by decoupling product stereochemistry from the configuration of the starting material.[4,5]

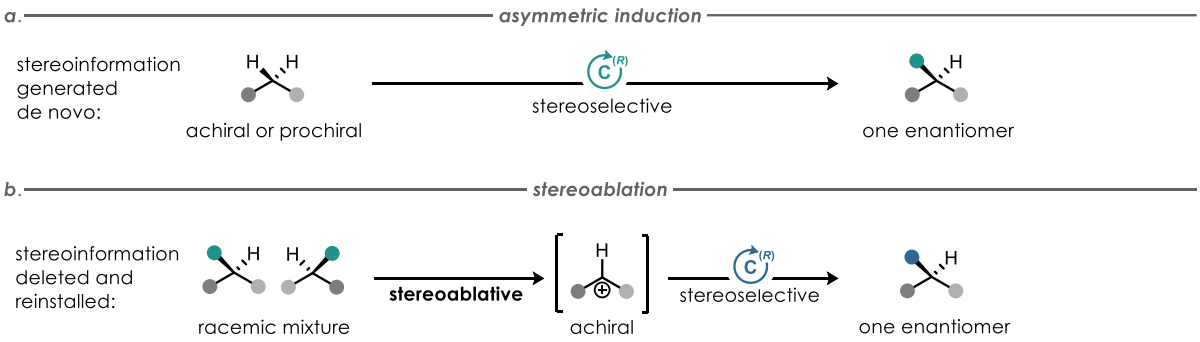

Scheme 1. Main concepts for the selective production of enantioenriched material. (a) Asymmetric induction generates stereoinformation de novo from achiral or prochiral substrates. (b) Stereoablation relies on deliberate deletion and subsequent reinstallation of stereoinformation. $C^{(R)}$ = chiral catalyst or reagent.

In modern terminology, stereoablation is most often encountered in the context of stereoablative catalysis, where the erasure of chirality in a racemic mixture is deliberately coupled to an ensuing enantioselective transformation of the resulting common prochiral intermediate, thereby installing

[a] Enantioenrichment can, in principle, also arise thermodynamically, e.g. when two enantiomers exist in equilibrium within a chiral environment that renders them diastereomeric and therefore unequal in energy. In such cases, a small free energy difference ($\Delta G \neq 0$) between the enantiomeric pair results in a non-racemic equilibrium composition, which, in most cases, has limited practical impact.

a new stereogenic element under catalytic control (Scheme 1b).[6,7] However, the original definition of stereoablation refers solely to a chemical process in which an existing stereogenic element in a molecule is eliminated,[4] without any implication on neither the nature and lifetime of a prochiral intermediate, nor on a subsequent reinstallation of chirality. In this broader sense, stereoablation serves as a strategic foundation for a broad variety of enantioselective catalytic processes in which stereochemical information is deliberately erased and *potentially* redefined.[8–11] In the following sections of this thesis, the term will thereby be used in its most general meaning, to discuss how stereoablation manifests within various important strategies for catalytic conversion of racemic substrates into enantioenriched products.

1.1.2 Enantioenrichment from Racemic Mixtures

1.1.2.1 Kinetic Resolution

Kinetic resolution (KR) represents one of the earliest and most fundamental strategies for obtaining enantioenriched compounds from racemic mixtures. The principle relies on a difference in reaction rates k between two enantiomers (i.e., *R* and *S*) of a racemic substrate when exposed to a chiral environment, typically a chiral catalyst, reagent, or enzyme.[12] Each enantiomer forms a distinct diastereomeric transition state (i.e., TS_R and TS_S) with the chiral catalyst, and if these transition states differ in free energy ($\Delta\Delta G^{\ddagger} \neq 0$), one enantiomer reacts faster than the other (e.g. $k_R > k_S$). Over time, the faster-reacting enantiomer is selectively transformed into some type of product, while the slower-reacting one accumulates, leading to enantiomeric enrichment in the residual starting material (Scheme 2a).[b] Notably, racemization does not take place in this scenario, as its barrier (ΔG_{rac}) lies higher in energy than each of the individual transition states for product formation ($\Delta G_{rac} > \Delta G^{\ddagger}_S > \Delta G^{\ddagger}_R$, Scheme 2b).

The conceptual origins of KR date back to PASTEUR's manual separation of the enantiomorphic crystals of sodium ammonium tartrate in 1848,[14] which was the first empirical observation that enantiomers could behave differently in a chiral environment. The first true chemical kinetic resolution, however, is often attributed to MARCKWALD and MCKENZIE's 1899 resolution of racemic mandelic acid esters using optically active menthol,[15] which introduced the idea of rate-dependent enantiodifferentiation in a chemical reaction. Since then, a vast array of KR methodologies have been developed, including enzymatic resolutions (e.g. lipase- or acylase-mediated esterifications and hydrolyses)[16] and non-enzymatic catalytic versions, such as hydrolytic and oxidative KR.[17,18] In this context, the oxidative kinetic resolution of various secondary alcohols

[b] Of course, the product of the KR may also be obtained in high enantiopurity, for an early example see here.[13]

raised to particular importance. NOYORI[19] and many others[20] developed a catalytic system, in which stereoablation accompanies the selective oxidation of one enantiomer to an achiral ketone intermediate. Herein, the stereoablative step is simultaneously the enantioselective step, providing multiple opportunities for further functionalization of the achiral byproduct. This concept was successfully adapted by other transformations,[21] highlighting the impact of stereoablative techniques in the field of KR.

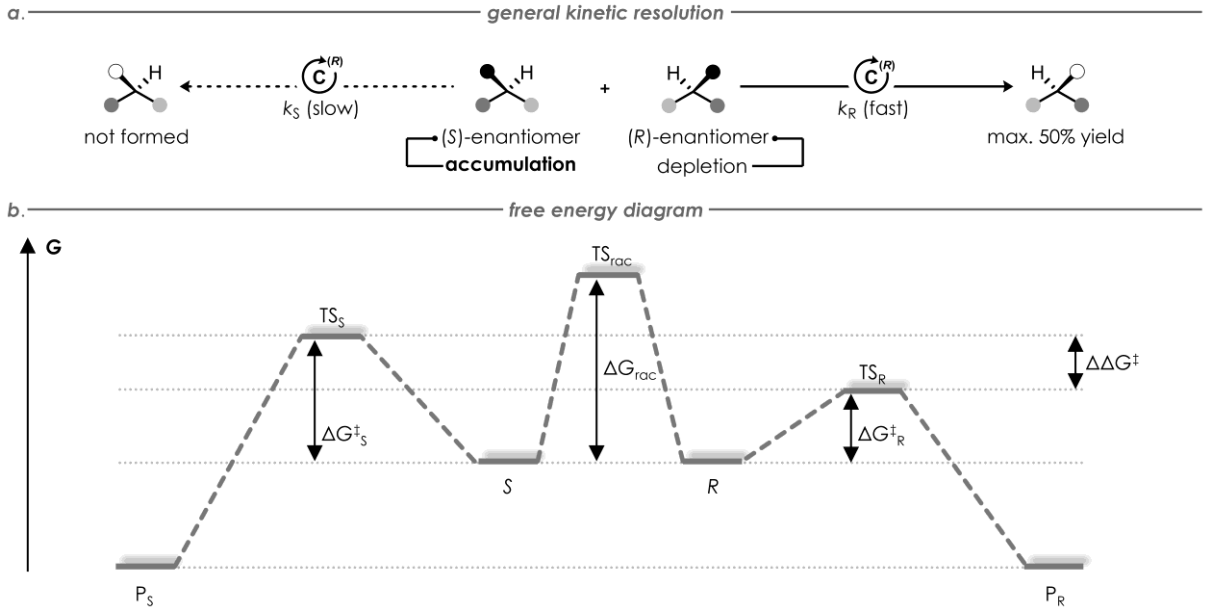

Scheme 2. The principle of KR. (a) One enantiomer of a racemic mixture is transformed into a byproduct, while the unreacted substrate is obtained in enantiopure form. $C^{(R)}$ = chiral catalyst or reagent. (b) Free energy diagram of a KR. P = product.

Despite its elegance and simplicity, KR suffers from the inherent limitation that, under ideal conditions, only a maximum yield of 50% can be achieved for a single enantiomer, since usually only one of the two enantiomers is transformed selectively. Once half of the racemic material has reacted, further conversion *reduces* rather than enhances the overall ee, or, in the case of oxidative KR, impairs the unreacted enantiomer's yield. This drawback fundamentally restricts the scalability of classical KR and provides the primary motivation for more elaborate, stereoablative catalytic processes to overcome the intrinsic yield limit. Naturally, this would require the other enantiomer to contribute to product formation as well, rendering the resolution to become a dynamic process.

1.1.2.2 Dynamic Kinetic Resolution

Dynamic kinetic resolution (DKR) extends the concept of KR by introducing a fast racemization step k_{rac} that directly interconverts the two enantiomers of a racemic substrate under the reaction conditions (Scheme 3a).[18,22] In contrast to classical KR, where racemization is not feasible

($\Delta G_{rac} > \Delta G^{\ddagger}$), DKR relies on a low racemization barrier (ΔG_{rac}) compared to the activation energy for the enantiodifferentiating step ($\Delta G^{\ddagger}$). Under these conditions, both enantiomers can undergo stereomutation (e.g. via sp^2-hybridzied intermediates or reversible bond rotation),[c] while the chiral catalyst selectively interacts with *one* of the two configurations, transforming it into product (Scheme 3b). Continuous regeneration of the faster-reacting enantiomer effectively channels the entire racemic mixture into a single enantioenriched product, thereby circumventing the 50% yield limit of classical KR. The dynamic balance between these two steps dictates the overall efficiency and enantioselectivity, since DKR can degenerate into a conventional KR if racemization proceeds too slowly. Conversely, when racemization is faster than selective conversion, full enantioconvergence can be achieved.

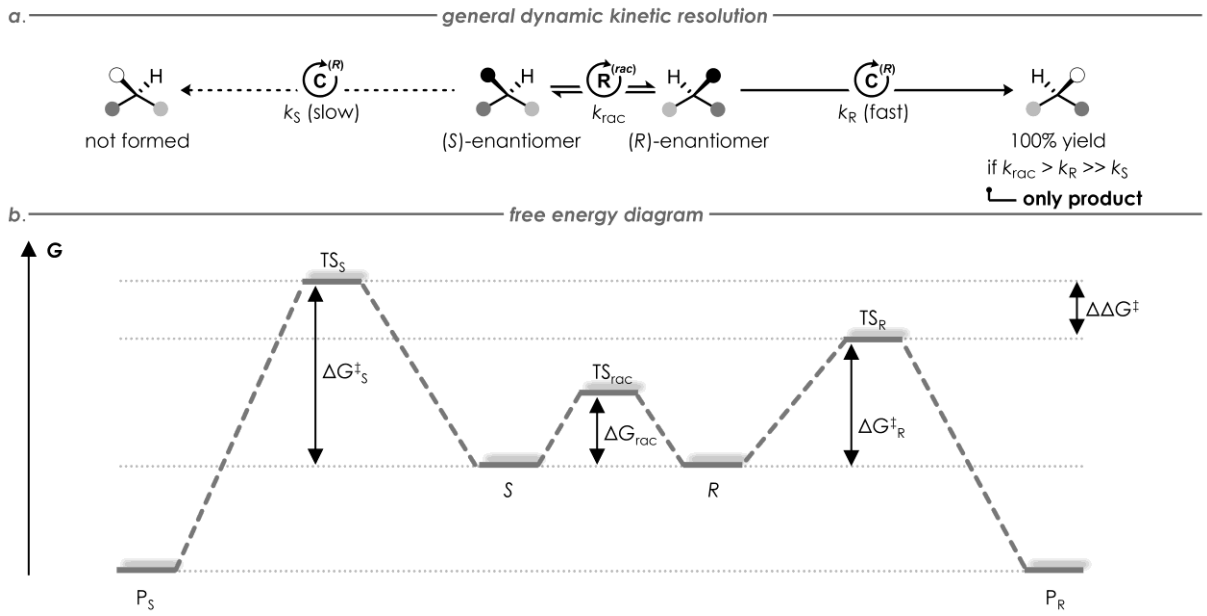

Scheme 3. The principle of DKR. (a) Fast equilibration of both enantiomers allows for a theoretical yield of 100%, even though still one enantiomer reacts selectively. $C^{(R)}$ = chiral catalyst or reagent. $R^{(rac)}$ = racemization catalyst. (b) Free energy diagram of a DKR. P = product.

Instructive early examples of DKR-related methodology include the work of NOYORI, WILLIAMS and BÄCKVALL, who independently demonstrated that a racemization catalyst and a chiral resolving agent can operate in tandem without mutual deactivation. The ruthenium-BINAP[d] hydrogenation systems developed by NOYORI and co-workers provided a mechanistic blueprint for dynamic enantioselective reductions of prochiral ketones,[25,26] while WILLIAMS and co-workers,[8,27] as well as BÄCKVALL and co-workers,[28] elegantly coupled transition-metal-mediated racemization with enzymatic acylation or hydrolysis for the DKR of racemic alcohols and amines. These studies established DKR as a general and powerful approach for achieving complete enantioconversion

[c] Most racemizations[23,24] are thermal, acid- or base-catalyzed, rely on Schiff bases, or redox and radical reactions.
[d] BINAP = 2,2'-bis(diarylphosphino)-1,1'-binaphthyl

through the coordinated interplay of stereomutation[e] and asymmetric catalysis, serving as trailblazers for a wide variety of transformations, such as enantioselective aldol reactions,[29] allylic substitutions,[30] and reductive aminations,[31] among many others.[f]

The potential of DKR lies in its theoretical 100% maximum yield of enantioenriched material, combined with the flexibility of coupling different racemization and asymmetric catalytic cycles. Nevertheless, the need to maintain a finely tuned balance between racemization and enantioselective transformation represents a persistent practical challenge. Inappropriate rate matching can lead to incomplete convergence or erosion of ee.[24] These considerations have inspired the development of integrated stereoablative catalytic systems, in which both the racemization and enantiodifferentiating steps are orchestrated within a single catalytic manifold, conceptually bridging DKR with the more general class of deracemization reactions discussed in the following section.

1.1.2.3 Deracemization

Deracemization represents the most direct strategy to obtain enantiopure compounds from racemic mixtures, ideally allowing for quantitative conversion into a single enantiomer without loss of material. In contrast to DKR, where racemization is coupled to a productive transformation step, deracemization converts both enantiomers of a racemate into one enantiomer of the *same* starting compound (Scheme 4a).[5,33] This process is intrinsically endergonic ($\Delta G = \Delta H - T\Delta S \approx +0.41$ kcal/mol at 298 K)[g] and formally violates microscopic reversibility,[36] hence, all successful deracemizations require external energy input to break the thermodynamic symmetry of enantiomer interconversion. Although the boundaries are fluid, catalytic deracemizations can be classified according to the topology of the stereochemical transformation into four mechanistic pathways:[5] 1) stereoinversion, which shares its initial step with 2) cyclic deracemization, and its final step with 3) linear deracemization. Attrition-enhanced deracemization 4) constitutes a powerful, yet niche technique, and is thereby treated separately (Scheme 4b–e).

---

[e] Stereomutation is a stereoablative process in its broadest sense,[6] since it also involves achiral intermediates.

[f] Not covered here but conceptually related to DKR are dynamic kinetic asymmetric transformations (DyKAT),[24,32] equilibrating diastereomeric (rather than enantiomeric) intermediates through different rates of the stereoisomers.

[g] This value stems from the entropy of mixing[34] for an ideal racemate. Since in achiral environments two enantiomers of one compound have identical enthalphy ($\Delta H = 0$),[35] deracemization changes only entropy ($\Delta S \neq 0$). The entropy of mixing (ΔS_{mix}) for two equally populated species is defined as $\Delta S_{mix} = R\ln 2$ per mole with $R = 1.987$ cal mol^{-1} K^{-1}. Thus, "unmixing" of the racemate to one enantiomer requires $T\Delta S_{mix} = RT\ln 2 \approx +0.41$ kcal mol^{-1} in free energy.

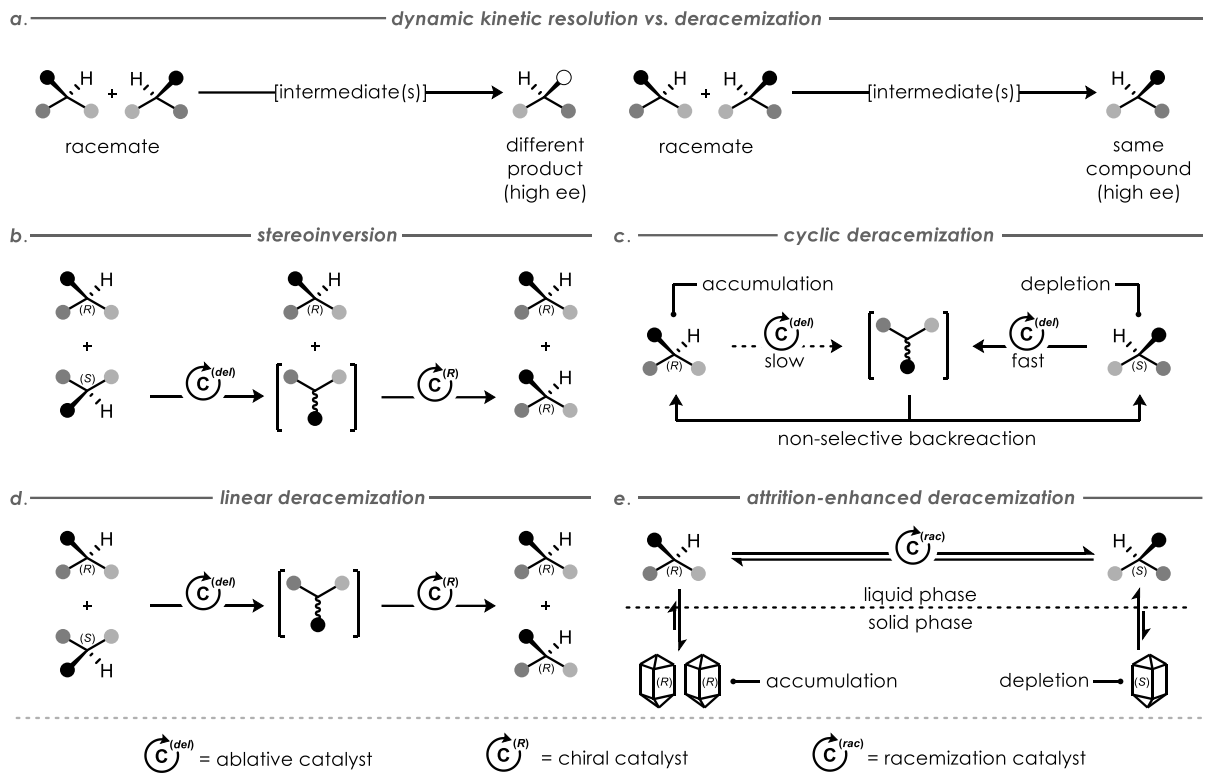

Scheme 4. (a) Distinction between DKR and deracemization. (b) Deracemization by stereoinversion. (c) Cyclic deracemization. (d) Linear deracemization. (e) The special case of attrition-enhanced deracemization.

Deracemization by stereoinversion usually relies on two synergistic catalytic regimes, wherein first one enantiomer loses its stereochemical identity in a stereoablative transformation (Scheme 4b). This achiral or prochiral compound is then selectively processed to the inverse enantiomer by a second catalyst with the opposite enantiopreference, ultimately enhancing the sample's optical purity. Since only one of the two enantiomers interacts with the stereoablative catalyst (i.e., constituting a matched pair), its mirror image remains untouched throughout the whole process, thus being accumulated, which additionally increases ee.[37] Insightful examples are mostly of biocatalytic nature and include enzymatic amino acid isomerization,[38] sequential oxidation–reduction cascades of alcohols and amines,[39] and a combination of enzymatic hydrolysis of acetates with MITSUNOBU inversion.[40] Since each processed molecule is inverted only once, stereoinversion theoretically achieves 100% yield but requires careful orchestration of chirality destruction and reformation within one process.

In the classical kinetic sense,[h] cyclic deracemization refers to an iterative process in which one enantiomer is selectively transformed into an achiral intermediate, followed by a non-selective

[h] A broader definition encompasses any repetitive, energy-driven cycle of stereoablation and reinstallation, irrespective of whether the forward step is enantioselective or not, including deracemization with participation of both enantiomers,[41] since the steady-state ee arises from asymmetric reconstitution rather than selective destruction.

backreaction to both enantiomers, resulting in gradual enrichment of the unreactive configuration (Scheme 4c). Apart from many chemo-enzymatic examples operating via this pathway,[42] BACH and co-workers demonstrated numerous photochemical variants of cyclic deracemization.[43] In their triplet-energy transfer deracemization of allenes (Scheme 5a),[44,45] a chiral photosensitizer selectively excites only *one* enantiomer within a short-lived catalyst–substrate complex, forming an achiral triplet diradical intermediate that relaxes to *either* enantiomer on the ground-state surface. Continuous excitation thus establishes a photochemical cycle of selective stereoablation and unselective reformation, leading to enrichment of one configuration. Similarly, their hydrogen-atom transfer (HAT) deracemizations (Scheme 5b)[46] proceed by selective abstraction of the stereogenic hydrogen atom from one enantiomer, followed by non-selective back HAT and tautomerization via an achiral enol intermediate. Here, the forward and reverse HAT steps occur on different potential-energy surfaces (i.e., proceed through different intermediate structures), breaking microscopic reversibility and enabling iterative erasure and regeneration of chirality.

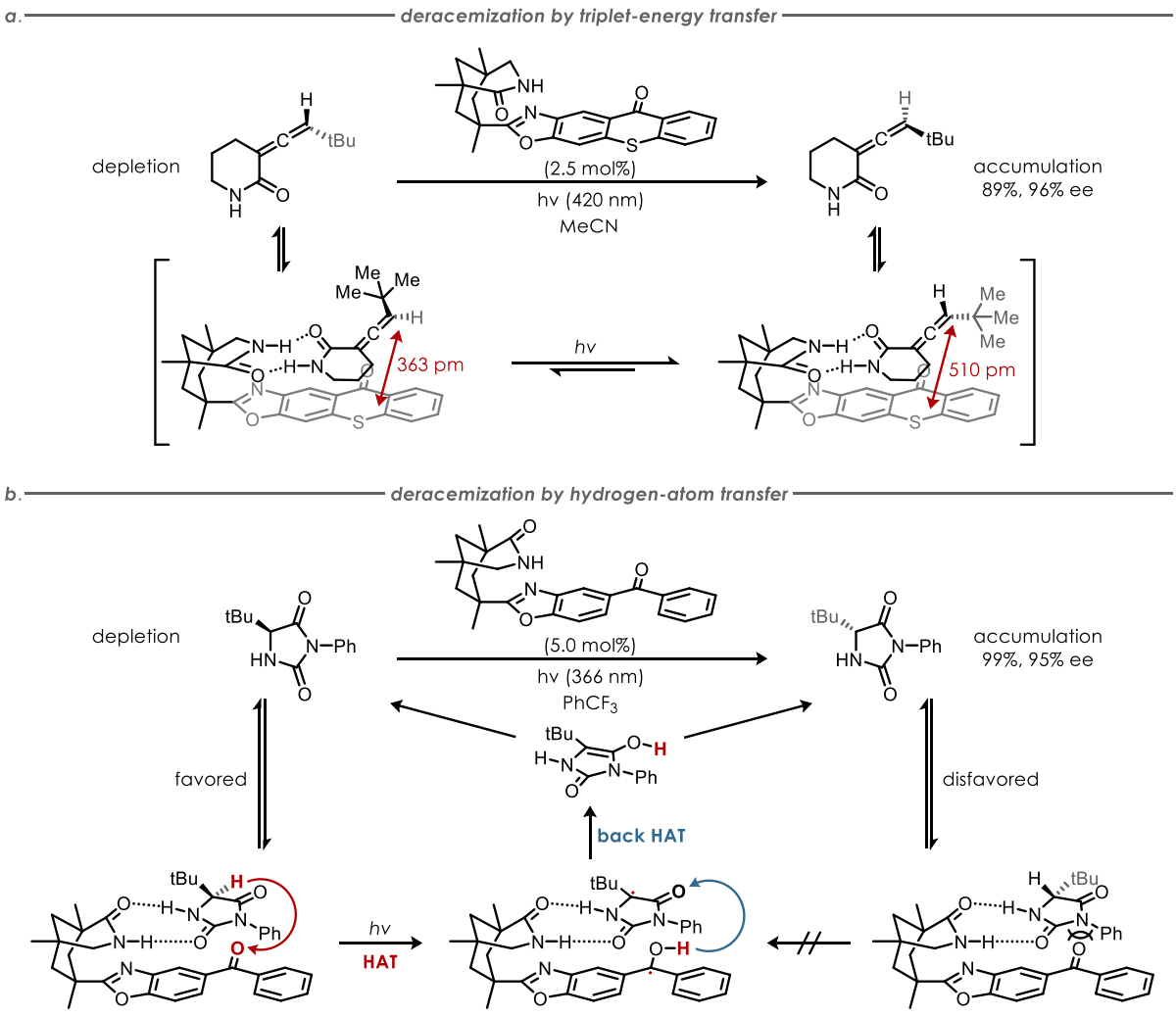

Scheme 5. (a) BACH and co-worker's photoinduced deracemization of allenes by triplet-energy transfer. (b) Similar deracemization of hydantoins by selective HAT.

In contrast to stereoinversion and cyclic variants, linear deracemization converts *both* enantiomers into a common achiral intermediate, followed by a selective reaction towards one preferred configuration in a continuous and unidirectional manner (Scheme 4d). A substantial amount of (photo-)redox-driven processes,[47,48] including photodehydrogenations,[49] operate on a linear sequence. An instructive borderline case between stereoinversion and linear deracemization is provided by MILLER, KNOWLES and co-workers, who used cyclic ureas as a model platform.[50] Here, both catalytic regimes, a chiral phosphate base and a cysteine-derived peptide HAT donor, collectively contribute to the overall enantioselection. The chiral phosphate preferentially deprotonates one activated enantiomer, generating an achiral radical intermediate. Subsequent HAT from the chiral peptide regenerates the C–H stereocenter with complementary enantioselectivity, reflecting the multiplicative combination of both chiral events in the product's ee (Scheme 6). Replacing either catalyst with an achiral analogue markedly reduced the enantioselectivity (58% ee and 72% ee, respectively), confirming the synergistic catalyst control of both the stereoablative (oxidation–deprotonation) and stereoreconstructive (HAT) steps.

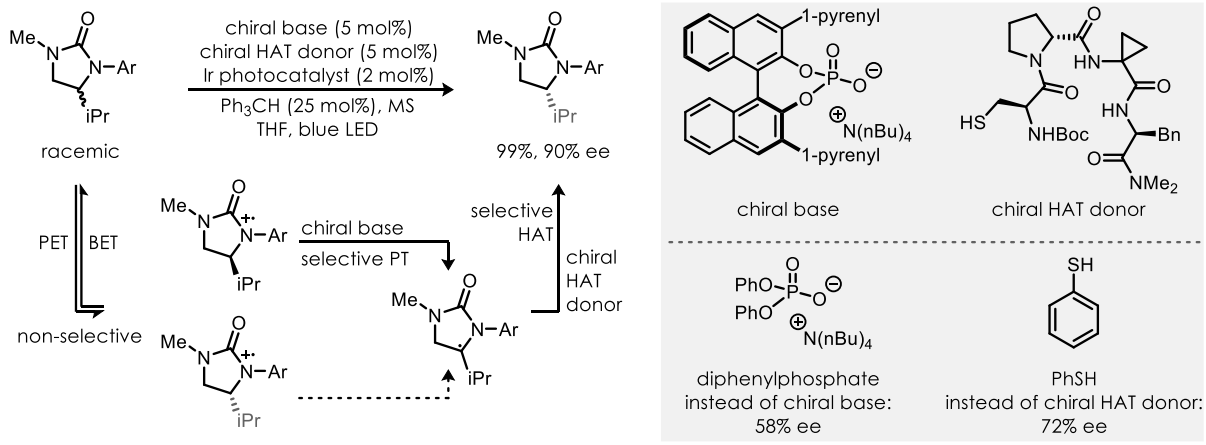

Scheme 6. Photoinduced deracemization of cyclic ureas through synergistic photoinduced electron-transfer (PET), proton transfer (PT), and HAT by MILLER, KNOWLES and co-workers. BET = back electron-transfer.

A mechanistically distinct form of deracemization occurs in the solid state through attrition-enhanced processes such as VIEDMA ripening.[51] Here, repeated grinding or stirring of conglomerate crystals in the presence of a solution-phase racemization catalyst induces dissolution–recrystallization cycles that selectively amplify one enantiomer in the solid phase (Scheme 4e). The continuous destruction and reformation of crystals mimic a macroscopic stereoablative process, where mechanical energy replaces photochemical or redox input.[52] Although limited to systems capable of forming enantiomorphous crystals,[53] this approach uniquely couples thermodynamic equilibration in solution with kinetic amplification in the solid phase to achieve complete deracemization.

Together, these pathways delineate the diverse mechanistic routes by which catalytic systems can achieve enantioenrichment via iterative stereoablation. While cyclic and attrition-enhanced methods rely on repeated destruction-reformation cycles to amplify ee dynamically, stereoinversion and linear deracemization involve discrete or single-pass transformations. Remarkably, the latter strategy represents a special case of so-called catalytic stereoablative transformations, which will be covered shortly in the next section.

1.1.2.4 Catalytic Stereoablative Transformations

Linear deracemization and catalytic stereoablative transformations share a mechanistic foundation in a way that both proceed through destruction of pre-existing chirality to form an achiral intermediate, followed by reinstallation of stereochemical information under chiral control. In linear deracemization, this intermediate reverts to the same molecular framework, yielding one enantiomer of the starting compound and thus effecting net deracemization. In contrast, the more general catalytic stereoablative transformations extend this concept to bond-forming reactions, where the achiral intermediate is converted into a *new* product of high enantiopurity.[9–11,54] The distinction to related systems such as DKR and dynamic kinetic asymmetric transformation (DyKAT)[i] lies in their naturally reversible racemization pathways by funneling all material through a single enantiomer,[24] whereas true stereoablative transformations feature irreversible racemization and prochiral intermediates that engage with the catalyst. A prototypical case of such a process is the palladium-catalyzed enantioselective allylic alkylation, originally developed by the TROST group[55] and extended by STOLTZ and co-workers.[56] In this transformation, racemic allylic electrophiles undergo oxidative addition to a Pd(0) complex to form an achiral η^3–allyl–Pd(II) intermediate, which completely erases the substrate's original stereochemical information. Subsequent nucleophilic attack on this symmetric complex occurs under the control of a chiral ligand, establishing new stereochemistry in the product with high enantioselectivity (Scheme 7).

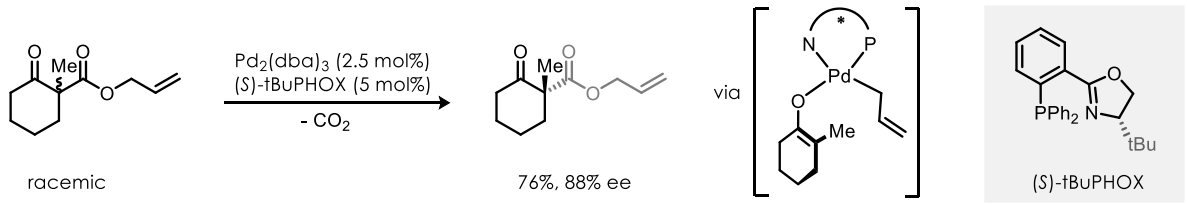

Scheme 7. Stereoablative Pd-catalyzed asymmetric allylic alkylation by STOLTZ and co-workers. dba = dibenzylideneacetone.

[i] DKR = independent racemization *prior* to engagement with chiral catalyst; DyKAT = chiral *catalyst-mediated* equilibration via diastereomeric complexes

Common to all strategies discussed thus far is the use of chiral, racemic mixtures as starting material, wherein stereoablation serves as the key to enantioconvergent product formation.[i] However, the concept of enantioselective convergence can be extended beyond racemic systems to encompass other types of mixtures, such as prochiral geometrical isomers (e.g., *E*/*Z*-olefins or imines), where, in the first step, chirality is generated rather than destroyed. These transformations are not necessarily stereoablative in nature but demonstrate the broader potential of enantioconvergent catalysis to operate across a larger chemical space, harnessing the full advantages of traditional asymmetric catalysis for prochiral as well as chiral feedstocks, thereby introducing greater degrees of freedom in catalyst design and reaction control. The following section aims to illustrate the possibilities and associated challenges on this frontier of stereochemical control.

1.1.3 Enantioenrichment from Geometrical Isomers

In transformations encompassing geometrical *E*/*Z*-isomers, stereochemical information does not arise from a pre-existing chiral center but from the spatial arrangement of substituents around a double-bond. Depending on how a chiral catalyst interacts with each isomer, two distinct outcomes are possible: the more common enantio*divergent* transformations, wherein the *E*- and *Z*-isomers yield *opposite* enantiomers, and rather rare enantio*convergent* processes, in which both geometrical isomers are funneled into a product with the *same* absolute configuration. To understand the uniqueness and rarity of the latter type, one must first understand the key parameters that dictate the stereochemical outcome of enantiodivergent reactions, best exemplified in catalytic hydrogenations and related processes.

1.1.3.1 Enantiodivergent Catalysis

The origin of enantiodivergent behavior in catalytic hydrogenations can mainly be rationalized through three selectivity quadrant models,[58] which differ in how the chiral catalyst distinguishes between geometrical isomers. In the steric quadrant model, first proposed by NOYORI[59] and HALPERN,[60] enantiodivergence arises purely from steric interactions, since the catalyst's chiral environment presents quadrants of differing spatial accessibility, and each substrate geometry (*E* or *Z*) aligns so that its smallest substituent (usually a proton) occupies the most hindered region (Scheme 8a). This reversal of substrate orientation causes hydrogen delivery to occur on opposite π-faces, yielding opposite enantiomers.[61,62] In the chelation-controlled model, a nearby heteroatom or functional group coordinates to the metal center and anchors the substrate in a fixed orientation

[i] Direct enantioconvergence of racemic mixtures via independent reaction pathways is possible,[57] but extremely rare.

prior to hydrogen addition.[63] Because *E*- and *Z*-isomers form distinct chelate geometries, the hydride inserts from opposite sides of the C=C or C=N bond, again leading to reversed stereochemical outcomes (Scheme 8b). Similarly, the secondary-interaction model accounts for cases where weak electronic forces, such as π–π stacking, C–H···π contacts, or n→π* interactions, govern face selectivity. Here, the differing spatial arrangement of π-systems in *E*- and *Z*-substrates inverts these non-covalent interactions, thereby switching the preferred enantioface of reduction (Scheme 8b).[64] Analogous phenomena have been observed in other asymmetric transformations, including allylic substitutions,[65,66,67,68] conjugate additions,[69,70] cyclopropanations,[71] and rearrangements.[72]

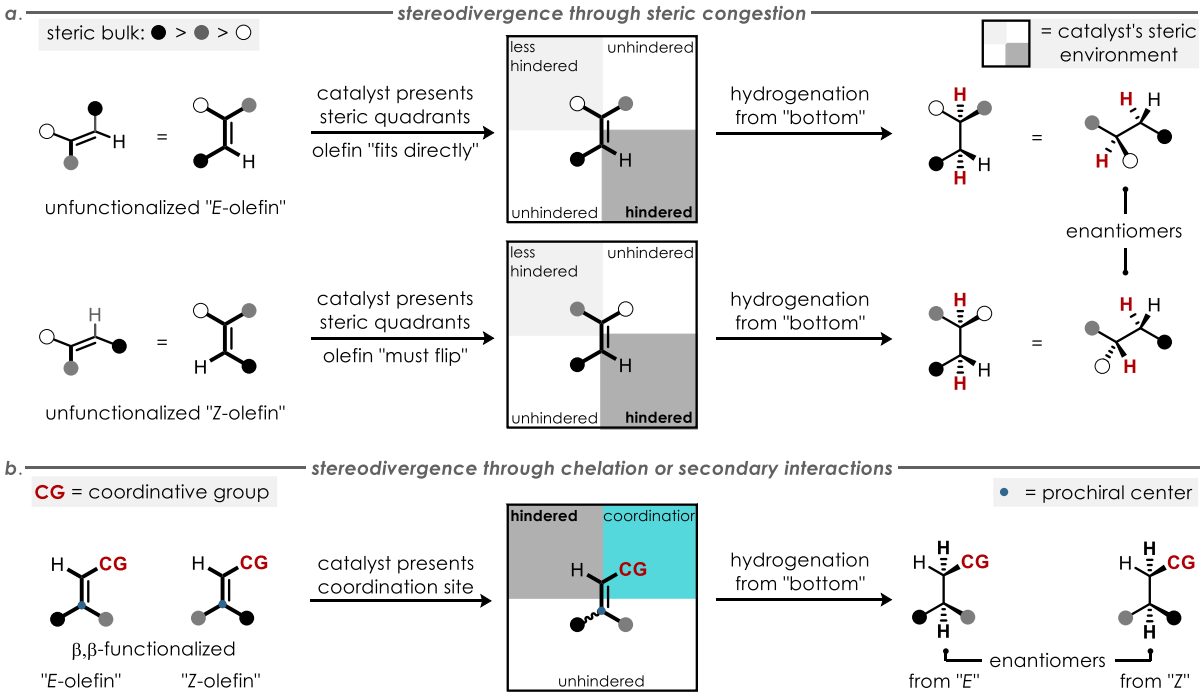

Scheme 8. Selectivity models for the asymmetric hydrogenations of trisubstituted olefins. (a) The steric quadrant model governs selectivity for unfunctionalized substrates. (b) Chelation or secondary interactions lead to stereodivergence for β,β-functionalized olefins in a similar way.

Together, these examples illustrate that enantiodivergence typically arises from the differential spatial orientation of geometrical isomers within the chiral pocket, whether governed by quadrant-type steric models, chelation control, or secondary-orbital interactions. Across these scenarios, the critical mechanistic feature is that the geometrical isomers are not dynamically equilibrated,[k] allowing the same catalyst isomer to translate structural difference into opposite enantiomeric products, a principle that is particularly appealing when the starting material is easily accessible in geometrically pure form. Achieving such switchable control, however, remains a significant challenge, as changes in olefin configuration often reduce both yield and ee,[65,66,68,69] demanding for

[k] Dependence on hydrogen pressure in presence of the catalyst can lead to direct *E*/*Z*-interconversion,[62] thus largely eroding the ee value.

catalytic systems that can directly process *E*/*Z*-*mixtures* from common WITTIG olefinations or cross metatheses to yield enantiomerically pure products.

1.1.3.2 Enantioconvergent Catalysis

Enantioconvergent reactions effectively erase stereochemical differences between starting isomers, expanding the scope of asymmetric catalysis beyond racemic mixtures to other configurationally complex feedstocks. Given their rarity, such transformations are often rather specific and substrate-dependent, however some commonalities can be found, even across multiple reaction types. In ruthenium- and rhodium-catalyzed stereoconvergent hydrogenations, once again chelation plays a decisive role: only when a strong coordinating group is bound to the prochiral carbon atom of an α,β-functionalized olefin, this anchor dominates substrate orientation within the catalytic pocket, rendering the substituents at the β-position largely irrelevant to facial selectivity (Figure 1, right).[73] As a result, both *E*- and *Z*-isomers approach the catalyst through the same coordination geometry, producing an identical enantiomer *irrespective* of their original configuration.

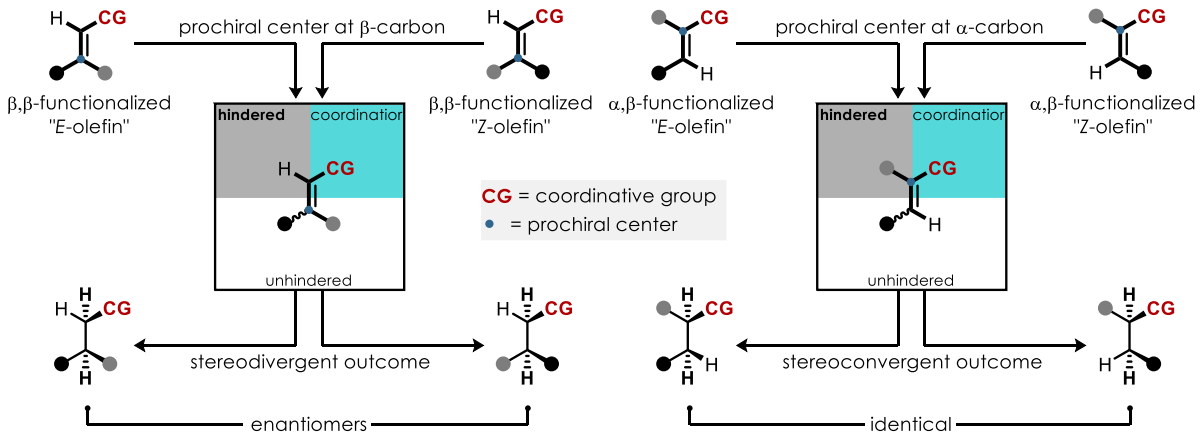

Figure 1. General models for divergent hydrogenations (left) in contrast to convergent hydrogenations (right) depending on the olefin functionalization.

Conceptually similar to catalytic stereoablative transformations (see Chapter 1.1.2.4) are enantioconvergent hydrogenations taking place through olefin isomerization. Herein, the catalyst must distinguish between the geometrical isomers with a marketed preference for the matched over the mismatched alkene and allow for rapid equilibration between the two isomers.[58] This mechanistic blueprint was supported experimentally by LU and co-workers,[74] who verified the existence of *E*/*Z*-isomerization under hydrogenation conditions previously hypothesized by BURK (Scheme 9).[75] In addition, independent studies from the groups of LIST[76] and MACMILLAN[77] on organocatalytic hydrogenations of unsaturated aldehydes showed rapid intramolecular equilibration of the α,β-unsaturated intermediates through single-bond rotation prior to hydrogen transfer.

Analogous effects have been observed in cooperative photo-enzymatic systems, such as in HARTWIG and co-worker's ester reductions,[78] wherein light-induced *E*/*Z*-isomerization continuously regenerates the reactive isomer that the enzyme selectively reduces, ultimately mimicking a dynamic kinetic resolution (see Chapter 1.1.2.2).

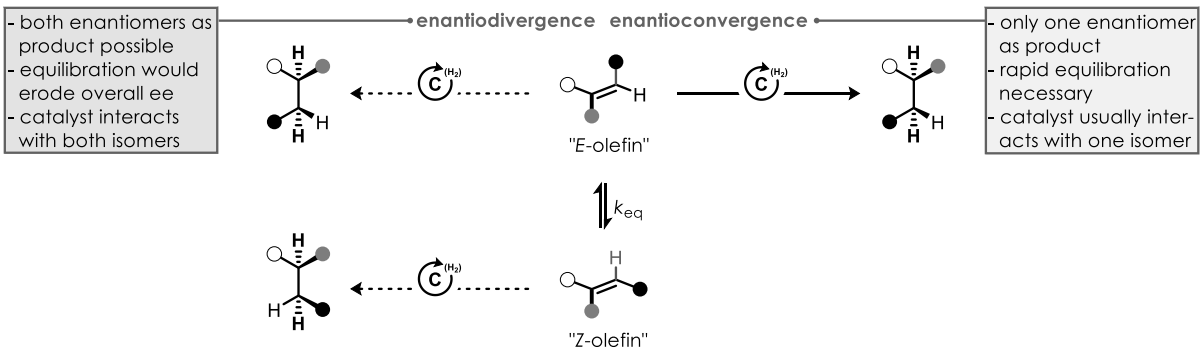

Scheme 9. Enantiodivergent vs. -convergent hydrogenation via olefin isomerization. $C^{(H2)}$ = hydrogenation catalyst.

Beyond hydrogenation, enantioconvergence via substrate isomerization has also been demonstrated in a variety of transition-metal-catalyzed C–C bond-forming reactions such as allylic alkylations[79] or homoallylic alcohol synthesis,[80] wherein both allylic isomers interconvert through a common achiral π-allyl intermediate prior to engaging with the productive catalytic cycle, ensuring identical enantioselective outcomes. Other systems achieve convergence through selective catalyst–substrate recognition rather than isomerization. For instance, the copper-catalyzed allylic borylations by MCQUADE and co-workers[81] as well as ZI's palladium-catalyzed hydrosulfonylations[82] exhibit sterically enforced facial bias: both *E*- and *Z*-isomers align such that borate or hydrogen delivery occurs from the same π-face. Similarly, UYEDA's enantioselective [4+1]-cycloadditions[83] and ARNOLD's engineered P411 enzymes[84] achieve complete enantioconvergence without any detectable isomer equilibration, as unfavorable steric or electronic interactions suppress the formation of the opposite enantiomer. These examples collectively demonstrate that enantioconvergent catalysis relies on either dynamic substrate equilibration or precisely tuned chiral environments that override inherent substrate geometry, thereby providing powerful access to stereodefined products from configurationally diverse starting materials.

1.1.4 Enantioenrichment from Constitutional Isomers?

By taking the concept of enantioconvergent catalysis to its logical extreme, the question arises if enantiopure products can in principle also emerge from constitutionally distinct substrates. Such a scenario would enable the transfer of stereochemical information not merely from *configurationally* related isomers, but from starting materials that differ in *connectivity*. A unique precedent for this

idea was reported by CHIRIK and co-workers, who observed that cobalt-catalyzed hydrogenation of both α-benzylstyrene and its double-bond isomer *trans*-methylstilbene furnished the same diphenylpropane enantiomer, albeit with modest enantioselectivity (Scheme 10a).[85] This outcome was attributed to rapid off-cycle alkene transposition promoted by the chiral cobalt hydride, allowing both constitutional isomers to funnel through a common intermediate before enantioselective hydrogenation. Although this observation offered limited synthetic utility at first glance, it introduced a crucial conceptual question: instead of converging constitutional isomers to a single enantiomer, could one diverge them to access both enantiomers using the *same* chiral catalyst?

In most asymmetric transformations of prochiral materials, the chiral catalyst acts as a translator of stereochemical information,[1,86] such that obtaining the opposite product enantiomer generally requires the catalyst's antipode. However, synthesizing both catalyst enantiomers is often costly and time-consuming. If instead constitutional isomerism could be exploited to achieve reconstitutional stereodivergence, that is, generation of opposite product enantiomers from constitutionally distinct substrates with the same chiral catalyst, this would offer a powerful alternative, especially if isomeric starting material construction is facile.[1] CHIRIK and co-workers demonstrated such behavior within the same catalytic system: hydrogenation of isomeric exo- and endocyclic alkenes of varying ring size produced opposite product configurations under otherwise identical conditions (Scheme 10b).[85] The stereochemical switch was traced to the position of the C=C bond and the differing coordination geometries of the substrates, with larger, more flexible rings reducing the extent of alkene isomerization and favoring genuine stereodivergence.

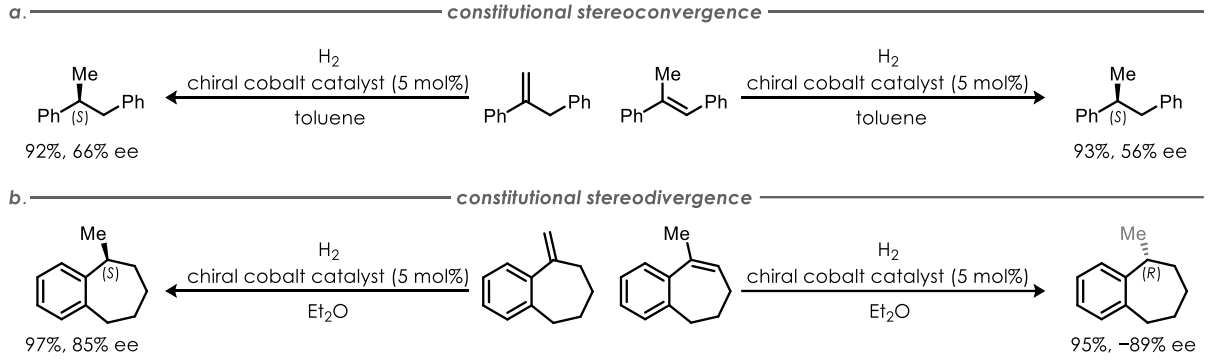

Scheme 10. (a) Observation of constitutional stereoconvergence in CHIRIK's hydrogenation of isomeric alkenes. (b) Isomeric exo- and endocyclic alkenes lead to stereodivergent outcomes, depending on their ring size (only seven-membered example shown, for a full representation see their publication).[85]

[1] For example, alkene synthesis via WITTIG olefination[87,88] or cross-metathesis[89,90] allows for a modular assembly.

The same phenomenon was reported by BLACKMOND and co-workers back in the 1990's during their hydrogenation of geraniol,[91,92] representing one of the few other examples of this form of reconstitutional stereodivergence. In both cases, catalyst-mediated alkene transposition coupled with connectivity-dependent enantioselective reduction proved key to the observed outcome. If generalized, this principle could allow selective access to either enantiomer of a desired product, an especially appealing prospect for pharmacologically active scaffolds such as chiral diarylmethanes,[93–95] where biological activity often depends critically on absolute configuration.

1.2 Chiral Diarylmethanes

1.2.1 Diarylmethanes as Privileged Structural Motif

Diarylmethanes constitute a fundamental pharmacophore present in more than 300 marketed or investigational drugs with broad activity profiles (Figure 2a).[93–95] Structurally, such active agents consist of a single carbon-bridged arene backbone, typically composed of two (substituted) phenyl or heteroaryl aromatics rings, connected through a linker to an aliphatic tertiary amine. The linker allows for conformational adaptation, typically comprising a short ethylene or propylene chain that may be branched, cyclic, extended by additional methylene units, or bear heteroatoms, while the terminal amine can be embedded in a piperidine or piperazine ring (Figure 2b).[96] Under physiological conditions, this protonated amine acts as an ionic anchor, enabling electrostatic interactions with human proteins like the H_1 histamine receptor.[97,98] The diaryl unit itself frequently engages in π–π stacking and hydrophobic interactions, thus supporting receptor binding due to its usually high lipophilicity.[99] A classical representative of a first generation H_1 antihistamine is the widely used Parkinson's medication diphenhydramine, which exhibits antihistaminic and anticholinergic activity while also blocking neuronal Na^+ channels and interacting with opioid receptors due to its ability to penetrate the blood-brain barrier.[100] Such multitarget behavior broadens therapeutic potential but can lead to adverse effects, including intoxication.[101] Attempts to improve selectivity by modifying the aryl substituents led to derivatives such as orphenadrine, wherein one phenyl group is replaced by an *o*-tolyl substituent, resulting in enhanced anticholinergic efficacy and use as a muscle relaxant and analgesic.[102,103] The related *p*-tolyl analogue neobenodine shows stronger antihistaminic effects,[93,102] underscoring how subtle changes in aryl substitution modulate both potency and receptor selectivity.

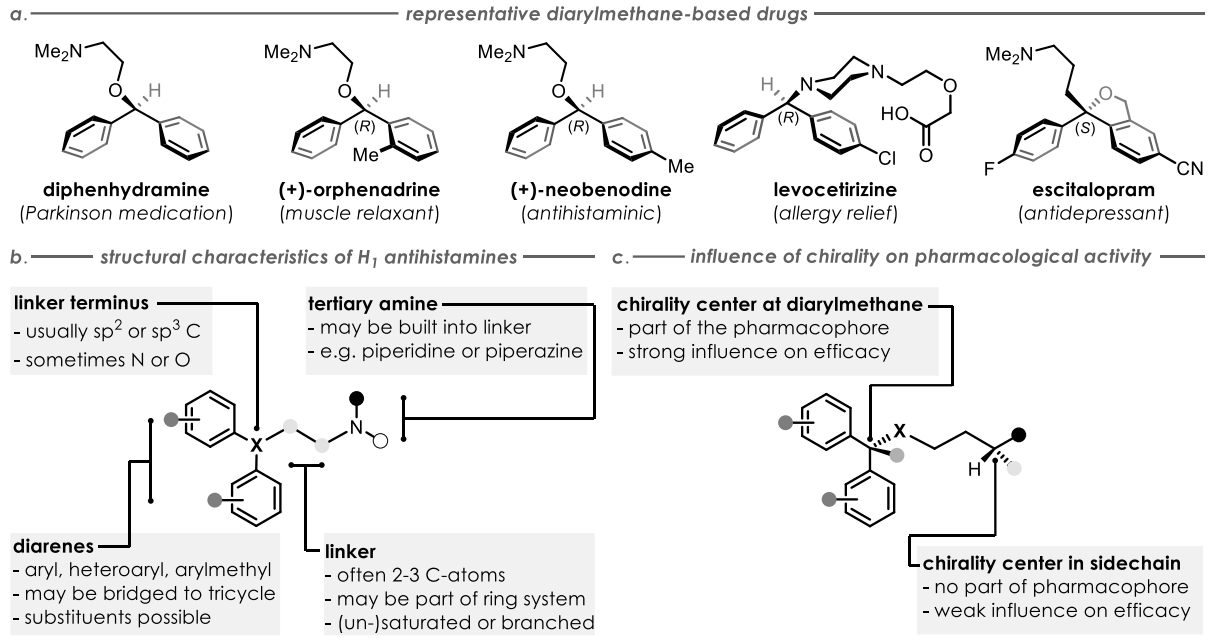

Figure 2. (a) Examples for diarylmethane-based drug molecules. (b) Common structural features of antihistamines. (c) Influence of chirality on activity.

Despite histamine itself being achiral,[97] many diarylmethane-based antihistamines and related drugs possess one or more chiral centers, which often critically govern potency through stereoselective receptor interactions (Figure 2c). Historically, most of these agents were marketed as racemates, however, isolation of the eutomer, the pharmacologically active enantiomer, has become standard practice. For instance, the second generation H_1 antihistamine levocetirizine, the (*R*)-enantiomer of cetirizine, was approved in 2007 and exhibits superior pharmacokinetics, including slower clearance.[104] Similarly, escitalopram, the (*S*)-enantiomer of citalopram, is twice as potent as its racemate and 27 times more potent than the (*R*)-distomer, which not only lacks activity but even *antagonizes* its counterpart.[105] These examples highlight the crucial role of enantioselective synthesis in developing diarylmethane-based pharmaceuticals and their common precursors.

1.2.2 Construction of Chiral Diarylmethanes

In modern catalysis, asymmetric methods for diarylmethane synthesis are manifold,[106,107] but can usually be classified into four principal construction logics (Figure 3): I. enantioselective desymmetrization of prochiral precursors, either at the central sp^3-hybridized carbon atom or within the sp^2-hybridized arene rings, II. stereocontrolled substitution, III. asymmetric addition onto prochiral precursors, including insertion reactions, and IV. intramolecular rearrangement. Each of these strategies provides distinct opportunities for introduction of asymmetry into the diarylmethane framework, while significantly differing in substrate scope, step-[108] and redox-[109] economy, as well as mechanistic control.

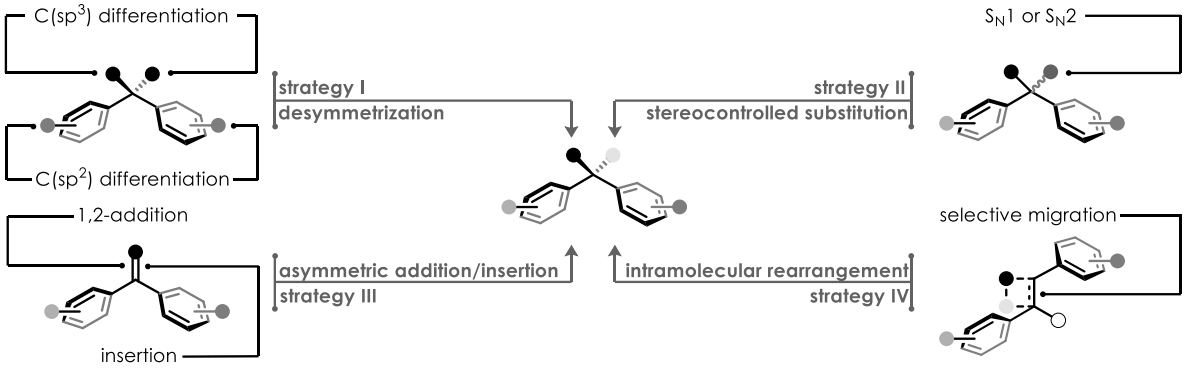

Figure 3. The four main tactics for the asymmetric assembly of diarylmethanes.

1.2.2.1 Enantioselective Desymmetrization

Among these strategies, desymmetrization conceptually represents the most straightforward route, converting a symmetry-related or prochiral precursor into a chiral diarylmethane through selective functionalization at one of two equivalent sites (Figure 3, strategy I). When applied at the benzylic sp^3-carbon, this approach typically proceeds through cross-coupling reactions in which a pre-installed directing group within the substrate governs differentiation of the two enantiotopic benzylic positions (usually hydrogen atoms).[110–112,113] Such directing elements ensure that only one site engages in metal coordination and subsequent bond formation, thereby establishing chirality in a single step. More recently, radical relay strategies have expanded this concept beyond traditional coordination control by combining careful ligand design with non-selective C–H abstraction prior to catalyst–substrate engagement. Such well-orchestrated catalytic regimes enabled groups like LU[114] and LIU[115] to achieve high levels of enantiocontrol without the need for pre-installed directing groups, marking a significant advance toward more general and substrate-tolerant desymmetrizations.

Similarly, sp^2-carbon differentiation often relies on more distal directing groups to steer C–H activation or electrophilic substitution selectively at one arene ring.[116–119] The challenge lies in achieving sufficient site discrimination within a substrate–catalyst coordination framework, which typically demands for highly engineered chiral metal catalysts capable of long-range stereochemical communication.[120,121] An elegant contribution by YOU and co-workers (Scheme 11) exploits intrinsic electronic differentiation between the two aryl rings combined with catalyst-controlled benzylic deprotonation and selective functionalization to build up unbiased chiral diarylpropanes, thus obviating the need for conventional directing elements.[122]

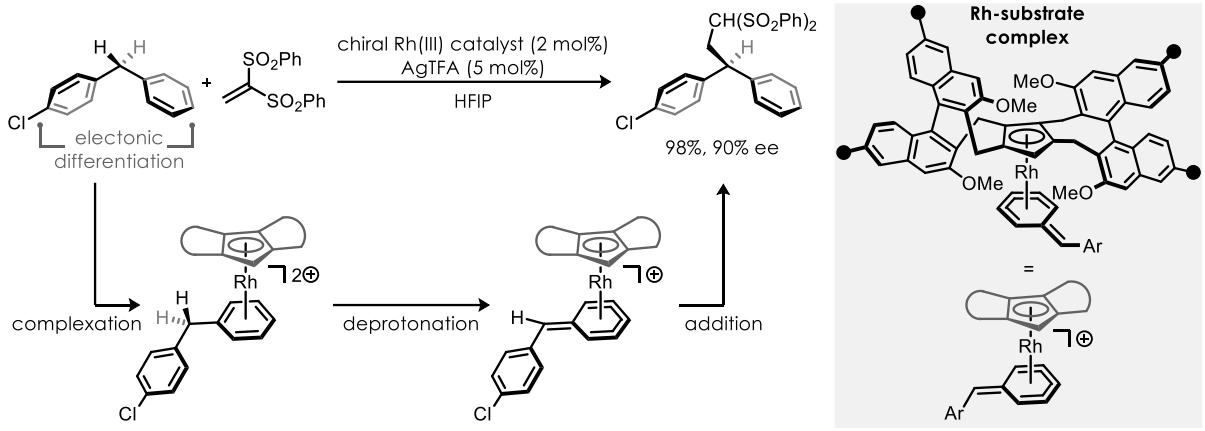

Scheme 11. Diarylmethane desymmetrization via electronic arene differentiation by YOU and co-workers.

Collectively, these desymmetrization processes can be viewed as a sequence of symmetry breaking, chiral induction, and enantioselective functionalization. The catalyst first establishes a non-equivalent environment around two otherwise identical reactive sites, either through direct coordination,[110–112,116–118] transient radical interaction,[114,115] or differential electronic activation,[122] thereby defining a stereochemical axis or center. Subsequent bond formation or substitution then locks this asymmetry into the molecular framework, producing a chiral diarylmethane from a symmetric or prochiral precursor in a *single* operation. This mechanistic logic also underpins the next major class of enantioselective diarylmethane syntheses, namely stereocontrolled substitution-based strategies.

1.2.2.2 Stereocontrolled Substitution

In most cases, stereocontrolled substitution strategies for diarylmethane synthesis rely on the presence of a suitable nucleofuge in benzylic position (e.g., a halide, ester or ether), which is displaced by an organometallic reagent in an enantiospecific fashion (Figure 3, strategy II).[123,124,125] Herein, the stereoinformation within the substrate must already be preset, enabling chirality transfer via S_N2-type inversion. In some systems this pathway can even be harnessed for enantiodivergent synthesis, as demonstrated by JARVO and co-workers,[125] who showed that judicious choice of reaction conditions allowed for selective access to either enantiomer of the product from the same enantioenriched precursor.

Notable mechanistic variants include allylic substitution via sp^2-centers,[126] circumventing the need of pre-installed chirality within the substrate through catalyst-controlled chiral π-allyl complexes. Conversely, stereoablative S_N1-type transformations, as reported by REISMAN[127] and LIU,[128] proceed through benzylic radical or cationic intermediates that lost all stereochemical memory. In these cases, asymmetry arises from enantioselective recombination with an arene substituent

governed by the chiral environment of the catalyst, a rare but conceptually important bridge between substitution-based and catalytic stereoablative transformations (see Chapter 1.1.2.4).[129,130] Altogether, these stereocontrolled substitution strategies highlight the breadth of approaches by which pre-functionalized benzylic or allylic substrates can be converted into chiral diarylmethanes, offering complementary precision to the symmetry-breaking logic of desymmetrization.

1.2.2.3 Asymmetric Addition and Insertion

The largest and most versatile class of enantioselective diarylmethane syntheses proceeds through asymmetric 1,2-additions or related insertion reactions into prochiral carbon–element π-bonds (Figure 3, strategy III).[131,132,133] Numerous highly optimized variants exist, often reaching excellent ee values. In all cases, the chiral catalyst must differentiate between the two enantiotopic faces of the π-system, which typically requires some sort of selective recognition handle within the substrate. One widely applied strategy involves addition of a carbon-centered radical or hydrogen atom onto the π-bond to generate an achiral benzylic radical intermediate.[134] Resembling a stereoablative substitution (see Chapter 1.2.2.2), the radical is subsequently intercepted by a chiral transition-metal catalyst, which enantioselectively installs a second arene unit at the benzylic position. Notable variations that bypass radical intermediates include direct HECK-type additions followed by controlled metal migration to avoid stereochemical scrambling,[135,136] as well as chiral phosphoric acid (CPA)-mediated benzylic reductions.[137]

A second major approach encompasses asymmetric reductions of benzophenones and 1,1-diarylalkenes or -imines. Herein, efficient enantioinduction critically depends on the catalyst's ability to distinguish between the two arene moieties, commonly achieved through steric bias (e.g., via *ortho*-substitution within one ring)[138,139,140,141] or distinct electronic properties (e.g., via arene decoration with electron-donating or -withdrawing groups).[64,142] A similar dependence on electronic arene differentiation is observed in carbene insertions, where stabilization of one transition state over the other relies on unequal π-donation or conjugation.[143,144] Consequently, challenging substrates that bear isosteric or isoelectronic residues typically yield low ee.[145–147] To overcome this limitation, SHI and co-workers introduced a selective η^6-$Cr(CO)_3$ coordination strategy that temporarily increases steric disparity between the arene rings, enabling high enantiodiscrimination even in systems with little electronic bias (Scheme 12).[148] Their approach predicated on the stabilities of $Cr(CO)_3$ arene complexes, adapted from a report by COREY and HELAL on their total synthesis of cetirizine.[149]

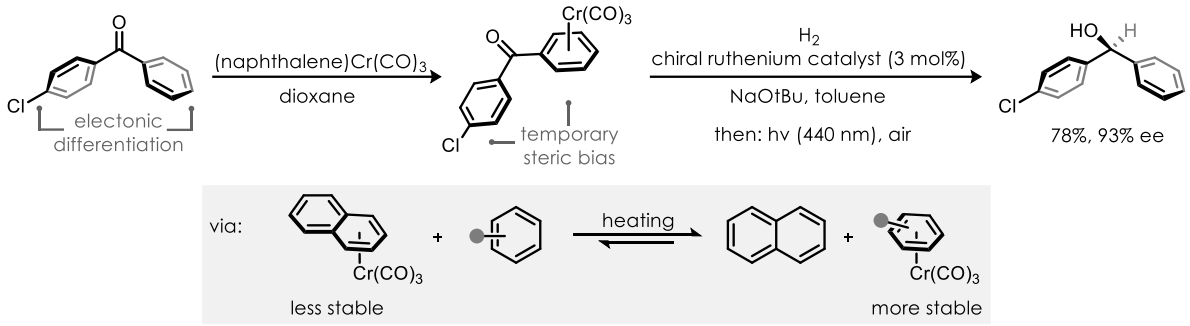

Scheme 12. Construction of chiral diarylmethanes via selective arene exchange and stereoselective asymmetric hydrogenation by SHI and co-workers.

Taken together, asymmetric addition and insertion-based strategies offer a straightforward and highly modular platform for constructing chiral diarylmethanes. Their traditional reliance on steric and electronic differentiation, however, can be overcome by tactics with a different design approach toward diarylmethane constructions such as intramolecular rearrangements.

1.2.2.4 Intramolecular Rearrangement

Representing the rarest class of enantioselective diarylmethane syntheses,[m] skeletal rearrangements (Figure 3, strategy IV) offer conceptually unique pathways by reconfiguring molecular connectivity rather than forging external C–C bonds. For example, YEUNG and co-workers developed a DKR-based semipinacol rearrangement that expands fluorenyl frameworks while simultaneously installing a stereogenic benzylic carbon and an axial chiral axis, demonstrating that a rearrangement step itself can serve as the stereodetermining event.[150] A mechanistically orthogonal approach was reported by CLAYDEN and co-workers, who achieved a stereospecific arene group transfer from lithiated ureas to generate diarylmethyl amines, showcasing how chirality can be translated through a controlled intramolecular anionic shift without the need for external chiral catalysts.[151] The most generalizable method so far was independently introduced by the groups of ZHU and SUN with their CPA-catalyzed HOUSE-MEINWALD rearrangements (Scheme 13). Herein, racemic epoxides undergo stereoablative ring opening upon protonation, followed by chiral counteranion-guided ring-expansion to form α,α-diaryl quaternary centers.[152,153] Remarkably, despite only showcasing a narrow substrate scope, the ring-expansion seems to proceed *independently* of the arene's steric or electronic properties. Although collectively rare and rather specific, these examples expand the conceptual repertoire of asymmetric diarylmethane synthesis by enabling enantioselective outcomes that would be difficult to achieve through previously covered techniques.

[m] More than 95% of reported examples encompass strategies I–III, leaving skeletal rearrangements (IV) as a rather niche technique.

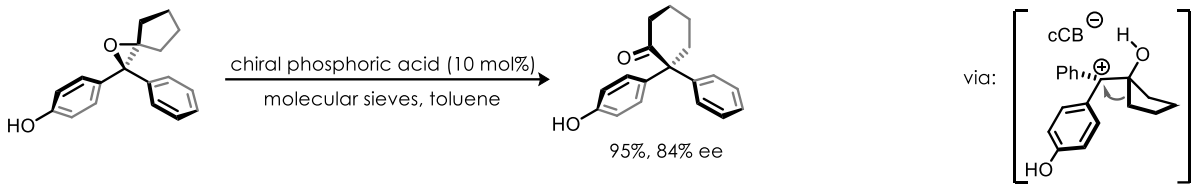

Scheme 13. CPA-catalyzed HOUSE-MEINWALD rearrangement by ZHU and co-workers and SUN and co-workers. cCB = chiral counter-base.

1.2.3 Rethinking Asymmetric Diarylmethane Assembly

All four strategic manifolds illustrate the diverse mechanistic logic by which stereochemical information can be introduced into the diarylmethane framework. While each tactic fundamentally exploits different principles of site differentiation, stereoinduction, or connectivity editing, their unified objective is the efficient construction of benzylic stereocenters with high enantioselectivity, enabling broad access to privileged medicinal scaffolds.[94,106,107] However, a common feature across all strategies is their mechanistic dependence on redox-activated starting materials to invoke the desired reactivity, which is often associated with additional pre- or post-modifications and thus unfavorable step-[108] and redox-economic[109] traits.[n] Some notable exceptions exist, among others,[121,122,154] most prominently for enantioselective hydrogenations of non-activated 1,1-diarylalkenes.[138,145,147,155,156] Nevertheless, even in these cases, high levels of enantiocontrol typically require inherent steric[145,156] or electronic[122] bias between the two aryl substituents or the presence of directing groups[138,147,154,155] to enforce selective π-facial differentiation. Substrates lacking such pre-installed asymmetry, particularly isosteric or electronically similar arenes, remain poorly addressed and often give low or erratic ee.[85,138,145,147] Although some rearrangement strategies[150] and cleverly engineered catalysts[121] have partially alleviated these constraints, their scope remains narrow and highly substrate-specific. Taken together, these limitations delineate a critical unmet challenge in asymmetric diarylmethane synthesis in the form of a general, modular, and ideally enantioconvergent catalytic strategy that circumvents both substrate pre-activation and structural bias. Addressing this challenge would provide access to enantioenriched diarylmethanes directly from simple, non-activated precursors and unlock a hardly accessible region of synthetic and medicinal chemical space.

Rare examples of enantioconvergent catalysis, whether achieved through stereoablative pathways or finely tuned chiral environments (see Chapter 1.1.3.2), are exceptionally powerful since they

[n] The term redox activation refers to stoichiometric pre-oxidation or pre-reduction, commonly in the form of reactive bonds like carbon–halogen (e.g., aryl halides),[111,120,129] carbon–metal (metal = Li, B, etc.),[115,117,126,135] carbon–nitrogen (e.g., imines, diazo compounds),[64,143,151] or carbon–oxygen (e.g., ketones, epoxides)[124,133,141,152,153] present in the starting material or reactant.

afford enantioenriched products from stereochemically unbiased feedstocks, such as racemates,[25,44,48] E/Z-isomeric mixtures,[76,77,80] or even constitutional isomers.[85] This reduction in substrate complexity is highly attractive for medicinal chemistry, where access to the eutomer *alone* is often required.[157] However, most known catalytic systems rely on substrate-dependent selectivity models (see Chapter 1.1.3.1), wherein subtle changes in steric or electronic structure can lead to enantiodivergent outcomes or even racemic erosion.[62] Key to most enantioconvergent solutions are substrate equilibration mechanisms, often enabled by stereoablative steps, rendering the initial stereochemical state irrelevant to the enantiodetermining step. Such systems posit a mechanistic blueprint for achieving broadly applicable stereoconvergence. A particularly instructive precedent was recently reported by PARK et al. in their semipinacol type I rearrangements of selenohydrins towards diarylmethanes.[158] Upon photocatalytic single-electron oxidation, carbon–selenium bond heterolysis leads to a carbocation intermediate, wherein the pre-existing stereochemistry at the β-carbon is erased prior to the bond-forming migration step (Scheme 14). Despite the overall transformation being racemic, this mechanistic insight implies that such a protocol could, in principle, be rendered enantioselective and -convergent by coupling stereoablation with asymmetric induction within the same catalytic framework, akin to ZHU's and SUN's asymmetric HOUSE-MEINWALD rearrangements.[152,153]

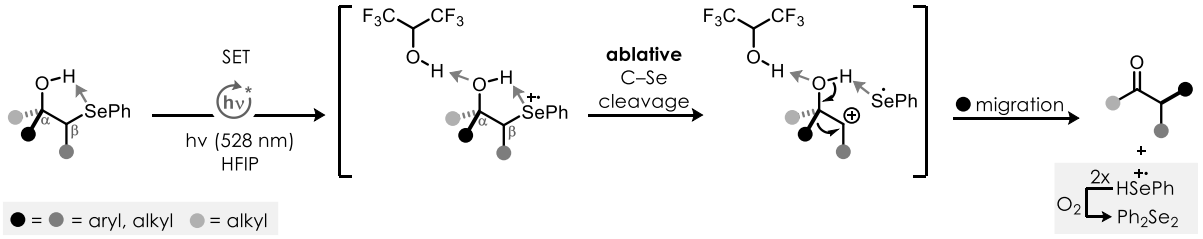

Scheme 14. Precedence for stereoablative diarylmethane synthesis from unbiased substrates by PARK et al. SET = single-electron transfer, hv* = photocatalyst, HFIP = 1,1,1,3,3,3-hexafluoro-2-propanol.

In summary, these developments illustrate the conceptual foundation for the global objective pursued in this thesis: to design a general and *enantioconvergent* catalytic manifold capable of transforming simple, *non-activated* precursors into enantioenriched diarylmethanes, *without* reliance on substrate bias or prior functional activation.

2 Objectives

The overarching working hypothesis of this thesis builds on the mechanistic observations by PARK et al. as a blueprint for asymmetric diarylmethane synthesis. A first retrosynthetic analysis revealed that selenohydrins could, in principle, be generated in situ from unbiased stilbenes through selenium-π-acid activation[159] and subsequent nucleophilic addition of water (Scheme 15a). Since each step in this sequence is expected to proceed enantiospecifically, the stilbene's geometrical configuration is initially reflected in the absolute configuration at the β-carbon of the resulting selenohydrin. However, a carbon–selenium bond cleavage, as demonstrated by PARK et al., renders this absolute configuration *irrelevant*, thus effectively "ablating" the intermediate (Scheme 14). If a chiral selenium catalyst was employed, it could then rebuild chirality after this stereoablative step, governing asymmetric induction while simultaneously mediating the initial LEWIS-acid activation of the stilbene.[160,161] The overall process thus mirrors a migratory TSUJI–WACKER (MTW) oxidation,[162] reimagined under photoredox selenium-π-acid dual catalysis,[163] and serves as this work's foundation (Scheme 15b).

Inspired by CHIRIK and co-worker's observations on constitutional stereodivergence, where double-bond position determines the enantiomeric outcome with a single chiral catalyst,[85] the question arises whether modifying stilbene connectivity can induce enantiomeric inversion in the product (Scheme 15c). If proven successful, such a switch would ensure the access towards eutomer diarylmethane drug precursors without synthesizing the catalyst's antipode, offering an efficient stereochemical control element given through the possibility of modular stilbene design.[87–90] Brought down to the essentials, this thesis' two main objectives are:

1) The development of a photoredox selenium-π-acid dual catalytic platform capable of converting *E*/*Z*-stilbene mixtures into chiral diarylmethanes by leveraging stereoablation as a convergence step, and
2) Harnessing stilbene substrate connectivity to achieve constitutional stereodivergence for the synthesis of (antihistamine) drug eutomers.

Together, these objectives embody the central theme of this thesis in seeking the strategic integration of stereoablation and enantioconvergence to expand asymmetric diarylmethane synthesis beyond pre-activated or biased substrates. In addition, these findings aim to contribute to the eutomer-selective access towards diarylmethane-based pharmaceuticals.

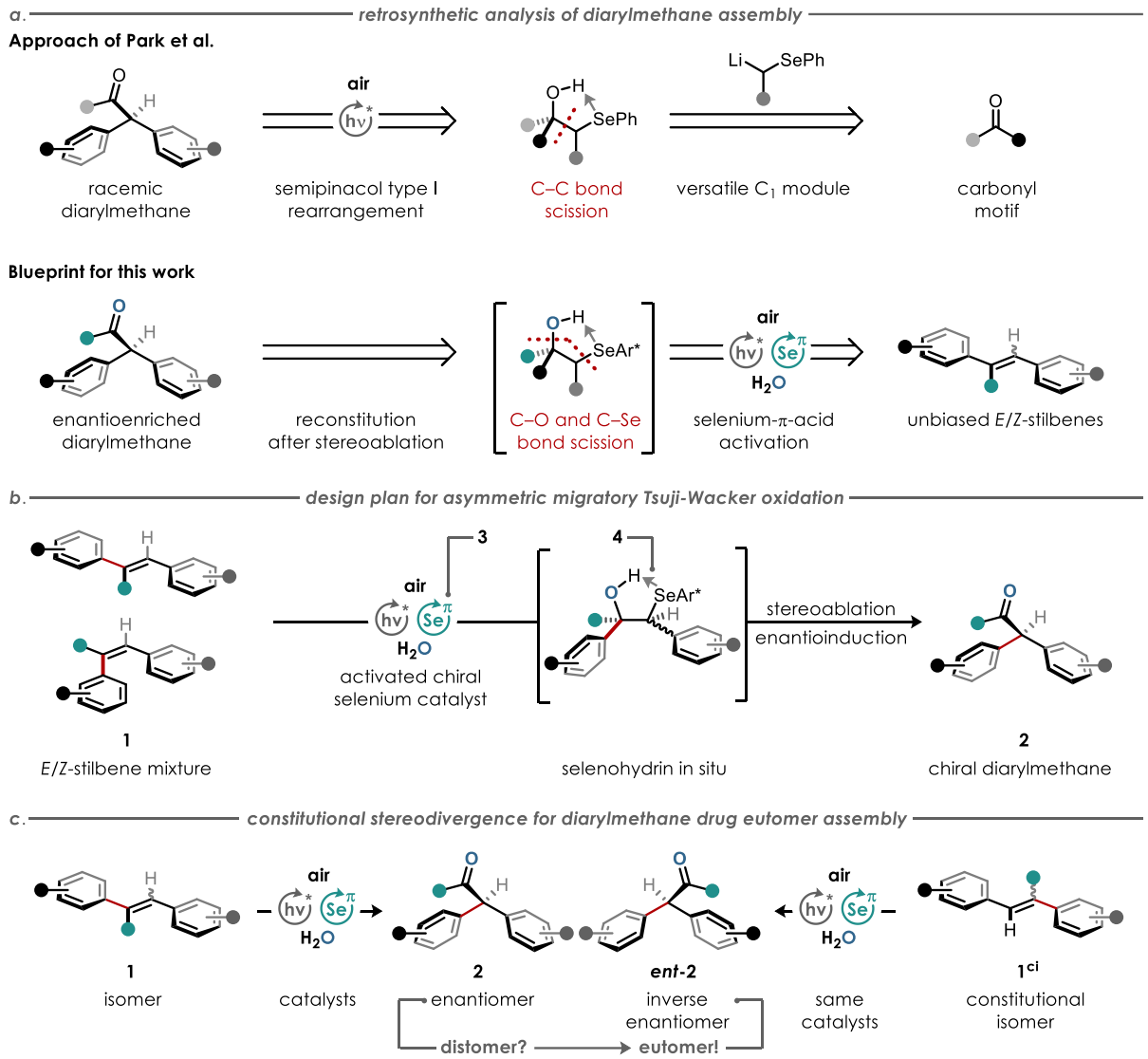

Scheme 15. Main objectives for the enantioconvergent migratory TSUJI-WACKER (MTW) oxidation towards diarylmethanes. (a) Retrosynthetic analysis of PARK et al. serving as blueprint for this thesis. Ar* = chiral arene backbone. (b) Design plan for overall oxidative rearrangement reaction starting from geometrical stilbene isomers **1** towards diarylmethanes **2** with incorporation of a stereoablative step and subsequent installation of the stereocenter under chiral control of a selenium catalyst **3**. (c) Control of reconstitutional stereodivergence by substrate connectivity towards eutomer-selective diarylmethane drug synthesis.

3 Results and Discussion

3.1 Asymmetric MTW Oxidation

3.1.1 Reaction Development

In their study on semipinacol type I rearrangements, PARK et al. primarily synthesized selenohydrins **4** via nucleophilic addition of seleniated carbanions to ketones (Scheme 15a).[158] However, purification proved challenging for selenohydrins bearing aromatic β-substituents, prompting the authors to develop alternative approaches using stilbenes **1** as starting materials. Two routes were explored: 1) epoxidation of stilbenes, followed by nucleophilic ring-opening of an in situ generated $PhSe^-$ (Scheme 16a), and 2) reaction with electrophilic PhSeBr, which functions as a π-acid[o] toward the C=C bond to form a seleniranium ion that undergoes MARKOVNIKOV-type hydration (Scheme 16b). Unexpectedly, rather than the anticipated selenohydrin **4a**, the latter pathway afforded the rearranged diarylmethane product **2a** directly from its stilbene precursor **1a**.

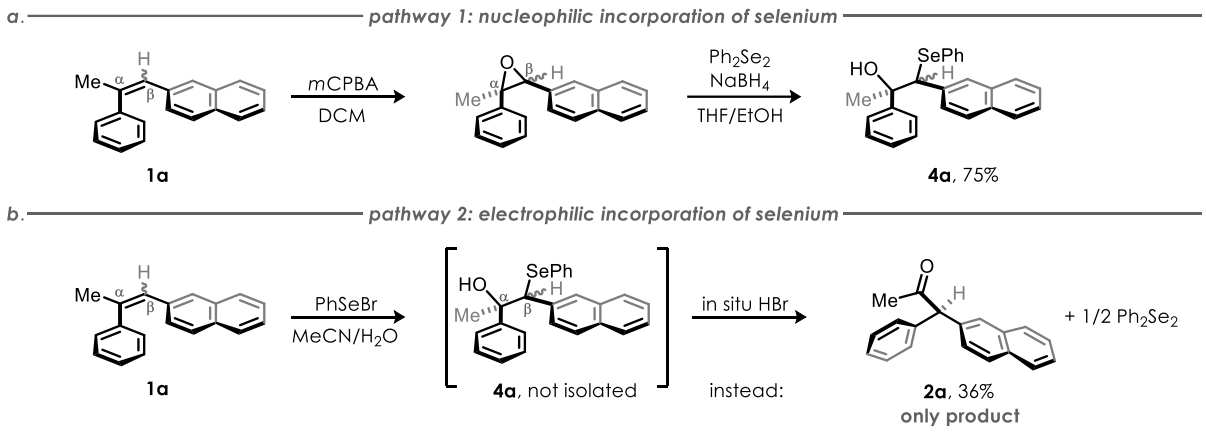

Scheme 16. Alternative synthetic strategies for selenohydrin **4a** assembly performed by Dr. Sooyoung Park.[165] (a) Nucleophilic incorporation of selenium via epoxidation and ring-opening by $PhSe^-$. (b) Electrophilic incorporation of selenium via seleniranium formation and ring-opening by water, which led directly to diarylmethane **2a**.

This observation was rationalized by assuming that HBr, stoichiometrically formed upon generation of the $PhSe^+$ π-acid in situ, protonates the chalcogen, thereby triggering a BRØNSTED-acid-induced semipinacol rearrangement.[166] Detection of diphenyldiselane (Ph_2Se_2) as a byproduct further suggested that a process catalytic in selenium might be achievable if the transient $PhSe^+$ species could be regenerated. This insight motivated the development of a photoredox/selenium-π-acid manifold, combining both selenium activation and the already established semipinacol rearrangement within a single catalytic system. Notably, a key prerequisite for productive reactivity in the study of PARK et al. was a solvent of high hydrogen-bond (H-bond) donicity, characterized

[o] i.e., a carbophilic LEWIS-acid,[164] which is used e.g. by the BREDER group for oxidative alkene functionalizations

by a KAMLET-TAFT α-parameter of >1.5.[167–169] In this regard, 1,1,1,3,3,3-hexafluoro-2-propanol (HFIP, α = 1.96) proved optimal, ensuring conformational rigidity of the selenohydrin through a rare intramolecular O–H···Se H-bond,[170] which facilitated the rearrangement.

For the ensuing optimization (Table 1), stilbene **1a** was chosen as the model substrate. Initial experiments with (super-)stoichiometric selenium electrophiles indeed directly led to the desired diarylmethane product **2a** by using water as the nucleophile in HFIP (entries 1–2). To render the process catalytic in selenium, two requirements were identified:

1) A suitable photoredox catalyst that activates the diselane precatalyst by single-electron transfer (SET) to unlock its LEWIS-acidic properties, while still modulating the nucleofugality of the selenium residue within the selenohydrin intermediate. Ideally, photocatalyst regeneration is secured by ambient air as terminal oxidant, thus affording only benign byproducts such as water.[171]
2) A proper redox hierarchy ensuring that the diselane (E_{pa}^{ox} = +1.35 V vs. SCE in MeCN for Ph_2Se_2)[172] quenches the excited state photocatalyst preferentially, ideally followed by the selenohydrin (E_{pa}^{ox} = +1.17–1.70 V vs. SCE in MeCN for alkyl(aryl)selanes),[173] while direct oxidation of the stilbene (E^{ox} = +1.15–1.78 V vs. SCE in MeCN)[174] should be avoided to suppress potential side reactivity.[p]

With this rationale in mind, exposure of stilbene **1a** to 10 mol% Ph_2Se_2 and 5 mol% of photoredox catalyst 2,4,6-tris(4-anisyl)pyrylium tetrafluoroborate (TAPT, $E^{red,*}$ = +1.84 V vs. SCE in MeCN)[173] under ambient air and temperature furnished ketone **2a** in respectable 29% yield, increasing to 77% upon heating to 55 °C (entries 3–4). Introduction of 1,2-dichloroethane (DCE) as a co-solvent greatly improved catalyst solubility and thus reproducibility (entry 5). On the basis of this ternary solvent mixture, the impact of sterically and electronically modified diselane catalysts was examined (entries 6–8), revealing electron-rich 2-anisyldiselane (E_{pa}^{ox} = +1.22 V vs. SCE in MeCN) to outperform all previous entries (entry 8), presumably due to its lower oxidation barrier (in comparison to entry 7) and negligible steric impact upon π-bond attack (in comparison to entry 6), furnishing ketone **2a** in 92% yield. Substitution of TAPT with milder photoredox catalysts such as dimethylated Rose Bengal (DMRB, $E^{red,*} \approx$ +1.36 V vs. SCE)[158] or 3CzClIPN ($E^{red,*}$ = +1.56 V vs. SCE),[176] or with related stronger pyrylium salts,[173] resulted in diminished performance (entries 9–13), revealing that the photoredox and selenium catalytic cycles operate cooperatively under finely balanced redox conditions, as evaluated on a first empirical basis.

[p] The anodic peak potential E_{pa}^{ox} is the potential at which the current reaches its maximum during an anodic (oxidation) process in a cyclovoltammetry (CV) experiment;[175] SCE = standard calomel electrode; MeCN = acetonitrile

Table 1. Optimization of the racemic migratory Tsuji-Wacker (MTW) oxidation performed by S. Park.[165]

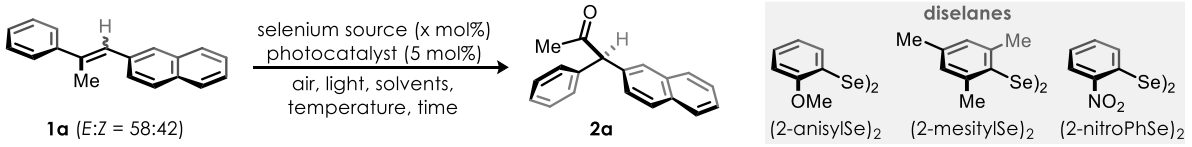

entry	selenium source (x)	photocatalyst	light (λ)	solvents (v:v, M)	temperature	time	NMR-yield
1	PhSeBr (100)	-	-	HFIP/H_2O (5:1; 0.25 M)	23 °C	18 h	45%[*]
2	PhSeBr (300)	-	-	HFIP/H_2O (5:1; 0.25 M)	23 °C	18 h	73%[*]
3	Ph_2Se_2 (10)	TAPT	447 nm	HFIP/H_2O (4:1; 0.1 M)	23 °C	10 h	29%
4	Ph_2Se_2 (10)	TAPT	447 nm	HFIP/H_2O (4:1; 0.1 M)	55 °C	10 h	77%
5	Ph_2Se_2 (10)	TAPT	447 nm	HFIP/DCE/H_2O (3:1:1; 0.1 M)	55 °C	18 h	71%
6	(2-mesitylSe)$_2$ (10)	TAPT	447 nm	HFIP/DCE/H_2O (3:1:1; 0.1 M)	55 °C	10 h	77%
7	(2-nitroPhSe)$_2$ (10)	TAPT	447 nm	HFIP/DCE/H_2O (3:1:1; 0.1 M)	55 °C	10 h	4%
8	(2-anisylSe)$_2$ (10)	TAPT	447 nm	HFIP/DCE/H_2O (3:1:1; 0.1 M)	55 °C	10 h	**92%**
9	Ph_2Se_2 (10)	DMRB	528 nm	HFIP/DCE/H_2O (3:1:1; 0.1 M)	55 °C	10 h	16%
10	Ph_2Se_2 (10)	3CzClIPN	447 nm	HFIP/DCE/H_2O (3:1:1; 0.1 M)	55 °C	16 h	51%
11	(2-anisylSe)$_2$ (10)	TTPT	447 nm	HFIP/DCE/H_2O (3:1:1; 0.1 M)	55 °C	10 h	84%
12	(2-anisylSe)$_2$ (10)	TPT	447 nm	HFIP/DCE/H_2O (3:1:1; 0.1 M)	55 °C	10 h	89%
13	(2-anisylSe)$_2$ (10)	MDPT	447 nm	HFIP/DCE/H_2O (3:1:1; 0.1 M)	55 °C	10 h	70%

[*] isolated yield

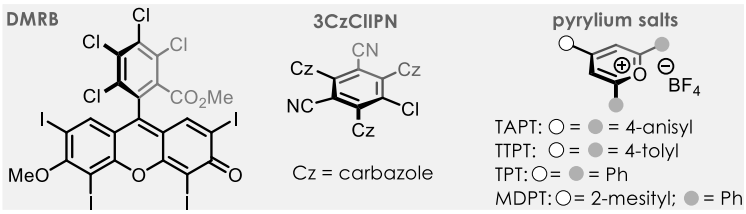

Control experiments (Table 2) underscored the necessity of all substoichiometric components, as omission of either the diselane or TAPT drastically reduced yields (entries 1–2). Replacement of HFIP with 2,2,2-trifluoroethanol (TFE, α = 1.51)[167,177] also diminished product formation, corroborating the need for a solvent of sufficiently high H-bond donicity (entry 3). Moreover, the reaction strictly requires light irradiation (entry 4), while changes within the atmosphere (entries 5–6) indicate a sweet spot regarding the oxygen concentration, which proved critical for the photocatalyst's turnover and substrate stability, consistent with an overall net-oxidative process.

Table 2. Control experiments.

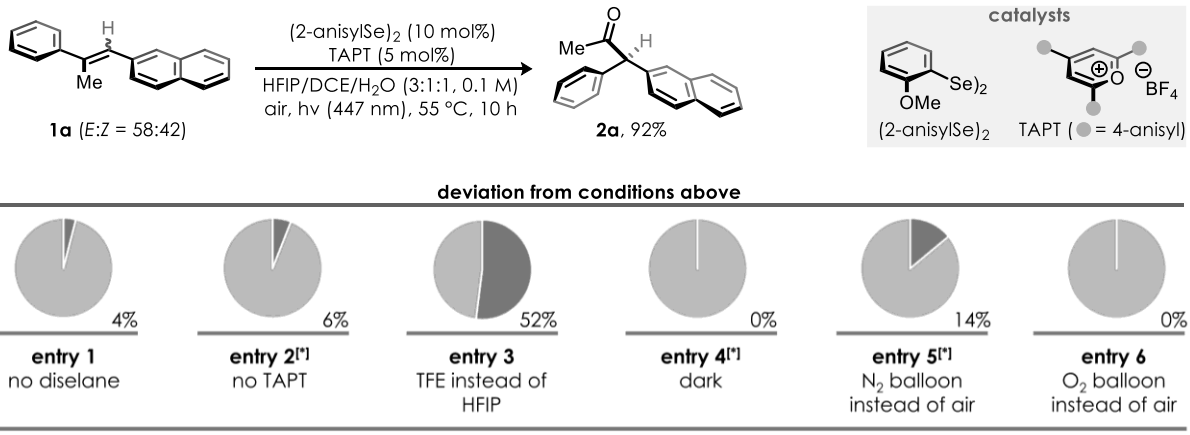

[*] the diselane was Ph_2Se_2

Following the initial racemic results, attention turned towards rendering the whole process enantioselective, completely under the control of a chiral, non-racemic selenium catalyst (Table **3**). While spirobiindane catalyst **3a**[178] was inactive at both 0 °C and 55 °C (entries 1–2), the MARUOKA–HASHIMOTO-type diselanes **3b** and **3c**, previously successful in asymmetric (imino-)lactonizations,[179] delivered ketone **2a** in up to −59% ee, albeit in moderate yield (entries 3–4). A major breakthrough was achieved with tetralin-based diselane **3d**, which was recently introduced by DENMARK and co-workers within their asymmetric di- and oxyamination reactions,[160,161] affording the desired ketone **2a** in 61% yield and 85% ee at 55 °C (entry 5). Gradual cooling of the reaction mixture led to a markedly increase in both yield and enantioselectivity (entries 6–8), culminating at 99% yield and 93% ee at 0 °C for the investigated scale of 0.5 mmol. Variations in the catalyst's ester substituent (**3e**–**3i**) decreased both yield and selectivity at 0 °C (entries 9–13), highlighting the naphthoate ester as a privileged motif, which is likely involved in π–π* interactions with the substrate at some point in the transformation, a feature that was examined in more detail in Chapter 3.1.3.2. In summary, the combination of a chiral diselane with a suitable photoredox catalyst in a ternary solvent system enabled the successful oxidative transformation of model stilbene **1a** into a diarylmethylketone with high yield and ee, respectively. This empirical optimization already serves as a proof of concept for the successful extension of PARK et al.'s semipinacol rearrangement towards an *enantioconvergent* diarylmethane synthesis by leveraging stereoablation as a key feature. The next step seeks to explore the generality of this method by applying the optimized conditions to various stilbenes differing in their electronic and steric properties.

Table 3. Evaluation of chiral, non-racemic selenium catalysts **3**. Experiments for entries 3–13 and asymmetric syntheses of MARUOKA–HASHIMOTO and DENMARK catalysts were performed by S. Park.[165]

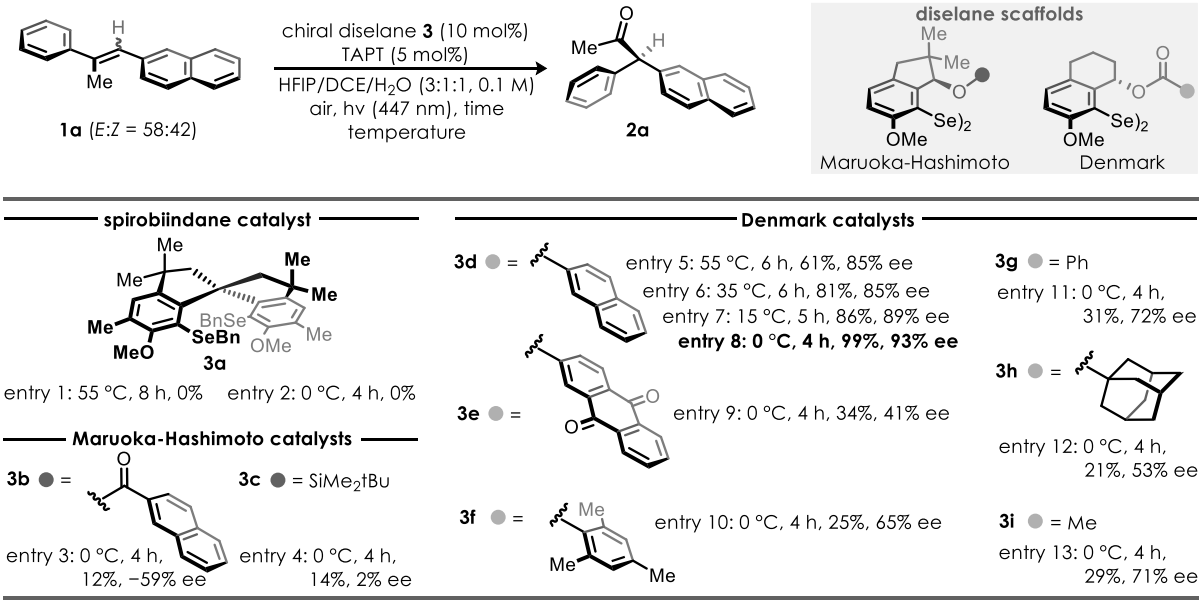

3.1.2 Reaction Generality

Before exploring the reaction scope, careful consideration was devoted to the assembly of the stilbene precursors. In alignment with this work's main objective, the central design principle was to evaluate enantioselectivity in the absence of pronounced steric bias between the two aryl substituents. Therefore, most derivatives featured *para*-substitution, minimizing spatial differentiation at the reactive site (i.e., the π-bond). At the same time, variation of the electronic properties of the arene units allowed assessment of both electron-rich and electron-deficient migrators, as well as the overall functional group tolerance of the catalytic system, thus providing a representative overview of the reaction's generality.

The modular synthesis of target stilbenes **1** was accomplished through two complementary routes (Scheme 17), chosen according to the substitution pattern of the arene under investigation. In route I, variation of the α-aryl unit was achieved by first preparing a phosphonium salt bearing a fixed β-aryl group,[180] followed by WITTIG olefination with the desired acetophenone.[181] Conversely, in route II, variation at the β-aryl position proceeded via formation of a hydrazone derived from a fixed α-aryl motif,[182] which then underwent copper-catalyzed WITTIG-type coupling with the corresponding aryl aldehyde.[183] Together, these two strategies provided a highly flexible synthetic platform, allowing for facile interchange of arene motifs simply by exchanging the corresponding precursors. Furthermore, the influence of the alkyl substituent at the vinylic position was examined by replacing the standard methyl group with various linear and branched alkyl residues, following either of the established routes. This modular approach ensured a consistent and efficient preparation of all substrate classes required for the subsequent catalytic investigation.

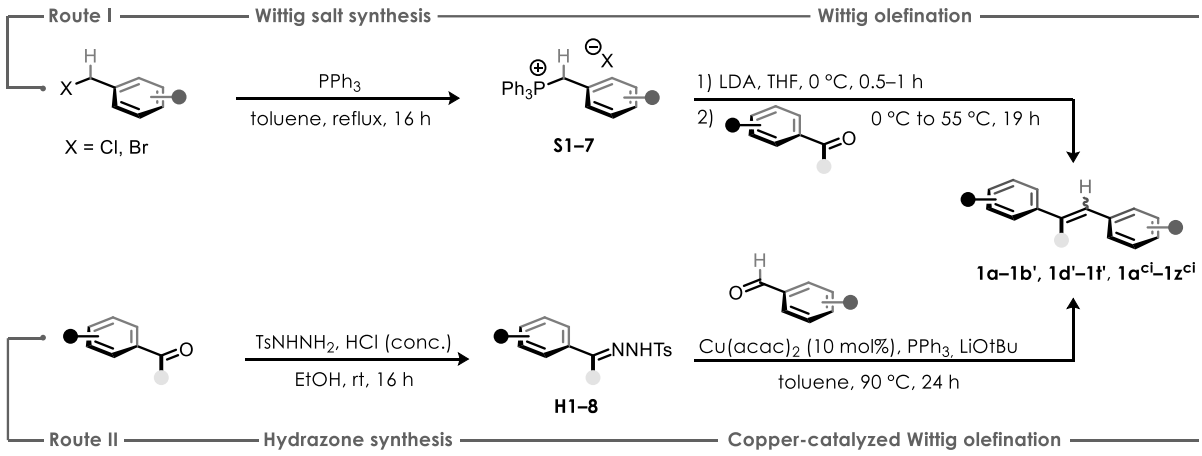

Scheme 17. Synthetic routes for the strategic assembly of *E*/*Z*-stilbenes. All stilbenes accessed via route II were synthesized by S. Park. For more details on the individual steps see his dissertation and the Experimental Part.[165]

Evaluation of the target reaction's scope, which was conducted on a 1 mmol scale, started with variation of the α-arene substituents (Table 4a). As anticipated from our design principles, steric effects within the arene rings had only a minor influence on stereoinduction. Unsubstituted and *para*-substituted stilbenes **1a–1j** delivered products with consistently high enantioselectivities (average ee = 89%), as was the case for electronically equivalent *ortho*- and *meta*-substituted derivatives **1p–1r** (average ee = 92%). Across the entire α-arene series, the global average ee was 88%, underscoring the method's pronounced performance, specifically regarding isosteric residues. A notable deviation was observed for substrates bearing weakly electron-withdrawing substituents (**1k**, **1n**, **1o**), which furnished the corresponding ketones with somewhat lower enantioselectivities (69–82% ee, average ee = 77%). We attribute this erosion to smaller differences in the stabilizing π–π* interactions of the catalyst's electron-deficient naphthoate backbone with the α-arene group, leading to less differentiated chiral control upon the migration step (see Figure 4). Conversely, ketone **2m**, bearing the strongly electron-deficient pinacolborane (Bpin), was produced with excellent enantioselectivity (97% ee), exceeding the ee of above-mentioned electron-poor analogues (**2k**, **2n**, **2o**). In this particular case, we suspect that a coordination of water, present in the solvent mixture, to the Bpin group results in the formation of an electron-rich ate complex (i.e., a pinacolboronate), which then exerts proper electronics for highly efficient catalytic conversion.

Variation of the β-arene unit revealed no clear correlation between steric or electronic features and enantioselectivity (Table 4b). In general, substrates **1s–c'** afforded ketones **2s–c'** in 50–93% ee, while also demonstrating broad functional group tolerance in this static arene terminus. Replacement of the β-aryl group with a benzoyloxy substituent afforded α-acyloxy ketone **2c'** in modest 40% yield and 61% ee. However, α-acyloxy ketones constitute valuable precursors to enantioenriched α-hydroxy ketones, being useful templates in asymmetric reactions and natural product synthesis,[184] and their formation indicates that photocatalytic activation of the chiral diselane is sufficiently rapid to outcompete direct alkene oxidation by the photocatalyst; an important mechanistic insight (see Table 5). This outcome also supports our previous hypothesis that the α-arene unit likely plays a critical role in the stereodetermining event through non-covalent interactions with the catalyst's naphthoate backbone, because the benzoyloxy substituent as well as the other β-aryl groups seem to be less relevant for the diselane's chiral induction.

The role of the vinylic alkyl substituent was probed by substituting the archetype methyl group with different residues (Table 4c). Various linear or functionalized *n*-alkyl chains (**1d'–g'**) consistently afforded products in high enantioselectivities (average ee = 89%), while the α-branched isopropyl stilbene **1h'** contrastingly provided only 4% yield at 44% conversion, indicating that increased steric bulk at this position disrupts productive catalyst–substrate

alignment. On the other hand, omission of the methyl group (i.e., replacement of Me with H) within substrate **1i'** led to its complete decomposition (100% conversion, 0% yield).

Table 4. Scope of the asymmetric MTW oxidation with (a) variation of the α-arene, (b) the β-arene, (c) the alkyl group and (d) unsuccessful examples. Ketones **2d–m**, **2p–2y**, **2a'–2g'**, **2m'**, and **2o'** were synthesized by S. Park.[165]

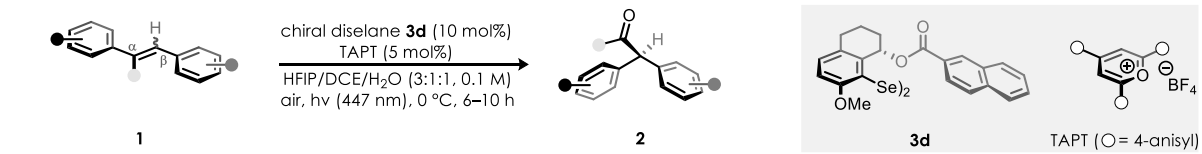

a. *variation of the α-arene group*

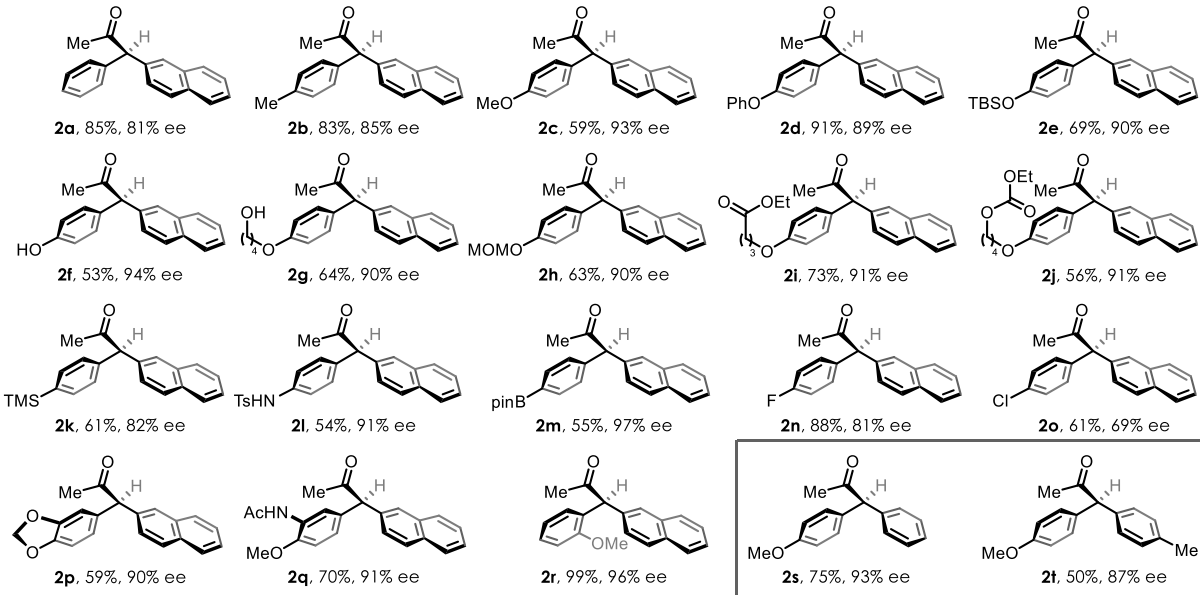

b. *variation of the β-arene group*

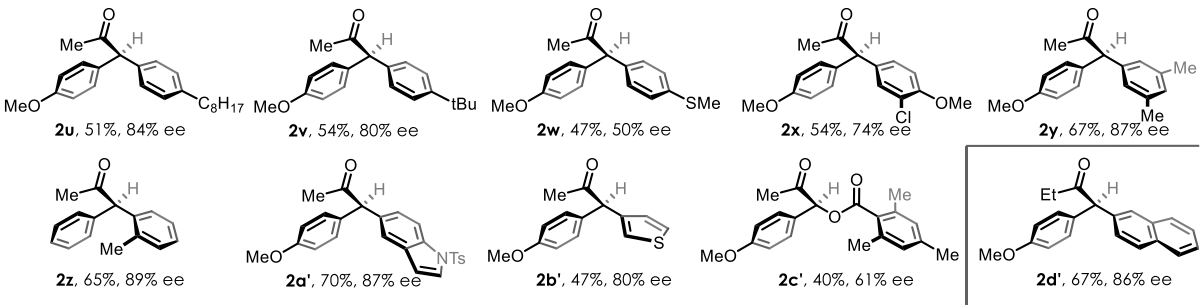

c. *variation of the alkyl group*

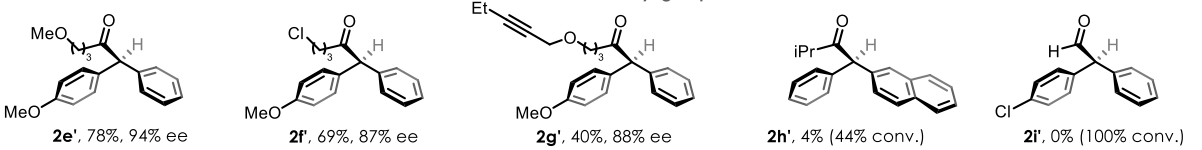

d. *unsuccessful examples*

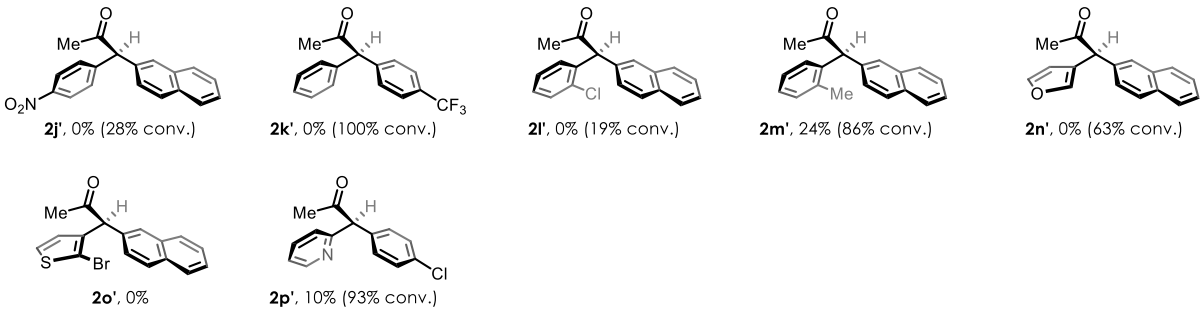

These observations support the notion that a linear α-alkyl substituent acts as a structural anchoring element, enabling the chiral diselane to effectively recognize the migrating unit located at the same carbon atom and thus secure productive transformation of the stilbene; a characteristic that was studied detailly in Chapter 3.1.3.4.

Besides α-alkyl-branched stilbenes, several arene substitution patterns proved unproductive or delivered target material in very low yield, likely due to mismatched electronic properties (Table **4**d). Strongly electron-deficient stilbenes (**1j'** and **1k'**) probably undergo slow seleniranium formation, rendering oxidative cleavage pathways initiated by sensitized oxygen kinetically competitive or even dominant.[185] Similarly, too electron-rich substrates (**1c**, **1f**, **1t**) appear prone to direct and rapid aerobic oxidation under the operative conditions, explaining their comparably modest yield.[186] Control experiments with **1c** (Scheme 18a) and **1k'** (Scheme 18b) performed in absence of the selenium catalyst (i.e., TAPT and stilbene only) produced identical carbonyl fragments and displayed similar conversion rates as was confirmed by their respective crude NMR spectra, supporting the hypothesis that these outcomes arise from direct photocatalyst-mediated side reactions rather than from impediments within the selenium catalytic cycle, a drawback that is more pronounced at higher temperatures (see Table 3, entry 5). Likewise, *ortho*-substitution within the α-arene can alter reactivity by forcing the arene out of conjugation with the central alkene through steric repulsion, thus reducing π-electron density. As indicated above, compound **2c**, derived from a highly electron-rich *para*-substituted stilbene, was obtained in reduced yield relative to its *ortho*-analogue **2r** (59% vs. 99%), which possesses a more balanced electronic profile (see Figure 5), while precursors of **2l'** and **2m'** appear to be too inert and thus susceptible to slow but gradual oxidative fragmentation. Finally, substrates bearing furan (**1n'**, 63% conversion, 0% yield), bromothiophene (**1o'**, 0% yield), or pyridine (**1p'**, 93% conversion, 0% yield) residues all proved incompatible. Remarkably, these heterocycles were fully tolerated in the semipinacol rearrangement step itself, as shown in the preliminary study by PARK et al.[158] Thus, the failure of these substrates does not originate from the rearrangement step but from interference in catalytic selenohydrin formation, most likely at the level of water addition to the seleniranium ion.

Collectively, these findings demonstrate that an efficient transformation requires stilbenes with balanced π-electron density and unhindered conjugation to support rapid electrophilic activation by the selenium-π-acid. Nevertheless, this broad scope illustrates the method's independence of steric and, to some degree, electronic bias between the two arene rings.

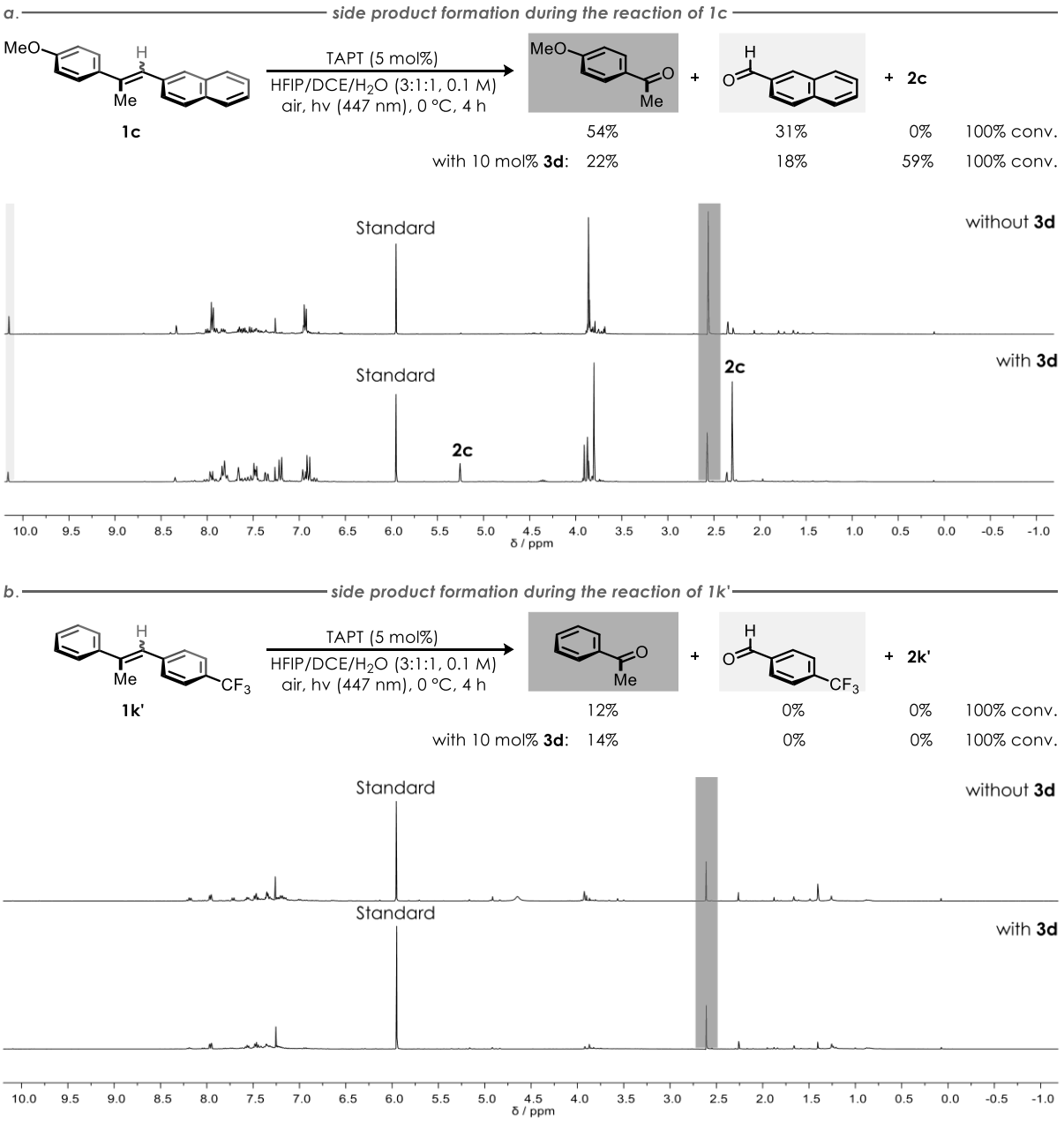

Scheme 18. Control reactions in the absence of chiral selenium catalyst **3d** with (a) low-yielding substrate **1c** and (b) unproductive stilbene **1k'**. In both cases, the same fragmentation products (grey boxes) were obtained with and without the selenium catalyst, respectively. Standard = 1,1,2,2-tetrachloroethane.

3.1.3 Mechanistic Investigations

Our empirical observations during reaction development and scope evaluation already provided several mechanistic insights that can be summarized into four main points:

1) The transformation likely proceeds through a selenohydrin intermediate that undergoes stereoablative C^{β}–Se bond cleavage, erasing the stereochemical information at the β-carbon and thereby enabling the enantioconvergent use of *E*/*Z*-stilbene mixtures.

2) Following this stereodestructive step, the chiral selenium catalyst controls the migratory rearrangement, steering the reaction toward a single absolute configuration, presumably through secondary non-covalent catalyst–substrate interactions.
3) The α-alkyl substituent plays a crucial dual role as it somehow acts as a recognition element for the chiral catalyst, contributing to stereoselectivity and regioselectivity during the nucleophilic opening of the seleniranium ion.
4) Finally, control experiments revealed that the same oxidative fragmentation products arise with or without the selenium catalyst (see Scheme 18), demonstrating that certain side reactions originate from direct photocatalytic oxidation of the stilbene.

These observations lead towards several unresolved mechanistic questions that must be addressed to fully understand the origins of enantioconvergence, stereocontrol, and side reactivity within this dual catalytic platform. In the following sections, we therefore seek to provide extensive mechanistic details by a combination of experimental assessment and computational calculations, with regard to these three queries:

1) Can a rapid pre-equilibrium (e.g., photochemical *E*/*Z*-isomerization) be excluded, ensuring that both stilbene isomers are genuinely accepted as substrates?
2) How does the chiral selenium catalyst differentiate between the two enantiomeric migration pathways once the initial stilbene configuration has been rendered irrelevant?
3) To what extent does the photocatalyst contribute to unproductive oxidative pathways?

3.1.3.1 Photochemical Isomerization and Decomposition

To evaluate whether photochemical *E*/*Z*-isomerization is responsible for regeneration of a single reactive stilbene isomer (e.g., *E*-**1a**) prior to productive conversion, we chromatographically separated the two geometrical isomers of **1a** and subjected them individually to the reaction conditions (Table 5). Diastereomerically enriched *E*-**1a** (*E*:*Z*-ratio = 92:8) delivered **2a** in 82% ee (entry 2), closely matching the enantioselectivity obtained from the standard *E*/*Z*-mixture (58:42, 81% ee, entry 1). In contrast, *Z*-**1a** (*E*:*Z*-ratio = 1:99) performed a lot worse (61% ee, entry 3), also regarding product formation (31% yield from *E*-**1a** vs. 5% yield from *Z*-**1a**, both after 1.5 h). Analysis of the recovered alkene revealed that *Z*-**1a** underwent faster photochemical isomerization than *E*-**1a**, reaching terminal *E*:*Z* ratios of 22:78 and 84:16, respectively. However, neither reached full equilibrium within the reaction timeframe, indicating that *E*/*Z*-isomerization is too slow to generate a single dominant reactive isomer, and thus chiral selenium catalyst **3d** must accept both *E*- and *Z*-stilbenes at the outset of catalysis. Photochemical isomerization was clearly faster in the absence of **3d** (entries 4–5), demonstrating that the selenium catalyst hampers photoinduced

isomerization while simultaneously accelerating productive formation of **2a**. This observation aligns with an on-cycle, selenium-mediated stereoablative process governing enantioconvergence.

Notably, slight product formation was visible even in the absence of the selenium catalyst for both *E*-**1a** (7%) and *Z*-**1a** (6%), consistent with initial control experiments (Table 2, entry 1) and STERN–VOLMER measurements (see Chapter 5.3.1).[187] We reasoned that this must be the consequence of a racemic background reaction, initiated by direct single-electron oxidation of stilbene **1a** by TAPT,[q] followed by nucleophilic addition of water as known from literature reports.[188] The resulting open-shell intermediate (i.e., a β-hydroxy radical) can undergo a semipinacol rearrangement to afford **2a**.[189] Due to the absence of any chiral control element, this nonselective pathway likely contributes to partial erosion of the observed ee.

Table 5. Impact of stilbene's *E*/*Z*-ratio on the product's ee and photochemical isomerization.

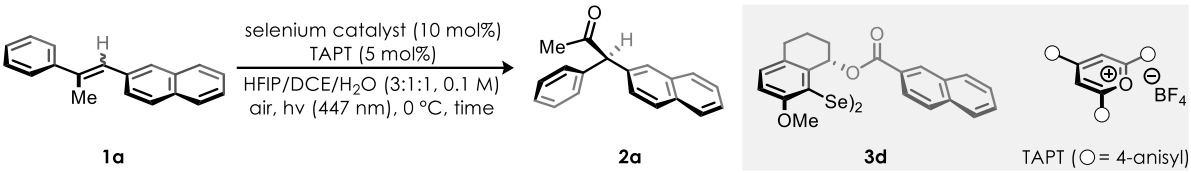

1a 2a 3d TAPT (○ = 4-anisyl)

entry	selenium catalyst	initial *E*:*Z*-ratio of 1a	terminal *E*:*Z*-ratio of 1a[*]	time	yield	ee[•]
1	**3d**	58:42	-	4 h	85%	81%
2	**3d**	92:8	84:16	1.5 h	31%	82%
3	**3d**	1:99	22:78	1.5 h	5%	61%
4	-	92:8	73:27	1.5 h	7%	-
5	-	1:99	34:66	1.5 h	6%	-

[*] determined by ^{1}H NMR analysis; [•] determined by chiral HPLC analysis

These findings raise the important mechanistic question on how the chiral selenium fragment remains sufficiently proximate to the substrate after C–Se bond cleavage to govern the ensuing enantioselective arene migration. In the case of PARK et al., upon generation of an open-shell species through single-electron oxidation, the C–Se$^{\bullet+}$ bond *heterolyzed* and the selenium fragment remained in proximity of the carbocation by a O–H···Se$^{\bullet}$ contact (see Scheme 14), whereas our data suggest the involvement of a carbon-centered radical and thus a C–Se *homolysis* prior to the migration step. To clarify the sequence from seleniranium formation, through stereoablative cleavage, to enantioselective aryl migration, we turned to density function theory (DFT) calculations to obtain a more detailed mechanistic picture.

q This process is also likely responsible for the observed fragmentation to acetophenone and 2-naphthaldehyde, upon reaction with oxygen. However, with less electron-rich systems, the fragmentation is of minor relevance (<5% impact).

3.1.3.2 Nature of Stereoselectivity within the Mechanism

As outlined above, conversion of stilbenes **1** into diarylmethanes **2** requires formation of an electrophilic cationic selenonium species, generated by single-electron oxidation of diselane **3d** by photoexcited TAPT, constituting a dual activation manifold previously characterized in detail for related transformations.[190] Consistent with this, STERN–VOLMER quenching experiments confirmed efficient fluorescence quenching of TAPT by **3d**, likely through a combination of static and dynamic pathways (see Chapter 5.3.1).[187] Exemplified for our model substrate, the resulting selenium-π-acid then undergoes reversible electrophilic addition to the C=C bond of **1a**, forming the corresponding seleniranium ion **5a**.[191,192] Because this step can occur on either π-face of each stilbene isomer, up to four diastereomeric seleniranium ions are possible. These intermediates are expected to interconvert rapidly, either through low-barrier selenenium extrusion from the iranium species[192] or via interolefinic selenenium transfer, processes well-documented in selenium-π-acid chemistry (Scheme 19).[193–196]

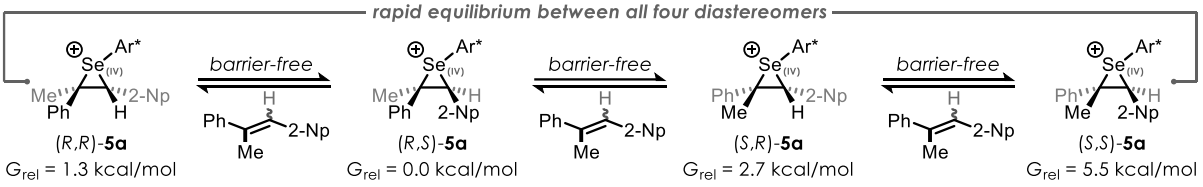

Scheme 19. Barrier-free equilibrium between the four diastereomeric seleniranium ions **5a** with their corresponding relative free GIBBS energies (G_{rel}) normalized to the energetically lowest isomer. These calculations were performed by Elias Harrer and are detailed in his Master Thesis.[197] 2-Np = 2-naphthyl.

Consequently, this initial addition step, which is typically stereodetermining in related asymmetric selenium-π-acid catalyzed alkene functionalizations,[193–196] cannot account for the stereoinduction in our system. None of the elementary processes within this pre-equilibrium alter the relative orientation of the aryl groups, and the chiral selenium catalyst shows no marked preference for either stilbene diastereomer or for a particular olefinic π-face.

Nucleophilic attack of water to iranium ion **5a** and subsequent deprotonation of the hydroxonium group furnishes a mixture of diastereomeric selenohydrins **4a** (see Scheme 22, step I), for which we could not find a kinetic or thermodynamic bias favoring the formation of a specific diastereomer over the others. Importantly, in all four cases the reaction proceeds with consistent regioselectivity, governed by differences in bond length and polarization between the Se–C_q (C_q = quaternary carbon) and Se–C_t (C_t = tertiary carbon) positions during nucleophilic attack of water. This regioselectivity is further rationalized by a stabilizing $\sigma_{CH} \rightarrow \sigma^*_{CO}$ hyperconjugative interaction that becomes available only when water attacks the quaternary carbon, lowering the energy of the protonated intermediate by more than 8 kcal/mol (Scheme 20). No comparable interaction exists when nucleophilic attack occurs at the tertiary carbon center, disfavoring that pathway.

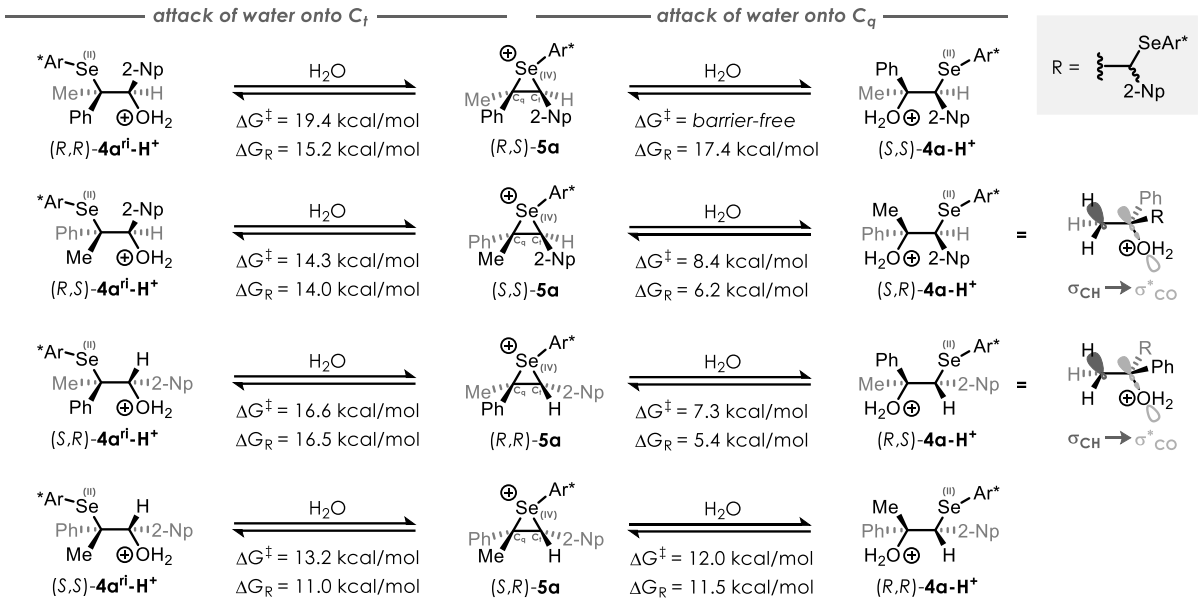

Scheme 20. Activation free energies ($\Delta G^‡$) and reaction free energies (ΔG_R) of both possible nucleophilic water attacks on the four diastereomeric seleniranium ions **5a** with schematic representation of beneficial orbital interactions in (*S*,*R*)-**4a-H$^+$** and (*R*,*S*)-**4a-H$^+$**. The calculations were performed by E. Harrer.[197] ri = regioisomer.

To confirm that the hydroxyl group incorporated into selenohydrins **4a** originates from the water co-solvent, we performed the reaction using ^{18}O-labelled water (i.e., $H_2{}^{18}O$) under otherwise identical conditions and analyzed the product by high-resolution mass spectrometry (HRMS).[165] Indeed, the majority of ketone **2a** (87%) contained the ^{18}O-label within the carbonyl oxygen (Scheme 21). The remaining unlabeled fraction (13%) likely arises from adventitious moisture as well as water generated in situ during photocatalyst turnover, where molecular oxygen participates in re-oxidation of the reduced TAPT catalyst.

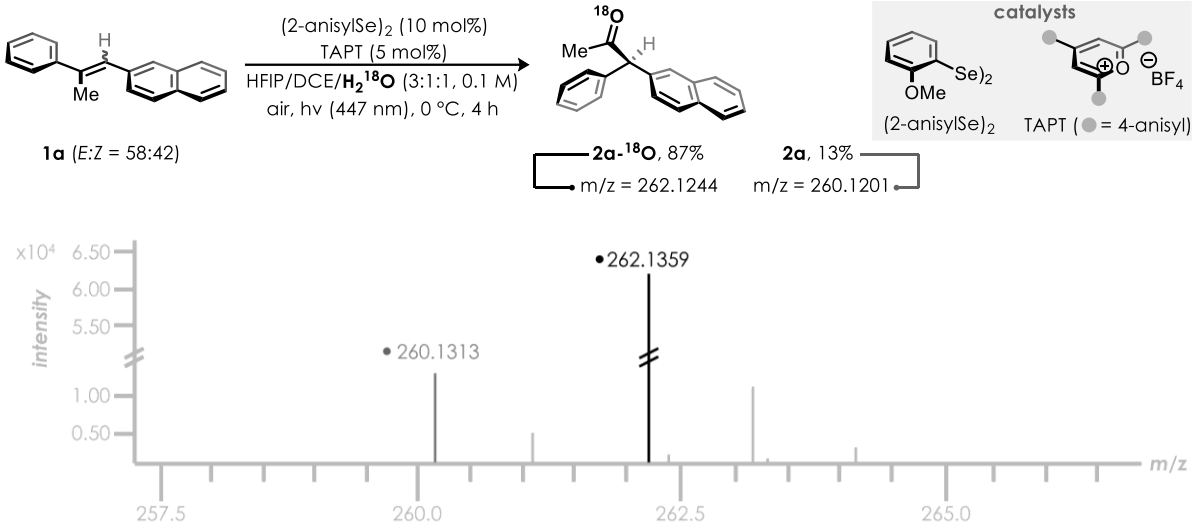

Scheme 21. HRMS (EI+, GC-MS, 70 ev) analysis for the ^{18}O-labelled water incorporation, performed by S. Park.[165]

Following proton-coupled electron transfer (PCET) from selenohydrins **4a**,[198] calculations indicate that the resulting open-shell species **6a** form a Se···O• interchalcogen bond (Scheme 22, step II). This interaction represents a mechanistic departure from the semipinacol rearrangement by PARK et al., which relied on an intramolecular O–H···Se•+ H-bond to maintain proximity between the selenium fragment and the developing cationic center.[158] This difference can be rationalized by the distinct solvent composition, since, in the present system, HFIP/H_2O provides a co-solvent mixture where water acts as a stronger H-bond acceptor (KAMLET–TAFT β-parameter 0.49 (H_2O) vs. 0.0 (HFIP)),[167–169] invoking a preference for the chalcogen bond over the H-bond.

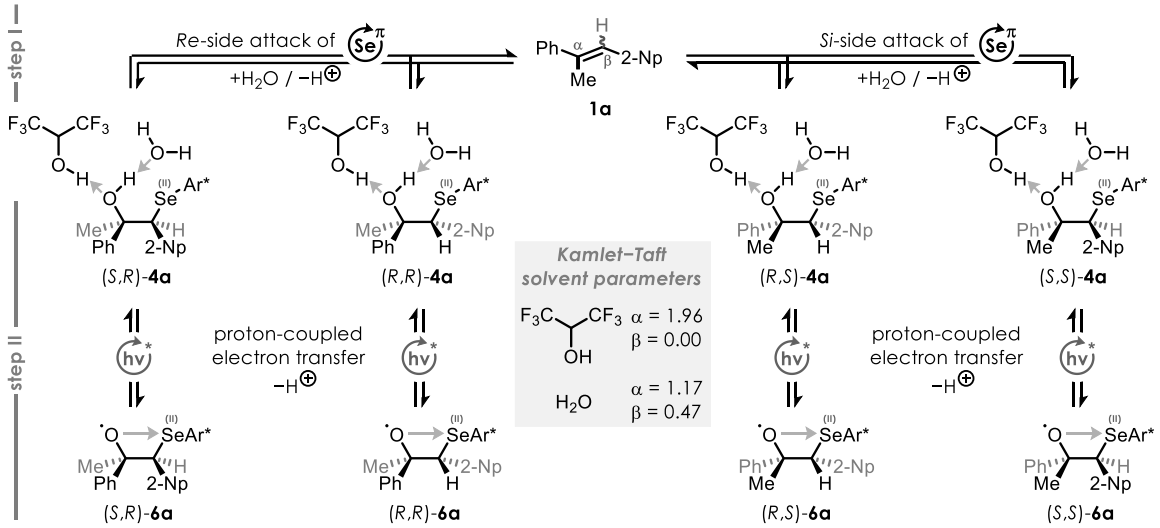

Scheme 22. Generation of reactive species **6a** from selenohydrin diastereomers **4a** by PCET based on the influence of the solvent mixture.

A key mechanistic distinction from the system of PARK et al. arises in the mode of C–Se bond cleavage. As indicated by the racemic background reactivity (Table 5, entries 4–5), σ-bond scission under the present conditions proceeds via homolysis, generating carbon-centered radicals **7a** (Scheme 23 and Scheme 37, step III). These radicals can undergo rotation around the central C–C σ-bond, enabling interconversion between s-*trans*-(1*S*)-**7a** into the more stable s-*cis*-(1*S*)-**7a** conformer due to a low rotational barrier of $\Delta E_{rot}^{\ddagger} < 12.2$ kcal/mol. An analogous relationship holds for the (1*R*)-**7a** manifold, where s-*cis*-(1*R*)-**7a** interconverts into s-*trans*-(1*R*)-**7a** (Scheme 37, step IV). Importantly, the transition state energies for the subsequent irreversible 1,2-aryl migration (Scheme 23, steps V–VI) are all higher than the rotamer interconversion barriers, allowing for a fast equilibrium between rotamers **7a**. Thus, from step IV onward, the system enters a CURTIN–HAMMETT regime,[199] in which the individual transition state energies of the respective **TSII**, rather than the equilibrium population of rotamers **7a**, dictate the observed stereochemical outcome.[r]

[r] If a CURTIN–HAMMETT scenario applies, one must consider both the equilibrium population and the barriers for the subsequent step. Significantly different barrier heights govern the reaction outcome regardless of the equilibrium population,[200] but when almost equal in energy,[201] the equilibrium distribution becomes decisive.

Within our manifold, the more stable s-*cis*-(1*S*)-**7a** also exhibits the lowest relative barrier for the rate-determining migration step ($\Delta G_{rel}^{\ddagger}$ = 16.4 kcal/mol, normalized to the global minimum), making it the dominant contributor to product formation. A two-dimensional relaxed surface scan (steps V−VI) indicates that aryl migration proceeds via a pseudo-concerted addition–elimination mechanism: radical attack on the aryl ring leads to a shallow, high-energy region associated with a transient three-membered ring structure **8a**, followed by rapid Se–O bond cleavage and spin-density relocation from the aryl fragment to the selenium center.

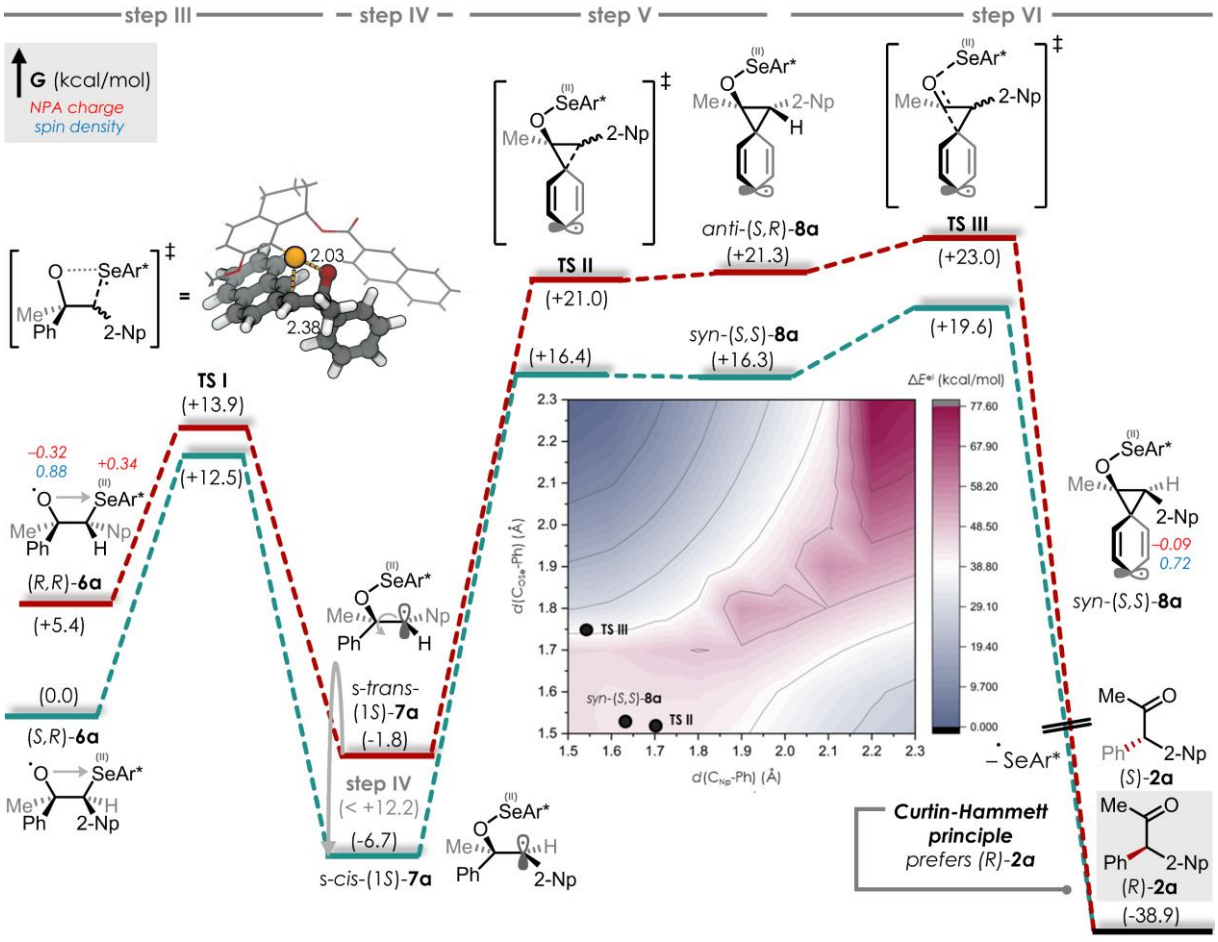

Scheme 23. Thermodynamics of the rate-determining enantioselective aryl migration within a proposed CURTIN–HAMMETT equilibrium shown for (*R*,*R*)-**6a** and (*S*,*R*)-**6a**. The other pair behaves similarly, furnishing (*R*)-**2a** preferentially from the more stable s-*trans*-(1*R*)-**7a** rotamer (see Scheme 37). GIBBS free energies and charge distributions were calculated by E. Harrer.[197] Barriers are normalized to the global minimum. (2-)Np = 2-naphthyl.

Major contributions to these barriers are secondary interactions between the catalyst's 2-naphthyl unit and the α-arene, as well as between the substrate's β-arene and the catalyst (Figure 4). The complementary transition states **TSII** from s-*cis*-(1*S*)-**7a** and s-*trans*-(1*S*)-**7a** both show π-stacking (more significant in the s-*cis*-conformer) and a $\sigma_{Ar-H} \rightarrow \pi^*$ interaction, while s-*cis*-(1*R*)-**7a** shows neither of these interactions. s-*trans*-(1*R*)-**7a** does not show $\sigma_{Ar-H} \rightarrow \pi^*$ interactions but π-stacking between the migrating α-arene and the catalyst's 2-naphthyl group. Overall, these interactions

induce differences in barrier heights, favoring s-*cis*-(1*S*)-**7a** over s-*trans*-(1*S*)-**7a** and s-*trans*-(1*R*)-**7a** over s-*cis*-(1*R*)-**7a**, both resulting in the preferred formation of (*R*)-**2a**.

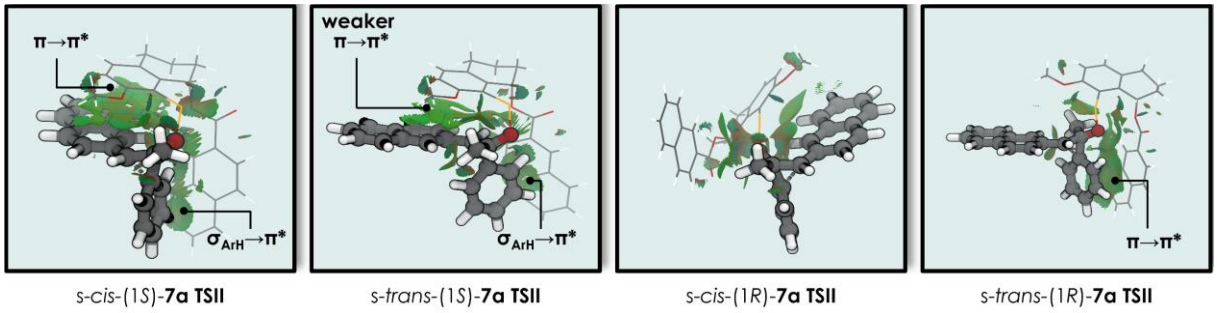

Figure 4. Decisive non-covalent interactions (NCIs) in the four diastereomeric transition states of the rate-determining steps. These NCI plots were calculated by E. Harrer.[197]

To rationalize the experimentally observed sensitivity toward substitution on the migrating arene (see Table 4), we computationally examined representative structures bearing different substituents on the α-arene.[197] Interestingly, the calculated GIBBS free energies (ΔG_{int}) of intermediates **8** increase with the electron-donating strength of *para*- and *meta*-substituents (Figure 5a). This trend stands in contrast to the experimental observation that *p*-chloro substrate **1o** afforded lower yield of **2o** than its *p*-methyl analogue **2b**, underscoring that side reactions (see Scheme 18) must be considered alongside intrinsic migratory aptitude. For *ortho*-substituted α-arenes, experiment and computation align more closely as the latter predicted significantly better reactivity for *o*-methoxy relative to *o*-chloro or *o*-methyl substrates, consistent with the higher yield and ee observed for **2r** compared to **2l'** and **2m'**. We attribute the increased barriers mainly to steric repulsion between the *ortho*-substituent and a) the α-methyl group and b) the hydrogen atom on the developing three-membered ring. In contrast, *o*-methoxy benefits from a stabilizing intramolecular H-bond (Figure **5**b), which lowers the migration barrier and additionally enhances enantioselectivity, since steric congestion disproportionately destabilizes the s-*trans*-(1*S*)-**7** rotamer, thereby amplifying the preference for the s-*cis*-(1*S*)-**7** conformer affording the observed (*R*)-product. Notably, only chloro- and methoxy- substitution induces substantial changes in bond order and π→σ* orbital interactions within the three-membered ring, suggesting a later transition state and thus faster bond cleavage, a feature absent in the methyl-substituted analogue.[197] Since electron-withdrawing groups generally accelerate the rearrangement, a similar rationale may explain the low barrier of s-*trans*-(1*R*)-**7**, which uniquely allows π-stacking between the migrating aryl group and the catalyst's 2-naphthyl moiety in **TSII** (see Figure 4). The π-energy of the catalyst's 2-naphthyl moiety is not influenced by any arene substituents, however, its π*-energy is lowered with the presence of electron-withdrawing groups on the migrating terminus, thus bringing the interacting orbitals closer together in terms of energy. The resulting stronger interaction serves as a through-space electron withdrawal from the aryl radical into the electron-poor naphthyl fragment, stabilizing the transition state.

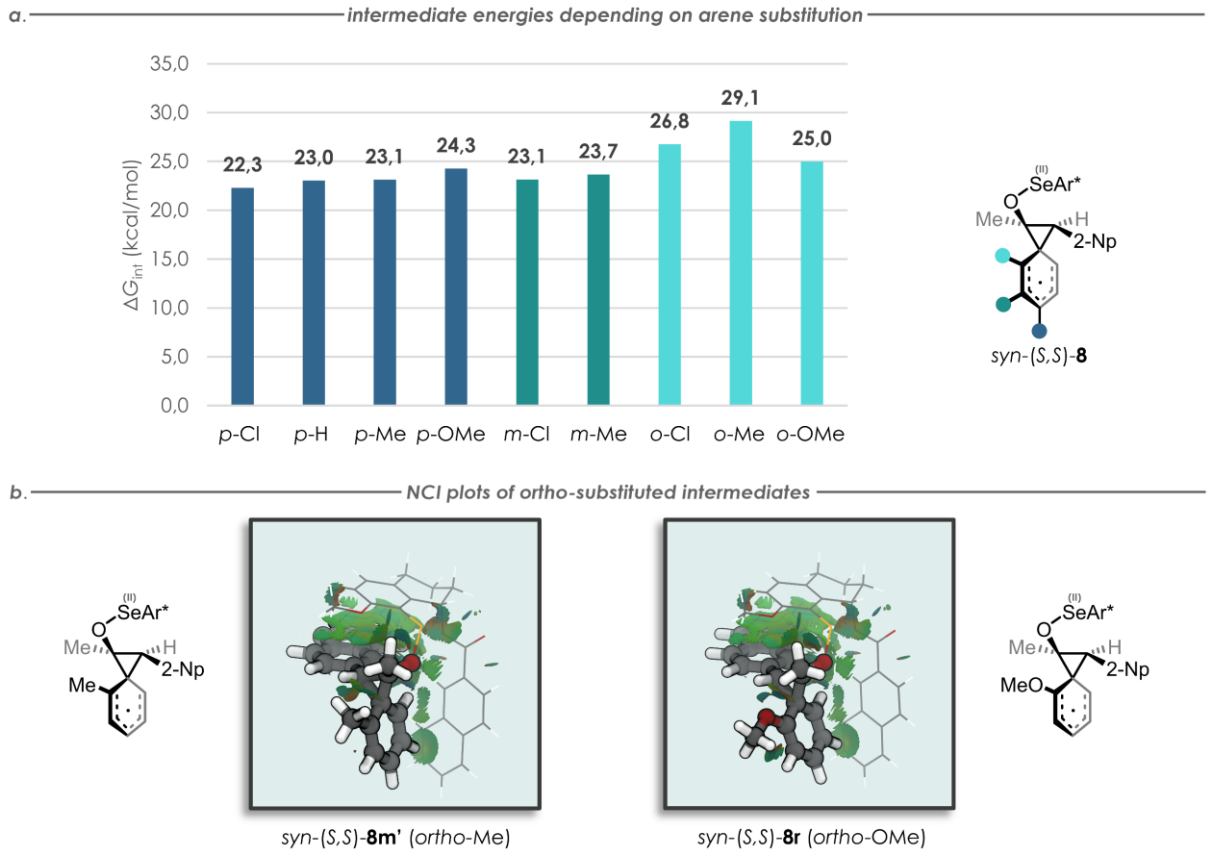

Figure 5. (a) Relative energies (ΔG_{int}) of intermediate **8** regarding different substitution patterns. (b) NCI plots of *ortho*-substituted arene rings showing steric repulsion for methyl substitution and H-bonding for methoxy substituents. These calculations were performed by E. Harrer.[197]

These computational insights enabled an experimentally testable prediction, as, according to STREITWIESER's rehybridization model,[202] the rate-limiting 1,2-arene migration (Scheme 23, steps V–VI) should exhibit an inverse kinetic isotope effect (KIE) due to rehybridization of the β-carbon atom from sp^2 in s-*cis*-(1*S*)-**7a** to sp^3 in (*R*)-**2a**. Thus, deuteration at the vinylic position in **1a** should lead to the observation of a secondary KIE (i.e., the C^{β}–D bond is not broken, but D influences the rehybridization rate in the rate-determining step). To test this prediction, we set out to prepare a deuterated isotopologue of the model substrate. However, direct synthesis of **1a-*d*** proved to be difficult (Scheme 24a), as we found a substantial amount of the deuterium label located at the methyl group after the WITTIG olefination step in the crude ^{1}H NMR spectrum, thus impairing the deuteration content at the critical vinylic position (Scheme 24b). We traced the origin of this deuterium scrambling to base-mediated enolization of acetophenone, followed by abstraction of deuterium from the WITTIG salt. To suppress this process, we replaced acetophenone with acetophenone-d_5, reasoning that additional deuterium labels at the methyl group would not influence the reaction rate due to their remote position. This modification furnished stilbene **1a-*d*$_4$** with full retention of the deuterium label at the vinylic position.

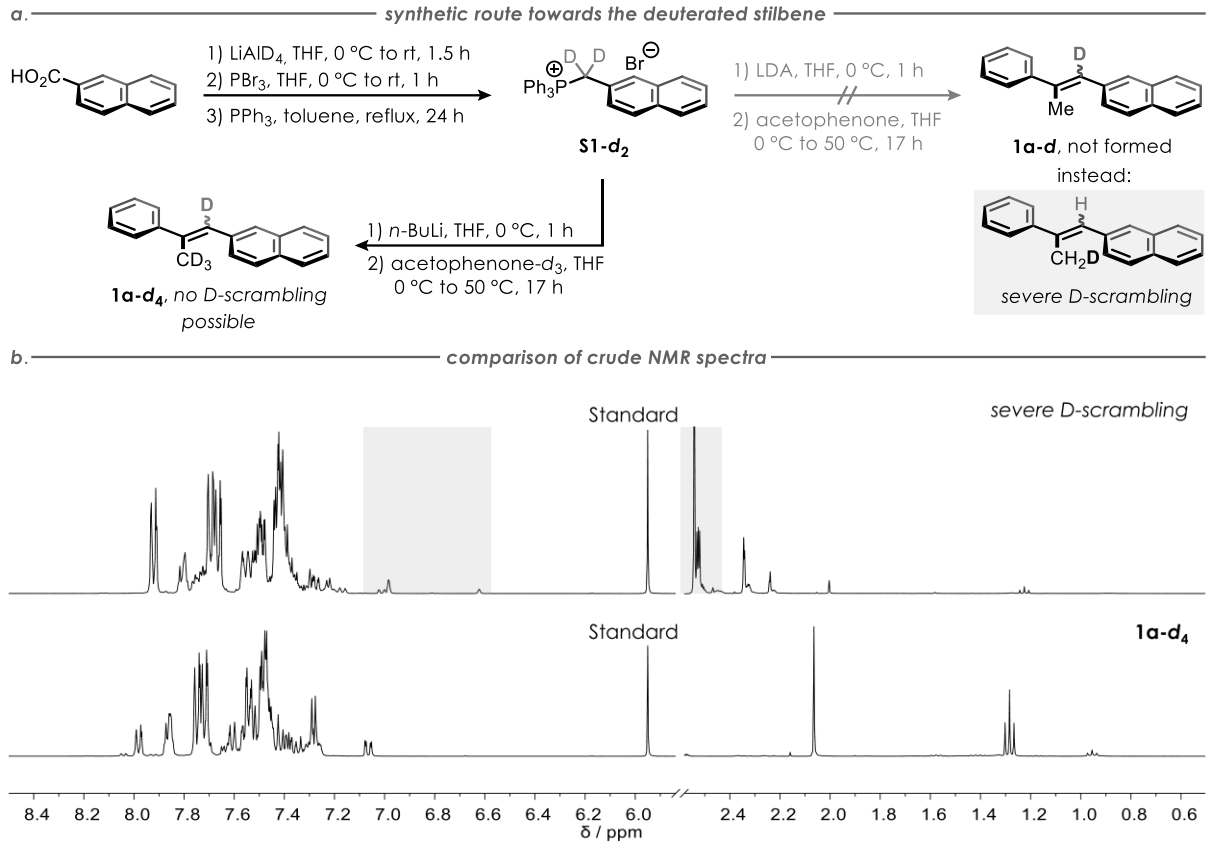

Scheme 24. (a) Synthetic endeavors towards a Cβ-deuterated stilbene based on reports by GUO et al. (reduction),[203] MURAYAMA et al. (bromination),[204] SATYANARAYANAJOIS et al. (WITTIG salt synthesis),[180] and DONG et al. (olefination).[181] (b) Comparison of the crude ^{1}H NMR spectra show proton signals in the double bond region (grey) and a complex pattern for the methyl group, indicating deuterium scrambling. These signals are not present in **1a-*d*$_4$** since the respective positions are fully deuterated.

The KIE experiment itself followed the method of SAUNDERS and SINGLETON,[205,206] which was later refined by LARROSA.[207] A solution of **1a** doped with 10 mol% of isotopologue **1a-*d*$_4$** was subjected to standard reaction conditions until it reached 83% conversion. Analysis of the remaining reactant composition confirmed that **1a-*d*$_4$** was depleted more rapidly than **1a**, corresponding to an inverse KIE of k_H/k_D = 0.89 ± 0.06, in good agreement with the calculated value of k_H/k_D = 0.80 (Scheme 25). This close match between theoretical prediction and experimental measurement strongly supports that 1,2-arene migration is indeed the rate-determining step, proceeding under the exclusive stereocontrol of the chiral selenium catalyst, with secondary noncovalent interactions dictating the formation of (*R*)-**2a**. Overall, the KIE measurement reinforces the mechanistic model derived from computation and corroborates the proposed stereoinduction pathway.

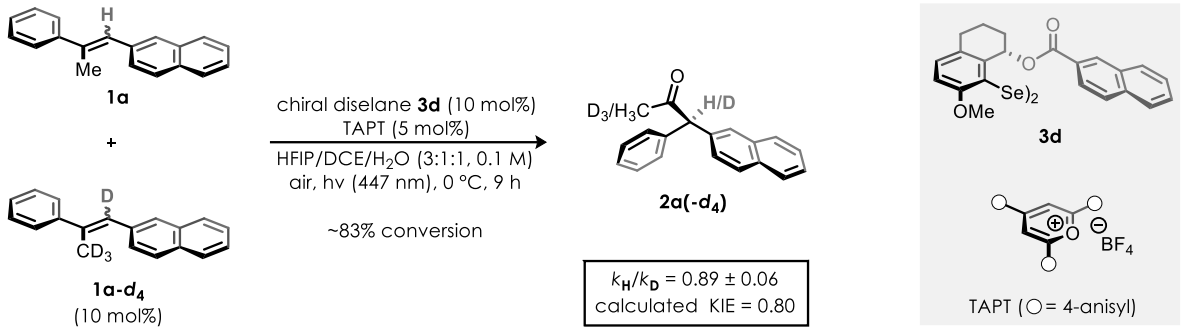

Scheme 25. Experimentally determined and theoretically confirmed KIE by E. Harrer.[197] For details on the exact procedure and calculations see Chapter 5.3.2.

3.1.3.3 Stilbene Connectivity in Constitutional Stereodivergence

The computational analysis provides a detailed picture of the mechanistic sequence, showing that enantioselection arises not from an initial preference of the chiral selenium catalyst for one olefinic π-face, but from an arene migration under CURTIN–HAMMETT control occurring after a stereoablative C–Se bond cleavage. In the rate-determining step, migration occurs from only one accessible hemisphere of the most stable conformers **7**, with the alternate hemisphere sterically shielded by the catalyst's naphthyl backbone (see Figure 4). These insights prompted us to ask whether exchanging the two arene groups in the stilbene substrate, effectively relocating the α-alkyl residue, would result in the *opposite* diarylmethane enantiomer, even when using the *same* catalyst enantiomer. Rooted in our substrate scope studies (see Table 4c), the linear α-alkyl substituent (usually a methyl group) was found to act as a structural anchor that controls regioselectivity during seleniranium opening (see Scheme 20). We believe that the same substituent dictates which of the two arene rings migrates and thus could enforce a constitution-dependent stereochemical outcome.

To experimentally verify this hypothesis, we used our modular stilbene synthesis platform (see Scheme 17) to prepare constitutional isomers of stilbenes **1** previously shown to be competent substrates. Importantly, generating these constitutional variants is far more practical than synthesizing the opposite enantiomer of the chiral selenium catalyst, which requires multi-step preparation.[160,161] When constitutional isomers $\mathbf{1}^{ci}$ were subjected to the standard reaction conditions, catalyst **3d** indeed furnished the inverted diarylmethane enantiomers ***ent*-2** in yields comparable to their mother substrates (26–86%, Table 6). Although the enantioselectivities were somewhat lower (−56 to −84% ee), this outcome is consistent with the computational prediction that less electron-rich or more sterically demanding migrating groups weaken the crucial secondary interactions that govern enantiodiscrimination (see Figure 5).

Table 6. Enantiomer-synthesis by constitutional stereodivergence. Compounds ***ent*-2r**, ***ent*-2s**, and ***ent*-2y** and their precursors were synthesized by S. Park.[165] Se^{π} = chiral diselane **3d**.

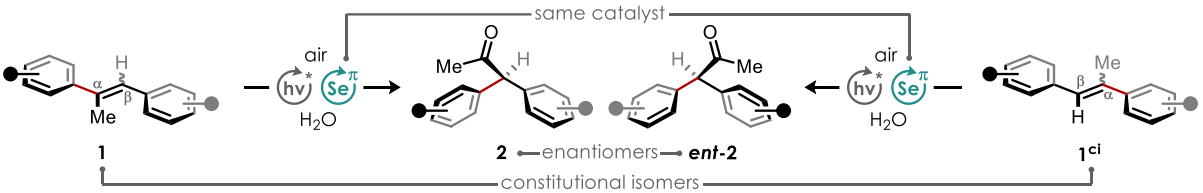

1a (*E*:*Z* = 58:42)	**2a**, 85%, 81% ee	***ent*-2a**, 86%, −82% ee	**1a^{ci}** (*E*:*Z* = 63:37)
1b (*E*:*Z* = 51:49)	**2b**, 83%, 85% ee	***ent*-2b**, 61%, −73% ee	**1b^{ci}** (*E*:*Z* = 65:35)
1c (*E*:*Z* = 49:51)	**2c**, 59%, 93% ee	***ent*-2c**, 79%, −69% ee	**1c^{ci}** (*E*:*Z* = 70:30)
1n (*E*:*Z* = 54:46)	**2n**, 88%, 81% ee	***ent*-2n**, 48%, −81% ee	**1n^{ci}** (*E*:*Z* = 57:43)
1r (*E*:*Z* = 38:62)	**2r**, 99%, 96% ee	***ent*-2r**, 83%, −81% ee	**1r^{ci}** (*E*:*Z* = 73:27)
1s (*E*:*Z* = 60:40)	**2s**, 75%, 93% ee	***ent*-2s**, 73%, −71% ee	**1s^{ci}** (*E*:*Z* = 60:40)
1y (*E*:*Z* = 58:42)	**2y**, 67%, 87% ee	***ent*-2y**, 80%, −56% ee	**1y^{ci}** (*E*:*Z* = 88:12)
1z (*E*:*Z* = 42:58)	**2z**, 65%, 89% ee	***ent*-2z**, 26%, −84% ee	**1z^{ci}** (*E*:*Z* = 40:60)

In summary, these results establish the first example of constitutional enantiodivergence outside the realm of hydrogenation chemistry.[85,91,92] Owing to the high modularity of the stilbene synthesis, this strategy provides a remarkably flexible means of accessing either diarylmethane enantiomer

using a single catalyst enantiomer, significantly expanding the synthetic utility of this enantioconvergent platform.

3.1.3.4 Chiral Discrimination of Isotopomeric Arene Rings

Our method's ability to deliver diarylmethanes bearing isosteric arene residues, such as *p*-substituted or unsubstituted aryl groups, with consistently high enantioselectivity (e.g., **2c**, **2s**, **2t**, **2e'** in Table 4) prompted a deeper examination of potential substitution effects within the aromatic rings. From our mechanistic calculations we had already learned that stereoselectivity does not originate from steric or electronic bias within the substrate but is instead governed by subtle energetic differences between competing transition states, enforced exclusively by the chiral selenium catalyst (see Figure 4). This insight suggested that even substrates lacking any intrinsic differentiation between the two aryl groups should still undergo highly selective asymmetric migration, as long as the catalyst can appropriately engage the alkene framework via the α-alkyl lynchpin.

To probe the directing influence of the α-methyl substituent in isolation, we synthesized pentadeuterated stilbene **1q'-*d*$_5$**,[s] in which the two arene rings (i.e., C_6H_5 and C_6D_6) are practically indistinguishable. Subjecting **1q'-*d*$_5$** to the standard asymmetric MTW oxidation did furnish the corresponding ketone **2q'-*d*$_5$**, however direct ee determination by chiral HPLC was impossible due to its isotopic symmetry. We therefore reduced the carbonyl group under COREY–BAKSHI–SHIBATA (CBS) conditions,[208] generating a diastereomeric mixture of secondary alcohol **5q'-*d*$_5$** in 86% yield (Scheme 26a). In this reduced product, chirality resides at two distinct positions, namely C^{α} (set during CBS reduction) and C^{β} (originating from the MTW step). Because these stereocenters influence different spectroscopic handles, we could deconvolute their contributions. Chiral HPLC resolves the C^{α} diastereomers, providing a ratio of $C^{\alpha,S}$:$C^{\alpha,R}$ = 71:29, consistent with the measured optical rotation (+3.0°) that is in agreement with literature data.[209] In turn, quantitative ^{13}C NMR distinguishes the *ipso*-carbon atoms of the non-deuterated phenyl ring, enabling quantification of the C^{β} configuration as $C^{\beta,S}$:$C^{\beta,R}$ = 68:32 (Scheme 26b). Combining both analyses allowed us to determine that (*S*)-**2q'-*d*$_5$** was formed in 82% ee, a value fully consistent with the enantioselectivities obtained for other isosteric diarylmethanes such as **2b** and **2t** (for details see Chapter 5.2.5).

[s] This stilbene was assembled via our standard protocol (Scheme 17, route I) from yet another deuterated acetophenone (this time with a pentadeuterated arene ring) and benzyltriphenylphosphonium bromide.

Taken together these results experimentally confirm that enantioselectivity in the MTW oxidation is dictated not by arene differentiation, but by catalyst-controlled transition-state organization, with the α-methyl substituent serving as the decisive structural anchor for both regio- and stereocontrol. Unlike prior enantioselective diarylmethane syntheses that rely on substrate-encoded differentiation (steric, electronic, or pre-functionalization cues), the present dual photoredox selenium-π-acid manifold provides a fundamentally new blueprint for enantioconvergent diarylmethane construction via remarkable catalyst-governed, post-stereoablative interactions.

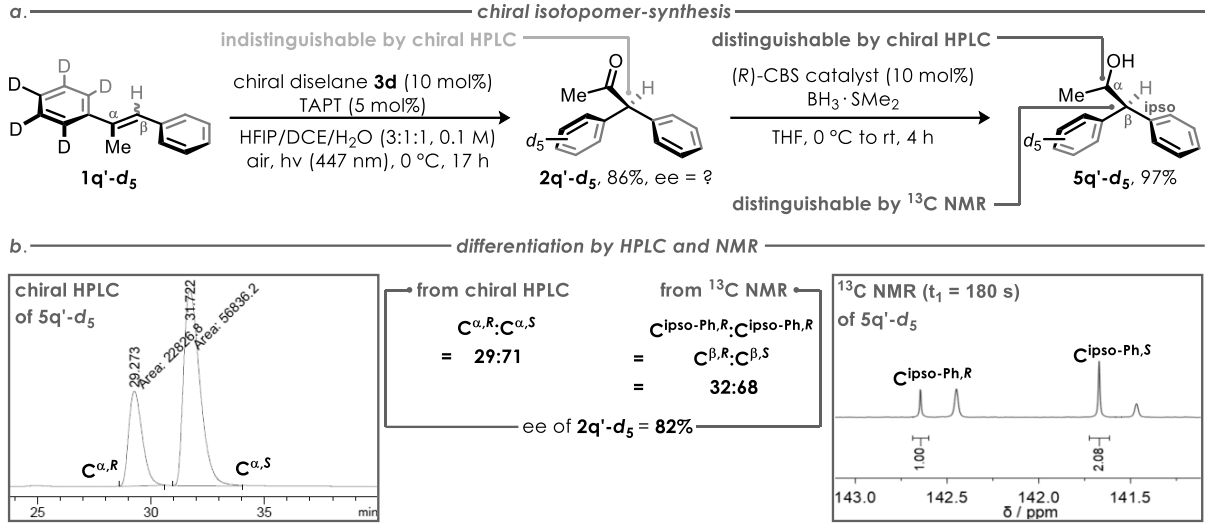

Scheme 26. (a) Synthesis of chiral isotopomer **2q'-*d*$_5$** and its derivatization to **5q'-*d*$_5$**. (b) Determination of the ee value by comparison of the complementary chiral HPLC and quantitative ^{13}C NMR measurements.

3.1.4 Diarylmethane Derivatization

With a general and enantioconvergent protocol for converting stilbenes into diarylmethanes established and its mechanistic foundations fully clarified, we next sought to demonstrate its synthetic utility through the expedient assembly of enantioenriched diarylmethane building blocks. Since the asymmetric MTW oxidation furnishes a versatile ketone handle at the benzylic stereocenter, numerous downstream derivatizations become accessible. Crucially, any follow-up transformations must preserve the high enantiopurity delivered in the oxidation step to ensure relevance for potential pharmacological applications. Given that the stereocenter resides α to a carbonyl group ($pK_a \approx 15.8$),[210] we avoided strongly acidic or basic conditions that might promote enolization and consequent erosion of enantiomeric excess. Being formed in 96% ee, we selected ketone **2r** (see Table 4) as the model substrate for these derivatization studies (Scheme 27). Guided by insights from our earlier CBS-based ketone reduction (see Scheme 26), simple hydride reduction with $LiAlH_4$ cleanly produced the corresponding secondary alcohol **9r** with excellent yield (99%) and stereochemical fidelity (96% ee).[211] Likewise, exposure of **2r** to TEBBE's olefination conditions

delivered 3,3-diarylpropene **10r** in 64% yield and 95% ee,[212] providing a concise entry to terpene-like building blocks.[213] A similarly high level of stereochemical preservation was obtained in the BAEYER–VILLIGER oxidation of **2r**, affording acetate **11r** in 52% yield and 93% ee,[214] while subsequent $LiAlH_4$ reduction provided diarylmethanol **12r** in 99% yield and 92% ee. This final sequence is particularly noteworthy, as it enables access to chiral benzhydrols, constituting key precursors in numerous diarylmethane-based pharmaceuticals,[94,106,107] in high overall enantiopurity, a feature that marks a longstanding challenge in the field (see Chapter 1.2.3).

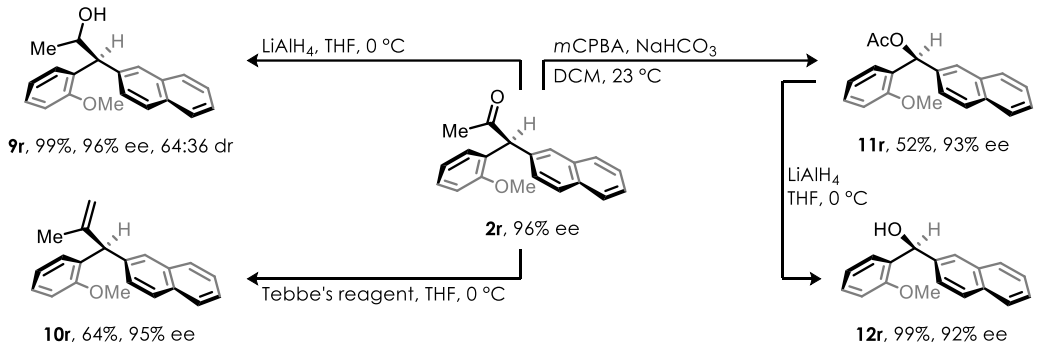

Scheme 27. Various derivatizations of ketone **2r**. Compounds **9r**, **11r**, and **12r** were synthesized by S. Park.[165]

These initial demonstrations highlight that the combination of our MTW protocol, BAEYER–VILLIGER oxidation, and mild reduction or hydrolysis constitutes a modular and stereochemically reliable blueprint for assembling privileged benzhydrol motifs *without* reliance on steric bias, electronic differentiation, or directing groups. This orthogonal synthetic platform lays the foundation for the next chapter, in which we apply this strategy to the streamlined preparation of diarylmethane-based drug scaffolds.

3.2 Diarylmethane Drug Eutomer Assembly

As discussed in Chapter 1.2.1, many antihistaminic and neuroactive agents can be accessed via a benzhydrol intermediate, requiring only one more *O*-alkylation step to unfold their bioactive potential. Conventional synthetic routes typically introduce the arene moiety early and implement critical arene decoration (i.e., methylation or dehalogenation) afterwards, often at the expense of step- and redox-economy.[133,140,141,146] In contrast, our asymmetric MTW platform offers a decisive strategic advantage as the arene unit *as a whole* can be selected and installed *a priori* within the stilbene precursor, enabling complete control over substitution patterns before rearrangement, an approach that becomes particularly powerful for the access of structures such as orphenadrine and

neobenodine.[95,96,103] To showcase this flexibility, we used our insights from the synthesis of enantioenriched benzhydrol intermediate **12r** (see Scheme 27) obtained in Chapter 3.1.4 to access two major classes of diphenhydramine-based targets: benzhydrol-based *O*-alkylated derivatives and benzhydrylamines from *O*-substitution (Scheme 28).

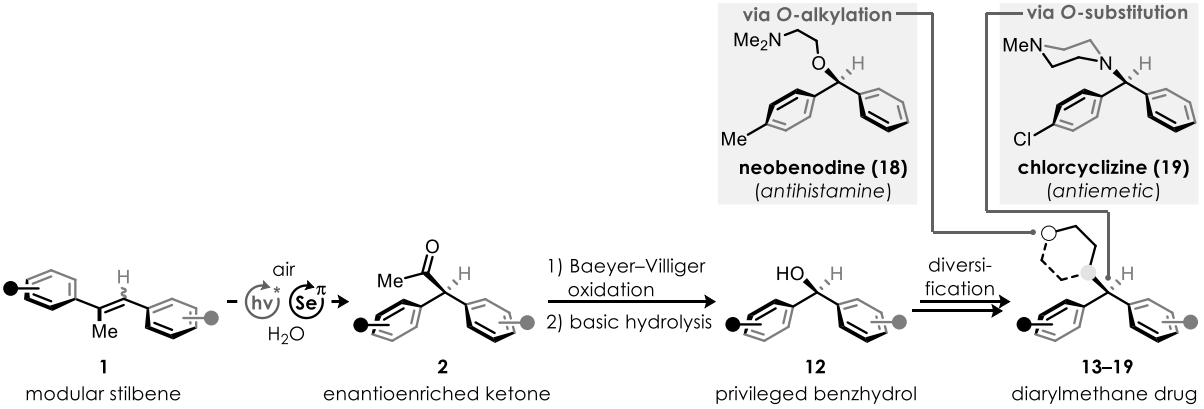

Scheme 28. Concept for the strategic assembly of benzhydrol- and benhydrylamine-based drugs.

3.2.1 Benzhydrol-based Targets

(*R*)-Orphenadrine (**13**) and its piperidine analogue **14** were chosen as our first target structures in the *O*-alkylation series (Scheme 29a). Application of the asymmetric MTW protocol to the common stilbene precursor **1z** delivered ketone **2z** in very high 89% ee (see also Table 4). BAEYER–VILLIGER oxidation followed by basic hydrolysis in methanolic K_2CO_3 afforded key benzhydrol **12z** with only minor erosion of stereoinformation (87% ee), which could be greatly enhanced to 98% ee by a single recrystallization step.[215] Subsequent WILLIAMSON etherification furnished (*R*)-orphenadrine (**13**) and its analogue **14** in overall yields of 24% and 18% over six steps,[216] both maintaining excellent 98% ee. Compared to our approach, which uniquely makes use of the stilbene's *alpha*-methyl group as a previously undecked stereochemical lynchpin (see Chapter 3.1.3.4), existing strategies toward (*R*)-orphenadrine rely heavily on the *ortho*-methyl substituent to induce stereocontrol. For instance, both CHAUMONT-OLIVE et al.[133] and SUI et al.[146] capitalized on a 1,2-addition strategy (Figure 3, strategy III) to acquire the benzhydrol intermediate, which was then transformed to the target compound in 54% total yield and 95% ee, as well as 83% total yield and 81% ee, respectively (Scheme 29b). The silylation strategy of KUMAR et al. reached outstanding 98% ee but, as indicated above, necessitated extra arene editing.[132] These comparisons underscore the distinct advantage and design flexibility of our MTW-based approach, particularly placed in a medicinal chemistry context where systematic arene variation is essential for the design of drug candidate libraries.

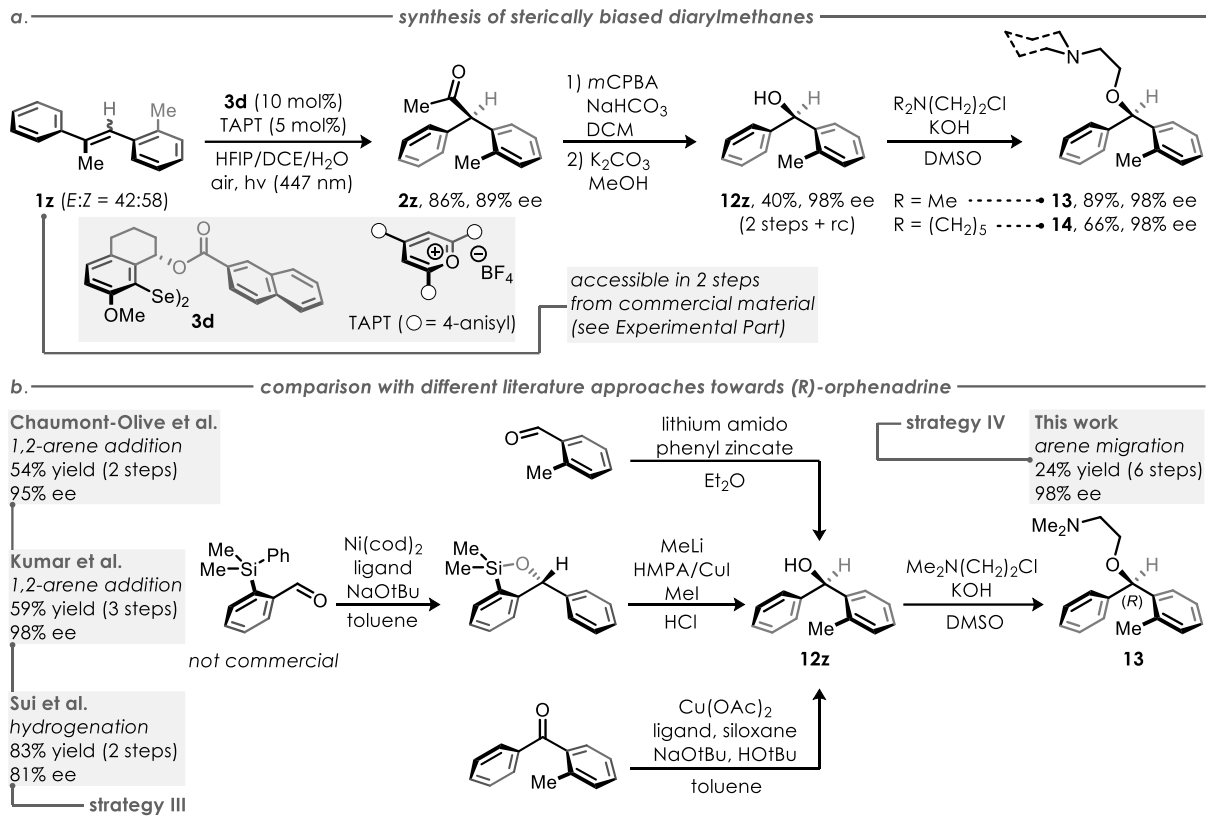

Scheme 29. (a) Total synthesis of (*R*)-orphenadrine (**13**) and its piperidine derivative **14** from stilbene **1z**. All synthetic efforts were carried out together with Jana Flügel, who provided excellent detailed descriptions in her Master Thesis.[217] rc = recrystalliazation. (b) Comparison with different approaches available in literature.

We next extended our synthetic efforts towards sterically unbiased *m*- and *p*-substituted diarylmethanes, a class traditionally difficult to convert into high-ee drug intermediates (Scheme **30**).[145,146] Electron-rich benzhydrol **12r'** was synthesized from ketone **2r'** in 25% overall yield (five steps) and 68% ee. Although attempts to transform **2r'** into N1L protein antagonist **15** via various methylation strategies were unsuccessful,[217] the benzhydrol itself retains cytotoxic activity as an inhibitor of tubulin polymerization, preserving its intrinsic value.[218]

Isosteric benzhydrol **12s'** was similarly converted into the eutomer (*S*)-cloperastine (**16**) in 15% overall yield and 81% ee, which possesses the superior antitussive activity and central nervous system profile relative to its (*R*)-distomer.[219] Likewise, our pentadeuterated 1,1-diphenylacetone **2q'-*d*$_5$**, whose ee was determined to be 82% (see Scheme 26), was successfully transformed into diphenhydramine-*d*$_5$ (**17**). Its optical rotation of −9.5° left us with the assumption that the enantiomeric excess was maintained during the reaction sequence as was the case for all previously discussed targets, with a total yield of 47% over five steps. Such isotopomers receive increasing attention in the context of pharmacokinetics,[220] and, if employed as the equivalent tritium-labelled compounds, might have potential in medicinal imaging applications.[220]

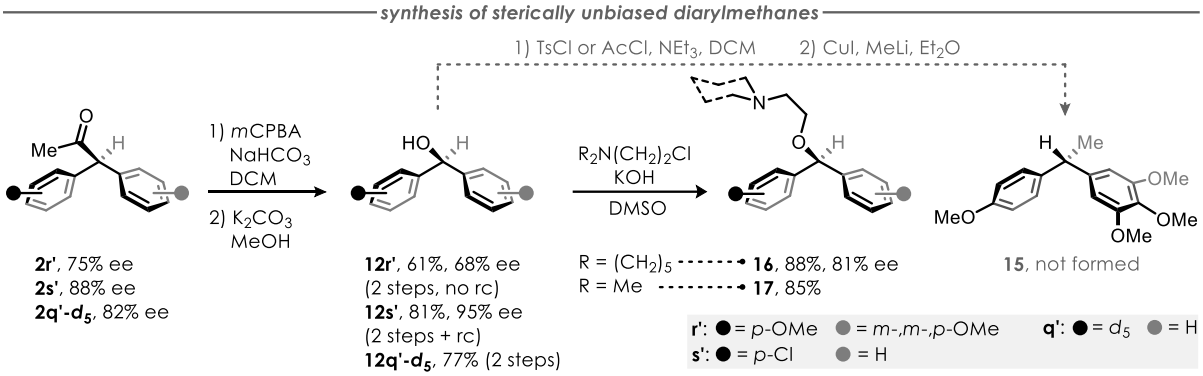

Scheme 30. Challenging total syntheses of sterically unbiased diarylmethanes (i.e., arene groups bearing *m*- and *p*-substituents). Targets **12r'**, **16** and their precursors were synthesized by J. Flügel.[217] rc = recrystallization.

As elaborated previously, a distinctive conceptual feature of our method is its ability to furnish *either* enantiomer of a diarylmethane by a simple constitutional change in the stilbene precursor, without the need to alter the catalyst *enantiomer*. By relocating the α-methyl group to the opposite alkene carbon (i.e., from C^{α} to C^{β}), we effectively redefine the migrating arene terminus,[t] which, according to our mechanistic studies, governs the stereochemical course of the rearrangement (see Table 6). This subtle change allows us to ensure the selective assembly of the actual pharmacologically active diarylmethane, effectively overcoming the stereochemical paradigm that bijectively connects *each* eutomer and distomer to *one* absolute catalyst configuration. To validate this principle, constitutional isomers **1t'** and **1t'**^{ci} were individually subjected to our asymmetric MTW conditions with the *same* chiral selenium catalyst **3d**, delivering the respective ketone enantiomers **2t'** and ***ent*-2t'** in good yields (76% and 85%, respectively) and high ee (85% and −91%, respectively). Both compounds could be further transformed to ultimately afford isosteric (*S*)- and (*R*)-neobenodine (**18**) in total yields of 28% and 36% and with ee values of 92% and −93% (Scheme **31**a), respectively, greatly showcasing that the above-mentioned bijectivity no longer holds true, at least for the diarylmethane examples provided here. Notably, our route towards neobenodine offers a uniquely modular and catalyst-economical pathway as it is independent of strategically placed substituents (e.g., *p*-Cl or *o*-Br) to enforce stereocontrol, unlike pathways from CHAUMONT-OLIVE et al.[133] or ZHOU et al.,[141] who capitalize on these biases (Scheme 31b). SUI et al. explicitly report a significant increase in ee with an additional *ortho*-substituent (25% vs. 92%), albeit with the cost of an additional redox-modifying step needed to remove this stereochemical handle (Scheme 31c).[146]

[t] In all cases examined, the migrating arene was always attached to the same carbon that bore the alkyl substituent.

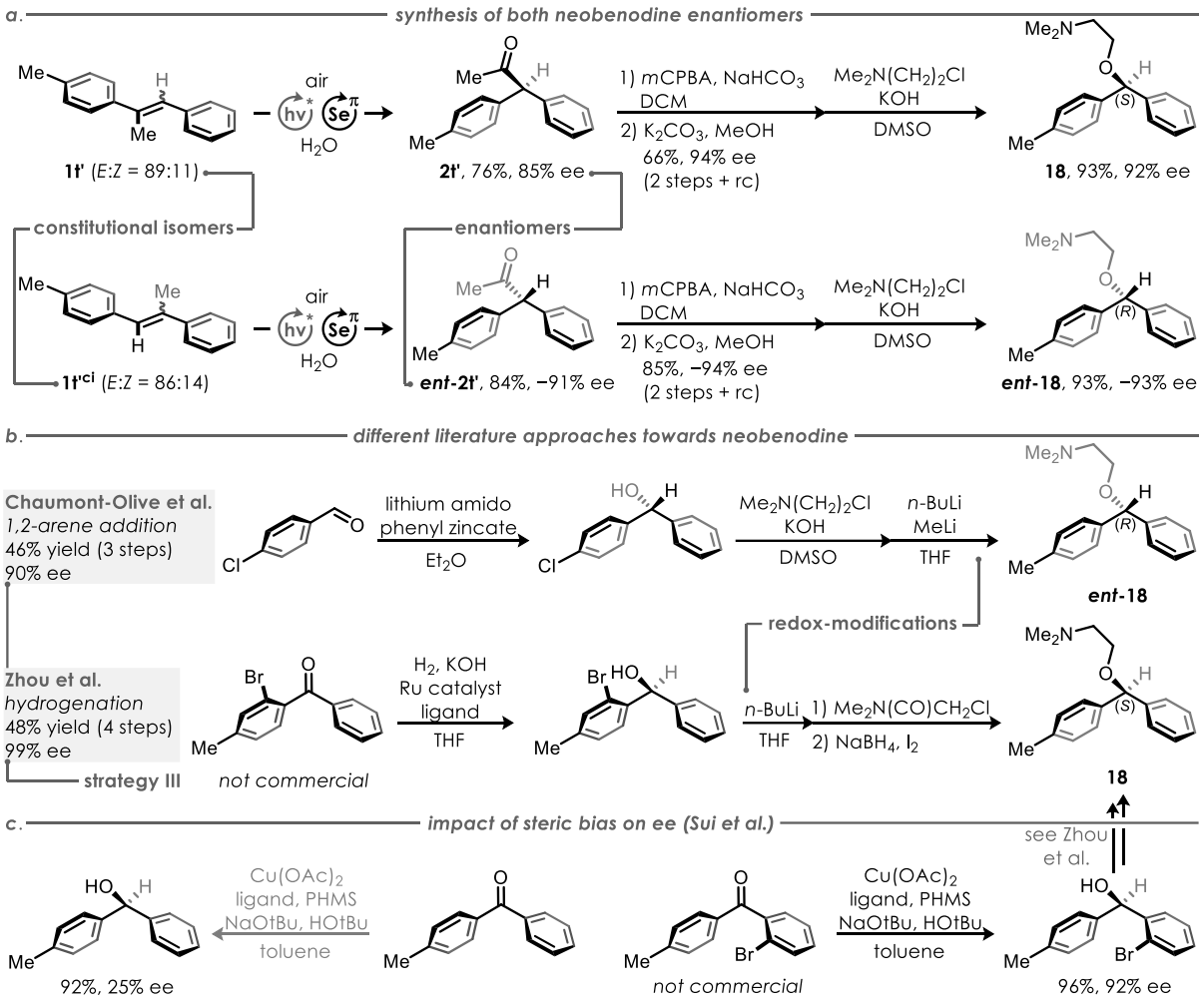

Scheme 31. (a) Total synthesis of both neobenodine enantiomers, performed by J. Flügel.[217] Se$^{\pi}$ = chiral diselane **3d**. (b) Various literature approaches towards neobenodine. (c) Impact of steric bias on the ee of the enantiodetermining step. PHMS = polymethylhydrosiloxane.

3.2.2 Benzhydrylamine-based Target

Building on the *O*-alkylation strategy described above, we next turned to the complementary class of *O*-substituted diarylmethanes, where the benzhydrol oxygen is replaced rather than functionalized (see Scheme 28). As a representative target, we selected chlorcyclizine (**19**), a first-generation antihistamine and antiemetic typically prepared by racemic reduction of 4-chlorobenzophenone (Figure 3, strategy III) followed by S_N1-type piperazine substitution.[221] In contrast, our approach aimed to exploit enantioenriched benzhydrol **12s'**, obtained in high ee of 95% from the asymmetric MTW oxidation and subsequent transformations, and to convert it into the target through a stereospecific substitution that would ideally preserve the stereochemical information. Our initial strategy relied on a MITSUNOBU reaction, which would couple **12s'** with piperazine under complete inversion of the benzylic stereocenter. However, the method usually requires nucleophiles with $pK_a \leq 11$,[222] rendering free piperazine ($pK_a \approx 37$)[210] unsuitable, while

its protonated form remained unreactive. We therefore evaluated the milder coupling protocol of HUANG and KANG,[223] which enables direct alcohol–amine substitution with (mono-)benzylic substrates, but steric congestion due to the second arene ring likely prevented product formation (Scheme 32a). We then turned to an S_N2-based approach, reasoning that conversion of the hydroxy group into a better nucleofuge might allow direct piperazine displacement. A one-pot mesylation–amination sequence indeed afforded chlorcyclizine, but only as a racemate (Scheme 32b).[224] To deduce the origin of this drastic erosion of stereoinformation, we opted to separate the two individual steps. Surprisingly, our reaction conditions, involving mesyl choride (MsCl) as reagent, did not produce the corresponding mesylate but the fully racemized benzylic chloride **20s'**, indicating fast in situ substitution at the strongly activated benzylic position. Despite this setback, we gained two important insights:

1) Erosion of stereoinformation likely originates in the first step of the sequence.
2) Chloride **20s'** is sufficiently stable to be chromatographically isolated and analyzed compared to the mesylate, which is in accordance with the nucleofugality scale proposed by MAYR and co-workers.[225]

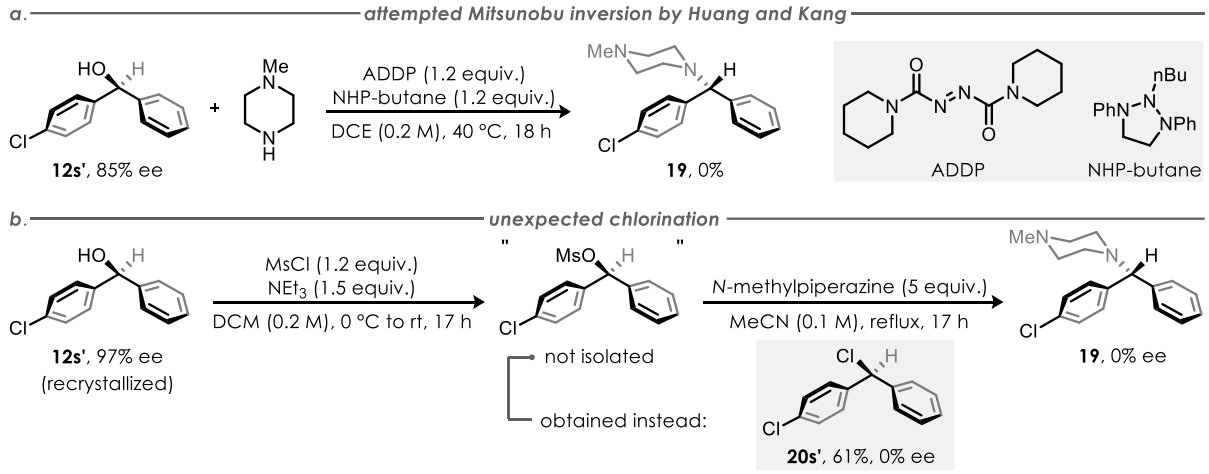

Scheme 32. (a) Initial attempt for the asymmetric assembly of chlorcyclizine (**19**) via a MITSUNOBU inversion, performed by Ludwig d'Heureuse.[223] (b) Mesylation strategy that unexpectedly yielded chloride **20s'**.[224]

To test whether chloride formation could proceed with at least partial conservation of stereoinformation, we turned to alcohol activation with thionyl chloride ($SOCl_2$). This approach afforded chloride **20s'** with significantly eroded ee (from 95% to 16%), but importantly, subsequent amination proceeded without any further loss of stereochemical integrity, confirming that the S_N2 step itself is stereospecific (Scheme 33a).[226] An APPEL reaction led to similar outcomes, leaving us with 12% ee (Scheme 33b).[227]

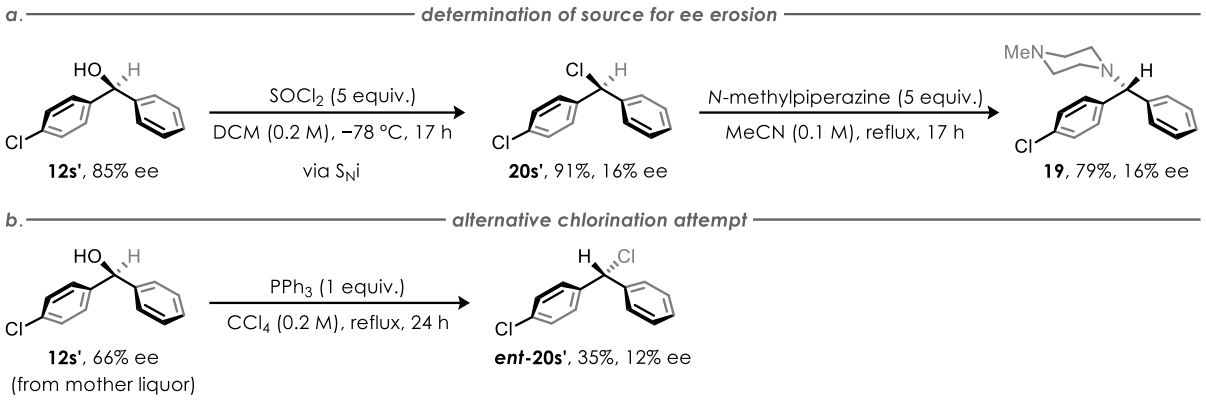

Scheme 33. (a) Chlorination of benzhydrol **12s'** with $SOCl_2$ and subsequent amination under retention of ee. (b) Chlorination via an APPEL reaction led to slightly worse ee with significantly lower yield.

Consequently, we broadened the search of suitable reaction conditions by screening a variety of alternative oxygen-based leaving groups at the benzylic center (Table 7).[228] While several acetates proved either too inert or led to ammonolysis (entries 2–6),[u] a carbonate led to complete decomposition upon activation with etherial boron trifluoride as LEWIS-acid (entries 7–8). Similarly, both a trichloroimidate and a diphenylphosphate did not furnish the product, respectively (entries 9–10), nor did any of these approaches improve the initial ee of 16% (entry 1).

Table 7. Screening of various leaving groups **X** at the benzhydryl carbon.

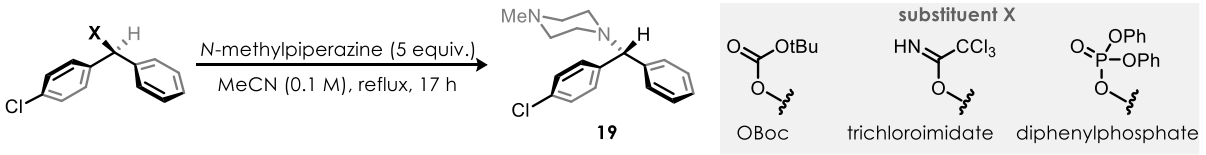

entry	substituent X	deviation from conditions above	conversion	NMR-yield	ee	comment
1	Cl	none	100%	79%[*]	**16%**	-
2	acetate	none	0%	0%	-	-
3	acetate	rt, $BF_3 \cdot OEt_2$ (1 equiv.) added	43%	0%	-	decomposition
4	trifluoroacetate	rt	100%	0%	-	aminolysis (96%)
5	monochloroacetate	rt	100%	0%	-	Cl-substitution (93%)
6	trichloroacetate	rt	75%	0%	-	hydrolysis (60%)
7	OBoc	none	0%	0%	-	-
8	OBoc	rt, $BF_3 \cdot OEt_2$ (1 equiv.) added	100%	0%	-	decomposition
9	trichloroimidate	none	~80%	0%	-	decomposition
10	diphenylphosphate	none	~80%	0%	-	decomposition

[*] isolated yield

Although the overall outcome remains modest, the sequence demonstrates a proof of principle for accessing enantioenriched benzhydrylamines such as chlorcyclizine (**19**) via our asymmetric MTW oxidation platform. The six-step route furnished eutomer (*R*)-**19** in 12% overall yield and 16% ee (see Scheme 33a), with clear identification of the step responsible for stereochemical erosion and confirmation of the stereospecificity of the C–N bond-forming substitution. These insights suggest

[u] Ammonolysis of esters results in the liberated alcohol (here the benzhydrol) and the corresponding amide.

that analogs of chlorcyclizine, including structurally related antihistamines such as (*R*)-cetirizine (see Figure 2a), should in principle be accessible through analogous sequences once a suitably mild and stereoretentive activation method for the benzylic alcohol is identified.

4 Conclusion

The investigations presented in this thesis set out to expand asymmetric diarylmethane synthesis beyond the constraints of redox pre-activated substrates, steric bias, and electronic differentiation. Guided by the mechanistic blueprint proposed by PARK et al. and inspired by constitutional stereodivergence concepts developed by CHIRIK and co-workers, we aimed to establish an enantioconvergent platform that strategically exploits stereoablation as key step to generate chiral diarylmethanes from readily accessible stilbenes. By addressing each of the critical questions formulated in the Objectives (see Chapter 2), this work provides a comprehensive conceptual and experimental foundation for a new class of stereocontrolled reconstitutive oxygenation reactions enabled by photoredox selenium-π-acid dual catalysis.

A central mechanistic insight of this thesis is the demonstration that unbiased stilbenes, irrespective of their initial *E*/*Z*-configuration, can be funneled into a single enantiomeric product through a deliberate stereoablative step (Scheme 34). Detailed experimental analysis and accompanying DFT studies established that the reaction proceeds through unselective π-facial attack by the selenium catalyst, reversible selenohydrin formation, and subsequent homolytic C–Se bond fragmentation. This radical-generating event erases the stereochemical information initially encoded in the alkene's configuration, enabling a true enantioconvergent process. The enantiodetermining migratory step is then governed by a CURTIN–HAMMETT scenario operating on rapidly equilibrating rotamers of a carbon-centered radical, where distinct secondary interactions with the chiral selenium catalyst guide selective aryl transposition. This mechanistic architecture constitutes a fundamentally new mode of asymmetric induction in diarylmethane synthesis.

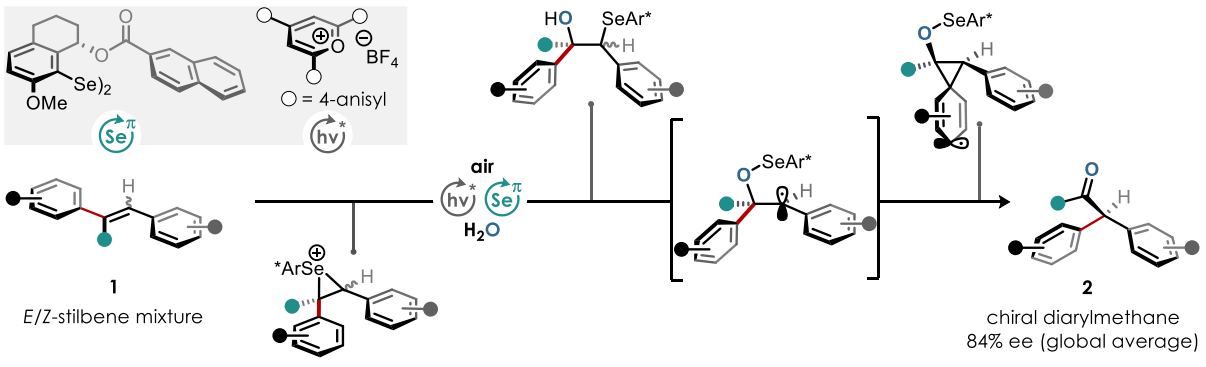

Scheme 34. The asymmetric migratory TSUJI–WACKER oxidation of stilbene diastereomers developed in this thesis.

Beyond this convergence principle, the thesis also confirms that stilbene *connectivity* can be leveraged as a powerful stereochemical control element. By relocating the alkyl substituent within the stilbene framework, constitutional isomers undergo the same catalytic sequence yet deliver opposite diarylmethane enantiomers from the *same* catalyst enantiomer (Scheme 35). This constitutional

stereodivergence obviates the need for catalyst antipodes and represents a conceptual inversion of traditional catalyst–enantioselectivity relationships. The successful realization of this strategy not only validates the initial hypothesis but also establishes stilbene design as a modular handle for programmable enantioinduction.

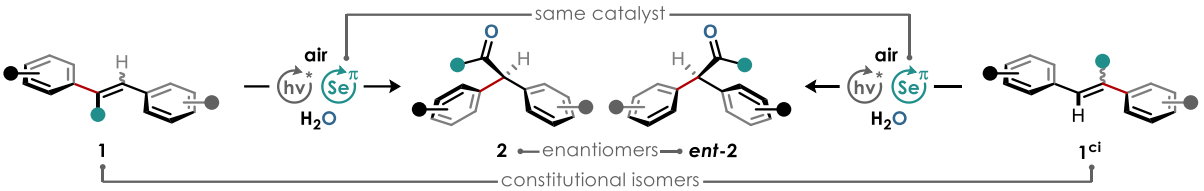

Scheme 35. Enantiomer-synthesis from constitutionally isomeric stilbenes by leveraging the *same* chiral catalyst.

With a robust mechanistic understanding in hand, the second major objective, applying this methodology to the synthesis of eutomeric diarylmethane pharmaceuticals, was pursued. The work presented demonstrates that the chiral α,α-diaryl ketones obtained through migratory TSUJI–WACKER oxidation serve as precursors for versatile benzhydryl intermediates that undergo a variety of mild, stereoretentive transformations (Scheme 36). This versatility was showcased through the concise syntheses of several antihistaminic and neuroactive drug targets, including (*R*)-orphenadrine, (*S*)-cloperastine, isotopically labelled (*S*)-diphenhydramine-d_5, and both enantiomers of neobenodine accessed through the constitutional stereodivergence principle. These applications highlight the method's independence from steric or electronic activation, its compatibility with isosteric arene pairs, and its ability to provide high ee values across a broad substrate spectrum. Even in more challenging contexts, such as the synthesis of (*R*)-chlorcyclizine, where the substitution of the benzylic oxygen proved prone to stereochemical erosion, the results establish a viable proof of concept for accessing benzhydrylamine frameworks enantioselectively from the same privileged benzhydrol intermediates.

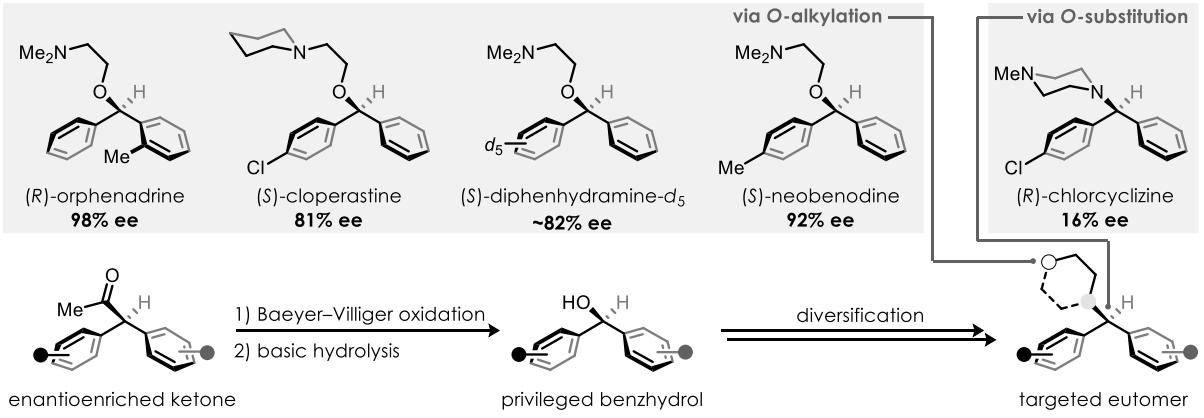

Scheme 36. Eutomer-synthesis of chiral diarylmethane drugs via privileged benzhydrol intermediates.

Altogether, the studies described herein establish a unified, mechanistically informed platform for enantioconvergent diarylmethane synthesis that merges stereoablation, enantiocontrol, and constitutional design elements into a single multicatalytic manifold. The ability to generate both eutomers and distomers from a single catalyst enantiomer, the independence from arene electronics or directing groups, and the seamless integration of the resulting benzhydrols into drug-relevant scaffolds constitute a conceptual and practical advance over existing state-of-the-art strategies. This thesis thus expands the synthetic logic available for constructing chiral diarylmethanes and underscores the potential of stereoablative catalysis in the development of future enantioselective rearrangement reactions.

In a broader context, these findings provide a blueprint for designing next-generation asymmetric methodologies that use temporary bond scission, catalyst-mediated "chiral memory rebuild," and substrate connectivity as complementary stereochemical control tools. By demonstrating how these principles can be harnessed in the context of pharmaceutically relevant motifs, this work contributes not only to fundamental mechanistic understanding but also to the stereocontrolled, modular assembly of diarylmethane drug candidates, an area poised for continued innovation in asymmetric synthesis and medicinal chemistry.

5 Experimental Part

5.1 General Remarks

5.1.1 Full Data Availability

Throughout the course of my PhD studies, most of the results presented in the Main Part of this thesis have already been published. It must be emphasized that all work presented herein is the product of in-depth cooperation between synthetic chemists, spectroscopists, and computational experts, guided by the expertise of our supervisors. Artificial intelligence was used solely to improve the linguistic clarity and style of this thesis. All scientific ideas, data, and interpretations originate entirely from me and my co-authors.

Most results within the optimization, reaction generality, mechanistic, and derivatization section can be found here: Frank, E.; Park, S.; Harrer, E.; Flügel, J. L.; Fischer, M.; Nuernberger, P.; Rehbein, J.; Breder, A. Asymmetric Migratory Tsuji-Wacker Oxidation Enables the Enantioselective Synthesis of Hetero- and Isosteric Diarylmethanes. *J. Am. Chem. Soc.* **2024**, *146*, 34383–34393.[229] The contribution of every co-author for their respective topic is highlighted within Scheme, Figure, or Table captions, as well as in the Experimental Part.

Results for the synthesis of diarylmethane drugs have been published here: Frank, E.; Flügel, J. L.; d'Heureuse, L.; Woick, S.; Breder, A. Enantioconvergent Synthesis of Diarylmethane Drugs via Privileged Benzhydrol Intermediates. *J. Org. Chem.* **2025**, just accepted.[230] The contribution of every co-author is also highlighted within the respective captions, as well as in the Experimental Part.

Experimental detail is only given for every compound synthesized by me, unless indicated otherwise. The remaining data can be found in the above-mentioned publications and additionally in the PhD Thesis of Dr. Sooyoung Park,[165] the Master Thesis of Elias Harrer,[197] and the Master Thesis of Jana Flügel,[217] as is also indicated in the Main Part if appropriate. Additional data that was collected in collaboration with others, like STERN–VOLMER measurements, are referenced.

5.1.2 Details on Material and Analytical Methods

Chemicals and solvents: All commercially available chemicals were purchased in high quality and used without further purification. Solvents for column chromatography were distilled prior to use. Moisture and oxygen-sensitive reactions were carried out using dry solvents from a MBraun Solvent Purification System (SPS) in flame-dried glassware under inert atmosphere of cobalt chloride-dried nitrogen. Current concentration of solutions containing organolithium compounds

was determined via titration with *N*-(2-tolyl)formamide in dry THF (0.1 M). The evaporation of solvents was carried out in a rotary evaporator at 40 °C, under reduced pressure. Room temperature (rt) was approximately 23 °C. Reactions at temperatures of 0 °C or below were conducted in a suitable freezing mixture (water/ice, acetone/dry ice) or a thermostat when run overnight. "Brine" refers to a saturated solution of sodium chloride in water. Column chromatography (CC): Acros Silica 60 (0.035–0.70 mm, 70–230 mesh ASTM) was used as the stationary phase with appropriate solvent mixtures applying forced flow. Purification by automated flash column chromatography was performed on a Advion puriFlash® 5.050 machine using either pre-packed puriFlash® columns or Acros Silica 60 self-packed columns. Thin-layer chromatography (TLC): Reactions were monitored by TLC on silica gel pre-coated aluminium sheets (Machery-Nagel, silica gel 60 G/UV254, 0.2 mm). Visualization was accomplished by exposure to UV light (λ = 254 nm or 365 nm) and by dipping the plates in a *p*-anisaldehyde staining solution (composition: 270 mL EtOH, 7.4 mL *p*-anisaldehyde, 10 mL conc. H_2SO_4), a potassium permanganate staining solution (composition: 3 g potassium permanganate, 20 g potassium carbonate, 5 mL 5% aq. NaOH, 300 mL H_2O), or a cerium molybdate staining solution (composition: 12 g ammonium molybdate, 235 mL H_2O, 0.5 g ceric ammonium molybdate, 15 mL H_2SO_4 conc.) followed by heating. Nuclear magnetic resonance (NMR): NMR spectra were recorded at room temperature using a Bruker Avance 300 NMR spectrometer (300 MHz for ^{1}H, 75 MHz for ^{13}C{^{1}H}), a Bruker Avance 400 or Bruker Avance III HD 400 NMR spectrometer (400 MHz for ^{1}H, 101 MHz for ^{13}C{^{1}H}, 61 MHz for ^{2}H, 377 MHz for ^{19}F{^{1}H}, and 162 MHz for ^{31}P{^{1}H}). Chemical shifts are reported in δ-scale in parts per million (ppm) and referenced to the residual proton signal of the used solvent: $CDCl_3$ (δ = 7.26 ppm, ^{1}H and ^{2}H; δ = 77.2 ppm, ^{13}C), THF-d_8 (δ = 3.58 ppm, ^{1}H). ^{19}F spectra are referenced to $CFCl_3$ and ^{31}P spectra to H_3PO_4. Coupling constants *J* are given in Hertz (Hz) and the multiplicities of the signals are abbreviated as: s = singlet, d = doublet, t = triplet, q = quartet, p = pentet, m = multiplet (denotes complex pattern), br = broad signal, and combinations of those. Signals are reported as follows: (multiplicity, coupling constant *J*, number of protons). Isomeric ratios (*E*:*Z*) were determined by the ratio of ^{1}H NMR integrals of the isolated products. For ^{1}H NMR yield determination, the solvent of the reaction mixture was removed under reduced pressure after reaction completion. The residue was taken up in $CDCl_3$ (2.5 mL), and an internal standard was added. Infrared spectroscopy (IR): IR spectra were recorded on an Agilent Cary630 FTIR spectrophotometer with the neat substances and are reported in cm^{-1}. High resolution mass spectrometry (HRMS): Mass spectra were obtained from the central analytic mass spectrometry facilities of the Faculty of Chemistry and Pharmacy, University of Regensburg. All mass spectra were recorded on a Finnigan MAT 95, Thermo Quest Finnigan TSQ 7000, Finnigan MATSSQ 710 A or an Agilent Q-TOF 6540 UHD instrument. X-ray structure analysis: Structure

determination of compounds by X-ray analysis was performed by the X-ray structure analysis department of the Faculty of Chemistry and Pharmacy, University of Regensburg. Data were collected on Rigaku Synergy DW, Mova / Ag or GV Cu-α / Cu-β single crystal diffractometers. High-performance liquid chromatography (HPLC): Enantiomeric ratios were determined by chiral HPLC measurements on an Agilent 1290 Infinity with the following columns provided by the company DAICEL: Chiralpak® IA-3 (4.6x250 mm, particle size 3 µm), Chiralpak® IB-3 (4.6x250 mm, particle size 3 µm), Chiralpak® IC-3 (4.6x250 mm, particle size 3 µm), Chiralpak® ID-3 (4.6x250 mm, particle size 3 µm), Chiralcel® OD-3 (4.6x250 mm, particle size 3 µm), Chiralcel® OJ-3 (4.6x250 mm, particle size 3 µm). Melting points (m.p.): Melting points were measured on a KRÜSS Opticron melting point meter M5000 without further correction of the values. Optical rotation ($[\alpha]_D^{20}$): Optical rotation of chiral non-racemic compounds was measured in $CHCl_3$ at 20 °C and 589 nm (sodium D-line) with a Jasco P-2000 polarimeter.

5.1.3 Irradiation Setup

All irradiation experiments were performed using custom built temperature-controlled metal blocks and commercially available blue LED lights (Rebel LXML PR01 0500 Royal Blue) operating at a constant current (700 mA) with an intensity maximum in the range of λ_{max} = 447 nm to 465 nm and an output power of 414 mW to 433 mW. The reaction vessel was either a 40 mL photo vial or a standard 100 mL round-bottom flask made of borosilicate glass, which had a distance of 1 cm to the LED. No filters were used (Figure 6).

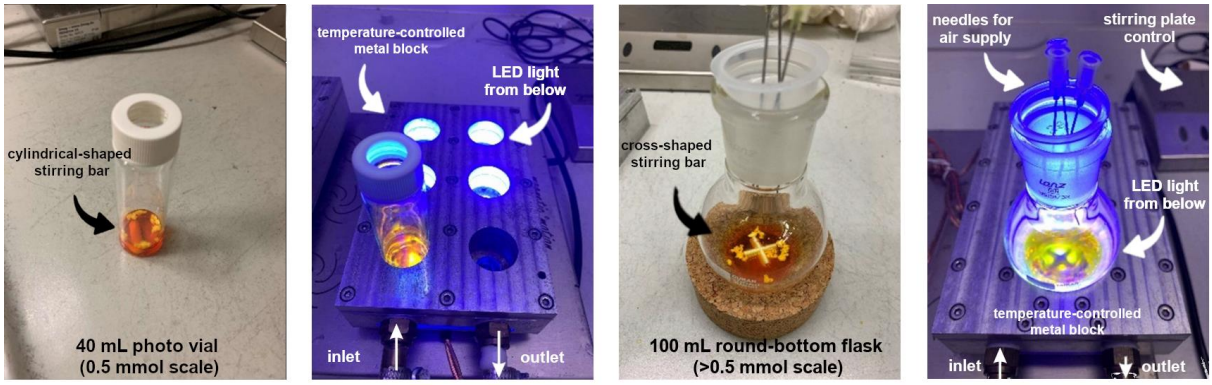

Figure 6. Irradiation setup used for 40 mL photo vials during optimization studies (left, left-center) and 100 mL round-bottom flasks for scope synthesis (right-center, right).

Optimization reactions shown in Table 1 and Table 2 were carried out on a small 0.5 mmol scale in carefully designed temperature-controlled irradiation setups (Figure 6, left and left-center). Regarding the scope and to ensure that the title transformation is still efficient upon upscaling (resulting in more reaction solution to maintain the concentration), the reaction vessel was changed

to a 100 mL round-bottom flask to decrease the irradiated layer thickness and increase the air-solvent interface (Figure 6, right-center and right). This presumably led to a higher oxygen concentration in the solution, further assisted by the change to a cross-shaped stirring bar, and thus to a shorter reaction time while maintaining a high yield. It must be noted that other than through the stirring speed, there is no control of the rate of oxygen intake into the reaction mixture, which is assumed to affect the reproducibility of the reaction.

5.2 Synthetic Work

5.2.1 Preparation of Photoredox Catalysts and Diselanes

The synthesis of 2,4,6-tris(4-methoxyphenyl)pyrylium tetrafluoroborate (TAPT), 2,4,6-tri-*p*-tolylpyrylium tetrafluoroborate (TTPT), 2,4,6-triphenylpyrylium tetrafluoroborate (TPT), 4-mesityl-2,6-diphenylpyrylium tetrafluoroborate (MDPT), methyl 2,3,4,5-tetrachloro-6-(2,4,5,7-tetraiodo-6-methoxy-3-oxo-3*H*-xanthen-9-yl)benzoate (DMRB), and 2,4,6-tri(9*H*-carbazol-9-yl)-5-chloroisophthalonitrile (3CzClIPN) was carried out by Dr. Sooyoung Park according to literature procedures.[165,229]

Preparation of selenium catalysts 1,2-dimesityldiselane ((2-mesitylSe)$_2$), 1,2-bis(2-nitrophenyl)diselane ((2-nitroPhSe)$_2$), 1,2-bis(2-methoxyphenyl)diselane ((2-anisylSe)$_2$), spirobiindane **3a**, MAROUKA–HASHIMOTO diselanes **3b** and **3c**, and DENMARK diselanes **3d–i** were carried out by Dr. Sooyoung Park, Christopher Schöll, and Ludwig d'Heureuse according to literature procedures.[165,229]

5.2.2 Optimization of Reaction Conditions

5.2.2.1 Initial Reaction Development and Control

A 40 mL photo vial equipped with a cylindrical stirring bar was charged with stilbene **1a** (*E*:*Z* = 58:42, 122 mg, 500 µmol), a selenium source, and a photoredox catalyst (5 mol%). A specified combination of solvents was added (Table 1). The flask was sealed with a rubber cap and equipped with needles for air supply. The solution was stirred with 450 rpm under irradiation of light at the indicated wavelength at 55 °C for a certain amount of time. While not being fully dissolved at the beginning, the stilbene was consumed over time during irradiation. The solvent of the crude mixture was removed under reduced pressure, and 1,3,5-trimethoxybenzene (0.5 equiv.) was added as internal standard for determination of NMR yield (reference signal at 6.03 ppm, s, 3H).

5.2.2.2 Evaluation of Chiral, Non-racemic Diselanes

A 100 mL round-bottom flask equipped with a cross-shaped stirring bar was charged with stilbene **1a** (*E*:*Z* = 58:42, 122 mg, 500 μmol), a chiral diselane **3** (10 mol%), and TAPT (12 mg, 25 μmol, 5.0 mol%). A 3:1:1 volumetric ratio of HFIP, DCE, and H_2O (5 mL in total, 0.1 M) was added. The flask was sealed with a rubber septum and equipped with needles for air supply. The solution was stirred with 500 rpm under irradiation of blue light (447 nm) at a constant temperature for a certain amount of time (Table 3). While not being fully dissolved at the beginning, the olefin was consumed over time during irradiation. The solvent of the crude mixture was removed under reduced pressure, and the residue was purified by silica gel column chromatography (R_f = 0.13 in *n*-hexanes:EtOAc = 20:1) to obtain the isolated ketone **2a**, and determine the ee value by chiral HPLC (IC-3, *n*-hexane:*i*-PrOH 95:5, flow rate 0.8 mL/min, 25 °C, t_R = 16.444 min (major), 18.711 min (minor)).

5.2.3 Synthesis of Starting Material

5.2.3.1 Preparation of Phosphonium Salts

General procedure **A** (WITTIG salt synthesis):[180] In a round-bottom flask, triphenylphosphine (1.05 equiv.) was dissolved in toluene (PhMe) or *o*-xylene (0.5 to 1.0 M). The respective chloro- or bromomethyl arene (1 equiv.) was added, and the solution was refluxed for 16 h. The resulting suspension was cooled slowly to rt, and the precipitate was collected by filtration, washed thoroughly with *n*-hexane, and dried under reduced pressure. The target phosphonium salt was used without further purification for subsequent transformations. Benzyltriphenylphosphonium bromide was commercially available.

(Naphthalen-2-ylmethyl)triphenylphosphonium bromide (S1)

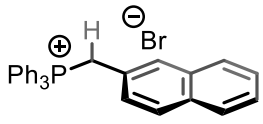

S1

General procedure **A**: Triphenylphosphine (13.9 g, 52.5 mmol, 1.05 equiv.), PhMe (50 mL, 1.0 M), and 2-(bromomethyl)naphthalene (11.5 g, 50.0 mmol) were used to afford phosphonium salt **S1** (22.7 g, 47.0 mmol, 94%) as a white solid.

m.p. 249.0 °C. **^{1}H NMR** (400 MHz, $CDCl_3$) δ / ppm = 7.72–7.65 (m, 9H), 7.63 (d, *J* = 8.0 Hz, 1H), 7.54 (ddd, *J* = 8.3, 7.2, 3.4 Hz, 6H), 7.50–7.44 (m, 3H), 7.39–7.29 (m, 2H), 7.10 (dt, *J* = 8.4, 1.8 Hz, 1H), 5.47 (d, *J* = 14.5 Hz, 2H). **^{13}C{^{1}H} NMR** (101 MHz, $CDCl_3$) δ / ppm = 135.0 (d, *J* = 3.1 Hz), 134.4 (d, *J* = 9.7 Hz), 132.9 (d, *J* = 3.5 Hz), 132.6 (d, *J* = 2.8 Hz), 131.2 (d, *J* = 7.3 Hz), 130.1 (d, *J* = 12.4 Hz), 128.6 (d, *J* = 4.3 Hz), 128.4 (d, *J* = 2.8 Hz), 127.8 (d, *J* = 1.7 Hz), 127.5 (d,

J = 1.7 Hz), 126.6 (d, *J* = 1.8 Hz), 126.4 (d, *J* = 1.1 Hz), 124.5 (d, *J* = 9.0 Hz), 117.8 (d, *J* = 85.5 Hz), 31.0 (d, *J* = 46.7 Hz). **^{31}P{^{1}H} NMR** (162 MHz, $CDCl_3$) δ / ppm = 23.6. **HRMS** (ESI) calcd. for $[C_{29}H_{24}P-Br]^+$ ([M−Br]$^+$), m/z = 403.1623, found: 403.1615. **IR** (ATR, neat) $\tilde{\nu}$ / cm^{-1} = 3653, 3056, 3012, 2859, 2784, 2184, 1439, 1111, 910, 723, 686.

(2-Methylbenzyl)triphenylphosphonium bromide (S2)

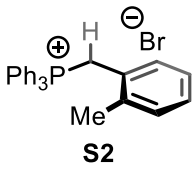

S2

General procedure **A**: Triphenylphosphine (8.26 g, 31.5 mmol, 1.05 equiv.), *o*-xylene (60 mL, 0.50 M), and 2'-methylbenzyl bromide (4.02 mL, 30.0 mmol) were used to afford phosphonium salt **S2** (13.1 g, 29.4 mmol, 98%) as a white solid.

m.p. 260.8 °C. **^{1}H NMR** (400 MHz, $CDCl_3$) δ / ppm = 7.71 (t, *J* = 6.3 Hz, 3H), 7.59–7.50 (m, 12H), 7.07 (t, *J* = 6.6 Hz, 1H), 6.96 (d, *J* = 6.9 Hz, 1H), 6.93–6.84 (m, 2H), 5.09 (d, *J* = 14.0 Hz, 2H), 1.58 (s, 3H). **^{13}C{^{1}H} NMR** (101 MHz, $CDCl_3$) δ / ppm = 138.5 (d, *J* = 5.9 Hz), 135.1 (d, *J* = 2.9 Hz), 134.1 (d, *J* = 9.8 Hz), 131.2 (d, *J* = 5.1 Hz), 130.9 (d, *J* = 3.3 Hz), 130.2 (d, *J* = 12.5 Hz), 128.7 (d, *J* = 3.9 Hz), 126.6 (d, *J* = 3.6 Hz), 125.4 (d, *J* = 8.7 Hz), 117.4 (d, *J* = 85.2 Hz), 28.3 (d, *J* = 47.1 Hz), 19.5. **^{31}P{^{1}H} NMR** (162 MHz, $CDCl_3$) δ / ppm = 22.6. **HRMS** (ESI) calcd. for $[C_{26}H_{24}P-Br]^+$ ([M−Br]$^+$), m/z = 367.1610, found: 367.1613. **IR** (ATR, neat) $\tilde{\nu}$ / cm^{-1} = 3056, 3012, 2859, 2184, 1588, 1487, 1439, 1405, 1320, 1111, 999, 917, 850, 783, 716.

(4-Methylbenzyl)triphenylphosphonium chloride (S3)

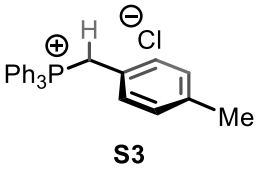

S3

General procedure **A**: Triphenylphosphine (5.51 g, 21.0 mmol, 1.05 equiv.), *o*-xylene (30 mL, 0.60 M), and 4'-methylbenzyl chloride (2.65 mL, 20.0 mmol) were used to afford phosphonium salt **S3** (6.44 g, 16.0 mmol, 80%) as an off-white solid.

m.p. 241.5 °C. **^{1}H NMR** (400 MHz, $CDCl_3$) δ / ppm = 7.76–7.63 (m, 9H), 7.58 (s, 6H), 6.88 (d, *J* = 6.9 Hz, 4H), 5.36–5.22 (m, 2H), 2.20 (s, 3H). **^{13}C{^{1}H} NMR** (101 MHz, $CDCl_3$) δ = 138.2 (d, *J* = 4.1 Hz), 134.9 (d, *J* = 3.0 Hz), 134.3 (d, *J* = 9.7 Hz), 131.3 (d, *J* = 5.6 Hz), 130.1 (d, *J* = 12.5 Hz), 129.5 (d, *J* = 3.3 Hz), 123.9 (d, *J* = 8.7 Hz), 118.0 (d, *J* = 85.5 Hz), 30.4 (d, *J* = 46.7 Hz), 21.1 (d, *J* = 1.2 Hz). **^{31}P{^{1}H} NMR** (162 MHz, $CDCl_3$) δ = 23.4. **HRMS** (ESI) calcd. for $[C_{26}H_{24}P-Cl]^+$ ([M−Cl]$^+$), m/z = 367.1610, found: 367.1613. **IR** (ATR, neat) $\tilde{\nu}$ / cm^{-1} = 3340, 3056, 3012, 2863, 2788, 2169, 1830, 1513, 1484, 1439, 1189, 1111, 999, 924, 824, 719, 690.

(4-Methoxybenzyl)triphenylphosphonium chloride (S4)

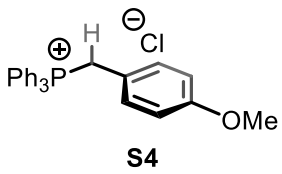

S4

General procedure **A**: Triphenylphosphine (11.0 g, 42.0 mmol, 1.05 equiv.), *o*-xylene (80 mL, 0.50 M), and 4'-methoxybenzyl chloride (5.45 mL, 40.0 mmol) were used to afford phosphonium salt **S4** (14.3 g, 34.2 mmol, 86%) as a white solid.

m.p. 227.5 °C. **^{1}H NMR** (400 MHz, $CDCl_3$) δ / ppm = 7.74–7.61 (m, 9H), 7.56 (td, *J* = 7.8, 3.5 Hz, 6H), 6.94 (dd, *J* = 8.8, 2.5 Hz, 2H), 6.56 (d, *J* = 8.4 Hz, 2H), 5.27 (d, *J* = 13.8 Hz, 2H), 3.65 (s, 3H). **^{13}C{^{1}H} NMR** (101 MHz, $CDCl_3$) δ = 159.6 (d, *J* = 3.7 Hz), 134.9 (d, *J* = 2.9 Hz), 134.4 (d, *J* = 9.7 Hz), 132.7 (d, *J* = 5.5 Hz), 130.1 (d, *J* = 12.5 Hz), 118.7 (d, *J* = 8.7 Hz), 118.0 (d, *J* = 85.3 Hz), 114.2 (d, *J* = 3.1 Hz), 55.2, 29.9 (d, *J* = 46.6 Hz). **^{31}P{^{1}H} NMR** (162 MHz, $CDCl_3$) δ = 23.1. **HRMS** (ESI) calcd. for $[C_{26}H_{24}OP-Cl]^+$ ($[M-Cl]^+$), m/z = 383.1559, found: 383.1559. **IR** (ATR, neat) $\tilde{\nu}$ / cm^{-1} = 3056, 3012, 2963, 2904, 2840, 2784, 2177, 1610, 1513, 1305, 1252, 1181, 1132, 1111, 1033, 910, 835, 719.

(4-Fluorobenzyl)triphenylphosphonium chloride (S5)

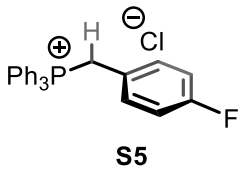

S5

General procedure **A**: Triphenylphosphine (5.51 g, 21.0 mmol, 1.05 equiv.), *o*-xylene (30 mL, 0.60 M), and 4'-fluorobenzyl chloride (2.39 mL, 20.0 mmol) were used to afford phosphonium salt **S5** (6.10 g, 15.0 mmol, 75%) as a white solid.

m.p. 312.6 °C. **^{1}H NMR** (400 MHz, $CDCl_3$) δ / ppm = 7.81–7.65 (m, 9H), 7.62–7.50 (m, 6H), 7.19.7.09 (m, 2H), 6.74 (t, *J* = 8.1 Hz, 2H), 5.70–5.58 (m, 2H). **^{13}C{^{1}H} NMR** (101 MHz, $CDCl_3$) δ = 162.6 (dd, *J* = 248.0, 4.3 Hz), 134.9 (d, *J* = 3.0 Hz), 134.5 (d, *J* = 9.8 Hz), 133.5 (dd, *J* = 8.1, 5.5 Hz), 130.1 (d, *J* = 12.5 Hz), 123.6 (dd, *J* = 8.7, 3.2 Hz), 118.0 (d, *J* = 85.6 Hz), 115.7 (dd, *J* = 21.5, 3.3 Hz), 29.6 (d, *J* = 46.7 Hz). **^{31}P{^{1}H} NMR** (162 MHz, $CDCl_3$) δ = 24.2. **^{19}F{^{1}H} NMR** (377 MHz, $CDCl_3$) δ = −113.9. **HRMS** (ESI) calcd. for $[C_{25}H_{21}FP-Cl]^+$ ($[M-Cl]^+$), m/z = 421.1327, found: 421.1333. **IR** (ATR, neat) $\tilde{\nu}$ / cm^{-1} = 3366, 3056, 3012, 2863, 2788, 2177, 1603, 1510, 1439, 1223, 1163, 1111, 999, 924, 842, 719, 690.

Triphenyl(4-(trifluoromethyl)benzyl)phosphonium bromide (S6)

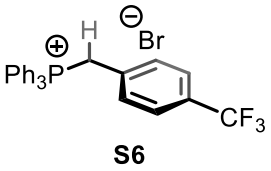

S6

General procedure **A**: Triphenylphosphine (5.51 g, 21.0 mmol, 1.05 equiv.), *o*-xylene (30 mL, 0.60 M), and 4'-trifluoromethylbenzyl bromide (4.78 g, 20.0 mmol) were used to afford phosphonium salt **S6** (9.76 g, 19.5 mmol, 97%) as a white solid.

m.p. 275.4 °C. **^{1}H NMR** (400 MHz, $CDCl_3$) δ / ppm = 7.75 (ddd, *J* = 22.5, 13.6, 7.5 Hz, 9H), 7.61–7.50 (m, 6H), 7.36 (d, *J* = 7.0 Hz, 2H), 7.26 (s, 2H), 5.79 (d, *J* = 15.3 Hz, 2H). **^{13}C{^{1}H} NMR** (101 MHz, $CDCl_3$) δ = 135.0 (d, *J* = 3.0 Hz), 134.6 (d, *J* = 10.0 Hz), 132.3 (d, *J* = 5.3 Hz), 130.1 (d, *J* = 12.7 Hz), 125.5–125.0 (m), 122.5 (q, *J* = 272.3 Hz), 117.6 (d, *J* = 86.0 Hz), 30.0 (d, *J* = 46.8 Hz). **^{31}P{^{1}H} NMR** (162 MHz, $CDCl_3$) δ = 24.8. **^{19}F{^{1}H} NMR** (377 MHz, $CDCl_3$) δ = −63.3. **HRMS** (ESI) calcd. for $[C_{26}H_{21}F_3P-Br]^+$ ($[M-Br]^+$), m/z = 371.1359, found: 371.1364. **IR** (ATR, neat) $\tilde{\nu}$ / cm^{-1} = 3056, 3012, 2863, 2784, 1618, 1439, 1327, 1163, 1111, 1070, 723, 690.

(4-Chlorobenzyl)triphenylphosphonium bromide (S7)

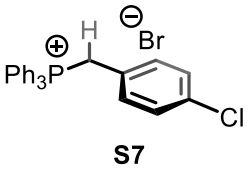

S7

General procedure **A**: Triphenylphosphine (7.36 g, 28.1 mmol, 1.05 equiv.), *o*-xylene (50 mL, 0.50 M), and 4'-chlorobenzyl bromide (5.49 g, 26.7 mmol) were used to afford phosphonium salt **S7** (11.7 g, 25.0 mmol, 94%) as a white solid.

m.p. 292.2 °C. **^{1}H NMR** (400 MHz, $CDCl_3$) δ / ppm = 7.82–7.69 (m, 9H), 7.59 (td, *J* = 7.9, 3.5 Hz, 6H), 7.12 (dd, *J* = 8.5, 2.5 Hz, 2H), 7.01 (d, *J* = 8.3 Hz, 2H), 5.58 (d, *J* = 14.7 Hz, 2H). **^{13}C{^{1}H} NMR** (101 MHz, $CDCl_3$) δ = 135.0 (d, *J* = 3.0 Hz), 134.6 (d, *J* = 9.9 Hz), 134.5 (d, *J* = 4.8 Hz), 133.2 (d, *J* = 5.5 Hz), 130.2 (d, *J* = 12.6 Hz), 128.9 (d, *J* = 3.4 Hz), 126.1 (d, *J* = 8.8 Hz), 117.8 (d, *J* = 85.8 Hz), 29.9 (d, *J* = 46.9 Hz). **^{31}P{^{1}H} NMR** (162 MHz, $CDCl_3$) δ = 24.0. **HRMS** (ESI) calcd. for $[C_{25}H_{21}ClP-Br]^+$ ($[M-Br]^+$), m/z = 387.1064, found: 387.1067. **IR** (ATR, neat) $\tilde{\nu}$ / cm^{-1} = 3418, 3056, 2859, 2788, 2177, 1537, 1491, 1439, 1111, 924, 839, 723, 690.

5.2.3.2 Preparation of *E*/*Z*-Stilbenes

Stilbenes **1d–m**, **1p–y**, **1a'–g'**, **1m'**, **1o'** and constitutional isomers **1r^{ci}**, **1s^{ci}**, **1y^{ci}** were synthesized by S. Park according to the procedure below or to similar literature methods.[165,182,183] Stilbenes **1r'**, **1t'**, and **1t'^{ci}** were synthesized by J. Flügel according to the procedure below.[217,230]

General procedure **B** (WITTIG olefination):[181] In a preheated Schlenk flask, a phosphonium salt (1.1 equiv.) was suspended in dry THF (0.2 M), and cooled down to 0 °C. LDA solution (in THF/heptane/ethylbenzene, 1.1 equiv.) was added dropwise to the flask, and the resulting mixture was stirred at 0 °C for 30 min. The respective ketone (1 equiv. dissolved in dry THF) was then added slowly to the flask, and the reaction mixture was allowed to warm to rt and subsequently heated to 40 °C for 16 h. Upon completion, the reaction was cooled down slowly to rt and quenched with sat. aq. NH_4Cl. The phases were separated, and the aqueous layer was extracted with EtOAc. The combined organic layer was washed with water and brine, dried over Na_2SO_4, filtered, and the solvent was removed under reduced pressure. The crude mixture was purified by silica gel column chromatography to afford the target stilbene. *Important note*: Some stilbenes contain 1,4-diphenylbutane as an impurity that was already present in the 2.0 M LDA solution purchased from Sigma Aldrich (product number: 361798) and was presumably formed from ethylbenzene (see above). Due to their identical R_f values, it was not always possible to remove 1,4-diphenylbutane from the target stilbene. To prove that this impurity originates from LDA solution, 5.0 mL were dissolved in dry THF, quenched with water, extracted with EtOAc, dried over Na_2SO_4, and concentrated to measure a crude NMR of that extract. The obtained NMR resonances are given as follows: **^{1}H NMR** (400 MHz, $CDCl_3$) δ = 7.21–7.14 (m, 2H), 7.11–7.05 (m, 3H), 2.55 (td, *J* = 7.4, 2.8 Hz, 2H), 1.61–1.55 (m, 2H). **^{13}C{^{1}H} NMR** (101 MHz, $CDCl_3$) δ = 142.6, 128.5, 128.4, 125.8, 35.9, 31.2.

2-(2-Phenylprop-1-en-1-yl)naphthalene (1a)

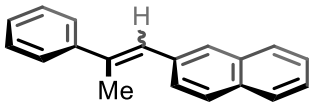

1a

General procedure **B**: Phosphonium salt **S1** (5.32 g, 11.0 mmol, 1.10 equiv.), dry THF (45 mL, 0.20 M), LDA solution (1.0 M, 11 mL, 11 mmol, 1.1 equiv.), and acetophenone (1.17 mL, 10.0 mmol) in 5.0 mL dry THF were used. Purification with silica gel column chromatography (hexanes:EtOAc = 40:1) afforded an *E*/*Z*-mixture of stilbene **1a** (*E*:*Z* = 58:42, 1.78 g, 7.29 mmol, 73%) as a white solid.

m.p. 95.3 °C. **TLC** R_f = 0.54 (hexanes:EtOAc = 19:1). **^{1}H NMR** (400 MHz, $CDCl_3$) δ / ppm = 7.87–7.80 (m, 4H, *E*), 7.72–7.66 (m, 1H, *Z*), 7.64–7.55 (m, 3H, *E*/*Z*), 7.53–7.44 (m, 5H, *E*/*Z*), 7.43–7.34 (m, 4H, *E*/*Z*), 7.34–7.20 (m, 6H, *E*/*Z*), 7.04–6.98 (m, 2H, *E*/*Z*), 6.65 (s, 1H, *Z*), 2.37 (d, *J* = 1.4 Hz, 3H, *E*), 2.27 (d, *J* = 1.5 Hz, 3H, *Z*). **^{13}C{^{1}H} NMR** (101 MHz, $CDCl_3$) δ = 144.1 (*E*), 142.2 (*Z*), 139.3 (*Z*), 138.0 (*E*), 136.0 (*E*), 135.4 (*Z*), 133.5 (*E*), 133.5 (*Z*), 132.3 (*E*), 132.1 (*Z*), 128.6 (*Z*), 128.5 (*E*+*Z*), 128.4 (*E*), 128.1 (*E*+*Z*), 128.0 (*Z*), 127.9 (*E*), 127.9 (*E*), 127.9 (*E*), 127.8 (*E*), 127.6 (*Z*), 127.4 (*E*), 127.3 (*Z*), 127.2 (*Z*), 127.2 (*Z*), 126.8 (*Z*), 126.2 (*E*), 126.2 (*E*), 125.9 (*Z*),

125.9 (*E*), 125.6 (*Z*), 27.3 (*Z*), 17.8 (*E*). **HRMS** (EI) calcd. for $[C_{19}H_{16}]^{\bullet+}$ ($[M]^{\bullet+}$), m/z = 244.1247, found: 244.1242. **IR** (ATR, neat) $\tilde{\nu}$ / cm^{-1} = 3056, 3023, 2967, 2911, 1625, 1593, 1495, 1446, 1379, 1271, 1074, 1029, 947, 902, 865, 820, 746, 697.

For mechanistic studies (see Table 5) the stilbene isomers were separated. Recrystallization of *E*/*Z*-**1a** from boiling *n*-hexane afforded *E*-**1a** (*E*:*Z* = 92:8) as a white solid. Its configuration was determined by a NOESY experiment.

^{1}H NMR (400 MHz, $CDCl_3$) δ / ppm = 7.84 (dd, *J* = 7.3, 3.3 Hz, 4H), 7.58 (d, *J* = 7.3 Hz, 2H), 7.54–7.45 (m, 3H), 7.41 (t, *J* = 7.6 Hz, 2H), 7.32 (t, *J* = 7.3 Hz, 1H), 7.00 (s, 1H), 2.38 (s, 3H). **^{13}C{^{1}H} NMR** (101 MHz, $CDCl_3$) δ = 144.1, 138.0, 136.0, 133.5, 132.3, 128.5, 128.1, 127.9, 127.9, 127.8, 127.8, 127.4, 126.3, 126.2, 125.9, 17.8.

Silica gel column chromatography (hexanes only) of *E*/*Z*-**1a** afforded *Z*-**1a** (*E*:*Z* = >1:99) as a white solid. Its configuration was determined by a NOESY experiment.

^{1}H NMR (400 MHz, $CDCl_3$) δ / ppm = 7.72–7.66 (m, 1H), 7.64–7.58 (m, 1H), 7.50 (d, *J* = 8.6 Hz, 1H), 7.47 (s, 1H), 7.40–7.33 (m, 2H), 7.32–7.20 (m, 5H), 7.01 (dd, *J* = 8.6, 1.7 Hz, 1H), 6.65 (s, 1H), 2.27 (d, *J* = 1.5 Hz, 3H). **^{13}C{^{1}H} NMR** (101 MHz, $CDCl_3$) δ = 142.2, 139.4, 135.4, 133.5, 132.1, 128.6, 128.5, 128.0, 128.0, 127.6, 127.4, 127.2, 127.2, 126.8, 125.9, 125.6, 27.3.

2-(2-(*p*-Tolyl)prop-1-en-1-yl)naphthalene (1b)

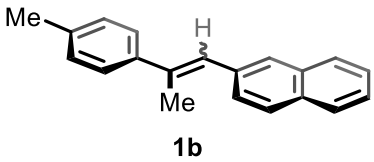

1b

General procedure **B**: Phosphonium salt **S1** (5.32 g, 11.0 mmol, 1.10 equiv.), dry THF (45 mL, 0.20 M), LDA solution (1.9 M, 5.8 mL, 11 mmol, 1.1 equiv.), and 4'-methylacetophenone (1.34 g, 10.0 mmol) in 5.0 mL dry THF were used. Purification with silica gel column chromatography (hexanes:EtOAc = 40:1) afforded an *E*/*Z*-mixture of stilbene **1b** (*E*:*Z* = 51:49, 2.33 g, 9.03 mmol, 90%) as a white solid. Assignments to each isomer are based on analogy to stilbene **1a**.

m.p. 90.0 °C. **TLC** R_f = 0.35 (hexanes:EtOAc = 19:1). **^{1}H NMR** (400 MHz, $CDCl_3$) δ / ppm = 7.91–7.84 (m, 4H, *E*), 7.77–7.71 (m, 1H, *Z*), 7.71–7.66 (m, 1H, *Z*), 7.59–7.48 (m, 7H, *E*/*Z*), 7.46–7.39 (m, 2H, *E*/*Z*), 7.29–7.23 (m, 2H, *E*/*Z*), 7.18 (d, *J* = 8.2 Hz, 2H, *E*/*Z*), 7.16–7.11 (m, 2H, *E*/*Z*), 7.10 (dd, *J* = 8.7, 1.6 Hz, 1H, *E*/*Z*), 7.05–7.02 (m, 1H, *E*/*Z*), 6.69–6.66 (m, 1H, *Z*), 2.44 (s, 3H, *E*/*Z*), 2.41 (d, *J* = 1.4 Hz, 3H, *E*), 2.40 (s, 3H, *E*/*Z*), 2.30 (d, *J* = 1.6 Hz, 3H, *Z*). **^{13}C{^{1}H} NMR** (101 MHz, $CDCl_3$) δ = 141.2, 139.2, 139.1, 137.9, 137.2, 136.8, 136.2, 135.7, 133.5, 132.2, 132.1, 129.3, 129.2, 128.3, 128.1, 128.0, 127.9, 127.9, 127.8, 127.8, 127.7, 127.6, 127.4, 127.1, 127.1, 126.5,

126.2, 126.0, 125.9, 125.8, 125.5, 27.3, 21.4, 21.3, 17.7. **HRMS** (EI) calcd. for $[C_{20}H_{18}]^{\bullet+}$ ($[M]^{\bullet+}$), m/z = 258.1043, found: 258.1042. **IR** (ATR, neat) $\tilde{\nu}$ / cm^{-1} = 3053, 3023, 2919, 2859, 1599, 1510, 1435, 1375, 1271, 902, 864, 816, 742.

2-(2-(4-Methoxyphenyl)prop-1-en-1-yl)naphthalene (1c)

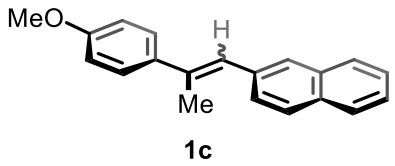

1c

General procedure **B**: Phosphonium salt **S1** (5.32 g, 11.0 mmol, 1.10 equiv.), dry THF (45 mL, 0.20 M), LDA solution (1.9 M, 5.8 mL, 11 mmol, 1.1 equiv.), and 4'-methoxyacetophenone (1.50 g, 10.0 mmol) in 5.0 mL dry THF were used. Purification with silica gel column chromatography (hexanes:EtOAc = 20:1 to 5:1) afforded an *E*/*Z*-mixture of stilbene **1c** (*E*:*Z* = 49:51, 2.34 g, 8.41 mmol, 84%) as a white semi-solid. Assignments to each isomer are based on analogy to stilbene **1a**.

TLC R_f = 0.34 (hexanes:EtOAc = 19:1). **^{1}H NMR** (400 MHz, $CDCl_3$) δ / ppm = 7.88–7.81 (m, 4H, *E*), 7.75–7.70 (m, 1H, *Z*), 7.69–7.64 (m, 1H, *Z*), 7.57–7.46 (m, 7H, *E*/*Z*), 7.43–7.36 (m, 2H, *E*/*Z*), 7.21–7.15 (m, 2H, *E*/*Z*), 7.08 (dd, *J* = 8.5, 1.8 Hz, 1H, *E*/*Z*), 6.99–6.94 (m, 3H, *E*/*Z*), 6.84 (d, *J* = 2.1 Hz, 1H, *E*/*Z*), 6.82 (d, *J* = 2.0 Hz, 1H, *E*/*Z*), 6.63 (d, *J* = 1.6 Hz, 1H, *Z*), 3.87 (s, 3H, *E*), 3.82 (s, 3H, *Z*), 2.37 (d, *J* = 1.3 Hz, 3H, *E*), 2.27 (d, *J* = 1.5 Hz, 3H, *Z*). **^{13}C NMR{^{1}H}** (101 MHz, $CDCl_3$) δ = 159.2, 158.8, 138.7, 137.4, 136.5, 136.2, 135.8, 134.2, 133.5, 133.5, 132.2, 132.1, 129.7, 128.0, 127.9, 127.9, 127.9, 127.8, 127.7, 127.7, 127.6, 127.4, 127.2, 127.2, 126.4, 126.3, 126.2, 125.9, 125.8, 125.5, 113.9, 113.9, 55.5, 55.3, 27.2, 17.7. **HRMS** (EI) calcd. for $[C_{20}H_{18}O]^{\bullet+}$ ($[M]^{\bullet+}$), m/z = 274.1352, found: 274.1355. **IR** (ATR, neat) $\tilde{\nu}$ / cm^{-1} = 3056, 3001, 2959, 2837, 2360, 1607, 1513, 1290, 1245, 1178, 1036, 828.

2-(2-(4-Fluorophenyl)prop-1-en-1-yl)naphthalene (1n)

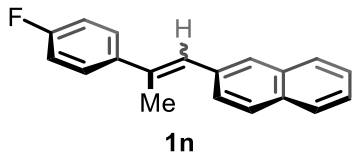

1n

General procedure **B**: Phosphonium salt **S1** (5.32 g, 11.0 mmol, 1.10 equiv.), dry THF (45 mL, 0.20 M), LDA solution (1.9 M, 5.8 mL, 11 mmol, 1.1 equiv.), and 4'-fluoroacetophenone (1.21 mL, 10.0 mmol) in 5.0 mL dry THF were used. Purification with silica gel column chromatography (hexanes:EtOAc = 70:1 to 30:1) afforded an *E*/*Z*-mixture of stilbene **1n** (*E*:*Z* = 54:46, 2.44 g, 9.32 mmol, 93%) as an off-white solid. Assignments to each isomer are based on analogy to stilbene **1a**.

m.p. 128.0 °C. **TLC** R_f = 0.51 (hexanes:EtOAc = 19:1). **^{1}H NMR** (400 MHz, $CDCl_3$) δ / ppm = 7.90–7.82 (m, 4H, *E*), 7.76–7.71 (m, 1H, *Z*), 7.69–7.65 (m, 1H, *Z*), 7.59–7.48 (m, 7H, *E*/*Z*), 7.45–7.40 (m, 2H, *E*/*Z*), 7.25–7.19 (m, 2H, *E*/*Z*), 7.15–7.08 (m, 2H, *E*/*Z*), 7.06–6.95 (m, 4H, *E*/*Z*), 6.68 (s, 1H, *Z*), 2.37 (d, *J* = 1.4 Hz, 3H, *E*), 2.28 (d, *J* = 1.6 Hz, 3H, *Z*). **^{13}C{^{1}H} NMR** (101 MHz, $CDCl_3$) δ = 163.4 (d, *J* = 33.4 Hz), 161.0 (d, *J* = 33.1 Hz), 140.1 (d, *J* = 3.3 Hz), 138.1, 137.9 (d, *J* = 3.4 Hz), 137.0, 135.8, 135.2, 133.5 (d, *J* = 1.3 Hz), 132.3, 132.2, 130.2, 130.1, 128.1, 127.9, 127.8, 127.8 (d, *J* = 1.7 Hz), 127.7, 127.6, 127.3, 127.2, 127.1, 126.3, 126.0, 125.9, 125.7, 115.5 (d, *J* = 21.2 Hz), 115.3 (d, *J* = 21.3 Hz), 27.1, 17.9. **^{19}F{^{1}H} NMR** (377 MHz, $CDCl_3$) δ = −115.6, −115.9. **HRMS** (EI) calcd. for $[C_{19}H_{15}F]^{\bullet+}$ ($[M]^{\bullet+}$), m/z = 262.1152, found: 262.1145. **IR** (ATR, neat) $\tilde{\nu}$ / cm^{-1} = 3056, 2967, 2911, 2855, 1595, 1505, 1222, 1159, 902, 816, 745.

2-(2-(4-Chlorophenyl)prop-1-en-1-yl)naphthalene (1o)

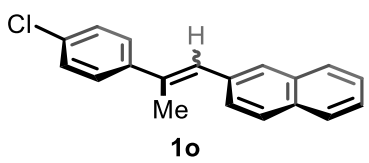

1o

General procedure **B**: Phosphonium salt **S1** (5.32 g, 11.0 mmol, 1.10 equiv.), dry THF (45 mL, 0.20 M), LDA solution (1.97 M, 5.60 mL, 11.0 mmol, 1.10 equiv.), and 4'-chloroacetophenone (1.3 mL, 10 mmol) in 5.0 mL dry THF were used. Purification with silica gel column chromatography (hexanes:EtOAc = 50:1 to 40:1) afforded an *E*/*Z*-mixture of stilbene **1o** (*E*:*Z* = 57:43, 2.34 g, 8.41 mmol, 84%) as a white solid. Assignments to each isomer are based on analogy to stilbene **1a**.

m.p. 91.6 °C. **TLC** R_f = 0.46 (hexanes:EtOAc = 19:1). **^{1}H NMR** (400 MHz, $CDCl_3$) δ / ppm = 7.89–7.81 (m, 4H, *E*), 7.75–7.70 (m, 1H, *Z*), 7.68–7.64 (m, 1H, *Z*), 7.56 (d, *J* = 8.6 Hz, 1H, *Z*), 7.50 (ddt, *J* = 6.2, 4.3, 2.5 Hz, 7H, *E*/*Z*), 7.44–7.34 (m, 4H, *E*/*Z*), 7.28–7.23 (m, 2H, *E*/*Z*), 7.21–7.14 (m, 2H, *E*/*Z*), 7.03 (dd, *J* = 8.6, 1.6 Hz, 1H, *Z*), 6.99 (s, 1H, *E*), 6.68 (s, 1H, *Z*), 2.35 (d, *J* = 1.3 Hz, 3H, *E*), 2.25 (d, *J* = 1.5 Hz, 3H, *Z*). **^{13}C{^{1}H} NMR** (101 MHz, $CDCl_3$) δ = 142.4, 140.5, 137.7, 136.8, 135.7, 135.1, 133.5, 133.1, 132.9, 132.3, 132.2, 129.9, 128.8, 128.6, 128.3, 128.1, 128.1, 128.0, 127.9, 127.8, 127.8, 127.6, 127.6, 127.5, 127.4, 127.4, 127.2, 126.3, 126.1, 126.0, 125.9, 26.9, 17.7. **HRMS** (EI) calcd. for $[C_{19}H_{15}Cl]^{\bullet+}$ ($[M]^{\bullet+}$), m/z = 278.0857, found: 278.0855. **IR** (ATR, neat) $\tilde{\nu}$ / cm^{-1} = 3056, 2971, 2915, 1595, 1491, 1435, 1375, 1092, 1014, 902, 828.

1-Methyl-2-(2-phenylprop-1-en-1-yl)benzene (1z)

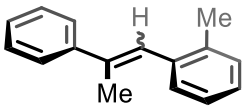

1z

General procedure **B**: Phosphonium salt **S2** (4.92 g, 11.0 mmol, 1.10 equiv.), dry THF (45 mL, 0.20 M), LDA solution (1.5 M, 7.3 mL, 11 mmol, 1.1 equiv.), and acetophenone (1.2 mL, 10 mmol) in 5.0 mL dry THF were used. Purification with silica gel column chromatography (hexanes:EtOAc = 40:1) afforded an *E*/*Z*-mixture of stilbene **1z** (*E*:*Z* = 42:58, 1.69 g, 8.11 mmol, 81%) as a yellow liquid. Assignments to each isomer are based on analogy to stilbene **1a**.

TLC R_f = 0.63 (hexanes:EtOAc = 19:1). **^{1}H NMR** (400 MHz, $CDCl_3$) δ / ppm = 7.60–7.55 (m, 2H, *E*), 7.41 (t, *J* = 7.7 Hz, 2H, *E*), 7.35–7.16 (m, 7H, *E*/*Z*), 7.12 (d, *J* = 7.7 Hz, 4H, *E*), 7.03 (t, *J* = 7.4 Hz, 1H, *Z*), 6.91–6.84 (m, 2H, *E*/*Z*), 6.79 (d, *J* = 7.7 Hz, 1H, *Z*), 6.56 (s, 1H, *Z*), 2.33 (s, 3H, *E*), 2.31 (s, 3H, *Z*), 2.28 (d, *J* = 0.9 Hz, 3H, *Z*), 2.15 (d, *J* = 0.8 Hz, 3H, *E*). **^{13}C{^{1}H} NMR** (101 MHz, $CDCl_3$) δ = 143.6, 141.7, 138.4, 137.7, 137.5, 137.3, 136.9, 136.3, 130.0, 130.0, 129.8, 129.4, 128.5, 128.1, 127.3, 127.0, 126.8, 126.8, 126.4, 126.1, 126.0, 125.5, 125.3, 36.0, 31.2, 26.0, 20.2, 20.2, 17.3. **HRMS** (EI) calcd. for $[C_{16}H_{16}]^{\bullet+}$ ($[M]^{\bullet+}$), m/z = 208.1247, found: 208.1250. **IR** (ATR, neat) $\tilde{\nu}$ / cm^{-1} = 3056, 3019, 2967, 2941, 2855, 1599, 1495, 1446, 1379, 1111, 1074, 1029, 913, 876, 753, 697.

2-(3-Methyl-2-phenylbut-1-en-1-yl)naphthalene (1h')

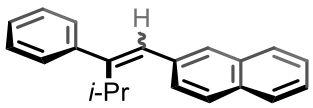

1h'

General procedure **B**: Phosphonium salt **S1** (5.32 g, 11.0 mmol, 1.10 equiv.), dry THF (45 mL, 0.20 M), LDA solution (2.0 M, 5.5 mL, 11 mmol, 1.1 equiv.), and isobutyrophenone (1.48 g, 10 mmol) in 5.0 mL dry THF were used. Purification with silica gel column chromatography (hexanes:EtOAc = 60:1) afforded an *E*/*Z*-mixture of stilbene **1h'** (*E*:*Z* = 90:10, 1.04 g, 3.80 mmol, 38%) as a yellow oil. Assignments to each isomer are based on analogy to stilbene **1a**.

TLC R_f = 0.57 (hexanes:EtOAc = 19:1). **^{1}H NMR** (400 MHz, $CDCl_3$) δ / ppm = 7.82–7.67 (m, 2H, *E*/*Z*), 7.64–7.59 (m, 2H, *E*/*Z*), 7.57–7.52 (m, 2H, *E*/*Z*), 7.47–7.36 (m, 5H, *E*/*Z*), 7.35–7.21 (m, 10H, *E*/*Z*), 7.17–7.11 (m, 4H, *E*/*Z*), 6.93 (dd, *J* = 8.6, 1.7 Hz, 2H, *E*/*Z*), 6.57 (s, 1H, *E*), 6.52 (s, 1H, *Z*), 3.41 (hept, *J* = 6.9 Hz, 1H, *Z*), 2.77 (hept, *J* = 7.2 Hz, 1H, *E*), 1.16 (d, *J* = 6.8 Hz, 6H, *E*), 1.11 (d, *J* = 6.9 Hz, 6H, *Z*). **^{13}C{^{1}H} NMR** (101 MHz, $CDCl_3$) δ = 150.1, 141.5, 135.5, 133.6, 132.2, 129.4, 129.2, 128.7, 128.5, 128.3, 128.1, 127.9, 127.6, 127.5, 127.2, 127.1, 126.1, 126.0, 125.9, 125.7, 125.2, 124.6, 37.7, 36.1, 31.3, 22.1. **HRMS** (EI) calcd. for $[C_{21}H_{20}]^{\bullet+}$ ($[M]^{\bullet+}$), m/z = 272.1565, found: 272.1558. **IR** (ATR, neat) $\tilde{\nu}$ / cm^{-1} = 3056, 2967, 1595, 1487, 1446, 1226, 1111, 902, 816, 757.

1-Chloro-4-styrylbenzene (1i')

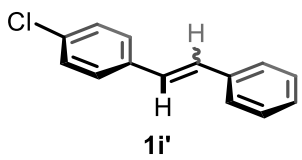

1i'

General procedure **B**: Benzyltriphenylphosphonium bromide (2.38 g, 5.50 mmol, 1.10 equiv.), dry THF (20 mL, 0.20 M), LDA solution (0.83 M, 6.6 mL, 5.5 mmol, 1.1 equiv.), and 4-chlorobenzaldehyde (703 mg, 5.00 mmol) in 5.0 mL dry THF were used. Purification with silica gel column chromatography (hexanes:EtOAc = 30:1) afforded an *E*/*Z*-mixture of stilbene **1i'** (*E*:*Z* = 50:50, 764 mg, 3.56 mmol, 71%) as a white semi-solid. Assignments to each isomer are based on analogy to stilbene **1a**.

TLC R_f = 0.55 (hexanes:EtOAc = 19:1). **^{1}H NMR** (400 MHz, $CDCl_3$) δ / ppm = 7.56–7.50 (m, 2H, *E*/*Z*), 7.49–7.43 (m, 2H, *E*/*Z*), 7.42–7.32 (m, 4H, *E*/*Z*), 7.26 (s, 6H, *E*/*Z*), 7.21 (d, *J* = 2.5 Hz, 4H, *E*/*Z*), 7.09 (d, *J* = 2.9 Hz, 2H, *Z*), 6.66 (d, *J* = 12.2 Hz, 1H, *E*), 6.56 (d, *J* = 12.2 Hz, 1H, *E*). **^{13}C{^{1}H} NMR** (101 MHz, $CDCl_3$) δ = 137.1, 137.0, 136.0, 135.8, 133.3, 132.9, 131.1, 130.3, 129.5, 129.1, 129.0, 128.9, 128.9, 128.5, 128.5, 128.0, 127.8, 127.5, 127.5, 126.7. **HRMS** (EI) calcd. for $[C_{14}H_{11}Cl]^{\bullet+}$ ($[M]^{\bullet+}$), m/z = 214.0549, found: 214.0547. **IR** (ATR, neat) $\tilde{\nu}$ / cm^{-1} = 3056, 3023, 1592, 1491, 1446, 1092, 910, 820, 731, 697.

2-(2-(4-Nitrophenyl)prop-1-en-1-yl)naphthalene (1j')

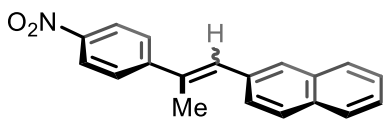

1j'

General procedure **B**: Phosphonium salt **S1** (5.32 g, 11.0 mmol, 1.10 equiv.), dry THF (45 mL, 0.20 M), LDA solution (1.9 M, 5.8 mL, 11 mmol, 1.1 equiv.), and 4'-nitroacetophenone (1.65 g, 10.0 mmol) in 5.0 mL dry THF were used. Purification with silica gel column chromatography (hexanes:EtOAc = 70:1 to 5:1) afforded an *E*/*Z*-mixture of stilbene **1j'** (*E*:*Z* = 97:3, 313 mg, 1.90 mmol, 19%) as a yellow solid. Assignments to each isomer are based on analogy to stilbene **1a**.

TLC R_f = 0.27 (hexanes:EtOAc = 19:1). **^{1}H NMR** (400 MHz, $CDCl_3$) δ / ppm = 8.25 (m, 4H, *E*/*Z*), 7.86 (m, 8H, *E*/*Z*), 7.70 (m, 4H *E*/*Z*), 7.51 (m, 6H, *E*/*Z*), 7.13 (s, 1H, *E*), 6.80 (s, 1H, *Z*), 2.40 (d, *J* = 1.4 Hz, 3H, *E*), 2.29 (d, *J* = 1.6 Hz, 3H, *Z*). **^{13}C{^{1}H} NMR** (101 MHz, $CDCl_3$) δ = 150.4, 146.8, 135.9, 134.8, 133.3, 132.5, 131.2, 128.3, 128.1, 127.9, 127.7, 127.2, 126.4, 126.3, 123.8, 17.5. **HRMS** (EI) calcd. for $[C_{19}H_{15}NO_2]^{\bullet+}$ ($[M]^{\bullet+}$), m/z = 289.1103, found: 289.1096. **IR** (ATR, neat) $\tilde{\nu}$ / cm^{-1} = 3064, 1588, 1513, 1338, 1111, 850, 753.

1-(2-Phenylprop-1-en-1-yl)-4-(trifluoromethyl)benzene (1k')

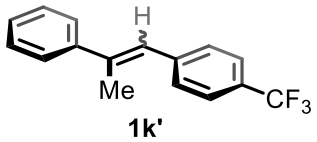

1k'

General procedure **B**: Phosphonium salt **S6** (4.4 g, 8.8 mmol, 1.1 equiv.), dry THF (35 mL, 0.20 M), LDA solution (1.0 M, 8.8 mL, 8.8 mmol, 1.1 equiv.), and acetophenone (0.93 mL, 8.0 mmol) in 5.0 mL dry THF were used. Purification with silica gel column chromatography (hexanes:EtOAc = 40:1) afforded an *E*/*Z*-mixture of stilbene **1k'** (*E*:*Z* = 53:47, 1.21 g, 4.62 mmol, 58%) as a white semi-solid. Assignments to each isomer are based on analogy to stilbene **1a**.

TLC R_f = 0.55 (hexanes:EtOAc = 19:1). **^{1}H NMR** (400 MHz, $CDCl_3$) δ / ppm = 7.65 (d, *J* = 8.2 Hz, 2H, *E*/*Z*), 7.56 (dd, *J* = 8.3, 1.2 Hz, 2H, *E*/*Z*), 7.48 (d, *J* = 8.4 Hz, 2H, *E*/*Z*), 7.45–7.39 (m, 2H, *E*/*Z*), 7.39–7.28 (m, 6H, *E*/*Z*), 7.19 (dd, *J* = 7.9, 1.7 Hz, 2H, *E*/*Z*), 7.05 (d, *J* = 8.4 Hz, 2H, *E*/*Z*), 6.87 (s, 1H, *E*), 6.51 (s, 1H, *Z*), 2.31 (d, *J* = 1.3 Hz, 3H, *E*), 2.26 (d, *J* = 1.5 Hz, 3H, *Z*). **^{13}C{^{1}H} NMR** (101 MHz, $CDCl_3$) δ = 143.5, 142.1 (d, *J* = 1.2 Hz), 141.7, 141.6, 141.4 (d, *J* = 1.3 Hz), 139.8, 129.5, 129.2, 128.8, 128.6, 128.3 (t, *J* = 32.5 Hz), 128.1, 127.9, 127.8, 127.5, 126.5, 126.2, 125.8 (d, *J* = 4.7 Hz), 125.5, 125.3 (q, *J* = 3.8 Hz), 124.9 (q, *J* = 3.8 Hz), 123.1 (d, *J* = 4.7 Hz), 27.3, 17.7. **^{19}F{^{1}H} NMR** (377 MHz, $CDCl_3$) δ = −62.9, −62.9. **HRMS** (EI) calcd. for $[C_{16}H_{13}F_3]^{\bullet+}$ ($[M]^{\bullet+}$), m/z = 262.0969, found: 262.0966. **IR** (ATR, neat) $\tilde{\nu}$ / cm^{-1} = 3056, 3027, 2922, 1614, 1320, 1163, 1111, 1066, 1018, 872, 757, 697.

2-(2-(2-Chlorophenyl)prop-1-en-1-yl)naphthalene (1l')

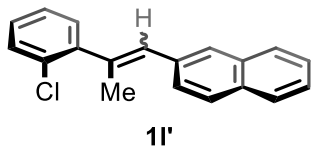

1l'

General procedure **B**: Phosphonium salt **S1** (5.32 g, 11.0 mmol, 1.10 equiv.), dry THF (45 mL, 0.20 M), LDA solution (1.9 M, 5.8 mL, 11 mmol, 1.1 equiv.), and 2'-chloroacetophenone (1.55 g, 10 mmol) in 5.0 mL dry THF were used. Purification with silica gel column chromatography (hexanes:EtOAc = 70:1 to 30:1) afforded an *E*/*Z*-mixture of stilbene **1l'** (*E*:*Z* = 57:43, 2.33 g, 8.37 mmol, 84%) as a colorless oil. Assignments to each isomer are based on analogy to stilbene **1a**.

TLC R_f = 0.61 (hexanes:EtOAc = 9:1). **^{1}H NMR** (400 MHz, $CDCl_3$) δ / ppm = 7.89–7.82 (m, 4H, *E*/*Z*), 7.71–7.66 (m, 1H, *E*), 7.63–7.57 (m, 1H, *Z*), 7.56–7.41 (m, 6H, *E*/*Z*), 7.40–7.34 (m, 4H, *E*/*Z*), 7.31–7.17 (m, 4H, *E*/*Z*) 7.13 (dd, *J* = 7.4, 1.8 Hz, 1H, *E*), 6.95 (d, *J* = 8.6 Hz, 1H, *Z*), 6.72 (d, 1H, *E*), 6.63 (s, 1H, *Z*), 2.33 (d, *J* = 0.5 Hz, 3H, *Z*), 2.26 (d, *J* = 0.9 Hz, 3H, *E*). **^{13}C{^{1}H} NMR** (101 MHz, $CDCl_3$) δ = 144.6, 141.3, 137.9, 137.1, 135.1, 134.7, 133.4, 133.3, 132.7, 132.4, 132.3, 132.1, 130.5, 130.1, 130.0, 129.9, 129.7, 128.5, 128.4, 128.2, 128.0, 127.9, 127.8, 127.7, 127.6, 127.5, 127.4, 127.4, 127.3, 126.8, 126.2, 126.1, 125.9, 125.8, 125.6, 26.2, 19.5. **HRMS** (EI) calcd. for

$[C_{20}H_{15}Cl]^{\bullet+}$ ($[M]^{\bullet+}$), m/z = 278.0862, found: 278.0857. **IR** (ATR, neat) $\tilde{\nu}$ / cm^{-1} = 3056, 2967, 2937, 1595, 1506, 1472, 1428, 1271, 1088, 1040, 947, 902, 816, 746.

2-(1-(Naphthalen-2-yl)prop-1-en-2-yl)furan (1n')

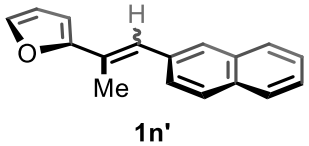

1n'

General procedure **B**: Phosphonium salt **S1** (4.3 g, 8.8 mmol, 1.1 equiv.), dry THF (35 mL, 0.20 M), LDA solution (2.0 M, 4.4 mL, 8.8 mmol, 1.1 equiv.), and 2-furylmethylketone (0.88 g, 8.0 mmol) in 5.0 mL dry THF were used. Purification with silica gel column chromatography (hexanes:EtOAc = 70:1 to 30:1) afforded an *E*/*Z*-mixture of stilbene **1n'** (*E*:*Z* = 95:5, 999 mg, 4.26 mmol, 53%) as a yellow oil. Assignments to each isomer are based on analogy to stilbene **1a**.

TLC R_f = 0.46 (hexanes:EtOAc = 19:1). **^{1}H NMR** (400 MHz, $CDCl_3$) δ / ppm = 7.86–7.79 (m, 4H, *E*/*Z*), 7.51 (dd, *J* = 8.7, 1.4 Hz, 1H, *E*), 7.49–7.44 (m, 3H, *E*/*Z*), 7.34 (dd, *J* = 8.5, 1.6 Hz, 1H, *Z*), 7.29 (s, 1H, *E*), 6.60 (s, 1H, *Z*), 6.46 (dd, *J* = 3.3, 1.8 Hz, 1H, *E*), 6.43 (d, *J* = 3.3 Hz, 1H, *E*), 6.30 (dd, *J* = 3.4, 1.8 Hz, 1H, *Z*), 6.17 (d, *J* = 3.4 Hz, 1H, *Z*), 2.28 (d, *J* = 1.3 Hz, 3H, *E*), 2.25 (d, *J* = 1.5 Hz, 3H, *Z*). **^{13}C{^{1}H} NMR** (101 MHz, $CDCl_3$) δ = 156.3, 153.9, 142.0, 141.3, 135.8, 135.2, 133.5, 132.4, 132.2, 128.0, 127.9, 127.7, 127.7, 127.6, 127.6, 127.6, 127.3, 127.3, 126.9, 126.7, 126.6, 126.2, 125.9, 125.8, 125.7, 124.3, 111.5, 111.0, 109.2, 106.6, 22.9, 15.1. **HRMS** (EI) calcd. for $[C_{17}H_{14}O]^{\bullet+}$ ($[M]^{\bullet+}$), m/z = 234.1045, found: 234.1036. **IR** (ATR, neat) $\tilde{\nu}$ / cm^{-1} = 3116, 3053, 2952, 2922, 1621, 1490, 1450, 1371, 1156, 1021, 902, 820, 738.

2-(1-(4-Chlorophenyl)prop-1-en-2-yl)pyridine (1p')

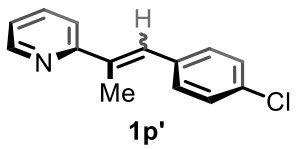

1p'

General procedure **B**: Phosphonium salt **S7** (5.2 g, 11 mmol, 1.1 equiv.), dry THF (45 mL, 0.20 M), LDA solution (1.85 M, 5.95 mL, 11.0 mmol, 1.10 equiv.), and 2-acetylpyridine (1.12 mL, 10.0 mmol) in 5.0 mL dry THF were used. Purification with silica gel column chromatography (hexanes:EtOAc = 4:1) afforded an *E*/*Z*-mixture of stilbene **1p'** (*E*:*Z* = 50:50, 2.14 g, 9.32 mmol, 93%) as a yellow liquid. Assignments to each isomer are based on analogy to stilbene **1a**.

TLC R_f = 0.23 (hexanes:EtOAc = 4:1). **^{1}H NMR** (400 MHz, $CDCl_3$) δ / ppm = 8.66–8.60 (m, 2H, *E*/*Z*), 7.74–7.66 (m, 1H, *Z*), 7.55–7.45 (m, 2H, *E*/*Z*), 7.43 (s, 1H, *Z*), 7.35 (s, 4H, *E*/*Z*), 7.22–7.17 (m, 1H, *E*), 7.16–7.12 (m, 1H. *E*), 7.07 (d, *J* = 8.5 Hz, 2H, *E*/*Z*), 7.02–6.96 (m, 1H, *E*), 6.83 (d, *J* = 8.5 Hz, 2H, *E*/*Z*), 6.59 (s, 1H, *Z*), 2.33 (d, *J* = 1.1 Hz, 3H, *E*), 2.27 (d, *J* = 1.3 Hz, 3H, *Z*). **^{13}C{^{1}H} NMR** (101 MHz, $CDCl_3$) δ = 160.1, 159.5, 149.7, 149.0, 139.4, 136.9, 136.8, 136.4, 136.3,

135.9, 132.8, 132.3, 130.8, 130.3, 129.2, 128.5, 128.3, 127.5, 124.1, 122.2, 122.1, 120.4, 25.0, 16.0. **HRMS** (EI) calcd. for $[C_{14}H_{12}ClN]^{\bullet+}$ ($[M]^{\bullet+}$), m/z = 229.0653, found: 229.0628. **IR** (ATR, neat) $\tilde{\nu}$ / cm^{-1} = 3049, 3001, 2971, 2915, 1700, 1584, 1491, 1431, 1092, 872, 816, 775, 746.

2-(1-Phenylprop-1-en-2-yl)naphthalene (1a^{ci})

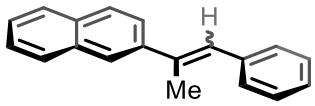

1a^{ci}

General procedure **B**: Benzyltriphenylphosphonium bromide (4.8 g, 11 mmol, 1.1 equiv.), dry THF (45 mL, 0.20 M), LDA solution (1.42 M, 7.75 mL, 11.0 mmol, 1.10 equiv.), and 2-acetonaphthone (1.70 g, 10.0 mmol) in 5.0 mL dry THF were used. Purification with silica gel column chromatography (hexanes:EtOAc = 40:1) afforded an *E*/*Z*-mixture of stilbene **1a^{ci}** (*E*:*Z* = 63:37, 1.96 g, 8.01 mmol, 80%) as a white solid. Assignments to each isomer are based on analogy to stilbene **1a**.

m.p. 126.8 °C. **TLC** R_f = 0.55 (hexanes:EtOAc = 19:1). **^{1}H NMR** (400 MHz, $CDCl_3$) δ / ppm = 8.00 (d, *J* = 1.4 Hz, 1H, *E*), 7.95–7.73 (m, 8H, *E*/*Z*), 7.59–7.42 (m, 9H, *E*/*Z*), 7.38–7.31 (m, 2H, *E*/*Z*), 7.15–7.09 (m, 2H, *E*/*Z*), 7.10–7.03 (m, 3H, *E*/*Z*), 6.66–6.61 (m, 1H, *Z*), 2.46 (d, *J* = 1.3 Hz, 3H, *E*), 2.36 (d, *J* = 1.5 Hz, 3H, *Z*). **^{13}C{^{1}H} NMR** (101 MHz, $CDCl_3$) δ = 141.2, 139.8, 138.5, 137.7, 137.3, 133.8, 133.6, 132.8, 132.6, 129.4, 129.2, 128.4, 128.3, 128.3, 128.1, 128.0, 128.0, 127.9, 127.8, 127.7, 127.2, 127.1, 126.8, 126.7, 126.3, 126.3, 126.0, 125.9, 125.9, 124.8, 124.5, 27.4, 17.6. **HRMS** (EI) calcd. for $[C_{19}H_{16}]^{\bullet+}$ ($[M]^{\bullet+}$), m/z = 244.1247, found: 244.1247. **IR** (ATR, neat) $\tilde{\nu}$ / cm^{-1} = 3056, 3027, 2967, 2933, 2855, 1595, 1491, 1438, 1129, 1275, 1182, 895, 857, 816, 746, 697.

2-(1-(*p*-Tolyl)prop-1-en-2-yl)naphthalene (1b^{ci})

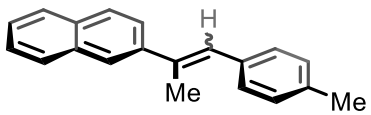

1b^{ci}

General procedure **B**: Phosphonium salt **S3** (4.43 g, 11.0 mmol, 1.10 equiv.), dry THF (45 mL, 0.20 M), LDA solution (1.42 M, 7.75 mL, 11.0 mmol, 1.10 equiv.), and 2-acetonaphthone (1.70 g, 10.0 mmol) in 5.0 mL dry THF were used. Purification with silica gel column chromatography (hexanes:EtOAc = 40:1) afforded an *E*/*Z*-mixture of stilbene **1b^{ci}** (*E*:*Z* = 65:35, 1.90 g, 7.36 mmol, 74%) as a white solid. Assignments to each isomer are based on analogy to stilbene **1a**.

m.p. 109.8 °C. **TLC** R_f = 0.58 (hexanes:EtOAc = 19:1). **^{1}H NMR** (400 MHz, $CDCl_3$) δ / ppm = 7.99 (d, *J* = 1.3 Hz, 1H, *E*), 7.93–7.80 (m, 5H, *E*/*Z*), 7.77 (dd, *J* = 8.5, 1.6 Hz, 3H, *E*/*Z*), 7.58–7.44

(m, 4H, *E*/*Z*), 7.43–7.31 (m, 3H, *E*/*Z*), 7.26 (s, 3H, *E*/*Z*), 7.04 (s, 1H, *E*), 6.93 (s, 3H, *E*/*Z*), 6.64–6.55 (m, 1H, *Z*), 2.45 (d, *J* = 1.3 Hz, 3H, *E*), 2.44 (s, 3H, *E*), 2.34 (d, *J* = 1.4 Hz, 3H, *Z*), 2.27 (s, 3H, *Z*). **^{13}C{^{1}H} NMR** (101 MHz, $CDCl_3$) δ = 141.4, 140.0, 137.6, 136.6, 136.4, 136.0, 135.6, 134.7, 133.8, 133.6, 132.8, 132.6, 129.3, 129.1, 129.0, 128.8, 128.3, 128.3, 128.1, 128.0, 127.9, 127.8, 127.7, 127.3, 127.0, 126.7, 126.3, 126.0, 125.8, 125.8, 124.8, 124.6, 27.4, 21.4, 21.2, 17.6. **HRMS** (EI) calcd. for $[C_{20}H_{18}]^{\bullet+}$ ($[M]^{\bullet+}$), m/z = 258.1403, found: 258.1409. **IR** (ATR, neat) $\tilde{\nu}$ / cm^{-1} = 3056, 3027, 2967, 2933, 2855, 1595, 1491, 1438, 1129, 1275, 1182, 895, 857, 816, 746, 697.

2-(1-(4-Methoxyphenyl)prop-1-en-2-yl)naphthalene (1c^{ci})

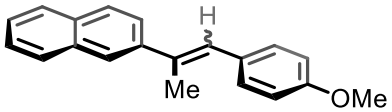

1c^{ci}

General procedure **B**: Phosphonium salt **S4** (4.61 g, 11.0 mmol, 1.10 equiv.), dry THF (45 mL, 0.20 M), LDA solution (2.06 M, 5.34 mL, 11.0 mmol, 1.10 equiv.), and 2-acetonaphthone (1.70 g, 10.0 mmol) in 5.0 mL dry THF were used. Purification with silica gel column chromatography (hexanes:EtOAc = 30:1) afforded an *E*/*Z*-mixture of stilbene **1c^{ci}** (*E*:*Z* = 70:30, 795 mg, 2.90 mmol, 29%) as a white solid. Assignments to each isomer are based on analogy to stilbene **1a**.

m.p. 125.2 °C. **TLC** R_f = 0.38 (hexanes:EtOAc = 19:1). **^{1}H NMR** (400 MHz, $CDCl_3$) δ / ppm = 7.95–7.93 (m, 1H, *E*), 7.90–7.71 (m, 8H, *E*/*Z*), 7.53–7.43 (m, 4H, *E*/*Z*), 7.38 (d, *J* = 8.5 Hz, 2H, *E*), 7.31 (dd, *J* = 8.4, 1.7 Hz, 1H, *Z*), 6.97 (s, 2H, *E*), 6.96–6.91 (m, 3H, *E*/*Z*), 6.66–6.60 (m, 2H, *Z*), 6.53 (s, 1H, *Z*), 3.86 (s, 3H, *E*), 3.71 (s, 3H, *Z*), 2.41 (d, *J* = 1.2 Hz, 3H, *E*), 2.30 (d, *J* = 1.5 Hz, 3H, *Z*). **^{13}C{^{1}H} NMR** (101 MHz, $CDCl_3$) δ = 158.4, 158.1, 141.5, 140.1, 136.6, 135.8, 133.8, 133.7, 132.7, 132.6, 131.1, 130.6, 130.3, 130.3, 128.3, 128.1, 128.0, 128.0, 127.9, 127.8, 127.7, 127.3, 126.7, 126.5, 126.3, 126.0, 125.8, 125.8, 124.7, 124.6, 113.8, 113.5, 55.4, 55.2, 27.3, 17.6. **HRMS** (EI) calcd. for $[C_{20}H_{18}O]^{\bullet+}$ ($[M]^{\bullet+}$), m/z = 274.1352, found: 274.1349. **IR** (ATR, neat) $\tilde{\nu}$ / cm^{-1} = 3056, 2967, 2837, 1607, 1573, 1506, 1461, 1297, 1252, 1178, 1111, 1033, 861, 828, 746.

2-(1-(4-Fluorophenyl)prop-1-en-2-yl)naphthalene (1n^{ci})

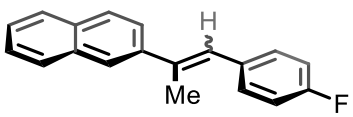

1n^{ci}

General procedure **B**: Phosphonium salt **S5** (4.48 g, 11.0 mmol, 1.10 equiv.), dry THF (45 mL, 0.20 M), LDA solution (1.42 M, 7.75 mL, 11.0 mmol, 1.10 equiv.), and 2-acetonaphthone (1.70 g, 10.0 mmol) in 5.0 mL dry THF were used. Purification with silica gel column chromatography (hexanes:EtOAc = 40:1) afforded an *E*/*Z*-mixture of stilbene **1n^{ci}**

(*E*:*Z* = 57:43, 1.57 g, 5.99 mmol, 60%) as a white solid. Assignments to each isomer are based on analogy to stilbene **1a**.

m.p. 139.3 °C. **TLC** R_f = 0.55 (hexanes:EtOAc = 19:1). **^{1}H NMR** (400 MHz, $CDCl_3$) δ / ppm = 7.99–7.95 (m, 1H, *E*), 7.93–7.71 (m, 8H, *E*/*Z*), 7.52 (ddd, *J* = 9.5, 5.6, 2.5 Hz, 4H, *E*/*Z*), 7.41 (dd, *J* = 8.5, 5.6 Hz, 2H, *E*/*Z*), 7.34–7.27 (m, 1H, *E*), 7.17–7.09 (m, 2H, *E*/*Z*), 7.03–6.95 (m, 3H, *E*/*Z*), 6.84–6.76 (m, 2H, *Z*), 6.57 (s, 1H, *Z*), 2.41 (d, *J* = 1.1 Hz, 3H, *E*), 2.33 (d, *J* = 1.4 Hz, 3H, *Z*). **^{13}C{^{1}H} NMR** (101 MHz, $CDCl_3$) δ = 161.6 (d, *J* = 246.2 Hz), 161.3 (d, *J* = 246.2 Hz), 141.0, 139.5, 138.4 (d, *J* = 1.8 Hz), 137.3 (d, *J* = 1.3 Hz), 134.5 (d, *J* = 3.6 Hz), 133.7, 133.7 (d, *J* = 3.7 Hz), 133.6, 132.8, 132.6, 130.9, 130.8, 130.7, 130.6, 128.3, 128.1, 128.0, 128.0, 127.8, 127.7, 127.2, 127.0, 126.8, 126.4, 126.2, 126.0, 126.0, 125.9, 124.9, 124.5, 115.2 (d, *J* = 21.0 Hz), 114.9 (d, *J* = 21.0 Hz), 27.2, 17.5. **^{19}F{^{1}H} NMR** (377 MHz, $CDCl_3$) δ = −115.9, −116.3. **HRMS** (EI) calcd. for $[C_{19}H_{15}F]^{\bullet+}$ ($[M]^{\bullet+}$), m/z = 262.1152, found: 262.1148. **IR** (ATR, neat) $\tilde{\nu}$ / cm^{-1} = 3056, 2967, 2933, 2855, 1599, 1506, 1435, 1223, 1156, 898, 857, 820, 783, 738.

1-Methyl-2-(1-phenylprop-1-en-2-yl)benzene (1z^{ci})

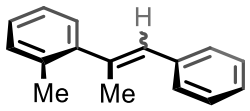

1z^{ci}

General procedure **B**: Benzyltriphenylphosphonium bromide (4.77 g, 11.0 mmol, 1.10 equiv.), dry THF (45 mL, 0.20 M), LDA solution (1.40 M, 7.86 mL, 11.0 mmol, 1.10 equiv.), and 2'-methylacetophenone (1.32 mL, 10.0 mmol) in 5.0 mL dry THF were used. Purification with silica gel column chromatography (hexanes:EtOAc = 40:1) afforded an *E*/*Z*-mixture of stilbene **1z^{ci}** (*E*:*Z* = 40:60, 507 mg, 2.43 mmol, 24%) as a yellow oil. Assignments to each isomer are based on analogy to stilbene **1a**.

TLC R_f = 0.60 (hexanes:EtOAc = 19:1). **^{1}H NMR** (400 MHz, $CDCl_3$) δ / ppm = 8.04 (d, *J* = 4.5 Hz, 4H, *E*/*Z*), 7.95–7.88 (m, 2H, *Z*), 7.88–7.80 (m, 8H, *E*/*Z*), 7.77–7.68 (m, 2H, *E*/*Z*), 7.52–7.47 (m, 2H, *E*), 7.13 (s, 1H, *E*), 7.04 (s, 1H, *Z*), 3.02 (s, 3H, *Z*), 2.85 (d, *J* = 1.3 Hz, 3H, *Z*), 2.80 (d, *J* = 1.2 Hz, 3H, *E*), 2.79 (s, 3H, *E*). **^{13}C{^{1}H} NMR** (101 MHz, $CDCl_3$) δ = 145.9, 142.2, 139.2, 138.6, 138.2, 137.7, 134.9, 134.7, 130.5, 130.3, 129.3, 129.1, 128.6, 128.4, 128.4, 128.1, 128.0, 127.1, 127.1, 127.0, 126.6, 126.5, 126.3, 125.8, 27.6, 20.1, 20.0, 19.3. **HRMS** (EI) calcd. for $[C_{16}H_{16}]^{\bullet+}$ ($[M]^{\bullet+}$), m/z = 208.1247, found: 208.1248. **IR** (ATR, neat) $\tilde{\nu}$ / cm^{-1} = 3060, 3023, 2967, 2930, 2859, 1737, 1599, 1491, 14433, 1375, 1238, 1044, 917, 865, 760, 727, 697.

1-Chloro-4-(1-phenylprop-1-en-2-yl)benzene (1s')

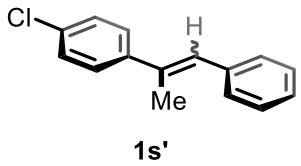

1s'

General procedure **B**: Benzyltriphenylphosphonium bromide (4.77 g, 11.0 mmol, 1.10 equiv.), dry THF (45 mL, 0.20 M), LDA solution (0.83 M, 13 mL, 11 mmol, 1.1 equiv.), and 4'-chloroacetophenone (1.30 mL, 10.0 mmol) in 5.0 mL dry THF were used. Purification with silica gel column chromatography (hexanes:EtOAc = 40:1) afforded an *E*/*Z*-mixture of stilbene **1s'** (*E*:*Z* = 57:43, 2.11 g, 9.23 mmol, 92%) as a white semi-solid. Assignments to each isomer are based on analogy to stilbene **1a**.

TLC R_f = 0.58 (hexanes:EtOAc = 19:1). **^{1}H NMR** (400 MHz, $CDCl_3$) δ / ppm = 7.61–7.55 (m, 2H, *E*), 7.55–7.44 (m, 7H, *E*/*Z*), 7.43–7.34 (m, 3H, *E*/*Z*), 7.29–7.20 (m, 4H, *E*/*Z*), 7.13–7.07 (m, 2H, *Z*), 6.96 (s, 1H, *E*), 6.63 (s, 1H, *Z*), 2.39 (d, *J* = 1.3 Hz, 3H, *E*), 2.32 (d, *J* = 1.5 Hz, 3H, *Z*). **^{13}C{^{1}H} NMR** (101 MHz, $CDCl_3$) δ = 142.4, 140.5, 138.1, 137.4, 137.4, 136.3, 133.0, 132.8, 129.8, 129.3, 129.1, 128.8, 128.5, 128.4, 128.2, 128.1, 127.4, 126.8, 126.5, 26.9, 17.5. **HRMS** (EI) calcd. for $[C_{15}H_{13}Cl]^{\bullet+}$ ($[M]^{\bullet+}$), m/z = 228.0700, found: 228.0702. **IR** (ATR, neat) $\tilde{\nu}$ / cm^{-1} = 3057, 3023, 2967, 2915, 2855, 1897, 1595, 1491, 1439, 1402, 1178, 1092, 1014, 917, 857, 820, 746, 697.

5.2.4 Diarylmethane-Synthesis via MTW

Ketones **2d–m**, **2p–y**, **2a'–g'**, **2m'**, **2o'**, ***ent*-2r**, ***ent*-2s**, and ***ent*-2y** were synthesized by S. Park according to the procedure below.[165,229] Ketones **2r'**, **2t'**, and ***ent*-2t'** were synthesized by J. Flügel according to the procedure below.[217,230]

General procedure **C** (asymmetric migratory TSUJI–WACKER oxidation): A 100 mL round-bottom flask equipped with a cross-shaped stirring bar, was charged with a stilbene (indicated *E*/*Z*-ratio, 1 or 2 mmol, 1 equiv.), selenium catalyst **3d** (10 mol%), and TAPT (5 mol%). A 3:1:1 volumetric ratio of HFIP, DCE, and H_2O (10 or 20 mL in total, 0.10 M) was added. The flask was sealed with a rubber septum and equipped with needles for air supply. The solution was stirred with 550 rpm under irradiation of blue light (447 nm) at 0 °C for a certain amount of time to achieve full consumption of the stilbene. While not being fully dissolved at the beginning, the stilbene was consumed over time during irradiation. The solvent of the crude mixture was removed under reduced pressure, and the residue was purified by silica gel column chromatography to afford the target ketone. Unsuccessful attempts (Table 4) followed this exact procedure (1 mmol scale).

For determination of retention times for chiral HPLC analysis, the respective stilbene (0.5 mmol, 1 equiv.), (2-anisylSe)$_2$ (18 mg, 50 μmol, 10 mol%), and TAPT (12 mg, 25 μmol, 5.0 mol%) in a

3:1:1 volumetric ratio of HFIP, DCE, and H_2O (5 mL in total, 0.1 M) were used under otherwise identical conditions.

(*R*)-1-(Naphthalen-2-yl)-1-phenylpropan-2-one (2a)

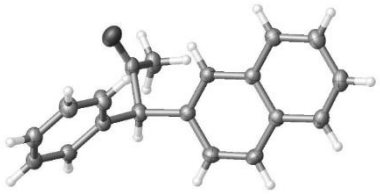

General procedure **C**: Stilbene **1a** (*E*:*Z* = 58:42, 244 mg, 1.00 mmol), selenium catalyst **3d** (82 mg, 0.10 mmol, 10 mol%), TAPT (24 mg, 50 μmol, 5.0 mol%), and HFIP, DCE, and H_2O (3:1:1, 10 mL in total, 0.10 M) were used. Reaction time was 8 h. Purification with silica gel column chromatography (hexanes:EtOAc = 20:1) afforded ketone **2a** (220 mg, 850 μmol, 85%, 81% ee) as an ivory solid. Recrystallization from boiling *n*-hexane afforded a colorless prism-shaped crystal, allowing X-ray analysis to determine the **2a**'s absolute configuration to be *R*.

m.p. 102.3 °C (recryst.). **TLC** R_f = 0.25 (hexanes:EtOAc = 20:1). **^{1}H NMR** (400 MHz, $CDCl_3$) δ / ppm = 7.92–7.82 (m, 3H), 7.76 (s, 1H), 7.57–7.49 (m, 2H), 7.46–7.39 (m, 3H), 7.38–7.32 (m, 3H), 5.36 (s, 1H), 2.35 (s, 3H). **^{13}C{^{1}H} NMR** (101 MHz, $CDCl_3$) δ / ppm = 206.5, 138.3, 135.9, 133.5, 132.6, 129.1, 128.8, 128.5, 127.9, 127.7, 127.7, 127.4, 127.2, 126.3, 126.1, 65.0, 30.2. **HRMS** (EI) calcd. for $[C_{19}H_{16}O]^{\bullet+}$ ($[M]^{\bullet+}$), m/z = 260.1201, obs.: 260.1203. **IR** (ATR, neat) $\tilde{\nu}$ / cm^{-1} = 3056, 1715, 1599, 1495, 1357, 1156, 816, 746, 701. **HPLC** (IC-3, *n*-hexane:*i*-PrOH 95:5, flow rate 0.8 mL/min, 220 nm, 25 °C) t_R = 16.444 min (90.5%), 18.711 min (9.5%). **Optical Rotation** $[\alpha]_D^{20}$ = −60.0 (*c* = 0.985, $CHCl_3$). **X-ray** CCDC: 2333303.

(*S*)-1-(Naphthalen-2-yl)-1-phenylpropan-2-one (*ent*-2a)

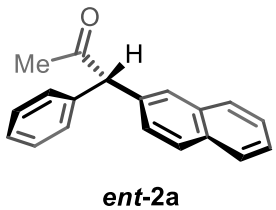

***ent*-2a**

General procedure **C**: Stilbene **1a^{ci}** (*E*:*Z* = 63:37, 244 mg, 1.00 mmol), selenium catalyst **3d** (82 mg, 0.10 mmol, 10 mol%), TAPT (24 mg, 50 μmol, 5.0 mol%), and HFIP, DCE, and H_2O (3:1:1, 10 mL in total, 0.10 M) were used. Reaction time was 8 h. Purification with silica gel column chromatography (hexanes:EtOAc:DCM = 40:1:20) afforded inversed ketone ***ent*-2a** (224 mg, 860 μmol, 86%, −82% ee) as an ivory solid. Determination of absolute configuration is based on analogy to ketone **2a**.

m.p. 102.3 °C. **TLC** R_f = 0.54 (hexanes:EtOAc:DCM = 40:1:20). **^{1}H NMR** (400 MHz, $CDCl_3$) δ / ppm = 7.85–7.75 (m, 3H), 7.67 (s, 1H), 7.51–7.44 (m, 2H), 7.41–7.32 (m, 3H), 7.31–7.26 (m, 3H), 5.29 (s, 1H), 2.30 (s, 2H). **^{13}C{^{1}H} NMR** (101 MHz, $CDCl_3$) δ / ppm = 206.7, 138.4, 135.9,

133.6, 132.7, 129.2, 128.9, 128.6, 128.0, 127.8, 127.8, 127.5, 127.3, 126.4, 126.2, 65.2, 30.4. Analytical data regarding **HRMS** and **IR** is identical to that of compound **2a**. **HPLC** (IC-3, *n*-hexane:*i*-PrOH 95:5, flow rate 0.8 mL/min, 220 nm, 25 °C) t_R = 15.889 min (9.1%), 17.962 min (90.9%). **Optical Rotation** $[\alpha]_D^{20}$ = +46.7 (*c* = 1.0, $CHCl_3$).

(*R*)-1-(Naphthalen-2-yl)-1-(*p*-tolyl)propan-2-one (2b)

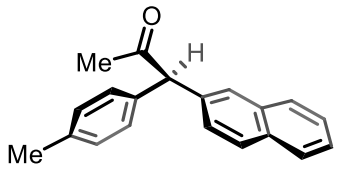

2b

General procedure **C**: Stilbene **1b** (*E*:*Z* = 51:49, 258 mg, 1.00 mmol), selenium catalyst **3d** (82 mg, 0.10 mmol, 10 mol%), TAPT (24 mg, 50 µmol, 5.0 mol%), and HFIP, DCE, and H_2O (3:1:1, 10 mL in total, 0.10 M) were used. Reaction time was 7 h. Purification with silica gel column chromatography (hexanes:EtOAc = 20:1) afforded ketone **2b** (229 mg, 830 µmol, 83%, 85% ee) as a yellow oil. Determination of absolute configuration is based on analogy to ketone **2a**.

TLC R_f = 0.10 (hexanes:EtOAc = 19:1). **^{1}H NMR** (400 MHz, $CDCl_3$) δ / ppm = 7.84–7.76 (m, 3H), 7.66 (s, 1H), 7.50–7.43 (m, 2H), 7.36 (dd, *J* = 8.5, 1.7 Hz, 1H), 7.17 (s, 4H), 5.26 (s, 1H), 2.34 (s, 3H), 2.29 (s, 3H). **^{13}C{^{1}H} NMR** (101 MHz, $CDCl_3$) δ / ppm = 206.9, 137.2, 136.2, 135.3, 133.6, 132.6, 129.6, 129.1, 128.5, 128.0, 127.7, 127.7, 127.3, 126.3, 126.1, 64.9, 30.3, 21.2. **HRMS** (EI) calcd. for $[C_{20}H_{18}O]^{\bullet+}$ ($[M]^{\bullet+}$), m/z = 274.1352, found: 274.1346. **IR** (ATR, neat) $\tilde{\nu}$ / cm^{-1} = 3053, 3023, 2922, 1715, 1603, 1510, 1353, 1156, 816, 746. **HPLC** (ID-3, *n*-hexane:*i*-PrOH 95:5, flow rate 0.8 mL/min, 254 nm, 25 °C) t_R = 10.347 min (92.3%), 11.449 min (7.7%). **Optical Rotation** $[\alpha]_D^{20}$ = −27.8 (*c* = 1.0, $CHCl_3$).

(*S*)-1-(Naphthalen-2-yl)-1-(*p*-tolyl)propan-2-one (*ent*-2b)

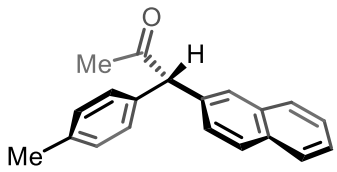

***ent*-2b**

General procedure **C**: Stilbene **1b**[ci] (*E*:*Z* = 65:35, 258 mg, 1.00 mmol), selenium catalyst **3d** (82 mg, 0.10 mmol, 10 mol%), TAPT (24 mg, 50 µmol, 5.0 mol%), and HFIP, DCE, and H_2O (3:1:1, 10 mL in total, 0.10 M) were used. Reaction time was 12 h. Purification with silica gel column chromatography (hexanes:EtOAc:DCM = 40:1:20) afforded inversed ketone ***ent*-2b** (168 mg, 610 µmol, 61%, −73% ee) as a yellow oil. Determination of absolute configuration is based on analogy to ketone **2a**.

TLC R_f = 0.10 (hexanes:EtOAc = 19:1). **^{1}H NMR** (400 MHz, $CDCl_3$) δ / ppm = 7.84–7.76 (m, 3H), 7.65 (s, 1H), 7.49–7.43 (m, 2H), 7.35 (dd, *J* = 8.5, 1.8 Hz, 1H), 7.16 (s, 4H), 5.25 (s, 1H), 2.33

(s, 3H), 2.29 (s, 3H). **^{13}C{^{1}H} NMR** (101 MHz, $CDCl_3$) δ / ppm = 206.9, 137.2, 136.2, 135.3, 133.6, 132.6, 129.6, 129.1, 128.5, 128.0, 127.7, 127.7, 127.3, 126.3, 126.1, 64.9, 30.3, 21.2. Analytical data regarding **HRMS** and **IR** is identical to that of compound **2b**. **HPLC** (ID-3, *n*-hexane:*i*-PrOH 95:5, flow rate 0.8 mL/min, 254 nm, 25 °C) t_R = 10.409 min (13.5%), 11.364 min (86.5%). **Optical Rotation** $[\alpha]_D^{20}$ = +25.0 (*c* = 1.0, $CHCl_3$).

(*R*)-1-(4-Methoxyphenyl)-1-(naphthalen-2-yl)propan-2-one (2c)

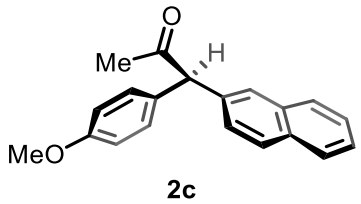

2c

General procedure **C**: Stilbene **1c** (*E*:*Z* = 49:51, 274 mg, 1.00 mmol), selenium catalyst **3d** (82 mg, 0.10 mmol, 10 mol%), TAPT (24 mg, 50 μmol, 5.0 mol%), and HFIP, DCE, and H_2O (3:1:1, 10 mL in total, 0.10 M) were used. Reaction time was 6 h. Purification with silica gel column chromatography (hexanes:THF = 10:1) afforded ketone **2c** (170 mg, 590 μmol, 59%, 93% ee) as a yellow oil. Determination of absolute configuration is based on analogy to ketone **2a**.

TLC R_f = 0.18 (hexanes:THF = 10:1). **^{1}H NMR** (400 MHz, $CDCl_3$) δ / ppm = 7.86–7.76 (m, 3H), 7.66 (s, 1H), 7.51–7.45 (m, 2H), 7.36 (dd, *J* = 8.5, 1.8 Hz, 1H), 7.25–7.17 (m, 2H), 6.95–6.87 (m, 2H), 5.25 (s, 1H), 3.80 (s, 3H), 2.30 (s, 3H). **^{13}C{^{1}H} NMR** (101 MHz, $CDCl_3$) δ / ppm = 207.0, 158.9, 136.3, 133.6, 132.6, 130.4, 130.3, 128.5, 128.0, 127.7, 127.6, 127.2, 126.3, 126.1, 64.4, 55.4, 30.2. **HRMS** (EI) calcd. for $[C_{20}H_{18}O_2]^{\bullet+}$ ($[M]^{\bullet+}$), m/z = 290.1301, found: 290.1302. **IR** (ATR, neat) $\tilde{\nu}$ / cm^{-1} = 3053, 3001, 2956, 2837, 1711, 1607, 1510, 1461, 1353, 1305, 1249, 1178, 1033, 813, 746. **HPLC** (IC-3, *n*-hexane:*i*-PrOH 90:10, flow rate 0.8 mL/min, 254 nm, 25 °C) t_R = 20.200 min (3.8%), 23.276 min (96.2%). **Optical Rotation** $[\alpha]_D^{20}$ = −26.9 (*c* = 1.0, $CHCl_3$).

(*S*)-1-(4-Methoxyphenyl)-1-(naphthalen-2-yl)propan-2-one (*ent*-2c)

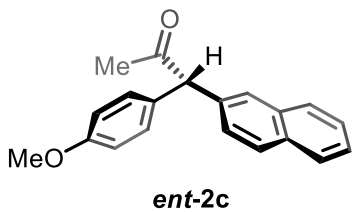

***ent*-2c**

General procedure **C**: Stilbene **1c^{ci}** (*E*:*Z* = 70:30, 274 mg, 1.00 mmol), selenium catalyst **3d** (82 mg, 0.10 mmol, 10 mol%), TAPT (24 mg, 50 μmol, 5.0 mol%), and HFIP, DCE, and H_2O (3:1:1, 10 mL in total, 0.10 M) were used. Reaction time was 6 h. Purification with silica gel column chromatography (hexanes:THF = 9:1) afforded inversed ketone ***ent*-2c** (230 mg, 790 μmol, 79%, −69% ee) as a yellow oil. Determination of absolute configuration is based on analogy to ketone **2a**.

TLC R_f = 0.23 (hexanes:THF = 9:1). **^{1}H NMR** (400 MHz, $CDCl_3$) δ / ppm = 7.85–7.77 (m, 3H), 7.66 (s, 1H), 7.51–7.44 (m, 2H), 7.36 (dd, *J* = 8.5, 1.8 Hz, 1H), 7.23–7.18 (m, 2H), 6.93–6.87 (m, 2H), 5.25 (s, 1H), 3.80 (s, 3H), 2.30 (s, 3H). **^{13}C{^{1}H} NMR** (101 MHz, $CDCl_3$) δ / ppm = 207.3, 159.3, 136.6, 133.9, 132.9, 130.7, 130.6, 128.8, 128.3, 128.0, 127.9, 127.5, 126.7, 126.4, 114.6, 64.7, 55.7, 30.5. Analytical data regarding **HRMS** and **IR** is identical to that of compound **2c**. **HPLC** (IC-3, *n*-hexane:*i*-PrOH 90:10, flow rate 0.8 mL/min, 254 nm, 25 °C) t_R = 20.033 min (84.7%), 23.151 min (15.3%). **Optical Rotation** $[\alpha]_D^{20}$ = +21.3 (*c* = 1.0, $CHCl_3$).

(*R*)-1-(4-Fluorophenyl)-1-(naphthalen-2-yl)propan-2-one (2n)

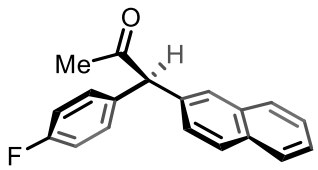

2n

General procedure **C**: Stilbene **1n** (*E*:*Z* = 54:46, 262 mg, 1.00 mmol), selenium catalyst **3d** (82 mg, 0.10 mmol, 10 mol%), TAPT (24 mg, 50 μmol, 5.0 mol%), and HFIP, DCE, and H_2O (3:1:1, 10 mL in total, 0.10 M) were used. Reaction time was 7 h. Purification with silica gel column chromatography (hexanes:EtOAc = 20:1) afforded ketone **2n** (246 mg, 880 μmol, 88%, 81% ee) as a yellow oil. Determination of absolute configuration is based on analogy to ketone **2a**.

TLC R_f = 0.13 (hexanes:EtOAc = 19:1). **^{1}H NMR** (400 MHz, $CDCl_3$) δ / ppm = 7.86–7.78 (m, 3H), 7.68 (s, 1H), 7.55–7.45 (m, 2H), 7.35 (dd, *J* = 8.5, 1.8 Hz, 1H), 7.28–7.20 (m, 2H), 7.08–7.00 (m, 2H), 5.28 (s, 1H), 2.30 (s, 3H). **^{13}C{^{1}H} NMR** (101 MHz, $CDCl_3$) δ / ppm = 206.8, 163.7, 161.2, 136.0, 134.5 (d, *J* = 3.3 Hz), 133.9, 133.0, 131.1 (d, *J* = 8.0 Hz), 129.1, 128.3, 128.1 (d, *J* = 7.7 Hz), 127.3, 126.8, 126.6, 116.0 (d, *J* = 21.4 Hz), 64.6, 30.6. **^{19}F{^{1}H} NMR** (377 MHz, $CDCl_3$) δ / ppm = −115.8. **HRMS** (EI) calcd. for $[C_{19}H_{15}FO]^{\bullet+}$ ($[M]^{\bullet+}$), m/z = 278.1101, found: 278.1095. **IR** (ATR, neat) $\tilde{\nu}$ / cm^{-1} = 3056, 2919, 1715, 1603, 1506, 1420, 1357, 1223, 1156, 1096, 1018, 816, 746. **HPLC** (ID-3, *n*-hexane:*i*-PrOH 95:5, flow rate 0.6 mL/min, 254 nm, 25 °C) t_R = 12.831 min (90.4%), 13.499 min (9.6%). **Optical Rotation** $[\alpha]_D^{20}$ = −103.6 (*c* = 1.0, $CHCl_3$).

(*S*)-1-(4-Fluorophenyl)-1-(naphthalen-2-yl)propan-2-one (*ent*-2n)

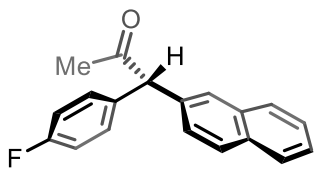

***ent*-2n**

General procedure **C**: Stilbene **1n^{ci}** (*E*:*Z* = 57:43, 262 mg, 1.00 mmol), selenium catalyst **3d** (82 mg, 0.10 mmol, 10 mol%), TAPT (24 mg, 50 μmol, 5.0 mol%), and HFIP, DCE, and H_2O (3:1:1, 10 mL in total, 0.10 M) were used. Reaction time was 10 h. Purification with silica gel column chromatography (hexanes:EtOAc = 20:1) afforded inversed

ketone ***ent*-2n** (134 mg, 480 µmol, 48%, −81% ee) as a yellow oil. Determination of absolute configuration is based on analogy to ketone **2a**.

TLC R_f = 0.13 (hexanes:EtOAc = 19:1). **^{1}H NMR** (400 MHz, $CDCl_3$) δ / ppm = 7.86–7.78 (m, 3H), 7.66 (s, 1H), 7.52–7.45 (m, 2H), 7.34 (dd, *J* = 8.5, 1.8 Hz, 1H), 7.26–7.20 (m, 2H), 7.07–7.00 (m, 2H), 5.27 (s, 1H), 2.30 (s, 3H). **^{13}C{^{1}H} NMR** (101 MHz, $CDCl_3$) δ / ppm = 206.5, 163.4, 160.9, 135.7, 134.2 (d, *J* = 3.3 Hz), 133.6, 132.7, 130.8 (d, *J* = 8.0 Hz), 128.8, 128.0, 127.8 (d, *J* = 7.4 Hz), 127.0, 126.5, 126.4, 115.7 (d, *J* = 21.5 Hz), 64.3, 30.3. **^{19}F{^{1}H} NMR** (377 MHz, $CDCl_3$) δ / ppm = −115.8. Analytical data regarding **HRMS** and **IR** is identical to that of compound **2n**. **HPLC** (ID-3, *n*-hexane:*i*-PrOH 95:5, flow rate 0.6 mL/min, 254 nm, 25 °C) t_R = 12.718 min (9.3%), 13.266 min (90.7%). **Optical Rotation** $[\alpha]_D^{20}$ = +103.6 (*c* = 1.0, $CHCl_3$).

(*R*)-1-(4-Chlorophenyl)-1-(naphthalen-2-yl)propan-2-one (2o)

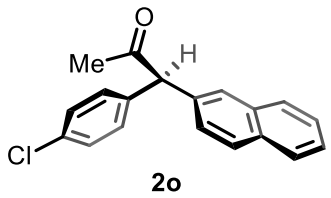

2o

General procedure **C**: Stilbene **1o** (*E*:*Z* = 57:43, 279 mg, 1.00 mmol), selenium catalyst **3d** (82 mg, 0.10 mmol, 10 mol%), TAPT (24 mg, 50 µmol, 5.0 mol%), and HFIP, DCE, and H_2O (3:1:1, 10 mL in total, 0.10 M) were used. Reaction time was 8 h. Purification with silica gel column chromatography (hexanes:EtOAc = 20:1) afforded ketone **2o** (179 mg, 610 µmol, 61%, 69% ee) as a yellow oil. Determination of absolute configuration is based on analogy to ketone **2a**.

TLC R_f = 0.14 (hexanes:EtOAc = 19:1). **^{1}H NMR** (400 MHz, $CDCl_3$) δ / ppm = 7.87–7.79 (m, 3H), 7.68 (s, 1H), 7.50 (quint, *J* = 5.2 Hz, 2H), 7.36–7.30 (m, 3H), 7.21 (d, *J* = 8.4 Hz, 2H), 5.27 (s, 1H), 2.31 (s, 3H). **^{13}C{^{1}H} NMR** (101 MHz, $CDCl_3$) δ / ppm = 206.2, 136.9, 135.4, 133.5, 133.4, 132.7, 130.5, 128.9, 128.9, 128.0, 127.8, 127.7, 127.0, 126.6, 126.4, 64.4, 30.3. **HRMS** (APCI) calcd. for $[C_{19}H_{15}ClO+NH_4]^+$ ($[M+NH_4]^+$), m/z = 312.1150, found: 312.1155. **IR** (ATR, neat) $\tilde{\nu}$ / cm^{-1} = 3056, 2922, 1715, 1599, 1491, 1409, 1353, 1271, 1156, 1092, 1014, 958, 813, 746. **HPLC** (ID-3, *n*-hexane:*i*-PrOH 95:5, flow rate 0.8 mL/min, 254 nm, 25 °C) t_R = 9.796 min (84.7%), 11.309 min (15.3%). **Optical Rotation** $[\alpha]_D^{20}$ = −83.8 (*c* = 1.0, $CHCl_3$).

(*R*)-1-Phenyl-1-(o-tolyl)propan-2-one (2z)

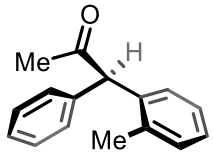

2z

General procedure **C**: Stilbene **1z** (*E*:*Z* = 42:58, 208 mg, 1.00 mmol), selenium catalyst **3d** (82 mg, 0.10 mmol, 10 mol%), TAPT (24 mg, 50 μmol, 5.0 mol%), and HFIP, DCE, and H_2O (3:1:1, 10 mL in total, 0.10 M) were used. Reaction time was 11 h. Purification with silica gel column chromatography (hexanes:EtOAc = 20:1) afforded ketone **2z** (145 mg, 650 μmol, 65%, 89% ee) as a colorless oil. Determination of absolute configuration is based on analogy to ketone **2a**.

TLC R_f = 0.15 (hexanes:EtOAc = 20:1). **^{1}H NMR** (400 MHz, $CDCl_3$) δ / ppm = 7.36–7.31 (m, 2H), 7.30–7.26 (m, 1H), 7.23–7.18 (m, 3H), 7.17–7.14 (m, 2H), 7.08–7.04 (m, 1H), 5.28 (s, 1H), 2.30 (s, 3H), 2.25 (s, 3H). **^{13}C{^{1}H} NMR** (101 MHz, $CDCl_3$) δ / ppm = 206.9, 137.6, 136.9, 136.8, 131.0, 129.5, 128.7, 128.5, 127.5, 127.3, 126.4, 61.9, 30.3, 20.1. **HRMS** (EI) calcd. for $[C_{16}H_{16}O]^{\bullet+}$ ($[M]^{\bullet+}$), m/z = 224.1196, found: 224.1201. **IR** (ATR, neat) $\tilde{\nu}$ / cm^{-1} = 3004, 2915, 2837, 1715, 1607, 1510, 1461, 1353, 1305, 1249, 1178, 1111, 1036, 831, 775, 738, 701. **HPLC** (IC-3, *n*-hexane:*i*-PrOH 95:5, flow rate 0.8 mL/min, 220 nm, 25 °C) t_R = 11.426 min (5.6%), 13.316 min (94.4%). **Optical Rotation** $[\alpha]_D^{20}$ = −89.3 (*c* = 1.0, $CHCl_3$).

(*S*)-1-Phenyl-1-(*o*-tolyl)propan-2-one (*ent*-2z)

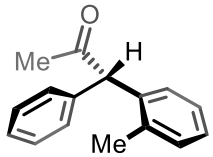

***ent*-2z**

General procedure **C**: Stilbene **1z^{ci}** (*E*:*Z* = 40:60, 208 mg, 1.00 mmol), selenium catalyst **3d** (82 mg, 0.10 mmol, 10 mol%), TAPT (24 mg, 50 μmol, 5.0 mol%), and HFIP, DCE, and H_2O (3:1:1, 10 mL in total, 0.10 M) were used. Reaction time was 11 h. Purification with silica gel column chromatography (hexanes:EtOAc = 20:1) afforded inversed ketone ***ent*-2z** (58.9 mg, 260 μmol, 26%, −84% ee) as a colorless oil. Determination of absolute configuration is based on analogy to ketone **2a**.

TLC R_f = 0.15 (hexanes:EtOAc = 19:1). **^{1}H NMR** (400 MHz, $CDCl_3$) δ / ppm = 7.47–7.41 (m, 2H), 7.40–7.35 (m, 1H), 7.30 (dt, *J* = 6.0, 3.0 Hz, 3H), 7.27–7.23 (m, 2H), 7.16 (dd, *J* = 5.2, 2.9 Hz, 1H), 5.38 (s, 1H), 2.40 (s, 3H), 2.35 (s, 3H). **^{13}C{^{1}H} NMR** (101 MHz, $CDCl_3$) δ / ppm = 206.9, 137.6, 136.9, 136.8, 131.0, 129.5, 128.7, 128.5, 127.5, 127.3, 126.4, 61.9, 30.3, 20.1. Analytical data regarding **HRMS** and **IR** is identical to that of compound **2z**. **HPLC** (IC-3, *n*-hexane:*i*-PrOH 95:5, flow rate 0.8 mL/min, 220 nm, 25 °C) t_R = 10.793 min (92.0%), 12.452 min (8.0%). **Optical Rotation** $[\alpha]_D^{20}$ = +71.3 (*c* = 1.0, $CHCl_3$).

(*S*)-1-(4-Chlorophenyl)-1-phenylpropan-2-one (2s')

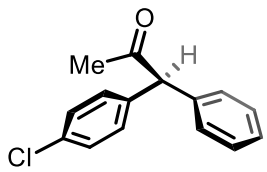

2s'

General procedure **C**: Stilbene **1s'** (*E*:*Z* = 57:43, 457 mg, 2.00 mmol), selenium catalyst **3d** (164 mg, 200 μmol, 10.0 mol%), TAPT (49 mg, 0.10 mmol, 5.0 mol%), and HFIP, DCE, and H_2O (3:1:1, 20 mL in total, 0.10 M) were used. Reaction time was 33 h. Purification with silica gel column chromatography (hexanes:EtOAc = 20:1) afforded ketone **2s'** (220 mg, 900 μmol, 45%, 88% ee) as a colorless oil. Determination of absolute configuration is based on analogy to ketone **2a**.

TLC R_f = 0.15 (hexanes:EtOAc = 19:1). **^{1}H NMR** (400 MHz, $CDCl_3$) δ / ppm = 7.35 (tt, *J* = 8.2, 1.8 Hz, 2H), 7.32–7.27 (m, 3H), 7.21 (dd, *J* = 7.1, 1.6 Hz, 2H), 7.17–7.13 (m, 2H), 5.08 (s, 1H), 2.24 (s, 3H). **^{13}C{^{1}H} NMR** (101 MHz, $CDCl_3$) δ = 206.1, 137.9, 137.0, 133.3, 130.4, 129.1, 129.0, 128.9, 127.7, 64.4, 30.2. **HRMS** (EI) calcd. for $[C_{15}H_{13}ClO]^{\bullet+}$ ($[M]^{\bullet+}$), m/z = 244.0649, found: 244.0645. **IR** (ATR, neat) $\tilde{\nu}$ / cm^{-1} = 3064, 3030, 1715, 1599, 1491, 1409, 1357, 1156, 1135, 1092, 1014, 813, 753, 701. **HPLC** (ID-3, *n*-hexane:*i*-PrOH 98:2, flow rate 0.8 mL/min, 220 nm, 25 °C) t_R = 8.963 min (94.0%), 9.342 min (6.0%). **Optical Rotation** $[\alpha]_D^{20} = -40.0$ (*c* = 1.0, $CHCl_3$).

5.2.5 Chiral Isotopomer Synthesis

The percentage of the major enantiomer of **2q'-*d*$_5$** can be calculated by using the following formula, with **x** being the percentage of the major enantiomer of **2q'-*d*$_5$** (in this case the *S*-enantiomer).

$$\frac{C^{\alpha,S}}{100}\mathrm{x} + \frac{C^{\alpha,R}}{100}(100 - \mathrm{x}) = C^{\beta,S} \qquad (5\text{-}1)$$

Since $C^{\alpha,S}$:$C^{\alpha,R}$ = 71.3:28.7 (from resolution of the α-center of **5q'-*d*$_5$** via chiral HPLC, Scheme 26) and $C^{\beta,S}$:$C^{\beta,R}$ = 67.5:32.5 (from resolution of the β-center of **5q'-*d*$_5$** in the quantitative ^{13}C NMR), the equation's solution is **x** = 91.1, which corresponds to an er value of 91.1:8.9 or an ee value of 82% for ketone **2q'-*d*$_5$**. As a control reaction, we exposed non-deuterated analogue of **2q'-*d*$_5$** (1,1-diphenylacetone) to the same CBS reduction conditions[208] and obtained almost the same isomer ratio from chiral HPLC (71.4:28.6), which excludes any potential influence of the deuterium atoms onto the ketone reduction compared to its protium analogue. All relevant compounds and their analytical data are listed below.

1-(1-Phenylprop-1-en-2-yl)benzene-2,3,4,5,6-*d*$_5$ (1q'-*d*$_5$)

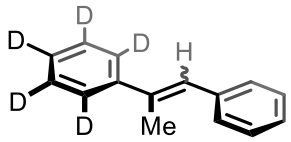

1q'-d_5

General procedure **B**: Benzyltriphenylphosphonium bromide (4.77 g, 11.0 mmol, 1.10 equiv.), dry THF (45 mL, 0.20 M), LDA solution (1.0 M, 11 mL, 11 mmol, 1.1 equiv.), and 1-(phenyl-d_5)ethan-1-one (1.17 mL, 10.0 mmol) in 5.0 mL dry THF were used. Purification with silica gel column chromatography (hexanes:EtOAc = 30:1) afforded an *E*/*Z*-mixture of stilbene **1q'-d_5** (*E*:*Z* = 53:47, 1.67 g, 8.38 mmol, 84%) as a white solid. Assignments to each isomer are based on analogy to stilbene **1a**.

m.p. 56.3 °C. **TLC** R_f = 0.55 (hexanes:EtOAc = 19:1). **^{1}H NMR** (400 MHz, $CDCl_3$) δ / ppm = 7.42 (m, 4H, *E*/*Z*), 7.33–7.26 (m, 1H, *Z*), 7.17–7.07 (m, 3H, *E*/*Z*), 7.02–6.97 (m, 2H, *E*/*Z*), 6.90 (d, *J* = 1.2 Hz, 1H, *E*), 6.52 (s, 1H, *Z*), 2.33 (d, *J* = 1.3 Hz, 3H, *E*), 2.25 (d, *J* = 1.5 Hz, 3H, *Z*). **^{13}C{^{1}H} NMR** (101 MHz, $CDCl_3$) δ = 143.9, 142.0, 138.8, 138.5, 137.8, 137.5, 129.3, 129.1, 128.3, 128.1 (d, *J* = 12.7 Hz), 128.0, 127.8, 127.7 (d, *J* = 7.7 Hz), 126.7, 126.6, 126.2, 125.7 (t, *J* = 22.7 Hz), 27.3, 17.6. **^{2}H NMR** (61 MHz, $CHCl_3$) δ / ppm = 7.65–7.19 (m, 5H). **HRMS** (EI) calcd. for $[C_{15}H_9D_5]^{\bullet+}$ ($[M]^{\bullet+}$), m/z = 199.1404, found: 199.1405. **IR** (ATR, neat) $\tilde{\nu}$ / cm^{-1} = 3056, 2967, 2915, 2274, 1599, 1495, 1439, 1375, 917, 861, 753, 731, 697.

(*S*)-1-Phenyl-1-(phenyl-d_5)propan-2-one (2q'-d_5)

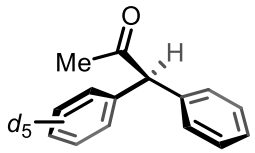

2q'-d_5

General procedure **C**: Stilbene **1q'-d_5** (*E*:*Z* = 53:47, 399 mg, 2.00 mmol), selenium catalyst **3d** (164 mg, 200 μmol, 10.0 mol%), TAPT (48.6 mg, 100 μmol, 5.00 mol%), and HFIP, DCE, and H_2O (3:1:1, 20 mL in total, 0.10 M) were used. Reaction time was 17 h. Purification with silica gel column chromatography (hexanes:EtOAc = 20:1) afforded ketone **2q'-d_5** (370 mg, 1.72 mmol, 86%, 82% ee) as a colorless oil. Determination of absolute configuration is based on analogy to ketone **2a**.

TLC R_f = 0.13 (hexanes:EtOAc = 19:1). **^{1}H NMR** (400 MHz, $CDCl_3$) δ / ppm = 7.37–7.32 (m, 2H), 7.30–7.27 (m, 1H), 7.25–7.22 (m, 2H), 5.13 (s, 1H), 2.25 (s, 3H). **^{13}C{^{1}H} NMR** (101 MHz, $CDCl_3$) δ / ppm = 206.6, 138.5, 138.3, 129.1, 128.9, 128.7 (t, *J* = 24.4 Hz), 128.4 (t, *J* = 24.4 Hz), 127.4, 126.9 (d, *J* = 24.3 Hz), 65.1, 30.2. **^{2}H NMR** (61 MHz, $CHCl_3$) δ / ppm = 7.34 (d, *J* = 6.1 Hz, 5H). **HRMS** (EI) calcd. for $[C_{15}H_9D_5O]^{\bullet+}$ ($[M]^{\bullet+}$), m/z = 215.1358, found: 215.1356. **IR** (ATR, neat) $\tilde{\nu}$ / cm^{-1} = 3064, 3027, 2274, 1715, 1603, 1495, 1454, 1420, 1357, 1156, 746, 701. **Optical Rotation** $[\alpha]_D^{20}$ = +3.0 (*c* = 10.0, $CHCl_3$). For non-deuterated analogue (1,1-diphenylacetone): $[\alpha]_D^{20}$ = +0.3 (*c* = 10.0, $CHCl_3$).

1-Phenyl-1-(phenyl-d_5)propan-2-ol (5q'-d_5)[208]

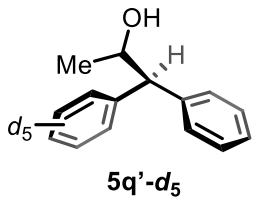

5q'-d_5

In a preheated Schlenk flask, (*R*)-(+)-2-methyl-CBS-oxazaborolidine (16 mg, 57 μmol, 10 mol%) was dissolved in dry THF (3 mL, 0.1 M) and cooled down to 0 °C. $BH_3 \cdot SMe_2$ solution (2.0 M in THF, 0.30 mL, 0.57 mmol, 1.0 equiv.) was added dropwise, and the mixture was stirred at 0 °C for 30 min. A solution of ketone **2q'-d_5** (123 mg, 57.0 μmol, 1.00 equiv.) in dry THF (2 mL) was added dropwise to the reaction mixture over a period of 10 min, which was then allowed to warm to rt and stirred for another 4 h. Upon completion, the reaction was quenched with MeOH (5 mL), and the solvent was removed under reduced pressure. The crude residue was purified by silica gel column chromatography (hexanes:EtOAc = 5:1) to afford a diastereomeric mixture of alcohol **5q'-d_5** (120 mg, 550 μmol, 97%) as a colorless oil.

For determination of retention times for chiral HPLC analysis (which can only separate the secondary alcohol centers), ketone **2q'-d_5** (261 mg, 1.21 mmol, 1.00 equiv.) was reduced with $NaBH_4$ (45.9 mg, 1.21 mmol, 1.00 equiv.) in MeOH (12 mL, 0.10 M) at 0 °C according to a literature procedure.[226]

TLC R_f = 0.15 (hexanes:EtOAc = 9:1). **^{1}H NMR** (400 MHz, $CDCl_3$) δ / ppm = 7.36 (dd, *J* = 8.2, 1.1 Hz, 2H), 7.30 (d, *J* = 7.4 Hz, 1H), 7.26 (s, 1H), 7.22–7.13 (m, 1H), 4.50 (dt, *J* = 12.3, 6.2 Hz, 1H), 3.79 (d, *J* = 8.7 Hz, 1H), 1.77 (br, 1H), 1.17 (d, *J* = 6.1 Hz, 3H). **^{13}C{^{1}H} NMR** (151 MHz, $CDCl_3$, t_1 = 180 s) δ / ppm = 142.6, 142.5, 141.7, 141.5, 128.9, 128.8, 128.7, 128.5 (t, *J* = 11.4 Hz), 128.3, 128.1 (t, *J* = 24.7 Hz), 127.8 (t, *J* = 23.9 Hz), 127.0, 126.6, 126.4, 126.1 (t, *J* = 24.2 Hz), 70.1, 60.6, 21.6. **^{2}H NMR** (61 MHz, $CHCl_3$) δ / ppm = 7.37 (d, *J* = 6.4 Hz, 5H). **HRMS** (APCI) calcd. for $[C_{15}H_{11}D_5O+NH_4]^+$ ($[M+NH_4]^+$), m/z = 235.1859, found: 235.1854. **IR** (ATR, neat) $\tilde{\nu}$ / cm^{-1} = 3567, 3422, 3060, 3027, 2930, 2971, 2274, 1603, 1491, 1454, 1372, 1256, 1118, 1081, 947, 880, 742, 701. **HPLC** (OD-3, *n*-hexane:*i*-PrOH 98:2, flow rate 0.5 mL/min, 220 nm, 25 °C) t_R = 29.273 min (28.7%), 31.722 min (71.3%). For non-deuterated analogue (1,1-diphenylpropan-2-ol): t_R = 27.750 min (28.6%), 30.200 min (71.4%). **Optical Rotation** $[\alpha]_D^{20} = -6.2$ (*c* = 1.9, $CHCl_3$).

5.2.6 Derivatization Studies

5.2.6.1 Synthesis of Expedited Building Blocks

Compounds **9r**, **11r**, and **12r** were synthesized by S. Park according to literature procedures and are detailed in his thesis.[165,229] The starting ketone **2r** used here was also synthesized by S. Park.

(*S*)-2-(1-(2-Methoxyphenyl)-2-methylallyl)naphthalene (10r)[212]

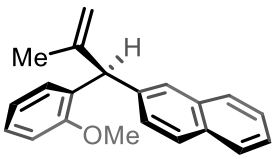

10r

In a preheated Schlenk flask, ketone **2r** (510 mg, 1.77 mmol) was dissolved in dry THF (4.40 mL, 400 μM), and the solution was cooled down to 0 °C. TEBBE's reagent (0.5 M in PhMe, 3.9 mL, 2.0 mmol, 1.1 equiv.) was added dropwise, and the reaction mixture was allowed to warm to rt and stirred for 1 h. The mixture was diluted with Et_2O (20 mL) and quenched with 0.1 M NaOH solution (2 mL). The resulting orange suspension was dried over Na_2SO_4 and filtered through a pad of celite. The filtrate was concentrated under reduced pressure. The resulting crude mixture was purified by silica gel column chromatography (hexanes:EtOAc = 40:1) to afford prop-1-ene **10r** (329 mg, 1.14 mmol, 64%, 95% ee) as a colorless oil.

TLC R_f = 0.45 (hexanes:EtOAc = 19:1). **^{1}H NMR** (400 MHz, $CDCl_3$) δ / ppm = 7.86–7.82 (m, 1H), 7.81–7.77 (m, 2H), 7.62 (s, 1H), 7.50–7.42 (m, 2H), 7.39 (dd, *J* = 8.5, 1.7 Hz, 1H), 7.26 (s, 1H), 7.09 (dd, *J* = 7.5, 1.7 Hz, 1H), 6.96–6.89 (m, 2H), 5.30 (s, 1H), 5.11 (s, 1H), 4.49 (s, 1H), 3.80 (s, 3H), 1.89 (s, 3H). **^{13}C{^{1}H} NMR** (101 MHz, $CDCl_3$) δ / ppm = 157.8, 148.0, 140.5, 133.9, 132.7, 131.5, 130.1, 128.9, 128.3, 128.0, 128.0, 127.8, 126.2, 125.8, 120.7, 114.5, 111.1, 56.1, 51.6, 24.1. **HRMS** (EI) calcd. for $[C_{21}H_{20}O]^{\bullet+}$ ($[M]^{\bullet+}$), m/z = 288.1509, found: 288.1517. **IR** (ATR, neat) $\tilde{\nu}$ / cm^{-1} = 3053, 2963, 2837, 1648, 1599, 1491, 1241, 1103, 898, 816, 746. **HPLC** (IA-3, *n*-hexane:*i*-PrOH 99:1, flow rate 0.6 mL/min, 254 nm, 25 °C) t_R = 6.946 min (2.7%), 7.445 min (97.3%). **Optical Rotation** $[\alpha]_D^{20} = -115.6$ (*c* = 1.0, $CHCl_3$).

5.2.6.2 Drug Synthesis

Compounds **13–16**, **18**, ***ent*-18** and their respective precursors were synthesized according to literature procedures by J. Flügel.[217] The attempted synthesis toward compound **15** was also performed by J. Flügel and is detailed in our joint publication.[230] For the assembly of benzhydrylamine **19**, alcohol **12s'** was subjected to numerous esterifications to improve its nucleofugality (Table 7). All acetates,[231] the "mesylate",[232] the carbonate,[233] the trichloroimidate,[234] and the diphenylphosphate[235] were synthesized by literature procedures and used immediately without isolation and determination of ee. For the attempted APPEL reaction, yielding compound **20s'**, another literature procedure was followed.[227]

General procedure **D** (BAEYER–VILLIGER oxidation and subsequent basic hydrolysis):[215] In a preheated Schlenk flask under nitrogen atmosphere, the respective ketone (1.0 equiv.) was dissolved in dry DCM (0.80 M). $NaHCO_3$ (3.0 equiv.) was added, and the reaction mixture was cooled to 0 °C. A suspension of *m*CPBA (1.5 equiv. in dry DCM) was added dropwise, and the

reaction mixture was allowed to warm to rt and stirred for a certain amount of time. If the SM was not fully consumed, another 1.0–1.5 equiv. of $NaHCO_3$ and *m*CPBA would be added, respectively. Upon completion, the solution was diluted with DCM, quenched with 10% (*w*/*w*) aq. Na_2SO_3 solution, and washed with sat. aq. $NaHCO_3$ solution. The organic layer was dried over $MgSO_4$, filtered, and the solvent was removed under reduced pressure.

The crude acetate was dissolved in MeOH (0.3 M), and K_2CO_3 (3.0 equiv.) was added. The reaction mixture was stirred at rt for a certain amount of time until full conversion was achieved. The solution was carefully neutralized with 1 M HCl and extracted with EtOAc. The combined organic layers were washed with brine, dried over $MgSO_4$, filtered, and the solvent was removed under reduced pressure. The pure product was obtained from silica gel column chromatography. An additional recrystallization step to enhance the compound's ee was carried out by dissolving the respective alcohol in the minimum possible amount of boiling hot *n*-hexane and letting the solution cool down slowly to rt. If no precipitation occurred, the solution was put in the fridge (3 °C) for 2 h. The resulting crystals were collected by filtration and washed carefully with cold *n*-hexane.

(*S*)-(4-Chlorophenyl)(phenyl)methanol (12s')

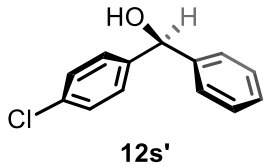

12s'

General procedure **D**: Ketone **2s'** (217 mg, 885 µmol, 88% ee) in dry DCM (4 mL, 0.8 M), $NaHCO_3$ (223 mg, 2.65 mmol, 3.00 equiv.), and *m*CPBA (229 mg, 1.33 mmol, 1.50 equiv.) in 5 mL dry DCM were used. Re-addition of $NaHCO_3$ (74 mg, 0.88 mmol, 1.0 equiv.) and *m*CPBA (153 mg, 880 µmol, 1.00 equiv.) in 4 mL dry DCM after 6 h. Reaction time was 18 h in total. Hydrolysis of the crude acetate with K_2CO_3 (365 mg, 2.64 mmol, 3.00 equiv.) in MeOH (3 mL, 0.3 M) took 18 h. Purification with silica gel column chromatography (hexanes:EtOAc = 9:1) afforded benzhydrol **12s'** (146 mg, 670 µmol, 76% over two steps, 85% ee) as a white solid. Recrystallization from hot *n*-hexane afforded **12s'** (99 mg, 456 µmol, 68%) with an enhanced ee value of 97%.

m.p. = 60.9 °C. **TLC** R_f = 0.10 (hexanes:EtOAc = 9:1). **^{1}H NMR** (400 MHz, $CDCl_3$) δ / ppm = 7.35 (d, *J* = 4.4 Hz, 4H), 7.31 (s, 4H), 7.29 (d, *J* = 4.6 Hz, 1H), 5.81 (d, *J* = 2.7 Hz, 1H), 2.15 (br, 1H). **^{13}C{^{1}H} NMR** (101 MHz, $CDCl_3$) δ / ppm = 143.6, 142.3, 133.4, 128.8, 128.7, 128.0, 126.7, 75.8. **HRMS** (EI) calcd. for $[C_{13}H_{11}ClO]^{\bullet+}$ ($[M]^{\bullet+}$), m/z = 218.0493, found: 218.0488. **IR** (ATR, neat) $\tilde{\nu}$ / cm^{-1} = 3567, 3262, 3064, 3030, 2878, 1599, 1491, 1405, 1185, 1088, 1014, 850, 798, 757, 701. **HPLC** (IA-3, *n*-hexane:*i*-PrOH 98:2, flow rate 0.8 mL/min, 220 nm, 25 °C) t_R = 31.235 min (1.6%), 33.953 min (98.4%). **Optical Rotation** $[\alpha]_D^{20}$ = +20.2 (*c* = 1.0, $CHCl_3$).

(*S*)-Phenyl(phenyl-d_5)methanol (12q'-d_5)

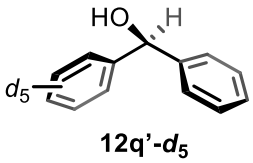

12q'-d_5

General procedure **D**: Ketone **2q'-d_5** (343 mg, 1.59 mmol, 82% ee) in dry DCM (5 mL, 0.8 M), $NaHCO_3$ (401 mg, 4.78 mmol, 3.00 equiv.), and *m*CPBA (412 mg, 2.39 mmol, 1.50 equiv.) in 3 mL dry DCM were used. Reaction time was 24 h. Hydrolysis of the crude acetate with K_2CO_3 (647 mg, 4.68 mmol, 3.00 equiv.) in MeOH (5 mL, 0.3 M) took 4 h. Purification with silica gel column chromatography (hexanes:EtOAc = 9:1) afforded benzhydrol **12q'-d_5** (227 mg, 1.20 mmol, 77% over two steps) as a white solid. Determination of ee value with chiral HPLC is impossible due to a lack of differentiation of the two enantiomers (estimation: 68% < ee < 82%).

m.p. = 67.4 °C. **TLC** R_f = 0.15 (hexanes:EtOAc = 9:1). **^{1}H NMR** (400 MHz, $CDCl_3$) δ / ppm = 7.39 (dd, *J* = 8.3, 1.4 Hz, 2H), 7.37–7.32 (m, 2H), 7.30–7.24 (m, 1H), 5.86 (s, 1H), 2.42–1.83 (br, 1H). **^{2}H NMR** (92 MHz, $CHCl_3$) δ / ppm = 7.47–7.31 (m, 5H). **^{13}C{^{1}H} NMR** (126 MHz, $CDCl_3$) δ / ppm = 143.9, 143.8, 128.6, 128.1 (t, *J* = 24.3 Hz), 127.7, 127.2 (t, *J* = 25.1 Hz), 126.7, 126.2 (t, *J* = 24.2 Hz), 76.4. **HRMS** (EI) calcd. for $[C_{13}H_7D_5O]^{\bullet+}$ ($[M]^{\bullet+}$), m/z = 189.1200, found: 189.1202. **IR** (ATR, neat) $\tilde{\nu}$ / cm^{-1} = 3545, 3362, 3064, 3030, 2878, 2274, 1495, 1454, 1137, 1047, 1014, 760, 731, 701.

(*S*)-*N,N*-Dimethyl-2-(phenyl(phenyl-d_5)methoxy)ethan-1-amine (17)[216]

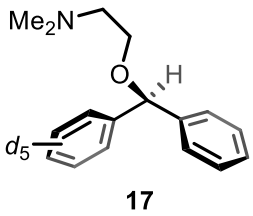

17

A preheated Schlenk flask was charged with benzhydrol **12q'-d_5** (90.6 mg, 479 μmol), KOH (269 mg, 4.79 mmol, 10.0 equiv.) and 2-chloro-*N,N*-dimethylethan-1-aminium chloride (138 mg, 957 μmol, 2.00 equiv.) under nitrogen atmosphere. This mixture was suspended in dry DMSO (2.5 mL, 0.20 M) and stirred for 18 h at rt. Upon completion, the reaction was quenched with 1 M aq. NaOH solution, diluted with Et_2O and stirred for 45 min. The layers were separated, and the aqueous layer was extracted with Et_2O. The combined organic layer was washed with 1 M aq. NaOH solution, dried over Na_2SO_4, filtered, and the solvent was removed under reduced pressure. Purification with silica gel column chromatography (hexanes:EtOAc = 7:3 + 1% (*v*/*v*) NEt_3) afforded (*S*)-diphenhydramine-d_5 (**17**) (106 mg, 410 μmol, 85%) as a colorless oil. Determination of *ee* value with chiral HPLC is impossible due to a lack of differentiation of the two enantiomers (estimation: 68% < *ee* < 82%).

TLC R_f = 0.13 (hexanes:EtOAc = 7:3 + 1% (*v*/*v*) NEt_3). **^{1}H NMR** (400 MHz, $CDCl_3$) δ / ppm = 7.37–7.28 (m, 4H), 7.26–7.21 (m, 1H), 5.37 (s, 1H), 3.57 (t, *J* = 6.0 Hz, 2H), 2.60 (t, *J* = 6.0 Hz, 2H), 2.27 (s, 6H). **^{2}H NMR** (61 MHz, $CHCl_3$) δ / ppm = 7.47–7.28 (m, 5H). **^{13}C{^{1}H} NMR**

(126 MHz, $CDCl_3$) δ / ppm = 142.4, 142.3, 128.5, 128.0 (t, *J* = 23.8 Hz), 127.5, 127.1, 127.0 (t, *J* = 24.7 Hz), 126.7 (t, *J* = 23.8 Hz), 84.1, 67.7, 59.1, 46.2. **HRMS** (APCI) calcd. for $[C_{17}H_{16}D_5NO+H]^+$ ($[M+H]^+$), m/z = 261.2025, found: 261.2013. **IR** (ATR, neat) $\tilde{\nu}$ / cm^{-1} = 2941, 2863, 2818, 2769, 2273, 1495, 1454, 1349, 1309, 1141, 1100, 734, 701. **Optical Rotation** $[\alpha]_D^{20}$ = −9.5 (*c* = 1.0, $CHCl_3$).

(*S*)-1-Chloro-4-(chloro(phenyl)methyl)benzene (20s')[226]

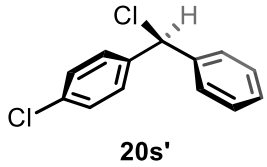

20s'

In a preheated Schlenk flask under nitrogen atmosphere, benzhydrol **12q'-*d*$_5$** (79.5 mg, 364 µmol, 97% ee) was dissolved in dry DCM (2 mL, 0.2 M) and cooled to −78 °C. $SOCl_2$ (132 µL, 1.82 mmol, 5.00 equiv.) was added dropwise and the resulting mixture was stirred at −78 °C for 17 h. Upon completion, the reaction was slowly warmed to rt and the solvent was removed under reduced pressure. Purification by silica gel column chromatography (hexanes:EtOAc = 20:1) afforded chloride **20s'** (78.6 mg, 332 µmol, 91%, 16% ee) as a colorless oil.

TLC R_f = 0.63 (hexanes:EtOAc = 9:1). **^{1}H NMR** (400 MHz, $CDCl_3$) δ / ppm = 7.45–7.31 (m, 9H), 6.12 (s, 1H). **^{13}C{^{1}H} NMR** (101 MHz, $CDCl_3$) δ / ppm = 140.7, 139.8, 134.1, 129.3, 128.8, 128.8, 128.4, 127.8, 63.5. **HRMS** (ESI) calcd. for $[C_{13}H_{10}Cl]^+$ ($[M-Cl]^+$), m/z = 201.0471, found: 201.0470. **IR** (ATR, neat) $\tilde{\nu}$ / cm^{-1} = 3064, 3030, 1595, 1491, 1409, 1215, 1088, 1014, 846, 801, 757, 701. **HPLC** (OD-3, *n*-hexane:*i*-PrOH 99.9:0.1, flow rate 0.6 mL/min, 220 nm, 25 °C) t_R = 16.361 min (57.9%), 17.310 min (42.1%). **Optical Rotation** $[\alpha]_D^{20}$ = +3.5 (*c* = 1.0, $CHCl_3$).

(*R*)-1-((4-Chlorophenyl)(phenyl)methyl)-4-methylpiperazine (19)[226]

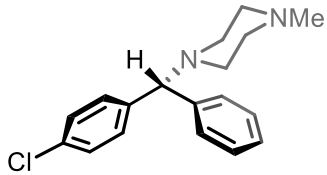

19

In a preheated Schlenk flask under nitrogen atmosphere, chloride **20s'** (78.6 mg, 332 µmol, 16% ee) was dissolved in dry MeCN (3 mL, 0.1 M). *N*-methylpiperazine (184 µL, 1.66 mmol, 5.00 equiv.) was added to the reaction mixture, which was refluxed at 82 °C for 17 h. Upon completion, the reaction was slowly cooled to rt and the solvent was removed under reduced pressure. The crude residue was dissolved in DCM (10 mL) and washed with 1 M aq. NaOH solution (2x 10 mL). The layers were separated, and the organic layer was dried over $MgSO_4$, filtered, and the solvent was removed under reduced pressure. Purification by silica gel column chromatography (hexanes:EtOAc = 1:3 + 1% (*v*/*v*) NEt_3) afforded (*R*)-chlorcyclizine (**19**) (78.8 mg, 260 µmol, 79%, 16% ee) as a colorless oil.

TLC R_f = 0.13 (hexanes:EtOAc = 2:3 + 1% (*v*/*v*) NEt_3). **^{1}H NMR** (400 MHz, $CDCl_3$) δ / ppm = 7.44–7.37 (m, 4H), 7.34–7.25 (m, 4H), 7.24–7.19 (m, 1H), 4.24 (s, 1H), 2.48 (s, 8H), 2.32 (s, 3H). **^{13}C{^{1}H} NMR** (101 MHz, $CDCl_3$) δ / ppm = 142.3, 141.5, 132.6, 129.2, 128.7, 128.7, 127.9, 127.2, 75.6, 55.4, 51.9, 46.0. **HRMS** (ESI) calcd. for $[C_{18}H_{21}ClN_2+H]^+$ ($[M+H]^+$), m/z = 301.1472, found: 301.1469. **IR** (ATR, neat) $\tilde{\nu}$ / cm^{-1} = 3060, 3027, 2963, 2937, 2796, 2691, 1487, 1454, 1290, 1144, 1088, 1010, 854, 805, 760, 701. **HPLC** (OD-3, *n*-hexane:(*i*-PrOH + 1% (*v*/*v*) Et_2NH) 98:2, flow rate 0.8 mL/min, 220 nm, 25 °C) t_R = 5.883 min (57.8%), 6.344 min (42.2%). **Optical Rotation** $[\alpha]_D^{20} = -25.3$ (*c* = 1.0, $CHCl_3$).

5.3 Mechanistic Details

5.3.1 Stern–Volmer Experiments

The following Stern–Volmer (SV) measurements and associated calculations were carried out by Marcel Fischer and are detailed in his ongoing dissertation,[187] as well as in our joint publication.[229] For the sake of completeness, the main results have been reprinted here.

Steady-state emission spectra were measured with a Horiba Fluorolog-3 spectrofluorometer. The irradiation source (450 W Xe-lamp) was centered around 443 nm. Emission was recorded between 475 and 800 nm. For time-resolved emission spectra, a home-built TCSPC-setup was used,[236] whose excitation source was centered around 443 nm and emission was recorded at 540 nm. Absorption spectra were recorded on an Agilent Cary 60 spectrophotometer between 190 and 1100 nm. All experiments were performed using MeCN of spectroscopic grade. Concentration of TAPT was held constant at 10 µM. The investigated quenchers were stilbene **1a**, chiral selenium catalyst **3d**, and selenohydrin **4a**, which was synthesized according to a literature procedure.[158] All quenchers were measured in a concentration range between 0.1 and 1.9 mM (Figure 7).

In the case of stilbene **1a** and selenohydrin **4a**, thermal decomposition of the photocatalyst was observed. The SV plots (Figure 8) for static emission have been corrected for this by calculating the number of excited molecules in each sample around the center of the cuvette. A scaling factor can be determined by calculating the fraction of this value for the pure sample and the ones corresponding to samples containing the quencher. The absorption of the quenchers is small compared to the absorption of TAPT at the irradiation wavelength and thus neglectable. For time-dependent measurements, contributions from catalyst decomposition are irrelevant, as the change in observed decay time is only dependent on the concentration of the quencher.

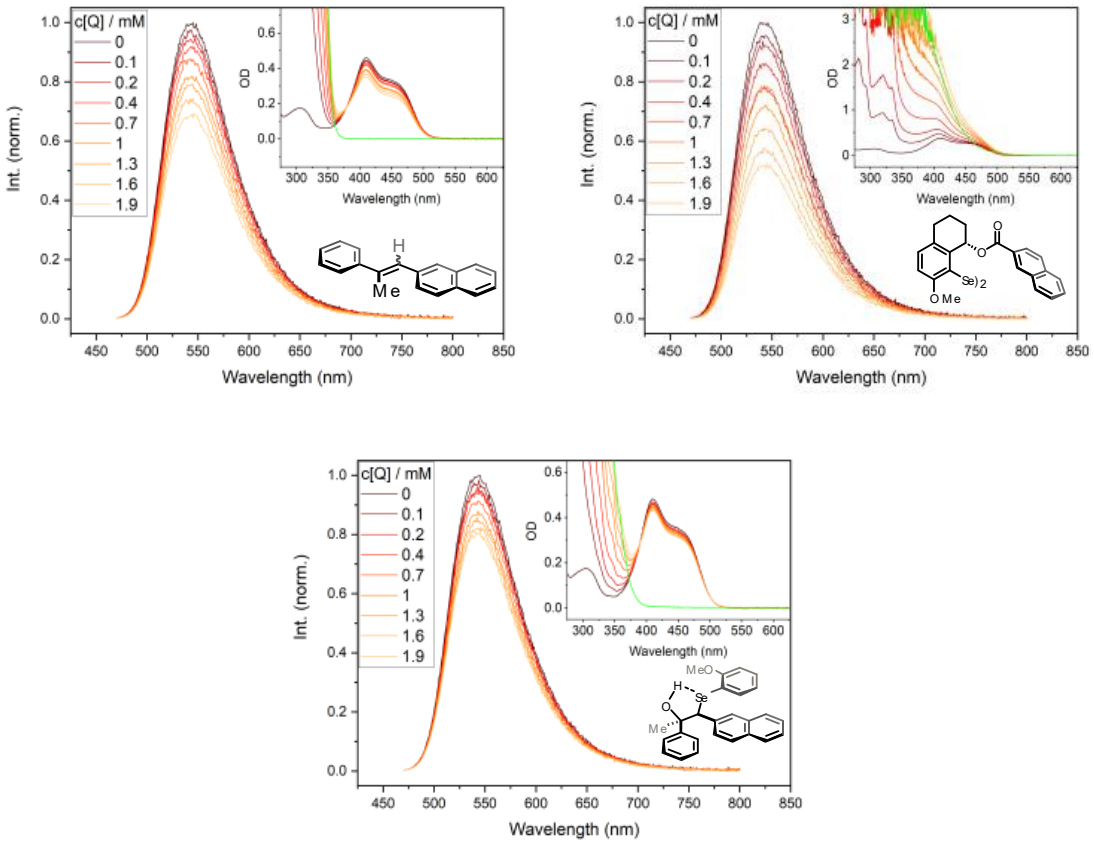

Figure 7. Normalized emission spectra of TAPT with addition of stilbene **1a** (left), selenium catalyst **3d** (right), and selenohydrin **4a** (center). The corresponding absorption spectra are shown as insets. The spectrum of the respective quencher is shown in green. These spectra were recorded by M. Fischer.[187]

For selenium catalyst **3d**, there is overlapping absorption present with TAPT at the excitation wavelength as well as an additional absorption which could not be assigned. As a result, we refrained from a correction of the static emission data, as the exact concentrations of each individual species are unknown and could not be determined accurately by analysis of the static absorption spectra. Only a correction for re-absorption of the selenium catalyst at the emission wavelength was applied in this case.

All dynamic quenching constants (K_d) have been calculated using the SV equation for dynamic quenching shown below, with τ being the excited-state lifetime at quencher concentration [Q].

$$\frac{\tau_0}{\tau} = 1 + K_d \cdot [\mathrm{Q}] \tag{5-2}$$

Where applicable, the static quenching constants (K_s) have been calculated by using the SV equation for combined quenching and fixing the K_d constant to the previously determined value, with I being the emission intensity at quencher concentration [Q].

$$\frac{\mathrm{I}_0}{\mathrm{I}} = 1 + K_d \cdot K_s \cdot [\mathrm{Q}]^2 + (K_d + K_s) \cdot [\mathrm{Q}] \tag{5-3}$$

For all three quenchers, similar K_d values were found (Table 8). K_s values for both the stilbene and the selenohydrin are also very similar. The K_s-value for the selenium catalyst could not be calculated because of the issue mentioned above.

Table 8. Dynamic (K_d) and static (K_s) SV constants for all quenchers.

SV constants	Stilbene 1a	Se-catalyst 3d	Selenohydrin 4a
K_d (L/µmol)	64.8 ± 0.5	54.9 ± 0.3	60.9 ± 1.8
K_s (L/µmol)	24	-	26

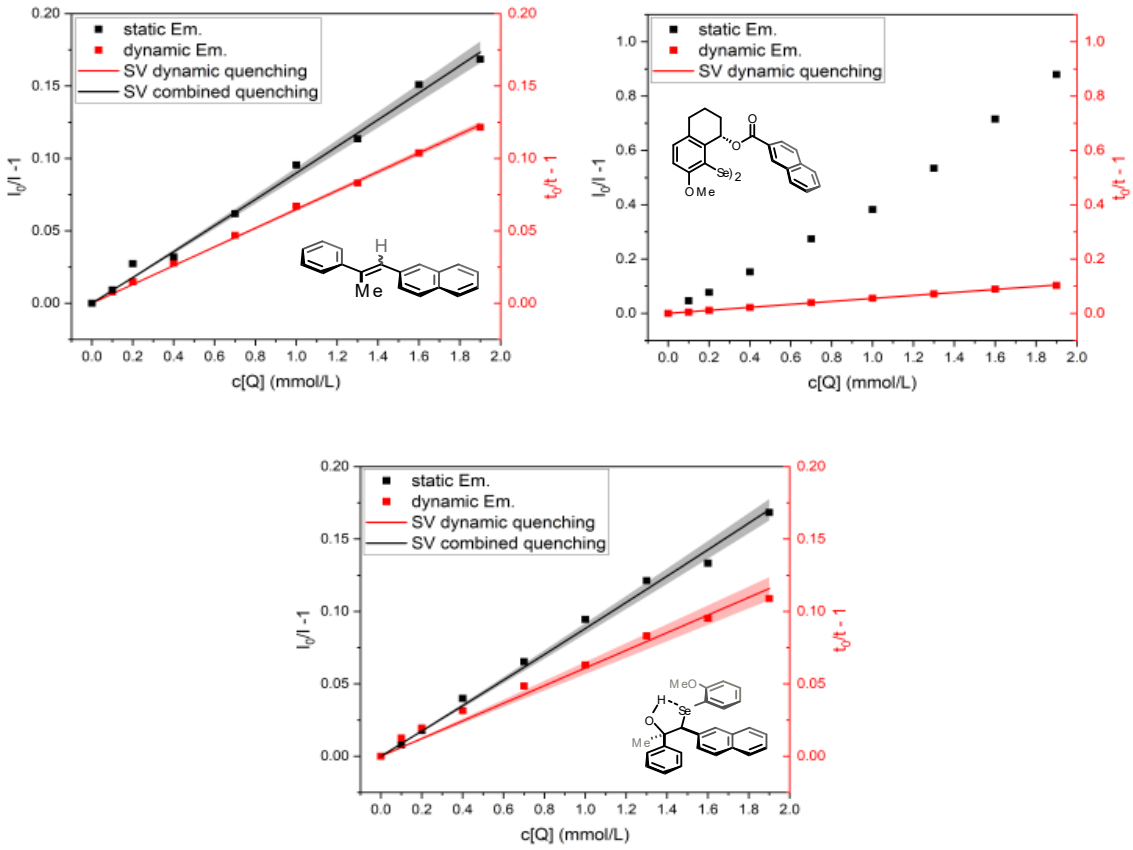

Figure 8. SV plots of the photocatalyst TAPT with addition of stilbene **1a** (left), selenium catalyst **3d** (right) and selenohydrin **4a** (center). The confidence values of the fits are shown in the corresponding colors. These spectra were recorded by M. Fischer.[187]

5.3.2 Details on the KIE Experiment

5.3.2.1 Preparation of the Deuterated Stilbene

Naphthalen-2-ylmethan-*d*$_2$-ol (S8)[203]

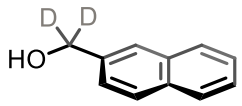

S8

In a preheated Schlenk flask, 2-naphthoic acid (2.58 g, 15.0 mmol) was added portion wise to a suspension of $LiAlD_4$ (1.26 g, 30.0 mmol, 2.00 equiv.) in dry THF (150 mL, 100 mM) at 0 °C. The resulting mixture was allowed to warm to rt and stirred for 1.5 h. Upon completion, the mixture was again cooled to 0 °C and $MgSO_4 \cdot 7\ H_2O$ was added to quench the reaction, followed by the addition of water (20 mL). The reaction was warmed to rt and continued to stir for another 30 min. The mixture was filtered through a pad of celite, washed with Et_2O, dried over $MgSO_4$, filtered, and the filtrate was concentrated under reduced pressure to afford a white solid. The crude alcohol **S8** (2.33 g, 14.5 mmol, 97%, >99% deuteration) was used for the next step without further purifications.

m.p. 147.6 °C. **TLC** R_f = 0.50 (hexanes:EtOAc = 1:1). **^{1}H NMR** (400 MHz, $CDCl_3$) δ / ppm = 7.87–7.78 (m, 4H), 7.53–7.44 (m, 3H), 2.00 (s, 1H). **^{13}C{^{1}H} NMR** (101 MHz, $CDCl_3$) δ / ppm = 138.3, 133.5, 133.1, 128.4, 128.0, 127.8, 126.3, 126.0, 125.6, 125.3, 65.0 (quint, J = 21.8 Hz). **^{2}H NMR** (61 MHz, $CDCl_3$) δ / ppm = 4.82 (s, 2D). **HRMS** (EI) calcd. for $[C_{11}H_8D_2O]^{\bullet+}$ ($[M]^{\bullet+}$), m/z = 160.0852, obs.: 160.0852. **IR** (ATR, neat) $\tilde{\nu}$ / cm^{-1} = 3243, 3056, 1603, 1506, 1454, 1353, 1182, 1126, 1088, 1051, 977, 906, 861, 798, 764, 731, 686.

2-(Bromomethyl-*d*$_2$)naphthalene (S9)[204]

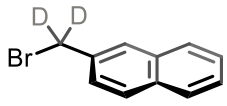

S9

In a preheated Schlenk flask, alcohol **S8** (2.31 g, 14.4 mmol) was dissolved in dry THF (70 mL, 0.20 M) and the resulting solution was cooled down to 0 °C. PBr_3 (2.05 mL, 21.6 mmol, 1.50 equiv.) was added dropwise to the mixture, which was allowed to warm to rt and stirred for 1 h. Upon completion, the reaction was quenched by the dropwise addition of water (10 mL). EtOAc (20 mL) was added, and the phases were separated. The aqueous layer was extracted with EtOAc (3x 10 mL). The combined organic layer was dried over $MgSO_4$, filtered, and the solvent was removed under reduced pressure. The crude mixture was purified by silica gel column chromatography (hexanes:EtOAc = 20:1) to afford bromide **S9** (2.81 g, 12.6 mmol, 87%, 99% deuteration) as a pale-yellow solid.

m.p. 58.6 °C. **TLC** R_f = 0.43 (hexanes:EtOAc = 19:1). **^{1}H NMR** (400 MHz, $CDCl_3$) δ / ppm = 7.88–7.82 (m, 4H), 7.55–7.49 (m, 3H). **^{13}C{^{1}H} NMR** (101 MHz, $CDCl_3$) δ / ppm = 135.1, 133.3,

133.2, 128.9, 128.1, 128.0, 127.8, 126.8, 126.7, 126.6, 33.8 (quint, J = 23.2 Hz). **^{2}H NMR** (61 MHz, $CDCl_3$) δ / ppm = 4.69 (s, 2D). **HRMS** (EI) calcd. for $[C_{11}H_7D_2Br]^{\bullet+}$ ($[M]^{\bullet+}$), m/z = 222.0001, obs.: 222.0008. **IR** (ATR, neat) $\tilde{\nu}$ / cm^{-1} = 3053, 1595, 1506, 1470, 1357, 1271, 1182, 1018, 962, 902, 857, 805, 731.

(Naphthalen-2-ylmethyl-*d*$_2$)triphenylphosphonium bromide (S1-*d*$_2$)

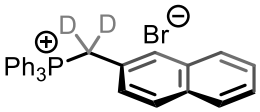

S1-*d*$_2$

General procedure **A**: Triphenylphosphine (3.06 g, 11.7 mmol, 1.05 equiv.), PhMe (22 mL, 0.50 M), and bromide **S9** (2.48 g, 11.1 mmol) were used to afford phosphonium salt **S1-*d*$_2$** (5.14 g, 10.6 mmol, 95%, 95% deuteration) as a white solid.

m.p. 251.1 °C. **^{1}H NMR** (400 MHz, $CDCl_3$) δ / ppm = 7.65 (dt, J = 20.0, 10.0 Hz, 10H), 7.52 (td, J = 7.9, 3.5 Hz, 6H), 7.45 (d, J = 8.6 Hz, 3H), 7.33 (dq, J = 14.4, 6.9 Hz, 2H), 7.08 (d, J = 8.5 Hz, 1H). **^{13}C{^{1}H} NMR** (101 MHz, $CDCl_3$) δ / ppm = 135.0 (d, J = 2.9 Hz), 134.4 (d, J = 9.8 Hz), 132.8 (d, J = 3.5 Hz), 132.6 (d, J = 2.8 Hz), 131.1 (d, J = 7.3 Hz), 130.1 (d, J = 12.6 Hz), 128.5 (d, J = 4.1 Hz), 128.3 (d, J = 2.6 Hz), 127.6 (d, J = 29.5 Hz), 126.4 (d, J = 18.5 Hz), 124.3 (d, J = 9.2 Hz), 117.6 (d, J = 85.6 Hz). **^{31}P{^{1}H} NMR** (162 MHz, $CDCl_3$) δ / ppm = 23.4. **^{2}H NMR** (61 MHz, $CHCl_3$) δ / ppm = 5.43 (s, 2D). **HRMS** (ESI) calcd. for $[C_{29}H_{22}D_2P-Br]^+$ ($[M-Br]^+$), m/z = 405.1736, found: 405.1735. **IR** (ATR, neat) $\tilde{\nu}$ / cm^{-1} = 3056, 3015, 2922, 1588, 1506, 1439, 1241, 1111, 820, 731, 690.

2-(2-Phenylprop-1-en-1-yl-1,3,3,3-*d*$_4$)naphthalene (1a-*d*$_4$)

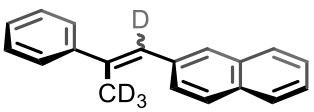

1a-*d*$_4$

General procedure **B**: Phosphonium salt **S1-*d*$_2$** (2.33 g, 4.80 mmol, 1.10 equiv.), dry THF (18 mL, 0.20 M), *n*-BuLi solution (2.1 M, 1.9 mL, 4.0 mmol, 1.1 equiv.), and acetophenone-*d*$_3$ (0.46 mL, 4.0 mmol) in 2.0 mL dry THF were used. Purification with silica gel column chromatography (hexanes:EtOAc = 40:1) afforded an *E*/*Z*-mixture of stilbene **1a-*d*$_4$** (*E*:*Z* = 55:45, 777 mg, 3.13 mmol, 78%, 98% deuteration) as a white solid.

m.p. 72.7 °C. **TLC** R_f = 0.50 (hexanes:EtOAc = 19:1). **^{1}H NMR** (400 MHz, $CDCl_3$) δ / ppm = 7.88–7.81 (m, 4H, *E*), 7.72–7.67 (m, 1H, *Z*), 7.65–7.56 (m, 3H, *E*/*Z*), 7.54–7.46 (m, 5H, *E*/*Z*), 7.44–7.35 (m, 4H, *E*/*Z*), 7.35–7.21 (m, 6H, *E*/*Z*), 7.02 (dd, J = 8.6, 1.7 Hz, 1H, *Z*). **^{13}C{^{1}H} NMR** (101 MHz, $CDCl_3$) δ = 144.0, 142.1, 139.0, 137.7, 135.9, 135.3, 133.5, 133.5, 132.2, 132.1, 128.6, 128.5, 128.4, 128.1, 128.0, 127.9, 127.7, 127.6, 127.4, 127.3, 127.2, 126.2, 126.1, 125.9, 125.9, 125.6,

26.3 (t, *J* = 18.3 Hz), 16.9 (t, *J* = 19.5 Hz). **^{2}H NMR** (61 MHz, $CHCl_3$) δ / ppm = 7.09 (s, 1D, *E*), 6.72 (s, 1D, *Z*), 2.39 (s, 3D, *E*), 2.28 (s, 3D, *Z*). **HRMS** (EI) calcd. for $[C_{19}H_{12}D_4]^{\bullet+}$ ($[M]^{\bullet+}$), m/z = 248.1498, found: 248.1493. **IR** (ATR, neat) $\tilde{\nu}$ / cm^{-1} = 3053, 2926, 2229, 1625, 1599, 1491, 1443, 1271, 1129, 1077, 1021, 947, 895, 857, 820, 753, 697.

5.3.2.2 Determination of KIE

Important note: Due to a better signal to noise ratio in the ^{2}H NMR, the additional deuterons at the methyl group were used for evaluation of KIE-related differences affecting the whole molecule instead of the vinylic deuterons. Since both deuterated positions are present in the same molecule, only a single KIE can be obtained by this approach (see pages 181–184).

The formulas shown below were used for the determination of the KIE value including its error (ΔKIE) and were previously reported by Saunders and Singleton (Table 12).[205,206]

F = conversion of starting material

R/R_0 = proportion of deuterated compound in recovered starting material (recov. SM) compared to the original starting material (orig. SM)

$$\mathbf{\Delta(R/R_0)} = \mathrm{R/R_0}\sqrt{\left(\frac{\Delta\text{recov. SM}}{\text{recov. SM}}\right)^2 + \left(\frac{\Delta\text{orig. SM}}{\text{orig. SM}}\right)^2} \tag{5-4}$$

$$\mathbf{KIE} = \frac{\log(1-\mathrm{F})}{\log[(1-\mathrm{F})\mathrm{R/R_0}]} \tag{5-5}$$

$$\mathbf{\Delta KIE} = \mathrm{KIE}\sqrt{\left(\frac{\Delta\mathrm{KIE_R}}{\mathrm{KIE}}\right)^2 + \left(\frac{\Delta\mathrm{KIE_F}}{\mathrm{KIE}}\right)^2} \tag{5-6}$$

$$\mathbf{\Delta KIE_R} = \frac{\partial\mathrm{KIE}}{\partial(\mathrm{R/R_0})}\Delta(\mathrm{R/R_0}) = \frac{-\log(1-\mathrm{F})}{(\mathrm{R/R_0})\log^2[(1-\mathrm{F})\mathrm{R/R_0}]}\Delta(\mathrm{R/R_0}) \tag{5-7}$$

$$\mathbf{\Delta KIE_F} = \frac{\partial\mathrm{KIE}}{\partial\mathrm{F}}\Delta\mathrm{F} = \frac{-\log(\mathrm{R/R_0})}{(1-\mathrm{F})\log^2[(1-\mathrm{F})\mathrm{R/R_0}]}\Delta\mathrm{F} \tag{5-8}$$

A 100 mL round-bottom flask was charged with 90 mol% of stilbene **1a** (*E*:*Z* = 58:42, 220 mg, 900 μmol) and 10 mol% of stilbene **1a-*d*$_4$** (*E*:*Z* = 55:45, 24.8 mg, 100 μmol). This mixture was dissolved in 5 mL THF and DMF-*d*$_7$ (7.78 μL, 100 μmol) was added as an internal deuterium standard. Four aliquots (0.5 mL each) were taken to determine the initial amount of deuterium relative to the DMF-*d*$_7$ standard (= **R$_0$**, see Table 10 by ^{2}H NMR analysis (92 MHz, 5.0 s delay, 4.4 s acquisition time, 512 scans).

The content of the NMR tubes was re-added to the 100 mL flask and the solvent was removed under reduced pressure with further drying under high vacuum to remove DMF traces. Selenium catalyst **3d** (82 mg, 0.10 mmol, 10 mol%), TAPT (24 mg, 50 μmol, 5.0 mol%), and a 3:1:1 volumetric ratio of HFIP, DCE, and H_2O (10 mL in total, 0.10 M) were added. The flask was sealed with a rubber septum and equipped with needles for air supply. The solution was stirred with 500 rpm under irradiation of blue light (447 nm) at 0 °C for 9 h. The solvent of the crude mixture was removed under reduced pressure, and the conversion was determined to be 83.3 ± 0.1% (= **F**, see Table 9) by ^{1}H NMR analysis (400 MHz, 2.0 s delay, 2.7 s acquisition time, 16 scans) using 1,1,2,2-tetrachloroethane (56 μL, 0.53 mmol, 0.53 equiv.) as internal standard. The content of the NMR tubes was re-added to the 100 mL flask and the remaining starting material was recovered by silica gel column chromatography (hexanes:EtOAc = 20:1) to afford the partly deuterated mixture of stilbene **1a** (39 mg, 0.16 mmol, 16% = 84% conversion) as a white solid.

The recovered starting material was dissolved in 3 mL THF and DMF-*d*$_7$ (7.78 μL, 100 μmol) was added as an internal deuterium standard. Four aliquots (0.5 mL each) were taken to determine the final amount of deuterium relative to the DMF-*d*$_7$ standard (= **R**, see Table 11) by ^{2}H NMR analysis (92 MHz, 5.0 s delay, 4.4 s acquisition time, 512 scans). It must be noted that the conversion of the starting material must be considered when comparing the deuterium ratios.

Table 9. Conversion of stilbene **1a** based on signal at 6.67 ppm (s, 0.9H) relative to the standard 1,1,2,2-tetrachloroethane at 5.95 ppm (s, 2H). Four separate acquisitions were done.

fid1	fid2	fid3	fid4	average (F)	stddev (ΔF)
83.2%	83.3%	83.3%	83.4%	83.3%	0.07%

Table 10. ^{2}H NMR integrations of stilbene **1a-*d*$_4$** starting material before the reaction. Four separate acquisitions were done.

signals	fid1	fid2	fid3	fid4	average (orig. SM)	stddev (Δorig. SM)
2.32–2.14 ppm	278.84	270.23	275.01	276.67	275.19	2.83
2.72 ppm (Standard)	600	600	600	600	600	0

Table 11. ^{2}H NMR integrations of recovered stilbene **1a-*d*$_4$** (83.3 ± 0.1% conversion). Standard integrals take the conversion into account. Four separate acquisitions were done.

signals	fid1	fid2	fid3	fid4	average (recov. SM)	stddev (Δrecov. SM)
2.32–2.14 ppm	226.93	212.38	222.08	223.25	221.16	4.81
2.72 ppm (Standard)	3750	3750	3750	3750	3750	0

Table 12. Determination of the ^{2}H KIE including its error.

signals	R/R$_0$	Δ(R/R$_0$)	KIE	ΔKIE	ΔKIE$_R$	ΔKIE$_F$
2.32–2.14 ppm	0.8037	0.0193	**0.8912**	**0.0583**	0.0246	0.0528
2.72 ppm (Standard)	1	0	1	0	0	0

5.3.3 Supporting Computational Material

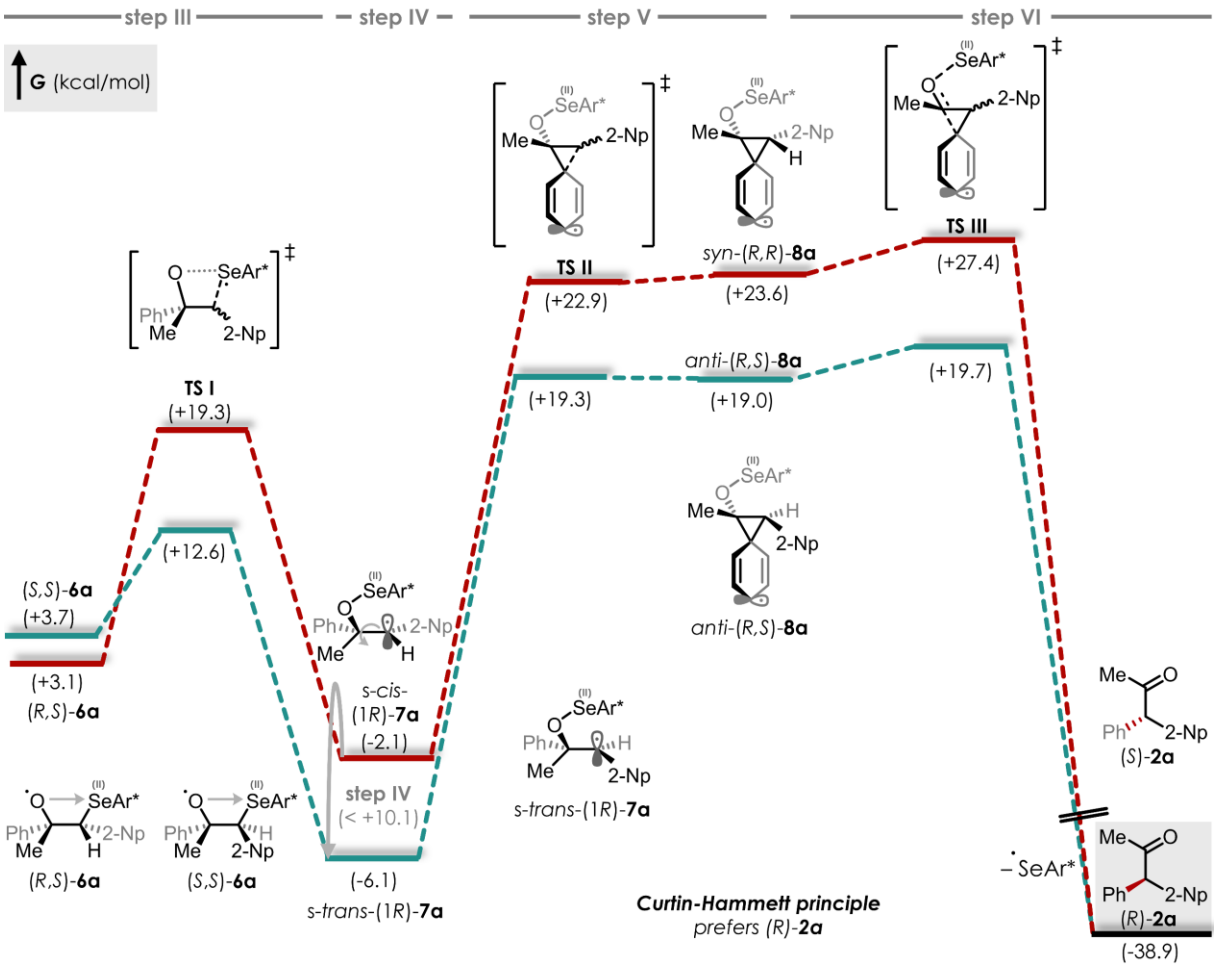

Scheme 37. Thermodynamics of the rate-determining enantioselective aryl migration. All energies are normalized to (*S*,*R*)-**6a**. Level of theory: ωB97M-V / def2-QZVPP @CPCM(ε = 27.5) // TPSS0-D4 / def2-SVP @CPCM(ε = 27.5). Torsion barrier height was approximated by means of relaxed surface scans. All calculations were performed by E. Harrer,[197] who also designed the overall graphic.

6 Literature

[1] P. I. Dalko, L. Moisan, *Angew. Chem. Int. Ed.* **2001**, *40*, 3726–3748.

[2] S. Bergens, B. Bosnich, *Comments Inorg. Chem.* **1987**, *6*, 85–90.

[3] J. T. Mohr, D. C. Behenna, A. M. Harned, B. M. Stoltz, *Angew. Chem. Int. Ed.* **2005**, *117*, 7084–7087.

[4] J. T. Mohr, D. C. Ebner, B. M. Stoltz, *Org. Biomol. Chem.* **2007**, *5*, 3571–3576.

[5] M. Huang, T. Pan, X. Jiang, S. Luo, *J. Am. Chem. Soc.* **2023**, *145*, 10917–10929.

[6] V. Bhat, E. R. Welin, X. Guo, B. M. Stoltz, *Chem. Rev.* **2017**, *117*, 4528–4561.

[7] J. T. Mohr, J. T. Moore, B. M. Stoltz, *Beilstein J. Org. Chem.* **2016**, *12*, 2038–2045.

[8] G. R. A. Adair, J. M. J. Williams, *Chem. Commun.* **2007**, 2608–2609.

[9] J. Zuo, Y.-H. Liao, X.-M. Zhang, W.-C. Yuan, *J. Org. Chem.* **2012**, *77*, 11325–11332.

[10] T. M. Kaiser, J. Yang, *Eur. J. Org. Chem.* **2013**, *2013*, 3983–3987.

[11] H. Shen, L. Yang, M. Xu, Z. Shi, K. Gao, X. Xia, Z. Wang, *Angew. Chem. Int. Ed.* **2025**, *64*, e202413198.

[12] E. L. Eliel, S. H. Wilen, N. L. Allinger, *Topics in stereochemistry. Volume 18*, John Wiley & Sons, New York, **1988**.

[13] V. S. Martin, S. S. Woodard, T. Katsuki, Y. Yamada, M. Ikeda, K. B. Sharpless, *J. Am. Chem. Soc.* **1981**, *103*, 6237–6240.

[14] L. Pasteur, *C. R. Acad. Sci. Paris* **1858**, *46*, 615–618.

[15] W. Marckwald, A. M. Kenzie, *Ber. Dtsch. Chem. Ges.* **1899**, *32*, 2130–2136.

[16] a) C. José, M. V. Toledo, L. E. Briand, *Crit. Rev. Biotechnol.* **2016**, *36*, 891–903; b) L. A. Harwood, L. L. Wong, J. Robertson, *Angew. Chem. Int. Ed.* **2021**, *60*, 4434–4447; c) R. M. Haak, C. Tarabiono, D. B. Janssen, A. J. Minnaard, J. G. de Vries, B. L. Feringa, *Org. Biomol. Chem.* **2007**, *5*, 318–323.

[17] a) S. E. Schaus, B. D. Brandes, J. F. Larrow, M. Tokunaga, K. B. Hansen, A. E. Gould, M. E. Furrow, E. N. Jacobsen, *J. Am. Chem. Soc.* **2002**, *124*, 1307–1315; b) D. E. Robinson, S. D. Bull, *Tetrahedron Asymm.* **2003**, *14*, 1407–1446; c) H. Pellissier, *Adv. Synth. Catal.* **2011**, *353*, 1613–1666; d) X. Bai, J. Yao, M. Zhang, Q. Peng, W. Li, X. Zhao, Y. Yin, Z. Jiang, *J. Am. Chem. Soc.* **2025**, *147*, 38942–38950.

[18] E. Vedejs, M. Jure, *Angew. Chem. Int. Ed.* **2005**, *44*, 3974–4001.

[19] S. Hashiguchi, A. Fujii, K.-J. Haack, K. Matsumura, T. Ikariya, R. Noyori, *Angew. Chem. Int. Ed.* **1997**, *36*, 288–290.

[20] a) Y. Nishibayashi, I. Takei, S. Uemura, M. Hidai, *Organometallics* **1999**, *18*, 2291–2293; b) E. M. Ferreira, B. M. Stoltz, *J. Am. Chem. Soc.* **2001**, *123*, 7725–7726; c) M. S. Sigman, D. R. Jensen, *Acc. Chem. Res.* **2006**, *39*, 221–229.

[21] a) M. Kitamura, I. Kasahara, K. Manabe, R. Noyori, H. Takaya, *J. Org. Chem.* **1988**, *53*, 708–710; b) C. Drago, L. Caggiano, R. F. W. Jackson, *Angew. Chem. Int. Ed.* **2005**, *44*, 7221–7223; c) T. Shao, Z. Li, F. Nie, Q. Li, X. Zhao, Z. Jiang, *Nat. Chem.* **2025**, *17*, 1722–1731.

[22] a) F. F. Huerta, A. B. E. Minidis, J.-E. Bäckvall, *Chem. Soc. Rev.* **2001**, *30*, 321–331; b) H. Pellissier, *Adv. Synth. Catal.* **2011**, *353*, 659–676.

[23] E. J. Ebbers, G. J. Ariaans, J. P. Houbiers, A. Bruggink, B. Zwanenburg, *Tetrahedron* **1997**, *53*, 9417–9476.

[24] J. Steinreiber, K. Faber, H. Griengl, *Chem. Eur. J.* **2008**, *14*, 8060–8072.

[25] R. Noyori, H. Takaya, *Acc. Chem. Res.* **1990**, *23*, 345–350.

[26] a) K.-J. Haack, S. Hashiguchi, A. Fujii, T. Ikariya, R. Noyori, *Angew. Chem. Int. Ed.* **1997**, *36*, 285–288; b) R. Noyori, T. Ohkuma, *Angew. Chem. Int. Ed.* **2001**, *40*, 40–73.

[27] a) J. V. Allen, J. M. Williams, *Tetrahedron Lett.* **1996**, *37*, 1859–1862; b) P. M. Dinh, J. A. Howarth, A. R. Hudnott, J. M. Williams, W. Harris, *Tetrahedron Lett.* **1996**, *37*, 7623–7626.

[28] a) A. L. E. Larsson, B. A. Persson, J.-E. Bäckvall, *Angew. Chem. Int. Ed.* **1997**, *36*, 1211–1212; b) B. A. Persson, A. L. E. Larsson, M. Le Ray, J.-E. Bäckvall, *J. Am. Chem. Soc.* **1999**, *121*, 1645–1650; c) B. Martín-Matute, M. Edin, K. Bogár, J.-E. Bäckvall, *Angew. Chem. Int. Ed.* **2004**, *43*, 6535–6539; d) J. Paetzold, J. E. Bäckvall, *J. Am. Chem. Soc.* **2005**, *127*, 17620–17621.

[29] a) D. E. Ward, V. Jheengut, O. T. Akinnusi, *Org. Lett.* **2005**, *7*, 1181–1184; b) C. Rodríguez-Franco, A. Ros, P. Merino, R. Fernández, J. M. Lassaletta, V. Hornillos, *ACS Catal.* **2023**, *13*, 12134–12141; c) S. Mondal, S. Mukherjee, T. K. Das, R. Gonnade, A. T. Biju, *ACS Catal.* **2017**, *7*, 3995–3999.

[30] a) J. Y. Hamilton, D. Sarlah, E. M. Carreira, *J. Am. Chem. Soc.* **2013**, *135*, 994–997; b) J. Wen, L. Zhang, C. He, S.-M. Song, J. L. Tyler, R. S. Paton, V. K. Aggarwal, *J. Am. Chem. Soc.* **2025**, *147*, 36940–36946; c) A. Berkessel, S. Mukherjee, F. Cleemann, T. N. Muller, J. Lex, *Chem. Commun.* **2005**, 1898–1900; d) C.-W. Cho, J.-R. Kong, M. J. Krische, *Org. Lett.* **2004**, *6*, 1337–1339.

[31] a) S. Hoffmann, M. Nicoletti, B. List, *J. Am. Chem. Soc.* **2006**, *128*, 13074–13075; b) V. N. Wakchaure, J. Zhou, S. Hoffmann, B. List, *Angew. Chem. Int. Ed.* **2010**, *49*, 4612–4614; c) X. Cheng, R. Goddard, G. Buth, B. List, *Angew. Chem. Int. Ed.* **2008**, *47*, 5079–5081.

[32] H.-J. Gais, *Eur. J. Org. Chem.* **2022**, *2022*.

[33] a) M. Rachwalski, N. Vermue, F. P. J. T. Rutjes, *Chem. Soc. Rev.* **2013**, *42*, 9268–9282; b) C. Aranda, G. Oksdath-Mansilla, F. R. Bisogno, G. de Gonzalo, *Adv. Synth. Catal.* **2020**, *362*, 1233–1257; c) J. Großkopf, T. Bach, *Angew. Chem. Int. Ed.* **2023**, *62*, e202308241.

[34] K. Faber, *Chem. Eur. J.* **2001**, *7*, 5004–5010.

[35] I. Prigogine, P. van Rysselberghe, *J. Electrochem. Soc.* **1963**, *110*, 97C.

[36] D. G. Blackmond, *Angew. Chem. Int. Ed.* **2009**, *48*, 2648–2654.

[37] J. H. Schrittwieser, J. Sattler, V. Resch, F. G. Mutti, W. Kroutil, *Curr. Opin. Chem. Biol.* **2011**, *15*, 249–256.

[38] a) I. Chibata, T. Tosa, R. Sano, *Appl. Microbiol.* **1965**, *13*, 618–624; b) Y. Hai, M. Jenner, Y. Tang, *J. Am. Chem. Soc.* **2019**, *141*, 16222–16226.

[39] a) C. C. Gruber, I. Lavandera, K. Faber, W. Kroutil, *Adv. Synth. Catal.* **2006**, *348*, 1789–1805; b) C. V. Voss, C. C. Gruber, K. Faber, T. Knaus, P. Macheroux, W. Kroutil, *J. Am. Chem. Soc.* **2008**, *130*, 13969–13972; c) C. V. Voss, C. C. Gruber, W. Kroutil, *Angew. Chem. Int. Ed.* **2008**, *47*, 741–745; d) G. Shin, S. Mathew, M. Shon, B.-G. Kim, H. Yun, *Chem. Commun.* **2013**, *49*, 8629–8631.

[40] a) Y. Shimada, K. Usuda, H. Okabe, T. Suzuki, K. Matsumoto, *Tetrahedron Asymm.* **2009**, *20*, 2802–2808; b) N. Bouzemi, I. Grib, Z. Houiene, L. Aribi-Zouioueche, *Catalysts* **2014**, *4*, 215–225.

[41] M. Huang, L. Zhang, T. Pan, S. Luo, *Science* **2022**, *375*, 869–874.

[42] a) F.-R. Alexandre, D. P. Pantaleone, P. P. Taylor, I. G. Fotheringham, D. J. Ager, N. J. Turner, *Tetrahedron Lett.* **2002**, *43*, 707–710; b) W. T. Lowther, N. Brot, H. Weissbach, J. F. Honek, B. W. Matthews, *Proc. Natl. Acad. Sci. USA* **2000**, *97*, 6463–6468; c) M. Alexeeva, A. Enright, M. J. Dawson, M. Mahmoudian, N. J. Turner, *Angew. Chem. Int. Ed.* **2002**, *41*, 3177–3180; d) G. Li, J. Ren, P. Yao, Y. Duan, H. Zhang, Q. Wu, J. Feng, P. C. K. Lau, D. Zhu, *ACS Catal.* **2014**, *4*, 903–908; e) X. Guo, Y. Okamoto, M. R. Schreier, T. R. Ward, O. S. Wenger, *Chem. Sci.* **2018**, *9*, 5052–5056.

[43] a) T. Kratz, P. Steinbach, S. Breitenlechner, G. Storch, C. Bannwarth, T. Bach, *J. Am. Chem. Soc.* **2022**, *144*, 10133–10138; b) X. Li, R. J. Kutta, C. Jandl, A. Bauer, P. Nuernberger, T. Bach, *Angew. Chem. Int. Ed.* **2020**, *59*, 21640–21647; c) M. Stierle, D. Bitterlich, J. Westermayr, T. Bach, *Chem. Sci.* **2025**, *16*, 19711–19719.

[44] A. Hölzl-Hobmeier, A. Bauer, A. V. Silva, S. M. Huber, C. Bannwarth, T. Bach, *Nature* **2018**, *564*, 240–243.

[45] M. Plaza, C. Jandl, T. Bach, *Angew. Chem. Int. Ed.* **2020**, *59*, 12785–12788.

[46] a) J. Großkopf, M. Plaza, A. Seitz, S. Breitenlechner, G. Storch, T. Bach, *J. Am. Chem. Soc.* **2021**, *143*, 21241–21245; b) R. J. Kutta, J. Großkopf, N. van Staalduinen, A. Seitz, P. Pracht,

S. Breitenlechner, C. Bannwarth, P. Nuernberger, T. Bach, *J. Am. Chem. Soc.* **2023**, *145*, 2354–2363; c) J. Großkopf, A. A. Heidecker, T. Bach, *Angew. Chem. Int. Ed.* **2023**, *62*, e202305274; d) M. Iglhaut, P. Freund, T. Bach, *Angew. Chem. Int. Ed.* **2025**, *64*, e202418873; e) M. Iglhaut, T. Bach, *Acc. Chem. Res.* **2025**, *58*, 777–786; f) P. Freund, M. Pauls, D. Babushkina, T. Pickl, C. Bannwarth, T. Bach, *J. Am. Chem. Soc.* **2025**, *147*, 1434–1439.

[47] a) G. R. A. Adair, J. M. J. Williams, *Chem. Commun.* **2005**, 5578–5579; b) A. D. Lackner, A. V. Samant, F. D. Toste, *J. Am. Chem. Soc.* **2013**, *135*, 14090–14093; c) M. Wan, S. Sun, Y. Li, L. Liu, *Angew. Chem. Int. Ed.* **2017**, *56*, 5116–5120; d) C. Onneken, T. Morack, J. Soika, O. Sokolova, N. Niemeyer, C. Mück-Lichtenfeld, C. G. Daniliuc, J. Neugebauer, R. Gilmour, *Nature* **2023**, *621*, 753–759.

[48] J.-W. Lee, B. List, *J. Am. Chem. Soc.* **2012**, *134*, 18245–18248.

[49] a) Z. Gu, L. Zhang, H. Li, S. Cao, Y. Yin, X. Zhao, X. Ban, Z. Jiang, *Angew. Chem. Int. Ed.* **2022**, *61*, e202211241; b) C. Zhang, A. Z. Gao, X. Nie, C.-X. Ye, S. I. Ivlev, S. Chen, E. Meggers, *J. Am. Chem. Soc.* **2021**, *143*, 13393–13400.

[50] N. Shin, J. Ryss, X. Zhang, S. Miller, R. Knowles, *Science* **2019**, *366*, 364–369.

[51] C. Viedma, *Phys. Rev. Lett.* **2005**, *94*, 65504.

[52] a) B. Kaptein, W. L. Noorduin, H. Meekes, W. J. P. van Enckevort, R. M. Kellogg, E. Vlieg, *Angew. Chem.* **2008**, *120*, 7336–7339; b) C. Viedma, J. E. Ortiz, T. de Torres, T. Izumi, D. G. Blackmond, *J. Am. Chem. Soc.* **2008**, *130*, 15274–15275; c) A. Lennartson, S. Olsson, J. Sundberg, M. Håkansson, *Angew. Chem. Int. Ed.* **2009**, *48*, 3137–3140; d) A. H. J. Engwerda, N. Koning, P. Tinnemans, H. Meekes, F. M. Bickelhaupt, F. P. J. T. Rutjes, E. Vlieg, *Cryst. Growth Des.* **2017**, *17*, 4454–4457.

[53] S. W. van Dongen, J. Maeda, B. Kaptein, P. Cardinael, A. Flood, G. Coquerel, W. L. Noorduin, *J. Am. Chem. Soc.* **2025**, *147*, 38508–38515.

[54] a) C. Fischer, G. C. Fu, *J. Am. Chem. Soc.* **2005**, *127*, 4594–4595; b) S. Ma, X. Han, S. Krishnan, S. C. Virgil, B. M. Stoltz, *Angew. Chem. Int. Ed.* **2009**, *48*, 8037–8041; c) M. Terada, Y. Toda, *J. Am. Chem. Soc.* **2009**, *131*, 6354–6355; d) M. Terada, T. Yamanaka, Y. Toda, *Chem. Eur. J.* **2013**, *19*, 13658–13662; e) X. Xie, L. Jing, D. Qin, W. He, S. Wu, L. Jin, G. Luo, *RSC Adv.* **2014**, *4*, 11605–11609; f) L. Zhang, H. Liu, T. G. Santiago, R. Martin, *J. Am. Chem. Soc.* **2025**, *147*, 44048–44054.

[55] B. M. Trost, D. L. van Vranken, *Chem. Rev.* **1996**, *96*, 395–422.

[56] J. T. Mohr, D. C. Behenna, A. M. Harned, B. M. Stoltz, *Angew. Chem. Int. Ed.* **2005**, *44*, 6924–6927.

[57] a) H. Ito, S. Kunii, M. Sawamura, *Nat. Chem.* **2010**, *2*, 972–976; b) M. Schober, P. Gadler, T. Knaus, H. Kayer, R. Birner-Grünberger, C. Gülly, P. Macheroux, U. Wagner, K. Faber, *Org.*

Lett. **2011**, *13*, 4296–4299; c) P. M. Lundin, G. C. Fu, *J. Am. Chem. Soc.* **2010**, *132*, 11027–11029.

[58] L. Massaro, J. Zheng, C. Margarita, P. G. Andersson, *Chem. Soc. Rev.* **2020**, *49*, 2504–2522.

[59] A. Miyashita, A. Yasuda, H. Takaya, K. Toriumi, T. Ito, T. Souchi, R. Noyori, *J. Am. Chem. Soc.* **1980**, *102*, 7932–7934.

[60] J. Halpern, *Science* **1982**, *217*, 401–407.

[61] a) W. S. Knowles, *Acc. Chem. Res.* **1983**, *16*, 106–112; b) T. L. Church, T. Rasmussen, P. G. Andersson, *Organometallics* **2010**, *29*, 6769–6781.

[62] C. A. Willoughby, S. L. Buchwald, *J. Am. Chem. Soc.* **1994**, *116*, 11703–11714.

[63] a) B. H. Lipshutz, J. M. Servesko, *Angew. Chem. Int. Ed.* **2003**, *42*, 4789–4792; b) J. Zhou, J. W. Ogle, Y. Fan, V. Banphavichit, Y. Zhu, K. Burgess, *Chem. Eur. J.* **2007**, *13*, 7162–7170; c) F. Maurer, U. Kazmaier, *J. Org. Chem.* **2013**, *78*, 3425–3428; d) Y. Liu, I. D. Gridnev, W. Zhang, *Angew. Chem. Int. Ed.* **2014**, *53*, 1901–1905; e) J. Engel, S. Mersmann, P.-O. Norrby, C. Bolm, *ChemCatChem* **2016**, *8*, 3099–3106.

[64] L. Wang, B. Wang, J. Lin, X. Meng, Q. Sun, W. Sun, *J. Am. Chem. Soc.* **2025**, *147*, 33581–33588.

[65] B. M. Trost, H. C. Shen, L. Dong, J.-P. Surivet, *J. Am. Chem. Soc.* **2003**, *125*, 9276–9277.

[66] S. Tominaga, Y. Oi, T. Kato, D. K. An, S. Okamoto, *Tetrahedron Lett.* **2004**, *45*, 5585–5588.

[67] a) H. Ito, C. Kawakami, M. Sawamura, *J. Am. Chem. Soc.* **2005**, *127*, 16034–16035; b) J. S. Cannon, S. F. Kirsch, L. E. Overman, *J. Am. Chem. Soc.* **2010**, *132*, 15185–15191; c) A. Guzman-Martinez, A. H. Hoveyda, *J. Am. Chem. Soc.* **2010**, *132*, 10634–10637.

[68] H. Ito, S. Ito, Y. Sasaki, K. Matsuura, M. Sawamura, *J. Am. Chem. Soc.* **2007**, *129*, 14856–14857.

[69] S.-Y. Wang, S.-J. Ji, T.-P. Loh, *J. Am. Chem. Soc.* **2007**, *129*, 276–277.

[70] a) D. Hirsch-Weil, K. A. Abboud, S. Hong, *Chem. Commun.* **2010**, *46*, 7525–7527; b) T. Sawano, A. Ashouri, T. Nishimura, T. Hayashi, *J. Am. Chem. Soc.* **2012**, *134*, 18936–18939; c) T. Q. Davies, J. J. Murphy, M. Dousset, A. Fürstner, *J. Am. Chem. Soc.* **2021**, *143*, 13489–13494.

[71] C. Zhong, S. Kunii, Y. Kosaka, M. Sawamura, H. Ito, *J. Am. Chem. Soc.* **2010**, *132*, 11440–11442.

[72] D. F. Fischer, A. Barakat, Z.-Q. Xin, M. E. Weiss, R. Peters, *Chem. Eur. J.* **2009**, *15*, 8722–8741.

[73] a) J. Halpern, D. P. Riley, A. S. C. Chan, J. J. Pluth, *J. Am. Chem. Soc.* **1977**, *99*, 8055–8057; b) A. S. C. Chan, J. J. Pluth, J. Halpern, *J. Am. Chem. Soc.* **1980**, *102*, 5952–5954; c) I. D.

Gridnev, T. Imamoto, *Chem. Commun.* **2009**, 7447–7464; d) I. D. Gridnev, Y. Liu, T. Imamoto, *ACS Catal.* **2014**, *4*, 203–219.

[74] P. Lu, H. Wang, Y. Mao, X. Hong, Z. Lu, *J. Am. Chem. Soc.* **2022**, *144*, 17359–17364.

[75] M. J. Burk, J. E. Feaster, W. A. Nugent, R. L. Harlow, *J. Am. Chem. Soc.* **1993**, *115*, 10125–10138.

[76] J. W. Yang, M. T. Hechavarria Fonseca, N. Vignola, B. List, *Angew. Chem. Int. Ed.* **2004**, *44*, 108–110.

[77] S. G. Ouellet, J. B. Tuttle, D. W. C. MacMillan, *J. Am. Chem. Soc.* **2005**, *127*, 32–33.

[78] Z. C. Litman, Y. Wang, H. Zhao, J. F. Hartwig, *Nature* **2018**, *560*, 355–359.

[79] a) G. Koch, A. Pfaltz, *Tetrahedron Asymm.* **1996**, *7*, 2213–2216; b) C. A. Falciola, A. Alexakis, *Angew. Chem. Int. Ed.* **2007**, *46*, 2619–2622.

[80] K.-X. Zhang, M.-Y. Liu, B.-Y. Yao, Q.-L. Zhou, L.-J. Xiao, *J. Am. Chem. Soc.* **2024**, *146*, 22157–22165.

[81] J. K. Park, H. H. Lackey, B. A. Ondrusek, D. T. McQuade, *J. Am. Chem. Soc.* **2011**, *133*, 2410–2413.

[82] Q. Zhang, D. Dong, W. Zi, *J. Am. Chem. Soc.* **2020**, *142*, 15860–15869.

[83] M. J. Behlen, C. Uyeda, *J. Am. Chem. Soc.* **2020**, *142*, 17294–17300.

[84] R. Mao, D. M. Taylor, D. J. Wackelin, S. J. Wu, K. M. Sicinski, F. H. Arnold, *Nat. Synth.* **2024**, *3*, 256–264.

[85] M. R. Friedfeld, M. Shevlin, G. W. Margulieux, L.-C. Campeau, P. J. Chirik, *J. Am. Chem. Soc.* **2016**, *138*, 3314–3324.

[86] E. B. Bauer, *Chem. Soc. Rev.* **2012**, *41*, 3153–3167.

[87] B. E. Maryanoff, A. B. Reitz, *Chem. Rev.* **1989**, *89*, 863–927.

[88] P. A. Byrne, D. G. Gilheany, *Chem. Soc. Rev.* **2013**, *42*, 6670–6696.

[89] A. K. Chatterjee, T.-L. Choi, D. P. Sanders, R. H. Grubbs, *J. Am. Chem. Soc.* **2003**, *125*, 11360–11370.

[90] A. Brotons-Rufes, S. Posada-Pérez, J. P. Martínez, S. P. Nolan, A. Poater, *Coord. Chem. Rev.* **2025**, *542*, 216827.

[91] Y. Sun, C. LeBlond, J. Wang, D. G. Blackmond, J. Laquidara, J. R. Sowa, *J. Am. Chem. Soc.* **1995**, *117*, 12647–12648.

[92] Y. Sun, J. Wang, C. LeBlond, R. A. Reamer, J. Laquidara, J. R. Sowa, D. G. Blackmond, *J. Organomet. Chem.* **1997**, *548*, 65–72.

[93] E. J. Ariëns, *Drug Design. Medicinal Chemistry: A Series of Monographs, Vol. 6*, Elsevier Science, Burlington, **1975**.

[94] F. Schmidt, R. T. Stemmler, J. Rudolph, C. Bolm, *Chem. Soc. Rev.* **2006**, *35*, 454–470.

[95] D. Ameen, T. J. Snape, *Med. Chem. Commun.* **2013**, *4*, 893–907.

[96] K. Müller, H. Prinz, M. Lehr, *Pharmazeutische/Medizinische Chemie. Arzneistoffe - von der Struktur zur Wirkung*, Wissenschaftliche Verlagsgesellschaft, Stuttgart, **2022**.

[97] G. J. Durant, C. R. Ganellin, M. E. Parsons, *J. Med. Chem.* **1975**, *18*, 905–909.

[98] P. Panula, P. L. Chazot, M. Cowart, R. Gutzmer, R. Leurs, W. L. S. Liu, H. Stark, R. L. Thurmond, H. L. Haas, *Pharmacol. Rev.* **2015**, *67*, 601–655.

[99] a) C. de Graaf, A. J. Kooistra, H. F. Vischer, V. Katritch, M. Kuijer, M. Shiroishi, S. Iwata, T. Shimamura, R. C. Stevens, I. J. P. de Esch et al., *J. Med. Chem.* **2011**, *54*, 8195–8206; b) S. Kuhne, A. J. Kooistra, R. Bosma, A. Bortolato, M. Wijtmans, H. F. Vischer, J. S. Mason, C. de Graaf, I. J. P. de Esch, R. Leurs, *J. Med. Chem.* **2016**, *59*, 9047–9061.

[100] a) F. Gonzalez, *Am. J. Hosp. Palliat. Care* **2009**, *26*, 474–475; b) F. Gengo, C. Gabos, J. K. Miller, *Clin. Pharmacol. Ther.* **1989**, *45*, 15–21; c) C.-C. Kuo, R.-C. Huang, B.-S. Lou, *Mol. Pharmacol.* **2000**, *57*, 135–143; d) K. D. Carr, J. M. Hiller, E. J. Simon, *Neuropeptides* **1985**, *5*, 411–414.

[101] a) L. Eckes, M. Tsokos, S. Herre, R. Gapert, S. Hartwig, *Forensic Sci. Med. Pathol.* **2013**, *9*, 145–153; b) F. C. Lowell, *Am. J. Nurs.* **1947**, *47*, 656; c) T. Nishino, S. Wakai, H. Aoki, S. Inokuchi, *Acute Med. Surg.* **2018**, *5*, 380–383; d) M. Taglialatela, H. Timmerman, L. Annunziato, *Trends Pharmacol. Sci.* **2000**, *21*, 52–56.

[102] R. F. Rekker, H. Timmerman, A. F. Harms, W. T. Nauta, *Arzneimittelforschung* **1971**, *21*, 688–691.

[103] S. Hunskaar, D. Donnell, *J. Int. Med. Res.* **1991**, *19*, 71–87.

[104] a) A. Pagliara, B. Testa, P. A. Carrupt, P. Jolliet, C. Morin, D. Morin, S. Urien, J. P. Tillement, J. P. Rihoux, *J. Med. Chem.* **1998**, *41*, 853–863; b) J.-P. Tillement, B. Testa, F. Brée, *Biochem. Pharmacol.* **2003**, *66*, 1123–1126; c) J. L. Devalia, C. de Vos, F. Hanotte, E. Baltes, *Allergy* **2001**, *56*, 50–57; d) E. Baltes, R. Coupez, H. Giezek, G. Voss, C. Meyerhoff, M. Strolin Benedetti, *Fundam. Clin. Pharmacol.* **2001**, *15*, 269–277.

[105] a) J. Waugh, K. L. Goa, *CNS Drugs* **2003**, *17*, 343–362; b) C. Sánchez, P. B. F. Bergqvist, L. T. Brennum, S. Gupta, S. Hogg, A. Larsen, O. Wiborg, *Psychopharmacol.* **2003**, *167*, 353–362; c) M. J. Owens, D. L. Knight, C. B. Nemeroff, *Biol. Psychiatry* **2001**, *50*, 345–350; d) A. Mørk, M. Kreilgaard, C. Sánchez, *Neuropharmacol.* **2003**, *45*, 167–173.

[106] M. Belal, Z. Li, X. Lu, G. Yin, *Sci. China Chem.* **2021**, *64*, 513–533.

[107] U. Gulati, R. Gandhi, J. K. Laha, *Chem. Asian. J.* **2020**, *15*, 3135–3161.

[108] P. A. Wender, V. A. Verma, T. J. Paxton, T. H. Pillow, *Acc. Chem. Res.* **2008**, *41*, 40–49.

[109] N. Z. Burns, P. S. Baran, R. W. Hoffmann, *Angew. Chem. Int. Ed.* **2009**, *48*, 2854–2867.

[110] B. M. Trost, D. A. Thaisrivongs, *J. Am. Chem. Soc.* **2009**, *131*, 12056–12057.

[111] S.-B. Yan, S. Zhang, W.-L. Duan, *Org. Lett.* **2015**, *17*, 2458–2461.

[112] J. H. Kim, S. Greßies, M. Boultadakis-Arapinis, C. Daniliuc, F. Glorius, *ACS Catal.* **2016**, *6*, 7652–7656.

[113] a) H. Wang, H.-R. Tong, G. He, G. Chen, *Angew. Chem. Int. Ed.* **2016**, *55*, 15387–15391; b) G. Chen, W. Gong, Z. Zhuang, M. S. Andrä, Y.-Q. Chen, X. Hong, Y.-F. Yang, T. Liu, K. N. Houk, J.-Q. Yu, *Science* **2016**, *353*, 1023–1027; c) F.-L. Zhang, K. Hong, T.-J. Li, H. Park, J.-Q. Yu, *Science* **2016**, *351*, 252–256.

[114] X. Cheng, H. Lu, Z. Lu, *Nat. Commun.* **2019**, *10*, 3549.

[115] W. Zhang, L. Wu, P. Chen, G. Liu, *Angew. Chem. Int. Ed.* **2019**, *58*, 6425–6429.

[116] B. Li, Z. Chao, C. Li, Z. Gu, *J. Am. Chem. Soc.* **2018**, *140*, 9400–9403.

[117] T. Morack, T. E. Myers, L. J. Karas, M. A. Hardy, B. Q. Mercado, M. S. Sigman, S. J. Miller, *J. Am. Chem. Soc.* **2023**, *145*, 22322–22328.

[118] X. Xiong, T. Zheng, X. Wang, Y.-L. S. Tse, Y.-Y. Yeung, *Chem* **2020**, *6*, 919–932.

[119] X. Yu, S. Liu, L. Wang, Y. Li, M. Huang, Z.-Y. Yan, H.-C. Li, Q. Zhang, X. Zhang, B.-F. Shi, *ACS Catal.* **2025**, *15*, 2540–2549.

[120] B. Kim, A. J. Chinn, D. R. Fandrick, C. H. Senanayake, R. A. Singer, S. J. Miller, *J. Am. Chem. Soc.* **2016**, *138*, 7939–7945.

[121] N. Aditya, S. Das, A. Datta, B. Maji, *J. Am. Chem. Soc.* **2025**, *147*, 27458–27470.

[122] W.-Q. Wu, P.-P. Xie, L.-Y. Wang, B.-B. Gou, Y. Lin, L.-W. Hu, C. Zheng, S.-L. You, H. Shi, *J. Am. Chem. Soc.* **2024**, *146*, 26630–26638.

[123] a) B. L. H. Taylor, E. C. Swift, J. D. Waetzig, E. R. Jarvo, *J. Am. Chem. Soc.* **2011**, *133*, 389–391; b) Q. Zhou, H. D. Srinivas, S. Dasgupta, M. P. Watson, *J. Am. Chem. Soc.* **2013**, *135*, 3307–3310.

[124] B. L. H. Taylor, M. R. Harris, E. R. Jarvo, *Angew. Chem. Int. Ed.* **2012**, *51*, 7790–7793.

[125] M. R. Harris, L. E. Hanna, M. A. Greene, C. E. Moore, E. R. Jarvo, *J. Am. Chem. Soc.* **2013**, *135*, 3303–3306.

[126] K. B. Selim, Y. Matsumoto, K. Yamada, K. Tomioka, *Angew. Chem. Int. Ed.* **2009**, *48*, 8733–8735.

[127] K. E. Poremba, N. T. Kadunce, N. Suzuki, A. H. Cherney, S. E. Reisman, *J. Am. Chem. Soc.* **2017**, *139*, 5684–5687.

[128] L. Liu, *Acc. Chem. Res.* **2022**, *55*, 3537–3550.

[129] Y.-Z. Wang, B. Sun, J.-F. Guo, X.-Y. Zhu, Y.-C. Gu, Y.-P. Han, C. Ma, T.-S. Mei, *Nat. Commun.* **2025**, *16*, 1108.

[130] Y.-Z. Wang, Z.-H. Wang, I. L. Eshel, B. Sun, D. Liu, Y.-C. Gu, A. Milo, T.-S. Mei, *Nat. Commun.* **2023**, *14*, 2322.

[131] a) T. Arao, K. Suzuki, K. Kondo, T. Aoyama, *Synthesis* **2006**, 3809–3814; b) M. Orlandi, M. J. Hilton, E. Yamamoto, F. D. Toste, M. S. Sigman, *J. Am. Chem. Soc.* **2017**, *139*, 12688–12695; c) J. Huang, C. Pei, H. Yang, B. Wu, W. Tang, *Angew. Chem. Int. Ed.* **2025**, *64*, e202505458; d) C. Yao, Y. Chen, R. Sun, C. Wang, Y. Huang, L. Li, Y.-M. Li, *Org. Biomol. Chem.* **2021**, *19*, 3644–3655.

[132] R. Kumar, Y. Hoshimoto, H. Yabuki, M. Ohashi, S. Ogoshi, *J. Am. Chem. Soc.* **2015**, *137*, 11838–11845.

[133] P. Chaumont-Olive, M. Rouen, G. Barozzino-Consiglio, A. Ben Abdeladhim, J. Maddaluno, A. Harrison-Marchand, *Angew. Chem. Int. Ed.* **2019**, *58*, 3193–3197.

[134] a) L. Wu, F. Wang, X. Wan, D. Wang, P. Chen, G. Liu, *J. Am. Chem. Soc.* **2017**, *139*, 2904–2907; b) Y.-G. Chen, B. Shuai, X.-T. Xu, Y.-Q. Li, Q.-L. Yang, H. Qiu, K. Zhang, P. Fang, T.-S. Mei, *J. Am. Chem. Soc.* **2019**, *141*, 3395–3399; c) Y. He, C. Liu, L. Yu, S. Zhu, *Angew. Chem. Int. Ed.* **2020**, *59*, 21530–21534; d) Z. Li, S. Wang, S.-C. Chen, X. Zhu, Z. Lian, D. Xing, *J. Am. Chem. Soc.* **2024**, *146*, 32235–32242; e) F. C. Raps, C. A. Jin, A. C. Brown, D. Sorigué, T. K. Hyster, *J. Am. Chem. Soc.* **2025**, *147*, 40547–40553.

[135] Z.-C. Wang, L. Gao, S.-Y. Liu, P. Wang, S.-L. Shi, *J. Am. Chem. Soc.* **2025**, *147*, 3023–3031.

[136] M. Seo, H. Kim, *J. Am. Chem. Soc.* **2025**, *147*, 41691–41698.

[137] X. Zhou, Q. Huang, J. Guo, L. Dai, Y. Lu, *Angew. Chem. Int. Ed.* **2023**, *62*, e202310078.

[138] X. Wang, A. Guram, S. Caille, J. Hu, J. P. Preston, M. Ronk, S. Walker, *Org. Lett.* **2011**, *13*, 1881–1883.

[139] a) F. Ling, S. Nian, J. Chen, W. Luo, Z. Wang, Y. Lv, W. Zhong, *J. Org. Chem.* **2018**, *83*, 10749–10761; b) J. Guan, Y. Luo, Q. Wang, J. Chen, W. Zhang, *Angew. Chem. Int. Ed.* **2024**, *63*, e202416313.

[140] W. Liu, J. Guo, S. Xing, Z. Lu, *Org. Lett.* **2020**, *22*, 2532–2536.

[141] J. Zhou, J. Ye, Y. Zhang, Z. Li, J. Li, D. Liu, W. Zhang, *Adv. Synth. Catal.* **2023**, *365*, 1275–1286.

[142] Z. Wang, L.-Y. Xue, Y. Xu, Q.-L. Zhou, *J. Am. Chem. Soc.* **2025**, *147*, 19491–19497.

[143] L.-L. Yang, D. Evans, B. Xu, W.-T. Li, M.-L. Li, S.-F. Zhu, K. N. Houk, Q.-L. Zhou, *J. Am. Chem. Soc.* **2020**, *142*, 12394–12399.

[144] a) Y.-T. Zhao, Y.-X. Su, X.-Y. Li, L.-L. Yang, M.-Y. Huang, S.-F. Zhu, *Angew. Chem. Int. Ed.* **2021**, *60*, 24214–24219; b) B. Yang, K. Cao, G. Zhao, J. Yang, J. Zhang, *J. Am. Chem. Soc.* **2022**, *144*, 15468–15474; c) W. Xu, T. Yamakawa, M. Huang, P. Tian, Z. Jiang, M.-H. Xu, *Angew. Chem. Int. Ed.* **2024**, *63*, e202412193; d) Y.-Z. Lin, S. Yuan, Y. Xu, H.-Y. Hu, X.-M. Zhao, Y.-G. Liang, S.-C. Zheng, *Angew. Chem. Int. Ed.* **2025**, e19102.

[145] J. Mazuela, J. J. Verendel, M. Coll, B. Schäffner, A. Börner, P. G. Andersson, O. Pàmies, M. Diéguez, *J. Am. Chem. Soc.* **2009**, *131*, 12344–12353.

[146] Y.-Z. Sui, X.-C. Zhang, J.-W. Wu, S. Li, J.-N. Zhou, M. Li, W. Fang, A. S. C. Chan, J. Wu, *Chem. Eur. J.* **2012**, *18*, 7486–7492.

[147] E. N. Bess, M. S. Sigman, *Org. Lett.* **2013**, *15*, 646–649.

[148] K. Li, W.-Q. Wu, Y. Lin, H. Shi, *Nat. Commun.* **2023**, *14*, 2170–2178.

[149] E. J. Corey, C. J. Helal, *Tetrahedron Lett.* **1996**, *37*, 4837–4840.

[150] Y. Liu, Y.-L. S. Tse, F. Y. Kwong, Y.-Y. Yeung, *ACS Catal.* **2017**, *7*, 4435–4440.

[151] J. Clayden, J. Dufour, D. M. Grainger, M. Helliwell, *J. Am. Chem. Soc.* **2007**, *129*, 7488–7489.

[152] D. Ma, C.-B. Miao, J. Sun, *J. Am. Chem. Soc.* **2019**, *141*, 13783–13787.

[153] H. Wu, Q. Wang, J. Zhu, *J. Am. Chem. Soc.* **2019**, *141*, 11372–11377.

[154] M. W. Gribble, S. Guo, S. L. Buchwald, *J. Am. Chem. Soc.* **2018**, *140*, 5057–5060.

[155] S. Song, S.-F. Zhu, Y.-B. Yu, Q.-L. Zhou, *Angew. Chem. Int. Ed.* **2013**, *52*, 1556–1559.

[156] J. Chen, C. Chen, C. Ji, Z. Lu, *Org. Lett.* **2016**, *18*, 1594–1597.

[157] I. Agranat, H. Caner, J. Caldwell, *Nat. Rev. Drug Discov.* **2002**, *1*, 753–768.

[158] S. Park, A. K. Dutta, C. Allacher, A. Abramov, P. Dullinger, K. Kuzmanoska, D. Fritsch, P. Hitzfeld, D. Horinek, J. Rehbein et al., *Angew. Chem. Int. Ed.* **2022**, *61*, e202208611.

[159] a) A. J. Cresswell, S. T.-C. Eey, S. E. Denmark, *Nat. Chem.* **2014**, *7*, 146–152; b) D. G. Garratt, G. H. Schmid, *Can. J. Chem.* **1974**, *52*, 3599–3606; c) L. Engman, *J. Org. Chem.* **1987**, *52*, 4086–4094.

[160] Z. Tao, B. B. Gilbert, S. E. Denmark, *J. Am. Chem. Soc.* **2019**, *141*, 19161–19170.

[161] E. M. Mumford, B. N. Hemric, S. E. Denmark, *J. Am. Chem. Soc.* **2021**, *143*, 13408–13417.

[162] a) J. Tsuji, *Synthesis* **1984**, *1984*, 369–384; b) Q. Feng, Q. Wang, J. Zhu, *Science* **2023**, *379*, 1363–1368; c) J. Sietmann, M. Tenberge, J. M. Wahl, *Angew. Chem. Int. Ed.* **2023**, *62*, e202215381.

[163] S. Ortgies, A. Breder, *Org. Lett.* **2015**, *17*, 2748–2751.

[164] S. Ortgies, A. Breder, *ACS Catal.* **2017**, *7*, 5828–5840.

[165] S. Park, Dissertation, University of Regensburg, **2025**.

[166] B. Maji, X.-H. Duan, P. M. Jüstel, P. A. Byrne, A. R. Ofial, H. Mayr, *Chem. Eur. J.* **2021**, *27*, 11367–11376.

[167] M. J. Kamlet, J. L. M. Abboud, M. H. Abraham, R. W. Taft, *J. Org. Chem.* **1983**, *48*, 2877–2887.

[168] Y. Marcus, *Chem. Soc. Rev.* **1993**, *22*, 409.

[169] Z. Cai, S. Li, Y. Gao, G. Li, *Adv. Synth. Catal.* **2018**, *360*, 4005–4011.

[170] a) L. A. P. Silks, R. Wu, R. B. Dunlap, J. D. Odom, *Phosphorus Sulfur Silicon Relat. Elem.* **1998**, *136*, 209–214; b) R. Michalczyk, J. G. Schmidt, E. Moody, Z. Li, R. Wu, R. B. Dunlap, J. D. Odom, L. A. P. Silks, *Angew. Chem. Int. Ed.* **2000**, *39*, 3067–3070.

[171] S. Ortgies, C. Depken, A. Breder, *Org. Lett.* **2016**, *18*, 2856–2859.

[172] M. Wilken, S. Ortgies, A. Breder, I. Siewert, *ACS Catal.* **2018**, *8*, 10901–10912.

[173] M. Martiny, E. Steckhan, T. Esch, *Chem. Ber.* **1993**, *126*, 1671–1682.

[174] a) S. M. Halas, K. Okyne, A. J. Fry, *Electrochim. Acta* **2003**, *48*, 1837–1844; b) X. Wu, A. P. Davis, A. J. Fry, *Org. Lett.* **2007**, *9*, 5633–5636; c) H. Roth, N. Romero, D. Nicewicz, *Synlett* **2016**, *27*, 714–723.

[175] P. Modiba, M. Matoetoe, A. M. Crouch, *J. Power Sources* **2012**, *205*, 1–9.

[176] E. Speckmeier, T. G. Fischer, K. Zeitler, *J. Am. Chem. Soc.* **2018**, *140*, 15353–15365.

[177] C. Reichardt, T. Welton, *Solvents and Solvent Effects in Organic Chemistry*, Wiley-VCH, Weinheim, **2011**.

[178] T. Lei, S. Graf, C. Schöll, F. Krätzschmar, B. Gregori, T. Appleson, A. Breder, *ACS Catal.* **2023**, *13*, 16240–16248.

[179] a) Y. Kawamata, T. Hashimoto, K. Maruoka, *J. Am. Chem. Soc.* **2016**, *138*, 5206–5209; b) Y. Otsuka, Y. Shimazaki, H. Nagaoka, K. Maruoka, T. Hashimoto, *Synlett* **2019**, *30*, 1679–1682.

[180] S. Satyanarayanajois, S. Villalba, L. Jianchao, G. M. Lin, *Chem. Bio. Drug Des.* **2009**, *74*, 246–257.

[181] D.-J. Dong, H.-H. Li, S.-K. Tian, *J. Am. Chem. Soc.* **2010**, *132*, 5018–5020.

[182] Y. Zhang, Y. Li, S.-F. Ni, J.-P. Li, D. Xia, X. Han, J. Lin, J. Wang, S. Das, W.-D. Zhang, *Chem. Sci.* **2023**, *14*, 10411–10419.

[183] Q. Sha, Y. Ling, W. Wang, Y. Wei, *Adv. Synth. Catal.* **2013**, *355*, 2145–2150.

[184] C. Palomo, M. Oiarbide, J. M. García, *Chem. Soc. Rev.* **2012**, *41*, 4150–4164.

[185] a) A. Rajagopalan, M. Lara, W. Kroutil, *Adv. Synth. Catal.* **2013**, *355*, 3321–3335; b) L. Yu, H. Cao, X. Zhang, Y. Chen, L. Yu, *Sustain. Energy Fuels* **2020**, *4*, 730–736.

[186] S. Qian, T. M. Lazarus, D. A. Nicewicz, *J. Am. Chem. Soc.* **2023**.

[187] M. Fischer, Dissertation, University of Regensburg, **2025**.

[188] X. Hu, G. Zhang, F. Bu, A. Lei, *ACS Catal.* **2017**, *7*, 1432–1437.

[189] S. Kumar Nanda, *Adv. Synth. Catal.* **2023**, *365*, 834–853.

[190] S. Ortgies, R. Rieger, K. Rode, K. Koszinowski, J. Kind, C. M. Thiele, J. Rehbein, A. Breder, *ACS Catal.* **2017**, *7*, 7578–7586.

[191] G. Borodkin, E. I. Chernyak, M. M. Shakirov, V. G. Shubin, *Russ. J. Org. Chem.* **1998**, *34*, 1563–1568.

[192] T. I. Sølling, S. B. Wild, L. Radom, *Chem. Eur. J.* **1999**, *5*, 509–514.

[193] T. Wirth, G. Fragale, M. Spichty, *J. Am. Chem. Soc.* **1998**, *120*, 3376–3381.

[194] S. E. Denmark, W. R. Collins, *Org. Lett.* **2007**, *9*, 3801–3804.

[195] S. E. Denmark, D. Kalyani, W. R. Collins, *J. Am. Chem. Soc.* **2010**, *132*, 15752–15765.

[196] H. Zhang, S. Lin, E. N. Jacobsen, *J. Am. Chem. Soc.* **2014**, *136*, 16485–16488.

[197] E. Harrer, Masterarbeit, University of Regensburg, **2023**.

[198] H. G. Yayla, H. Wang, K. T. Tarantino, H. S. Orbe, R. R. Knowles, *J. Am. Chem. Soc.* **2016**, *138*, 10794–10797.

[199] a) J. Burés, A. Armstrong, D. G. Blackmond, *J. Am. Chem. Soc.* **2012**, *134*, 6741–6750; b) T. Földes, Á. Madarász, Á. Révész, Z. Dobi, S. Varga, A. Hamza, P. R. Nagy, P. M. Pihko, I. Pápai, *J. Am. Chem. Soc.* **2017**, *139*, 17052–17063; c) C. Ali, D. G. Blackmond, J. Burés, *ACS Catal.* **2022**, *12*, 5776–5785.

[200] a) R. D. Otzenberger, K. B. Lipkowitz, B. P. Mundy, *J. Org. Chem.* **1974**, *39*, 319–321; b) P. J. Crowley, M. Robinson, M. G. Ward, *Tetrahedron* **1977**, *33*, 915–925; c) J. I. Seeman, *Chem. Rev.* **1983**, *83*, 83–134; d) L. Carballeira, I. Prez-Juste, *J. Comput. Chem.* **1998**, *19*, 961–976.

[201] B. Giese, B. Kopping, T. Göbel, J. Dickhaut, G. Thoma, K.J. Kulicke, F. Trach in *Organic Reactions*, John Wiley & Sons, Ltd, **2004**, pp. 301–856.

[202] a) A. Streitwieser, G. R. Ziegler, P. C. Mowery, A. Lewis, R. G. Lawler, *J. Am. Chem. Soc.* **1968**, *90*, 1357–1358; b) R. Faust, E. D. Glendening, A. Streitwieser, K. P. C. Vollhardt, *J. Am. Chem. Soc.* **1992**, *114*, 8263–8268; c) T. Zheng, J. R. Tabor, Z. L. Stein, F. E. Michael, *Org. Lett.* **2018**, *20*, 6975–6978.

[203] W.-T. Guo, B.-H. Zhu, Y. Chen, J. Yang, P.-C. Qian, C. Deng, L.-W. Ye, L. Li, *J. Am. Chem. Soc.* **2022**, *144*, 6981–6991.

[204] S. Murayama, Z. Li, H. Liang, Y. Liu, H. Naka, K. Maruoka, *Chem. Eur. J.* **2023**, *29*, e202301866.

[205] L. Melander, W. H. Saunders (Eds.) *Reaction Rates of Isotopic Molecules*, Wiley: New York, New York, **1980**.

[206] D. A. Singleton, A. A. Thomas, *J. Am. Chem. Soc.* **1995**, *117*, 9357–9358.

[207] C. Colletto, S. Islam, F. Juliá-Hernández, I. Larrosa, *J. Am. Chem. Soc.* **2016**, *138*, 1677–1683.

[208] S. E. Denmark, L. R. Marcin, M. E. Schnute, A. Thorarensen, *Org. Synth.* **1997**, *74*, 33.

[209] Y. Li, S. Yu, X. Wu, J. Xiao, W. Shen, Z. Dong, J. Gao, *J. Am. Chem. Soc.* **2014**, *136*, 4031–4039.

[210] D. H. Ripin, D. A. Evans, pKa Tables, Harvard University, **2005**.

[211] F. Chen, C. K. Tan, Y.-Y. Yeung, *J. Am. Chem. Soc.* **2013**, *135*, 1232–1235.

[212] S. H. Pine, G. S. Shen, H. Hoang, *Synthesis* **1991**, 165–167.

[213] a) E. Oldfield, F.-Y. Lin, *Angew. Chem. Int. Ed.* **2012**, *51*, 1124–1137; b) S. J. Harwood, M. D. Palkowitz, C. N. Gannett, P. Perez, Z. Yao, L. Sun, H. D. Abruña, S. L. Anderson, P. S. Baran, *Science* **2022**, *375*, 745–752.

[214] J. Zou, L. Xu, Y. Tang, W. Wang, Y. Cai, *Org. Lett.* **2022**, *24*, 7140–7144.

[215] K. Ravindar, P.-Y. Caron, P. Deslongchamps, *J. Org. Chem.* **2014**, *79*, 7979–7999.

[216] D. Sälinger, R. Brückner, *Chem. Eur. J.* **2009**, *15*, 6688–6703.

[217] J. L. Flügel, Masterarbeit, University of Regensburg, **2024**.

[218] M. Cushman, D. Nagarathnam, D. Gopal, H. M. He, C. M. Lin, E. Hamel, *J. Med. Chem.* **1992**, *35*, 2293–2306.

[219] P. Aliprandi, L. Cima, M. Carrara **2002**.

[220] J. Chen, Y.-Y. Zhu, L. Huang, S.-S. Zhang, S.-X. Gu, *Eur. J. Med. Chem.* **2025**, *287*, 117371.

[221] S. He, B. Lin, V. Chu, Z. Hu, X. Hu, J. Xiao, A. Q. Wang, C. J. Schweitzer, Q. Li, M. Imamura et al., *Sci. Transl. Med.* **2015**, *7*, 282ra49.

[222] K. C. K. Swamy, N. N. B. Kumar, E. Balaraman, K. V. P. P. Kumar, *Chem. Rev.* **2009**, *109*, 2551–2651.

[223] H. Huang, J. Y. Kang, *J. Org. Chem.* **2017**, *82*, 6604–6614.

[224] J. Cao, C. Ma, J. Zang, S. Gao, Q. Gao, X. Kong, Y. Yan, X. Liang, Q. Ding, C. Zhao et al., *Bioorg. Med. Chem.* **2018**, *26*, 3145–3157.

[225] a) B. Denegri, A. R. Ofial, S. Jurić, A. Streiter, O. Kronja, H. Mayr, *Chem. Eur. J.* **2006**, *12*, 1657–1666; b) B. Denegri, A. Streiter, S. Jurić, A. R. Ofial, O. Kronja, H. Mayr, *Chem. Eur. J.* **2006**, *12*, 1648–1656.

[226] G. Ana, P. M. Kelly, A. M. Malebari, S. Noorani, S. M. Nathwani, B. Twamley, D. Fayne, N. M. O'Boyle, D. M. Zisterer, E. F. Pimentel et al., *Pharmaceuticals* **2021**, *14*, 169.

[227] S. Newman, C. Bryan, D. Perez, M. Lautens, *Synthesis* **2011**, *2*, 342–346.

[228] M. B. Smith, *March's advanced organic chemistry. Reactions, mechanisms, and structure*, Wiley, Hoboken, New Jersey, **2025**.

[229] E. Frank, S. Park, E. Harrer, J. L. Flügel, M. Fischer, P. Nuernberger, J. Rehbein, A. Breder, *J. Am. Chem. Soc.* **2024**, *146*, 34383–34393.

[230] E. Frank, J. L. Flügel, L. d'Heureuse, S. Woick, A. Breder, *J. Org. Chem.* **2025**, just accepted.

[231] B. Denegri, O. Kronja, *J. Org. Chem.* **2009**, *74*, 5927–5933.

[232] J. Cao, C. Ma, J. Zang, S. Gao, Q. Gao, X. Kong, Y. Yan, X. Liang, Q. Ding, C. Zhao et al., *Bioorg. Med. Chem.* **2018**, *26*, 3145–3157.

[233] Y. Chen, M. Chen, Y. Liu, *Angew. Chem. Int. Ed.* **2012**, *51*, 6493–6497.

[234] N. Müller, O. Kováč, A. Rode, D. Atzl, T. Magauer, *J. Am. Chem. Soc.* **2024**, *146*, 22937–22942.

[235] P. Zhang, J. Xu, Y. Gao, X. Li, G. Tang, Y. Zhao, *Synlett* **2014**, *25*, 2928–2932.

[236] R. J. Kutta, Dissertation, University of Regensburg, **2013**.

7 Spectra

^{1}H NMR (400 MHz, $CDCl_3$) of **S1**

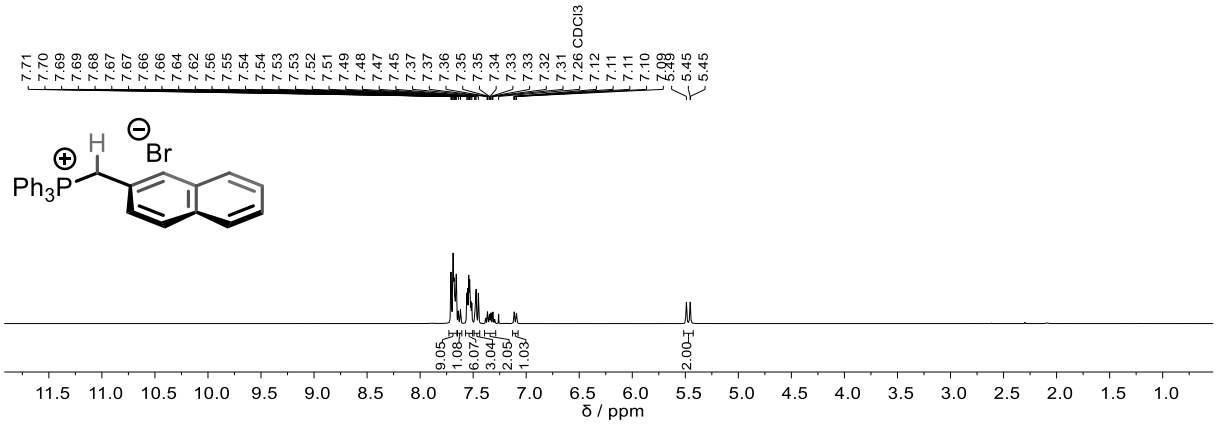

^{13}C{^{1}H} NMR (101 MHz, $CDCl_3$) of **S1**

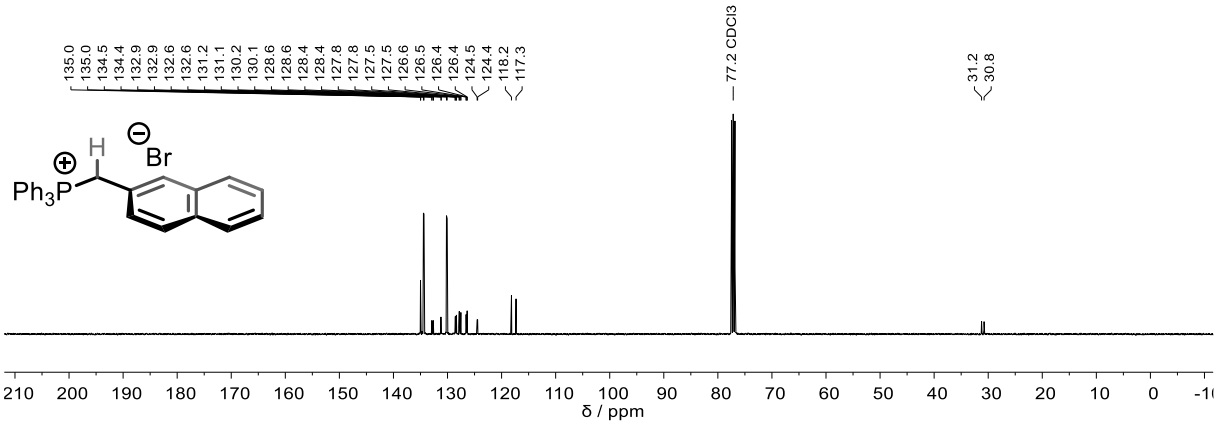

^{31}P{^{1}H} NMR (162 MHz, $CDCl_3$) of **S1**

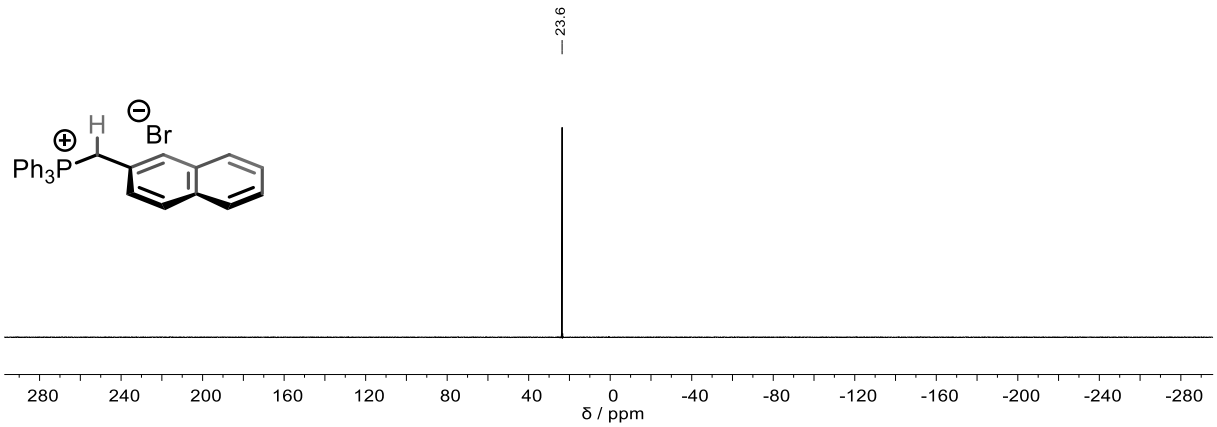

IR (ATR, neat) of **S1**

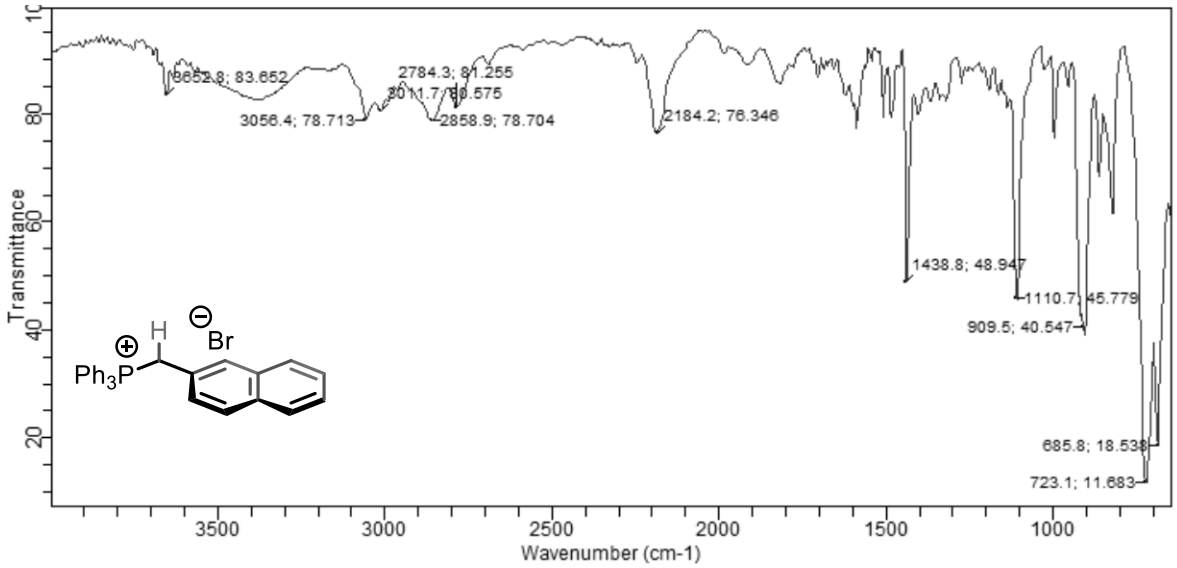

^{1}H NMR (400 MHz, $CDCl_3$) of **S2**

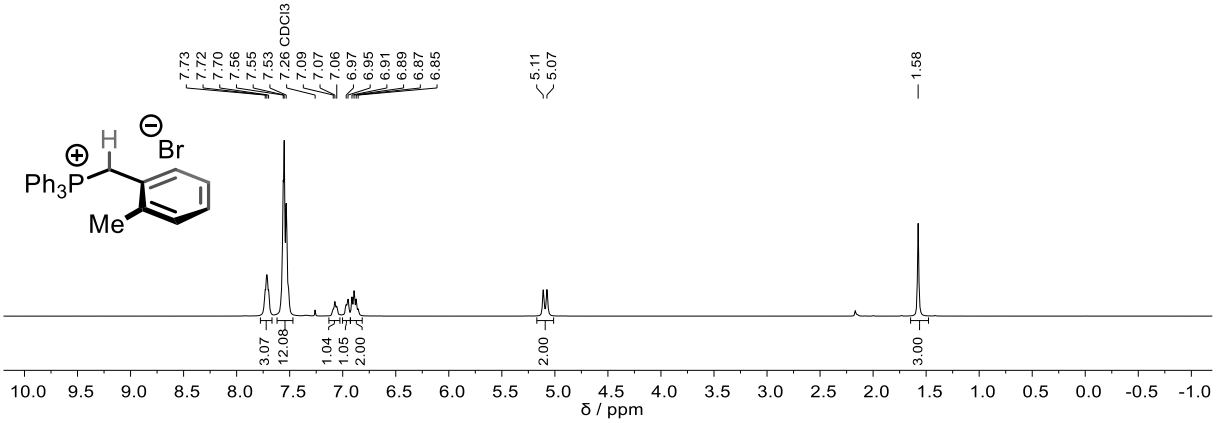

^{13}C{^{1}H} NMR (101 MHz, $CDCl_3$) of **S2**

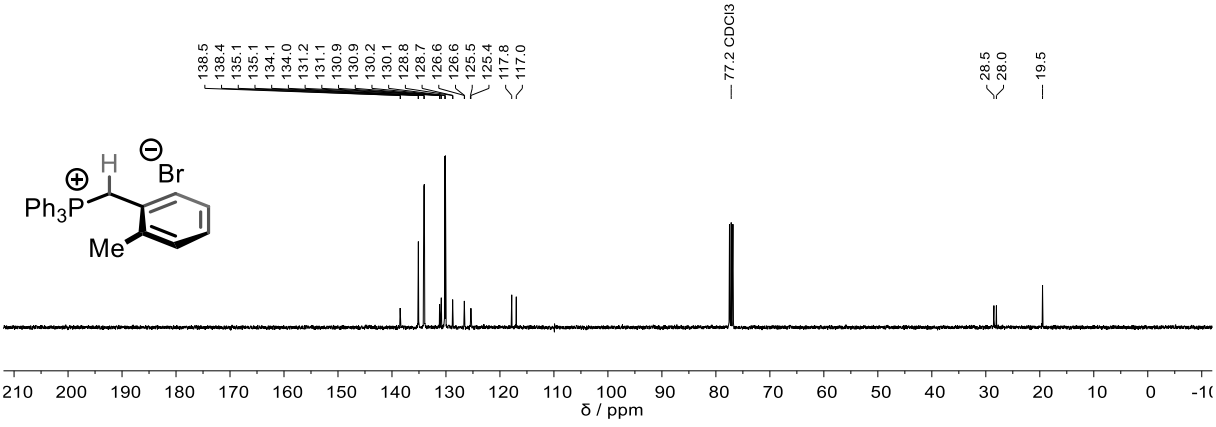

^{31}P{^{1}H} NMR (162 MHz, $CDCl_3$) of **S2**

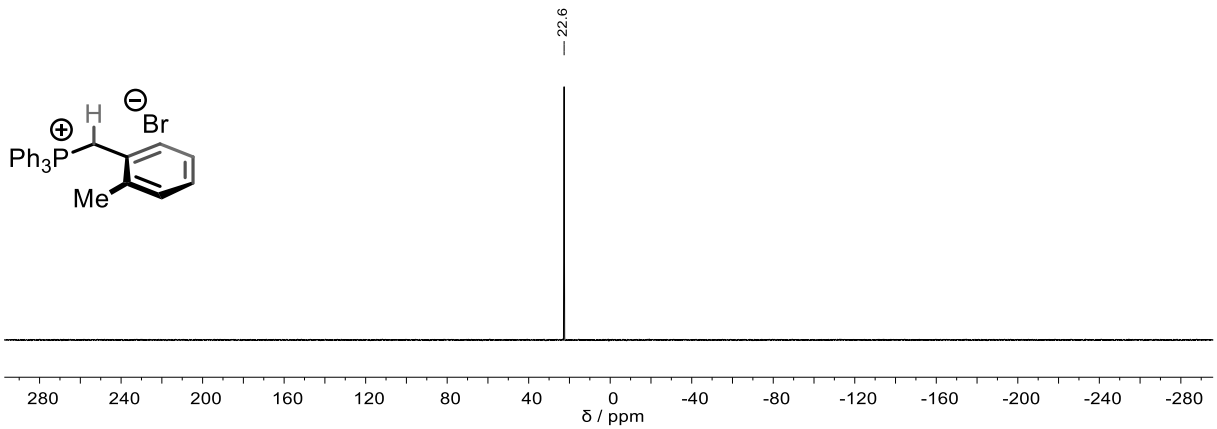

IR (ATR, neat) of **S2**

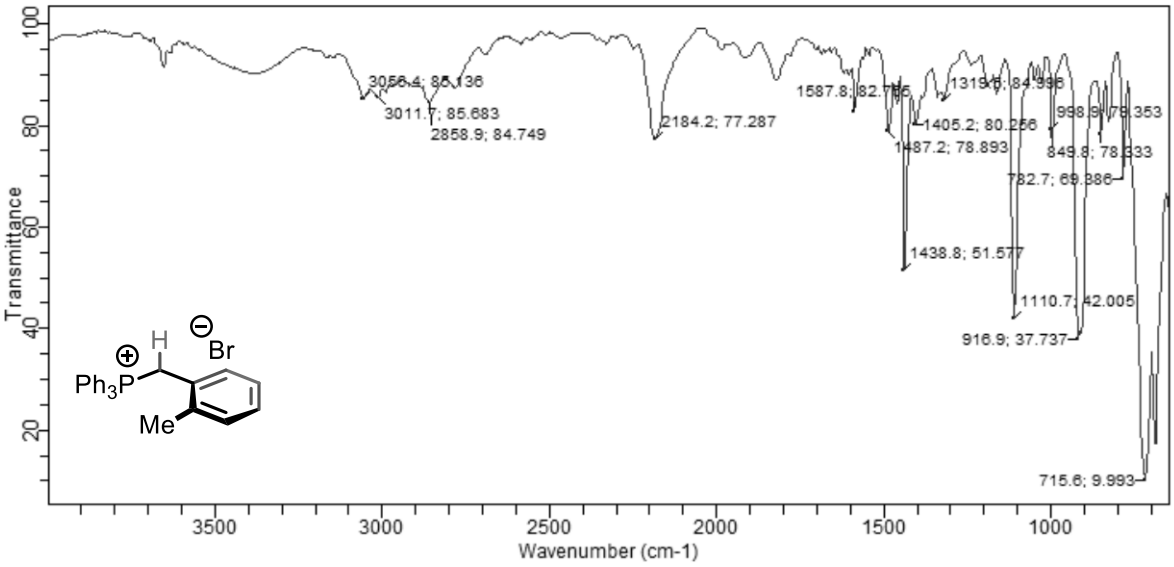

^{1}H NMR (400 MHz, $CDCl_3$) of **S3**

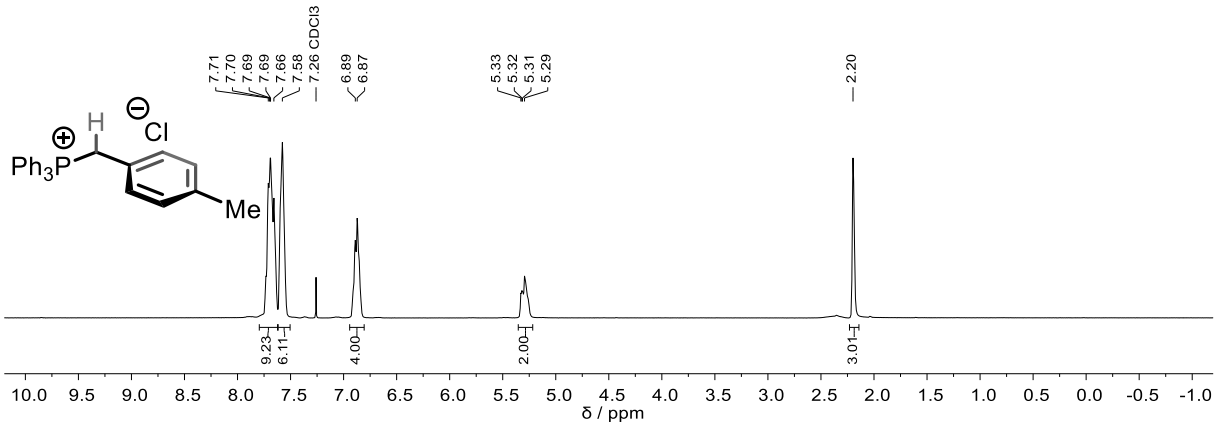

$^{13}C\{^{1}H\}$ NMR (101 MHz, $CDCl_3$) of **S3**

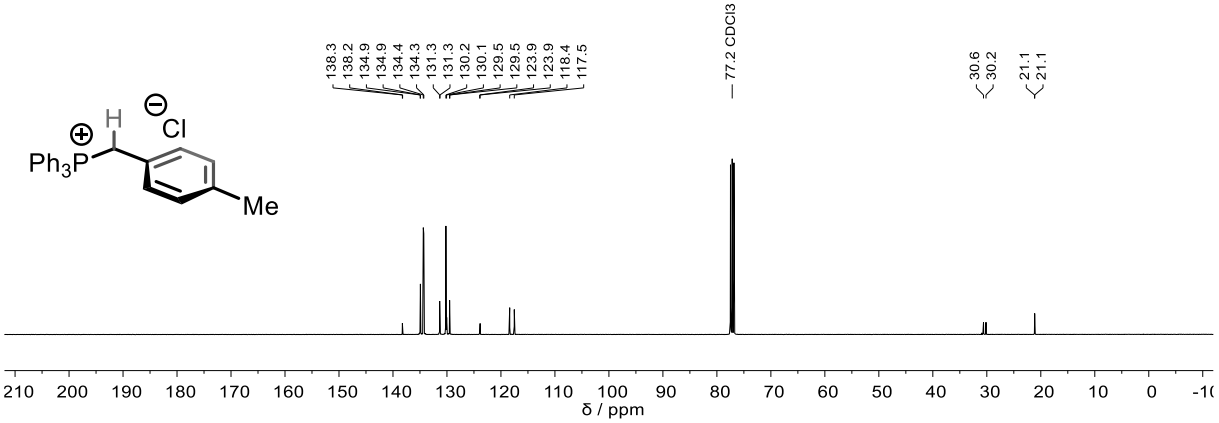

$^{31}P\{^{1}H\}$ NMR (162 MHz, $CDCl_3$) of **S3**

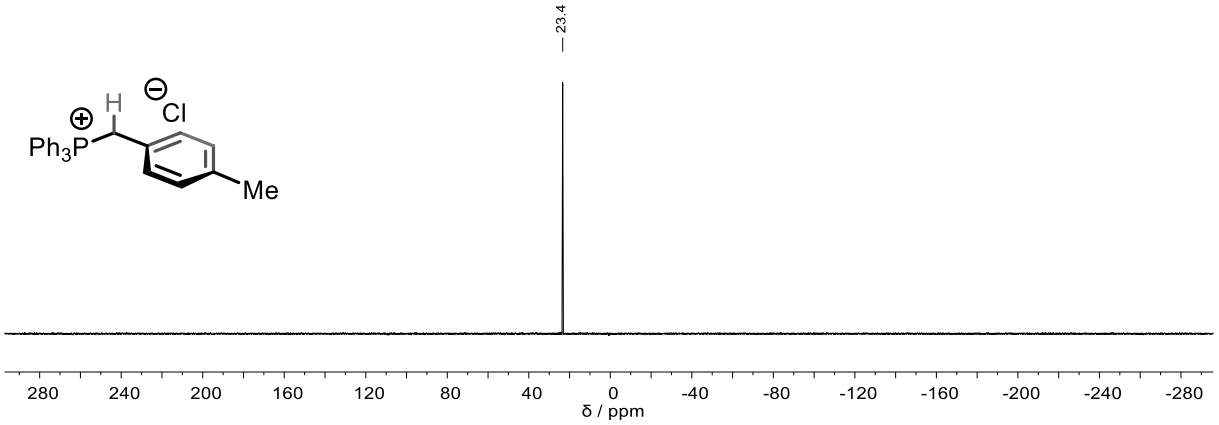

IR (ATR, neat) of **S3**

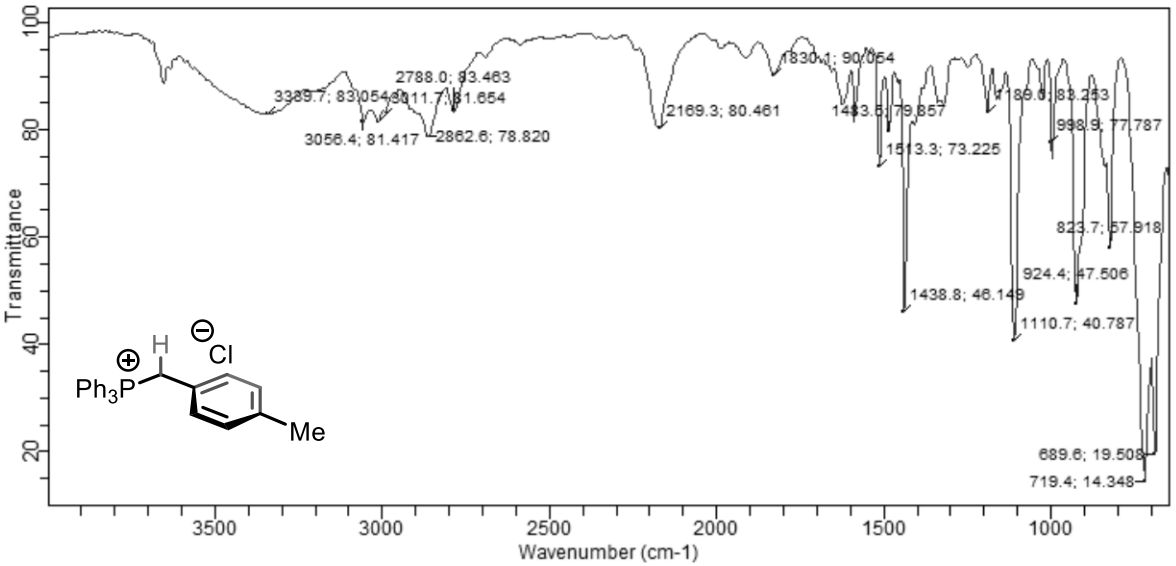

^{1}H NMR (400 MHz, $CDCl_3$) of **S4**

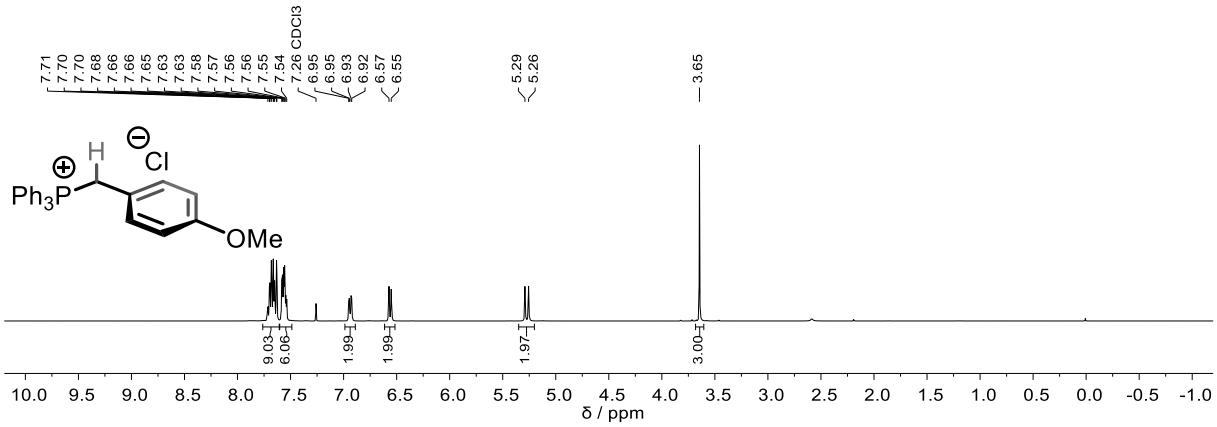

^{13}C{^{1}H} NMR (101 MHz, $CDCl_3$) of **S4**

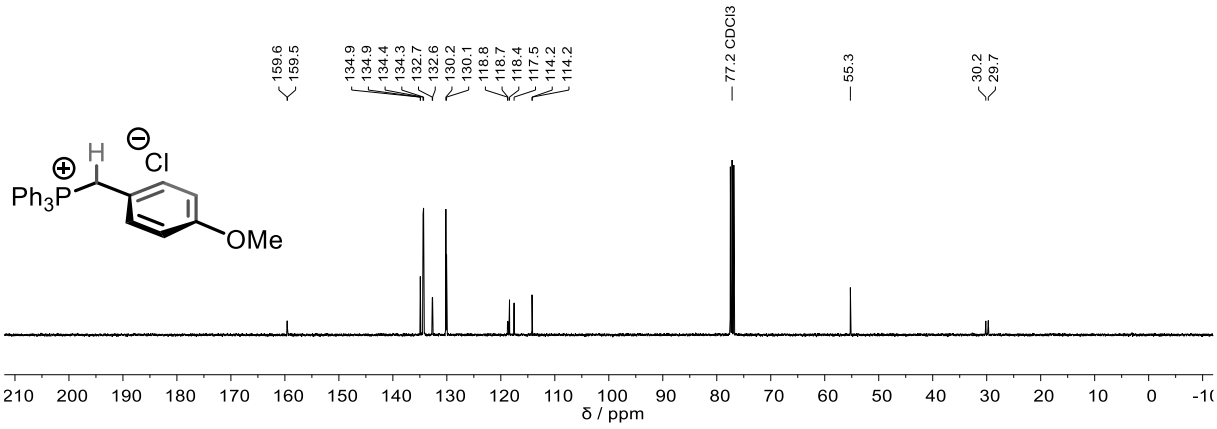

^{31}P{^{1}H} NMR (162 MHz, $CDCl_3$) of **S4**

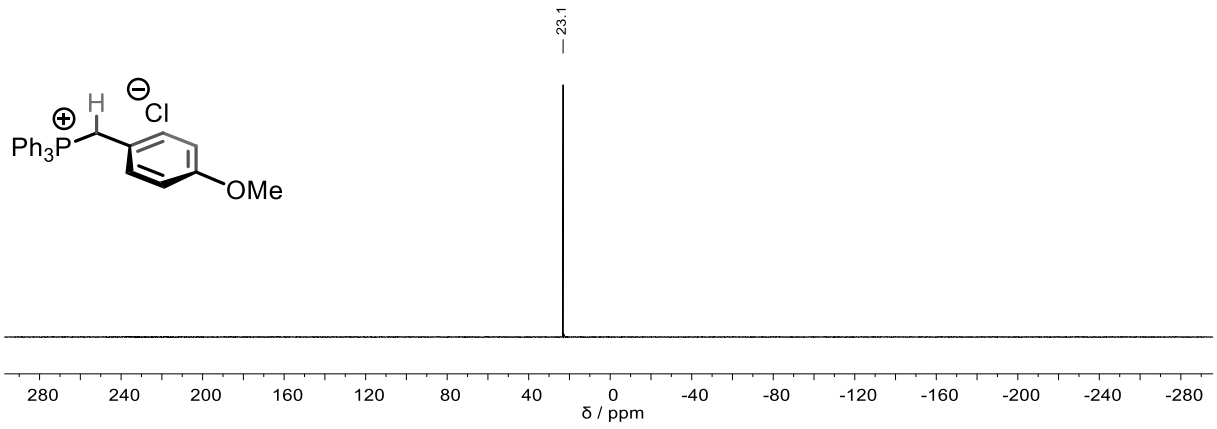

IR (ATR, neat) of **S4**

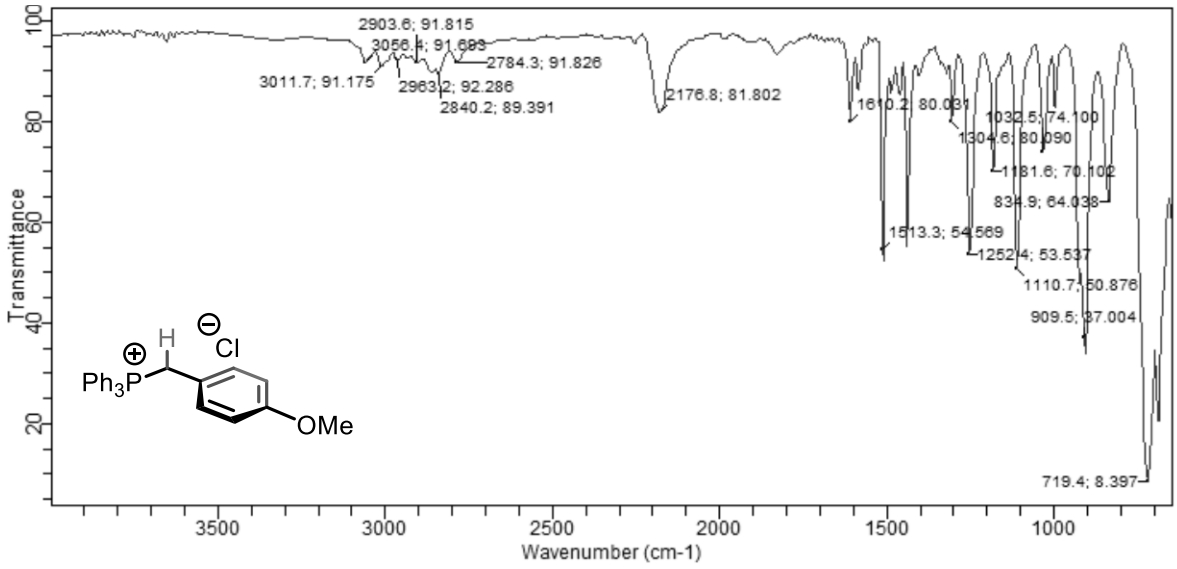

^{1}H NMR (400 MHz, $CDCl_3$) of **S5**

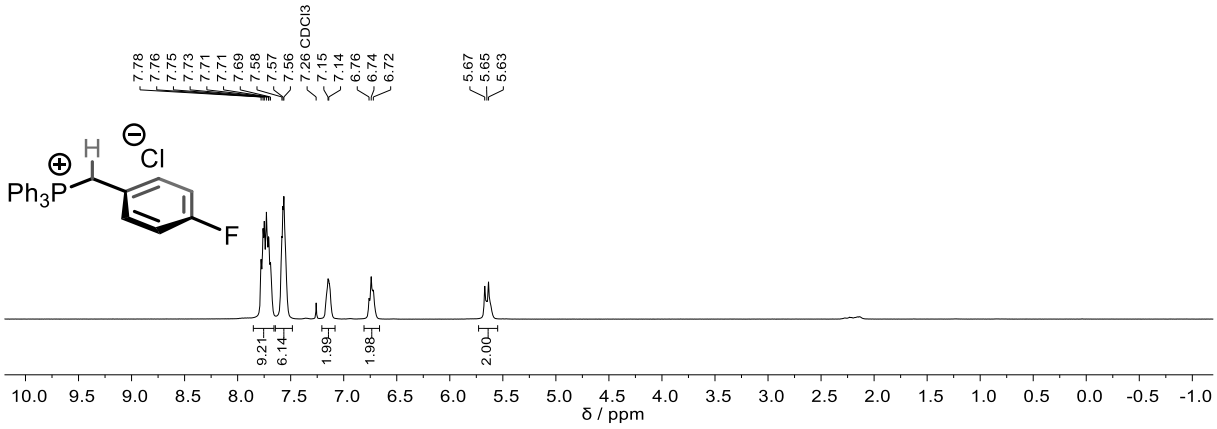

^{13}C{^{1}H} NMR (101 MHz, $CDCl_3$) of **S5**

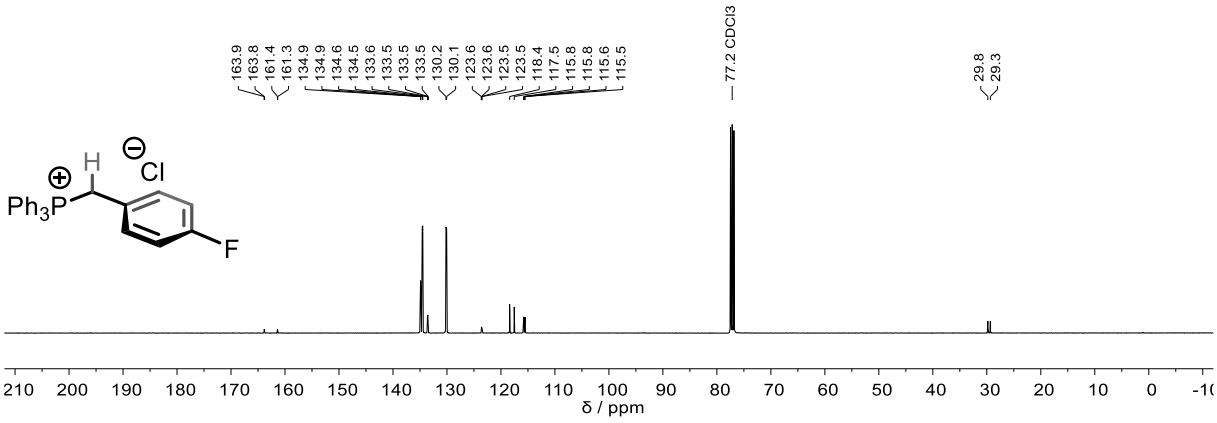

$^{31}P\{^{1}H\}$ NMR (162 MHz, $CDCl_3$) of **S5**

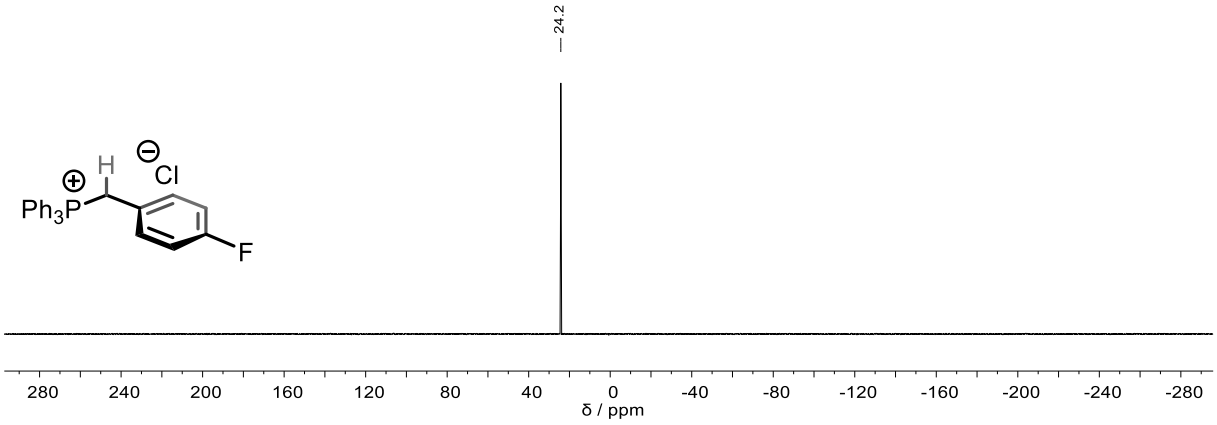

$^{19}F\{^{1}H\}$ NMR (377 MHz, $CDCl_3$) of **S5**

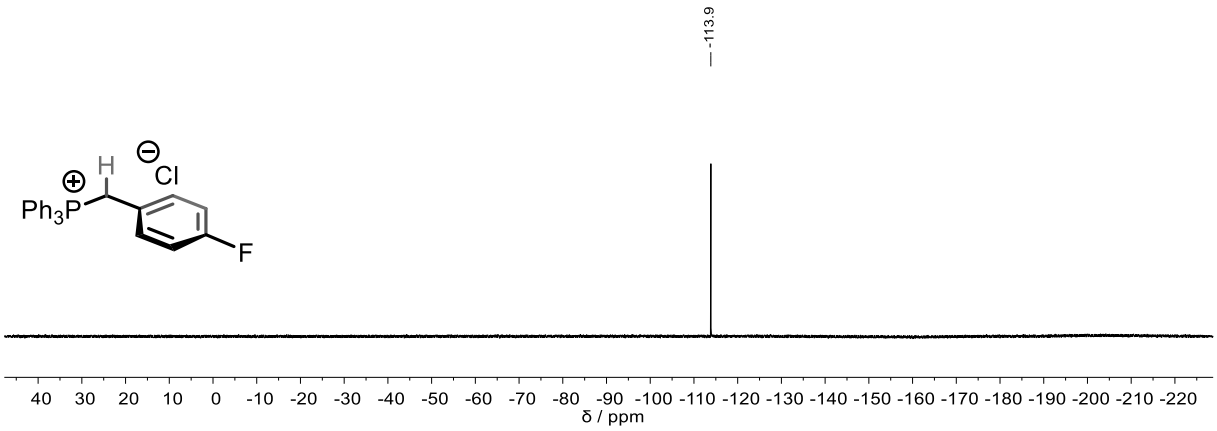

IR (ATR, neat) of **S5**

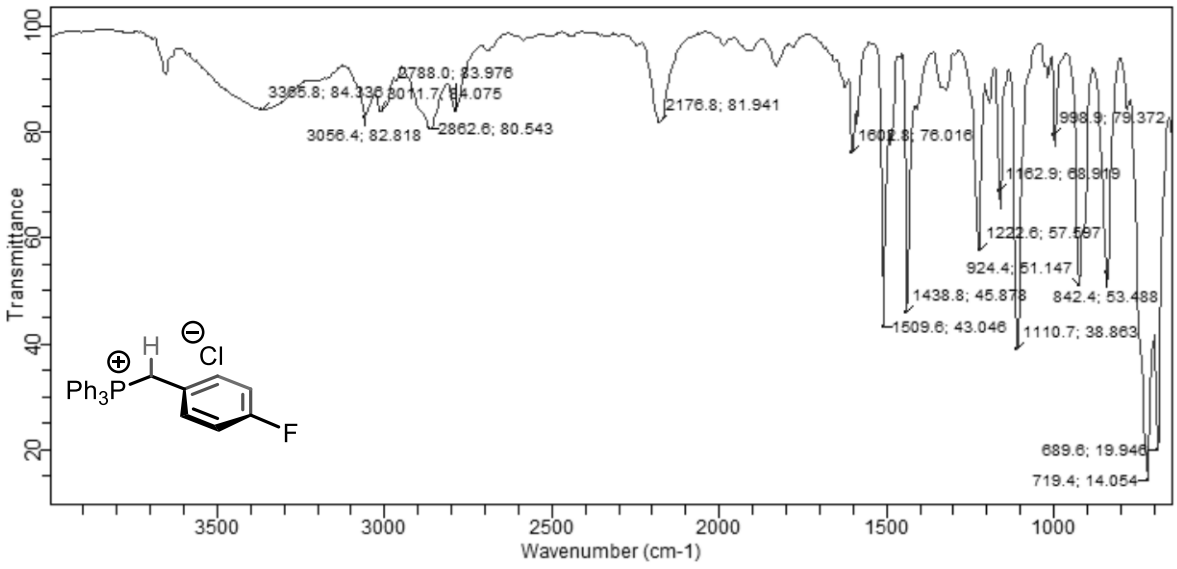

^{1}H NMR (400 MHz, $CDCl_3$) of **S6**

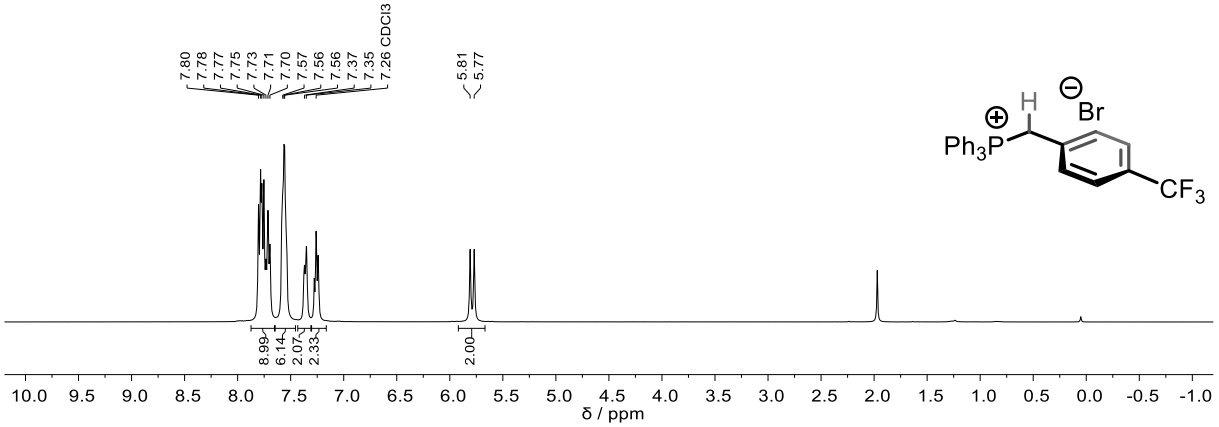

^{13}C{^{1}H} NMR (101 MHz, $CDCl_3$) of **S6**

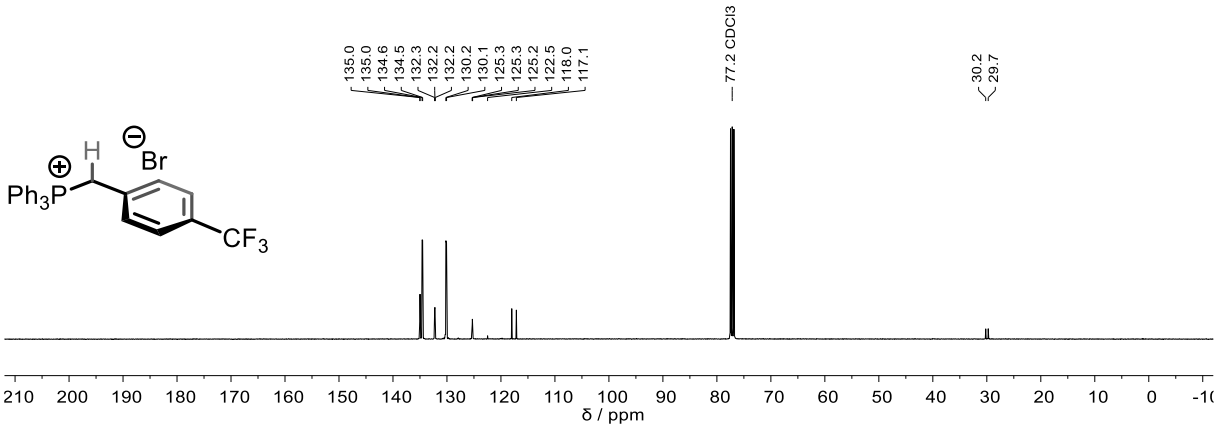

^{31}P{^{1}H} NMR (162 MHz, $CDCl_3$) of **S6**

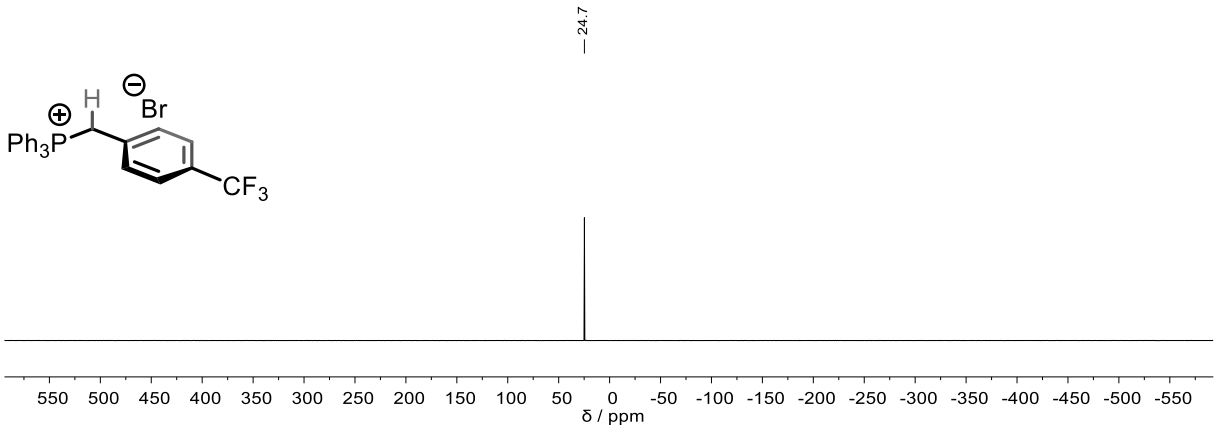

$^{19}F\{^{1}H\}$ NMR (377 MHz, $CDCl_3$) of **S6**

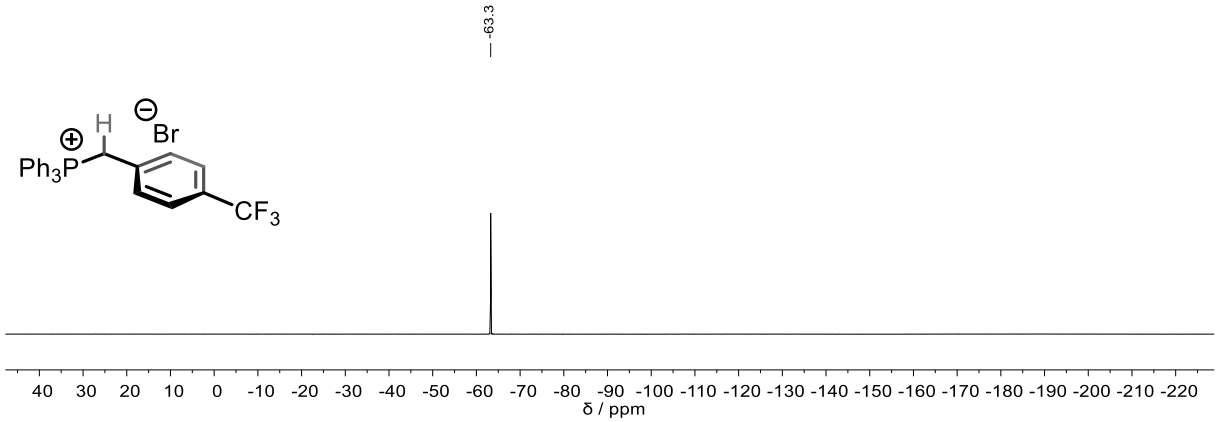

IR (ATR, neat) of **S6**

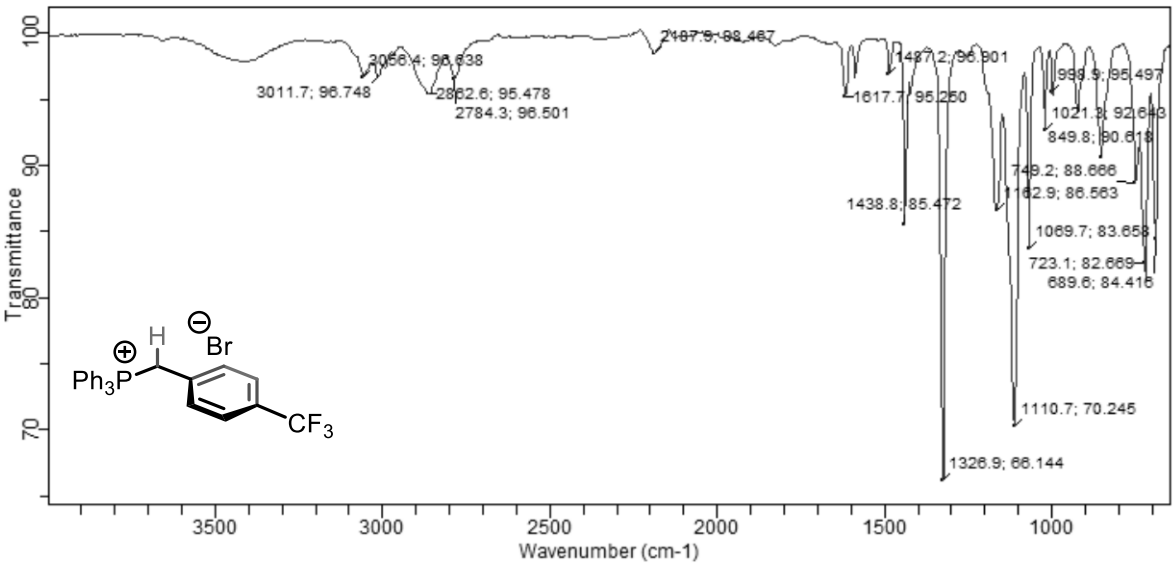

^{1}H NMR (400 MHz, $CDCl_3$) of **S7**

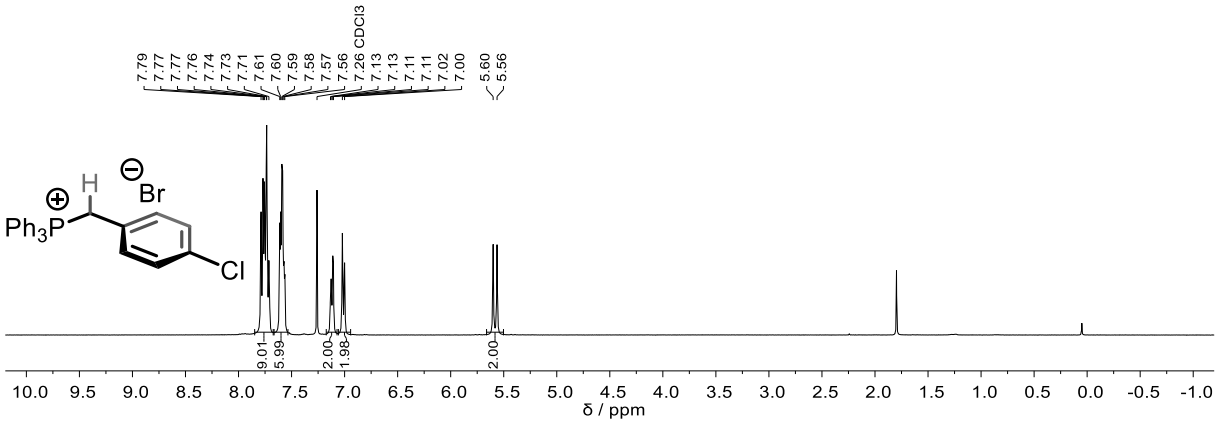

$^{13}C\{^{1}H\}$ NMR (101 MHz, $CDCl_3$) of **S7**

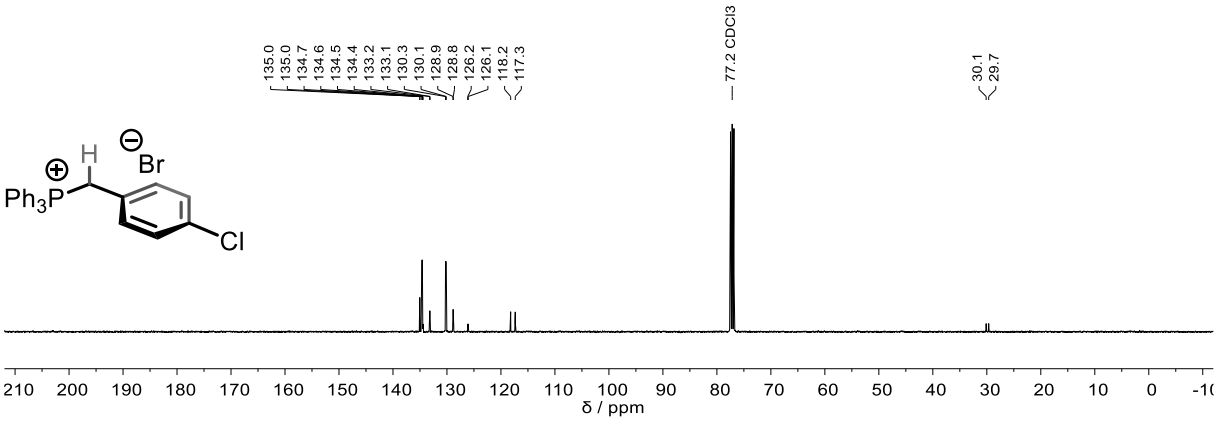

$^{31}P\{^{1}H\}$ NMR (162 MHz, $CDCl_3$) of **S7**

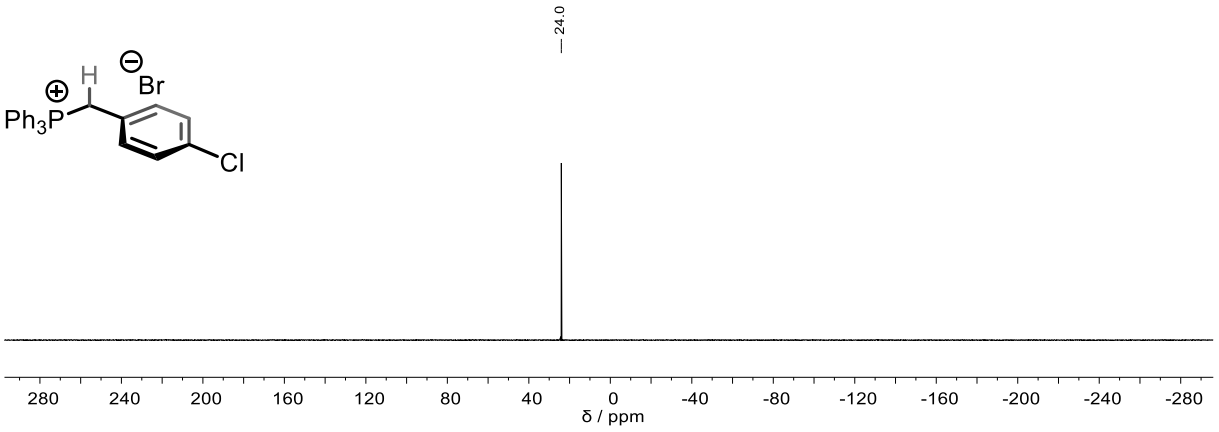

IR (ATR, neat) of **S7**

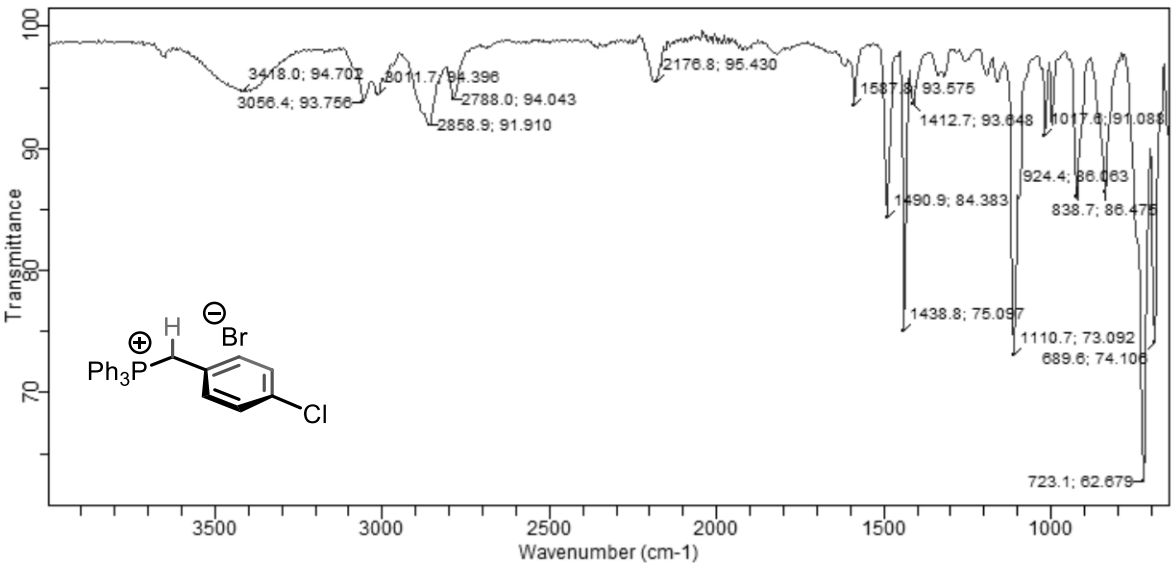

^{1}H NMR (400 MHz, $CDCl_3$) of *E*/*Z*-**1a** (*E*:*Z* = 58:42)

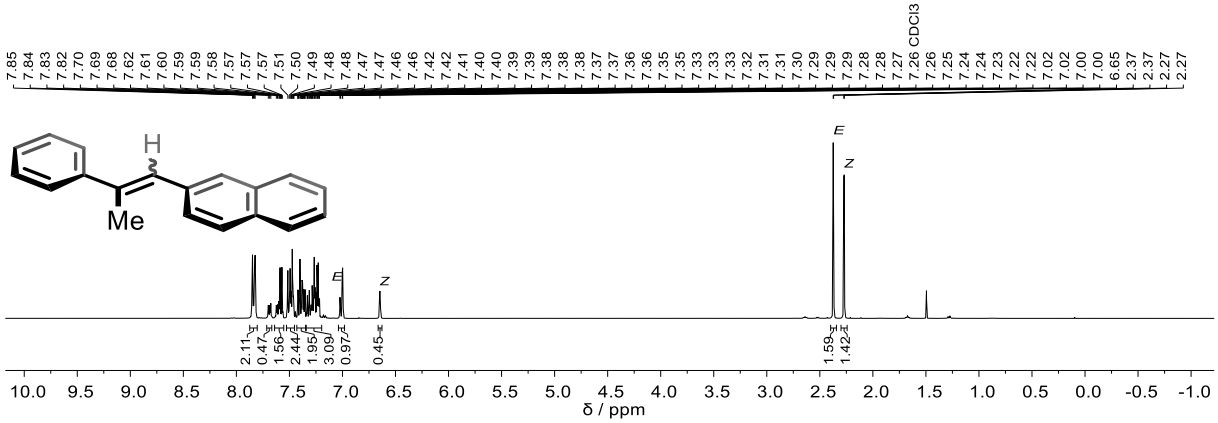

^{13}C{^{1}H} NMR (101 MHz, $CDCl_3$) of *E*/*Z*-**1a** (*E*:*Z* = 58:42)

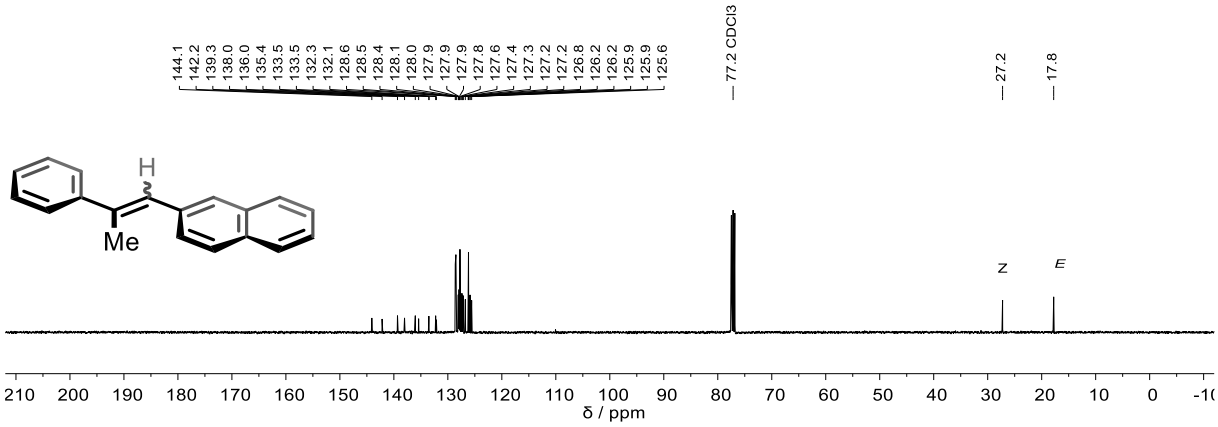

IR (ATR, neat) of *E*/*Z*-**1a**

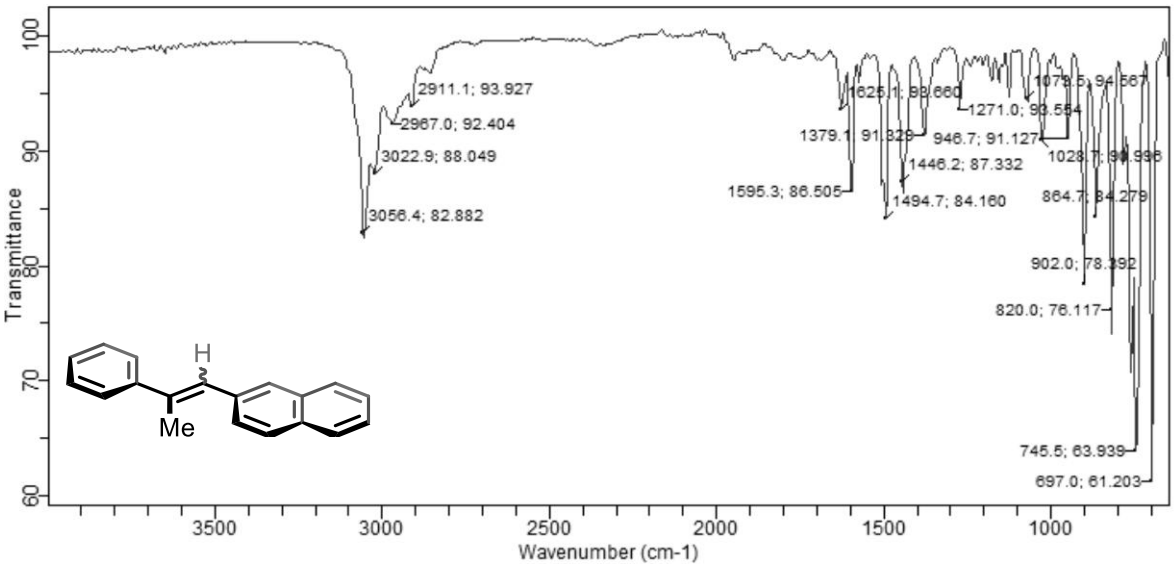

^{1}H NMR (400 MHz, $CDCl_3$) of *E*-**1a**

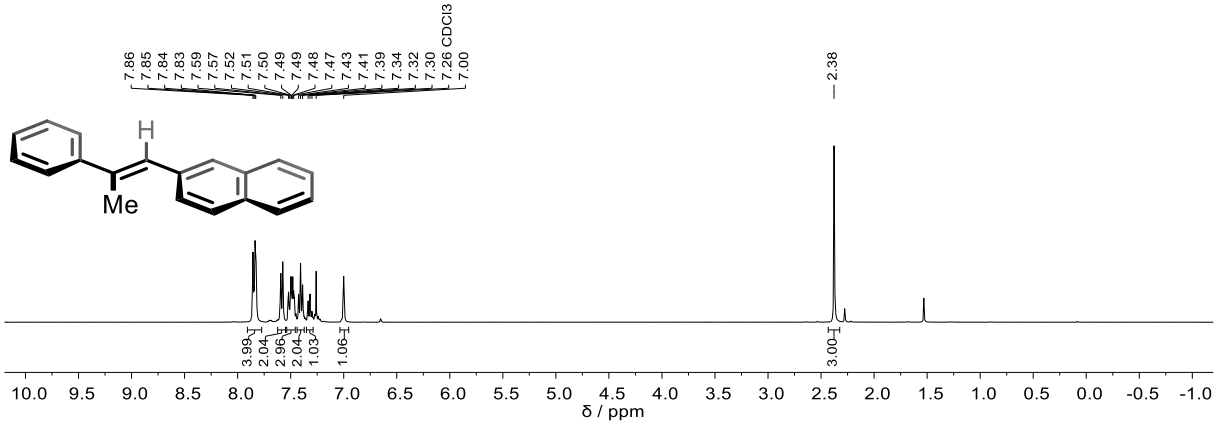

^{13}C{^{1}H} NMR (101 MHz, $CDCl_3$) of *E*-**1a**

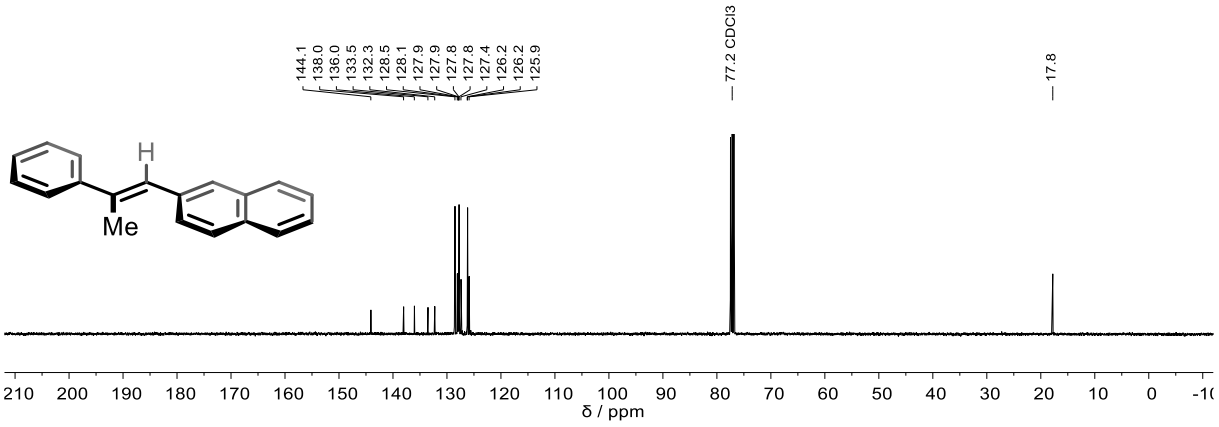

NOESY (400 MHz, $CDCl_3$) of *E*-**1a**

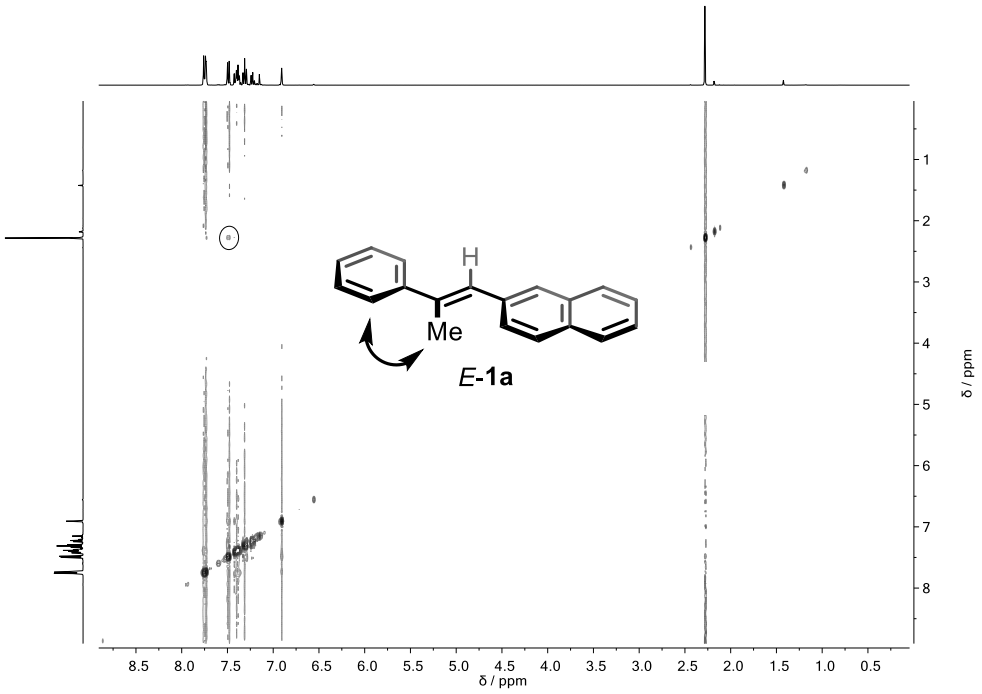

^{1}H NMR (400 MHz, $CDCl_3$) of *Z*-**1a**

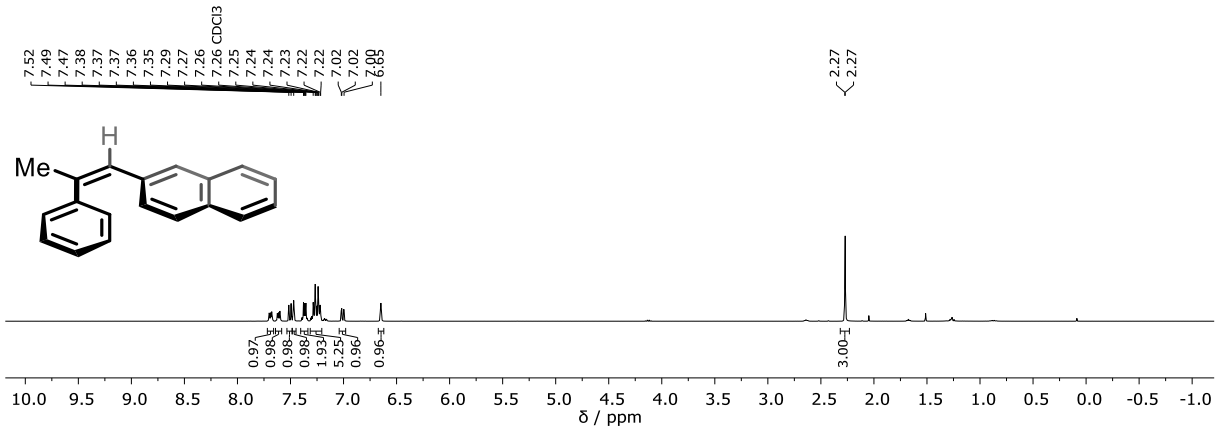

^{13}C{^{1}H} NMR (400 MHz, $CDCl_3$) of *Z*-**1a**

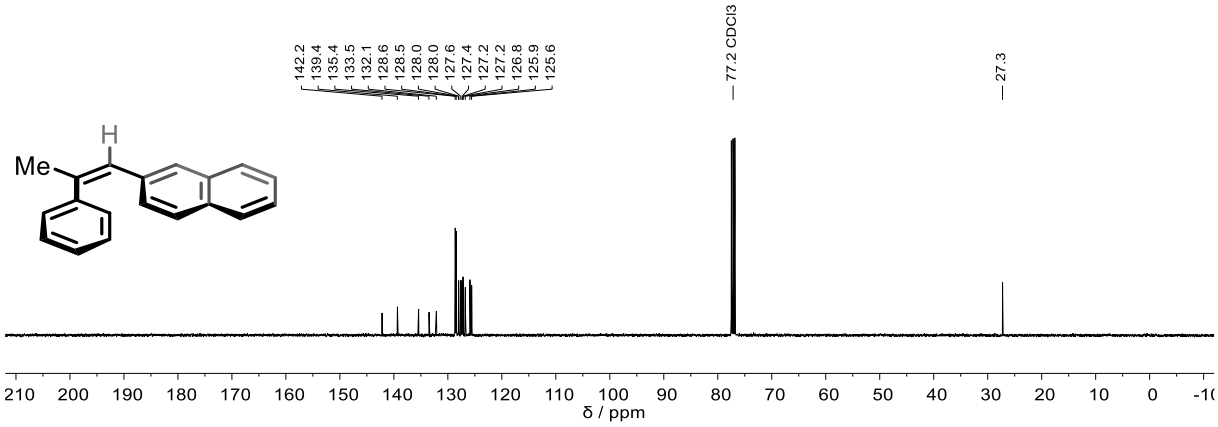

NOESY (400 MHz, $CDCl_3$) of *Z*-**1a**

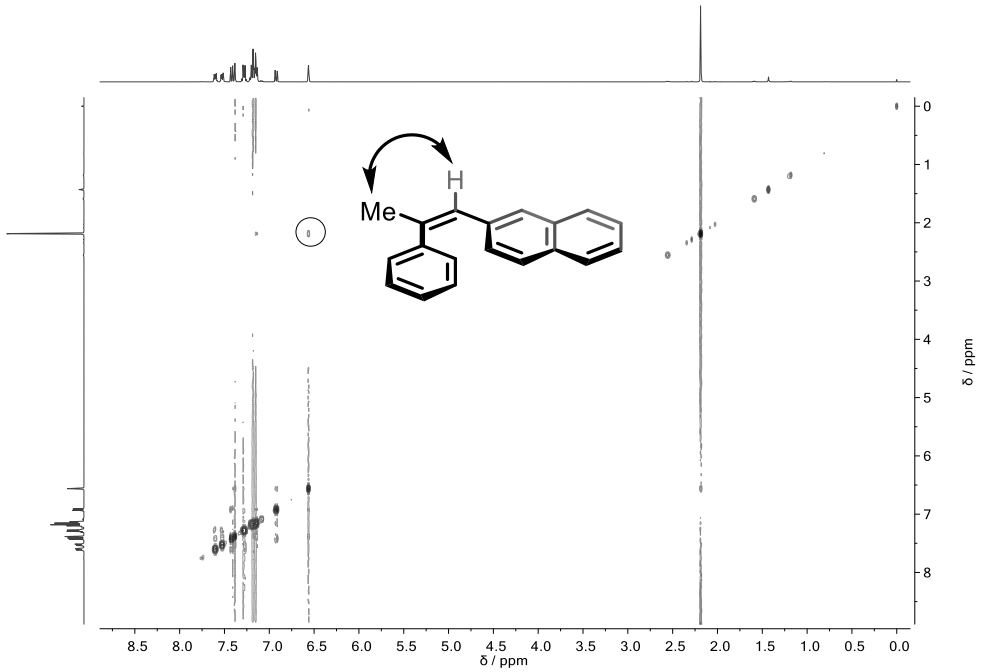

^{1}H NMR (400 MHz, $CDCl_3$) of **1b** (*E*:*Z* = 51:49)

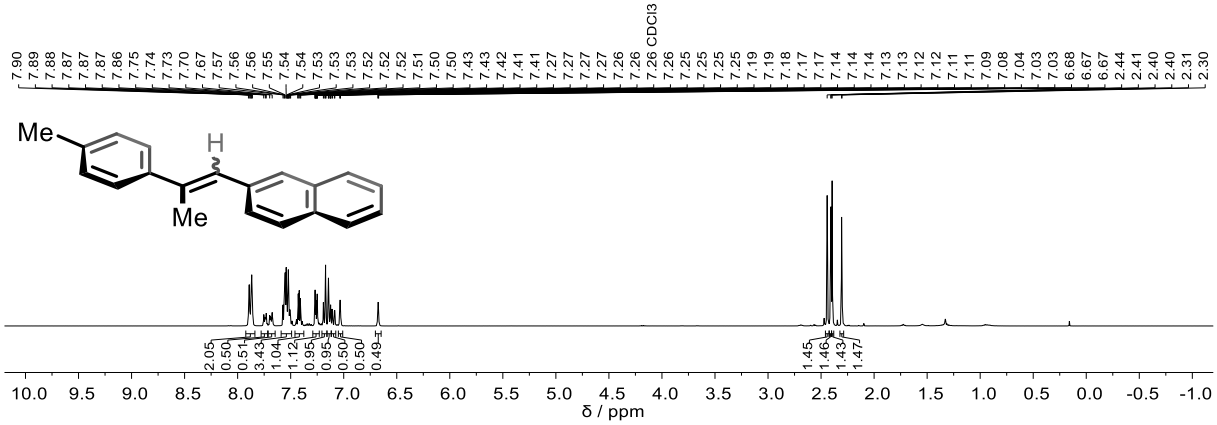

^{13}C{^{1}H} NMR (101 MHz, $CDCl_3$) of **1b** (*E*:*Z* = 51:49)

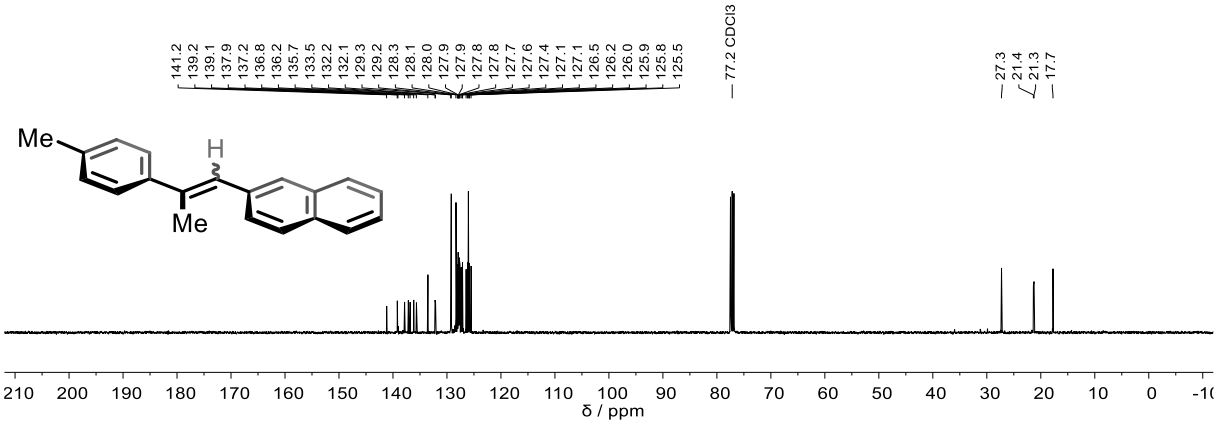

IR (ATR, neat) of **1b**

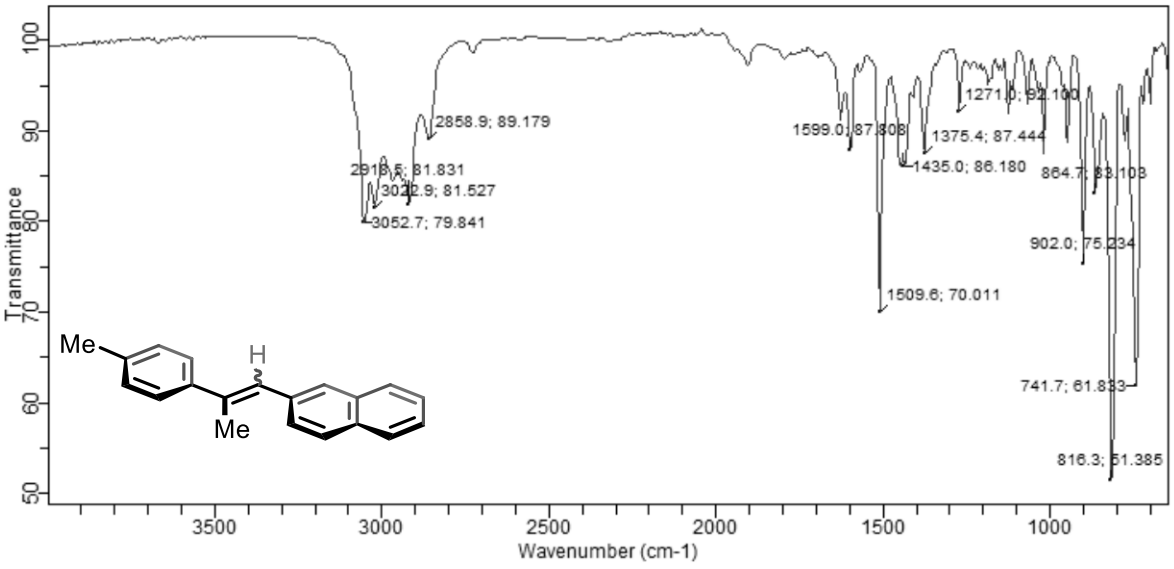

^{1}H NMR (400 MHz, $CDCl_3$) of **1c** (*E*:*Z* = 49:51)

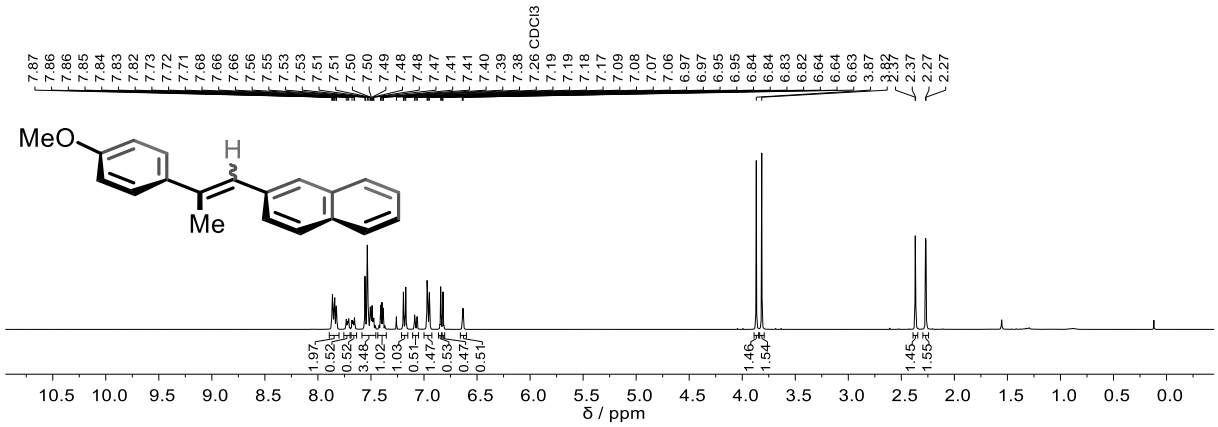

^{13}C{^{1}H} NMR (101 MHz, $CDCl_3$) of **1c** (*E*:*Z* = 49:51)

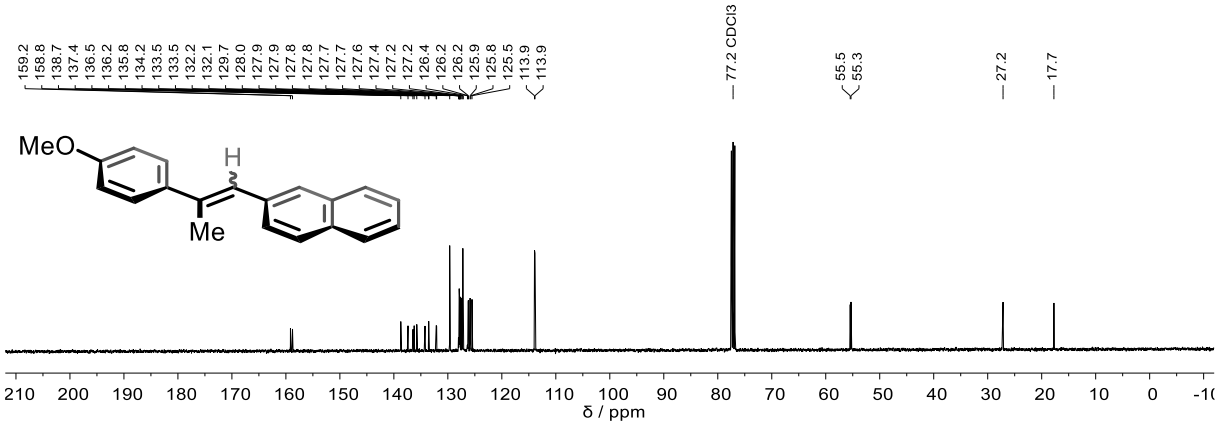

IR (ATR, neat) of **1c**

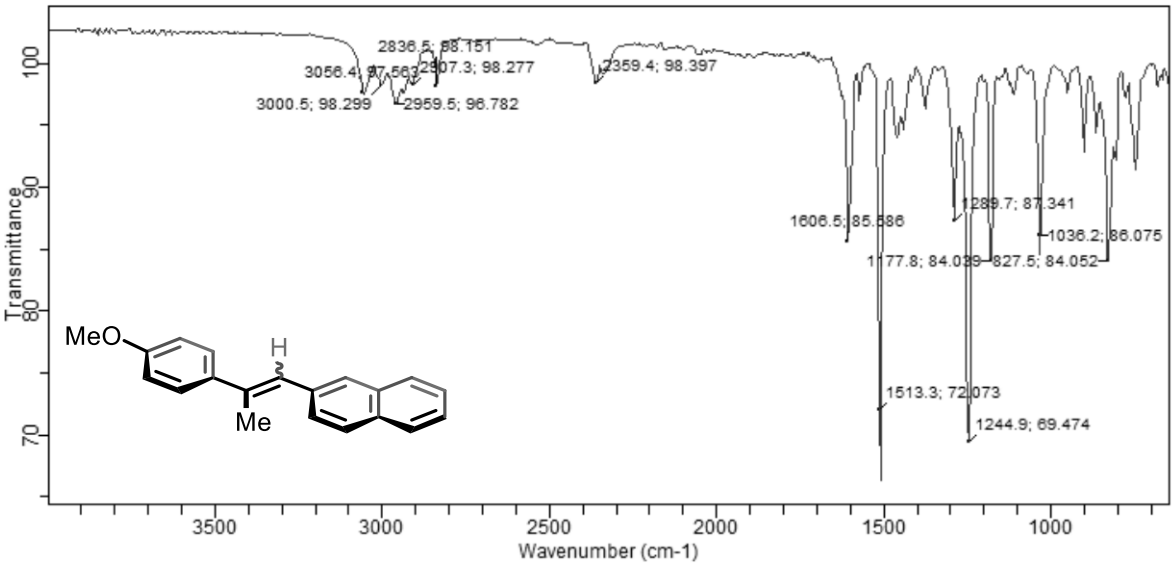

^{1}H NMR (400 MHz, $CDCl_3$) of **1n** (*E*:*Z* = 54:46)

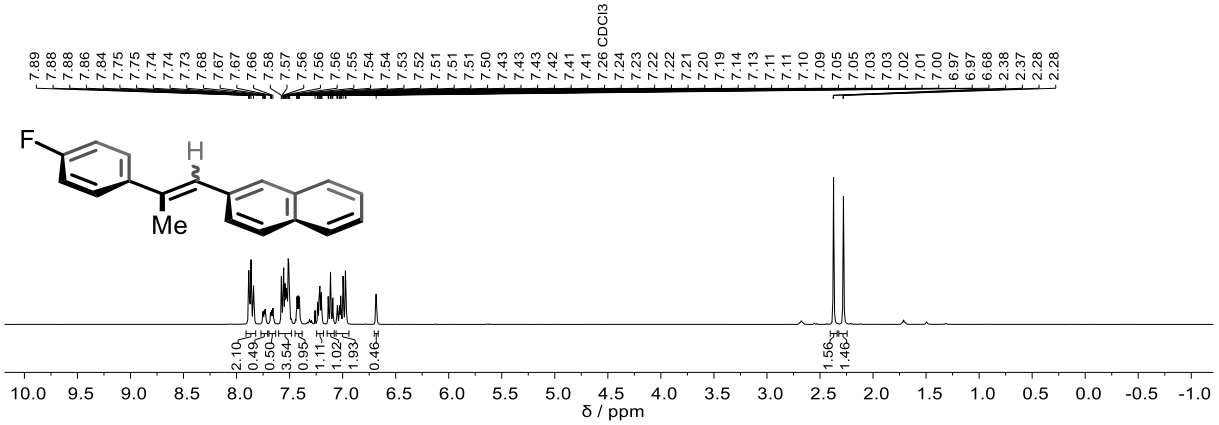

^{13}C{^{1}H} NMR (101 MHz, $CDCl_3$) of **1n** (*E*:*Z* = 54:46)

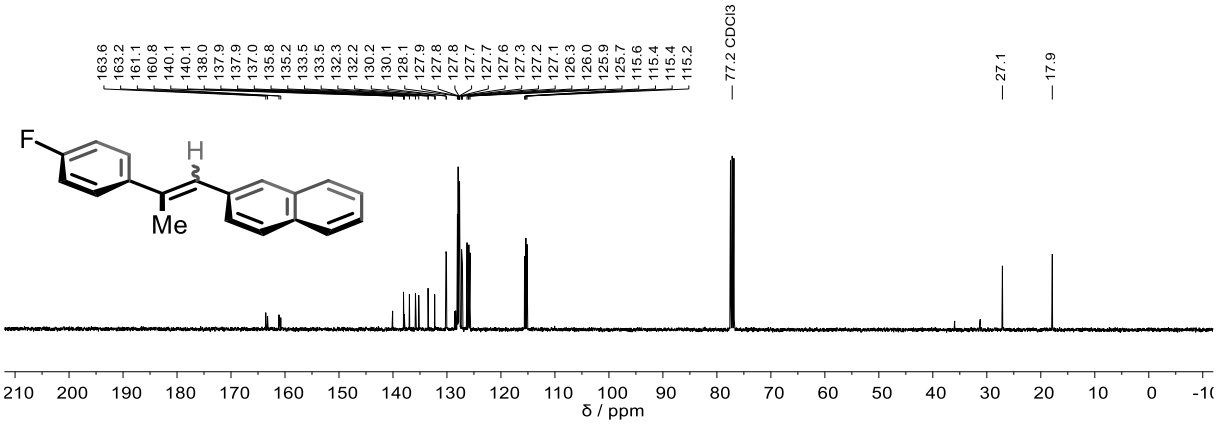

^{19}F{^{1}H} NMR (377 MHz, $CDCl_3$) of **1n** (*E*:*Z* = 54:46)

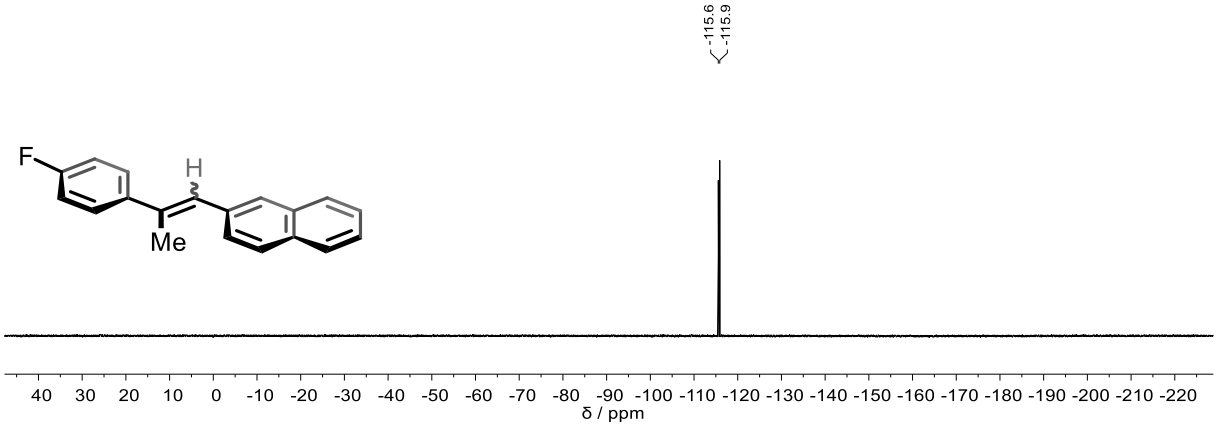

IR (ATR, neat) of **1n**

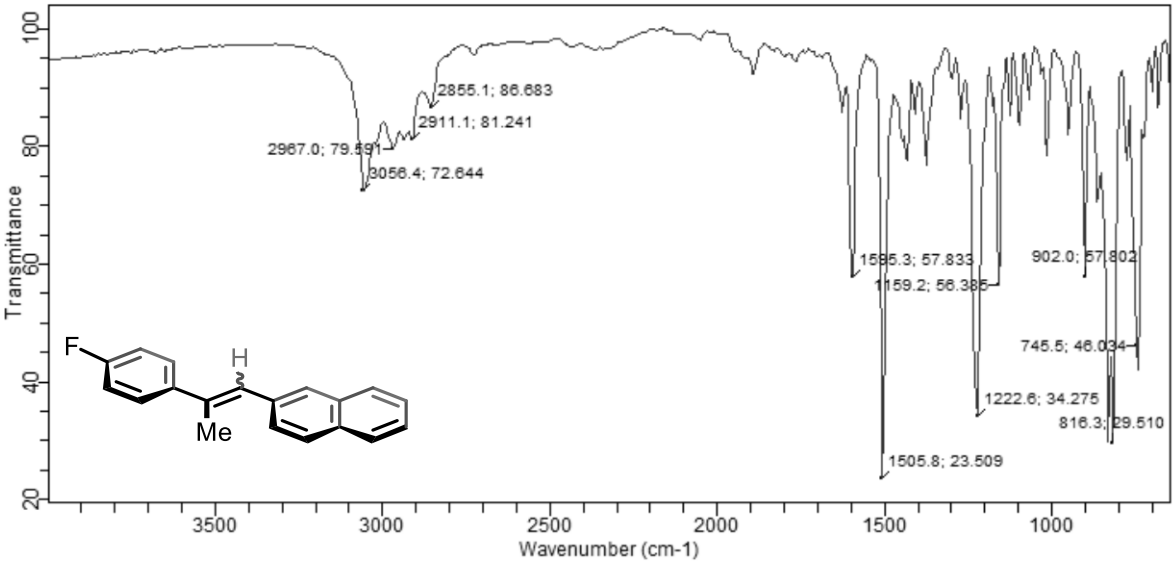

^{1}H NMR (400 MHz, $CDCl_3$) of **1o** (*E*:*Z* = 57:43)

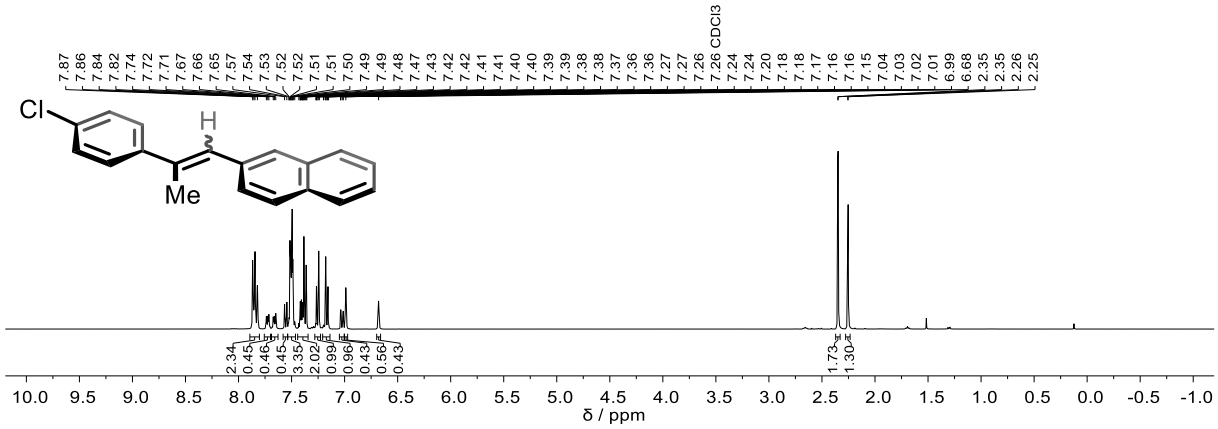

^{13}C{^{1}H} NMR (101 MHz, $CDCl_3$) of **1o** (*E*:*Z* = 57:43)

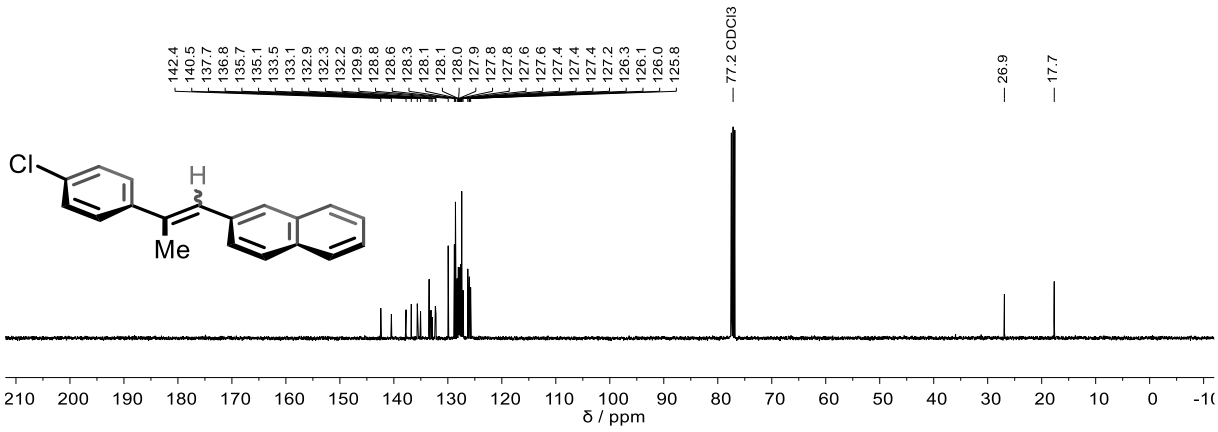

IR (ATR, neat) of **1o**

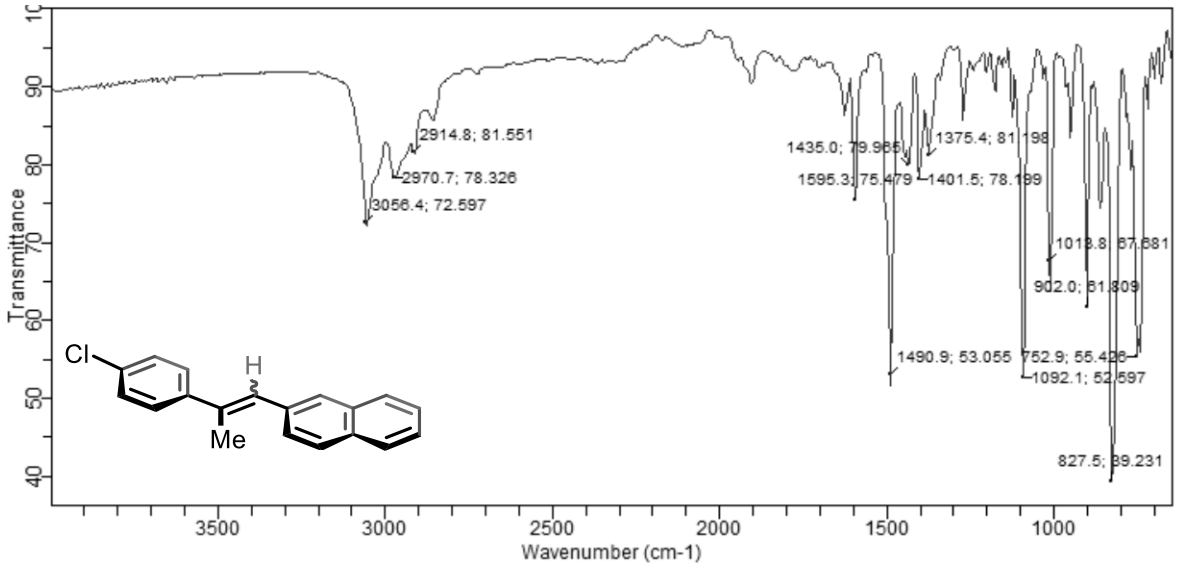

^{1}H NMR (400 MHz, $CDCl_3$) of **1z** (*E*:*Z* = 42:58)

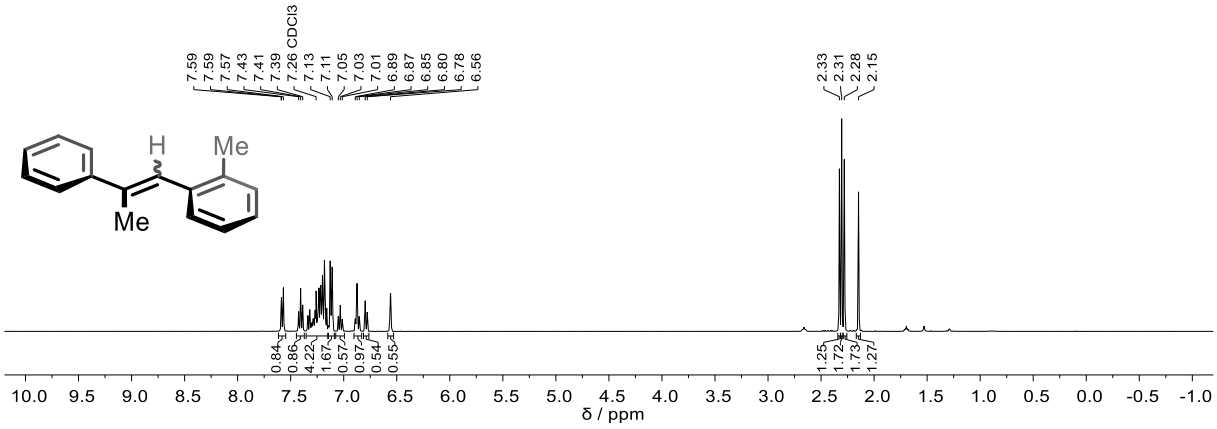

^{13}C{^{1}H} NMR (101 MHz, $CDCl_3$) of **1z** (*E*:*Z* = 42:58)

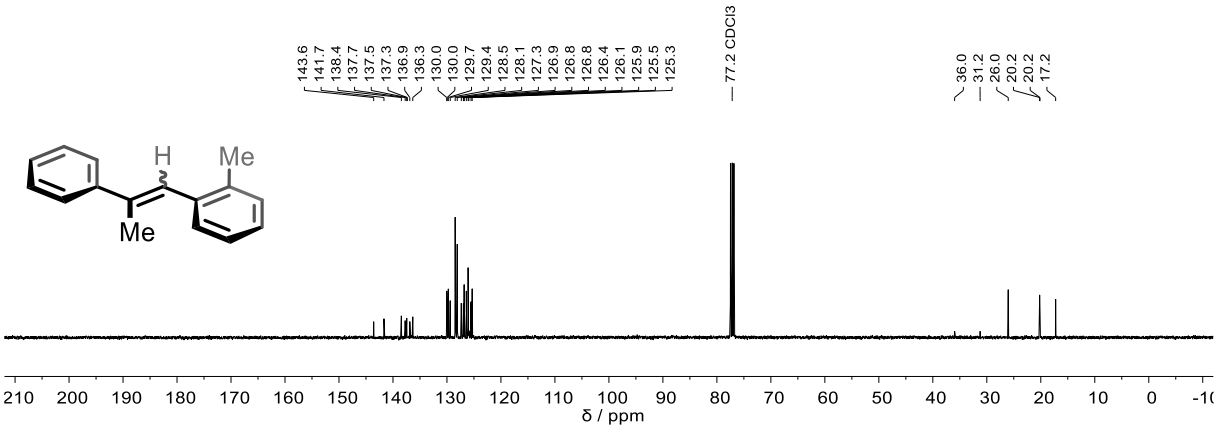

IR (ATR, neat) of **1z**

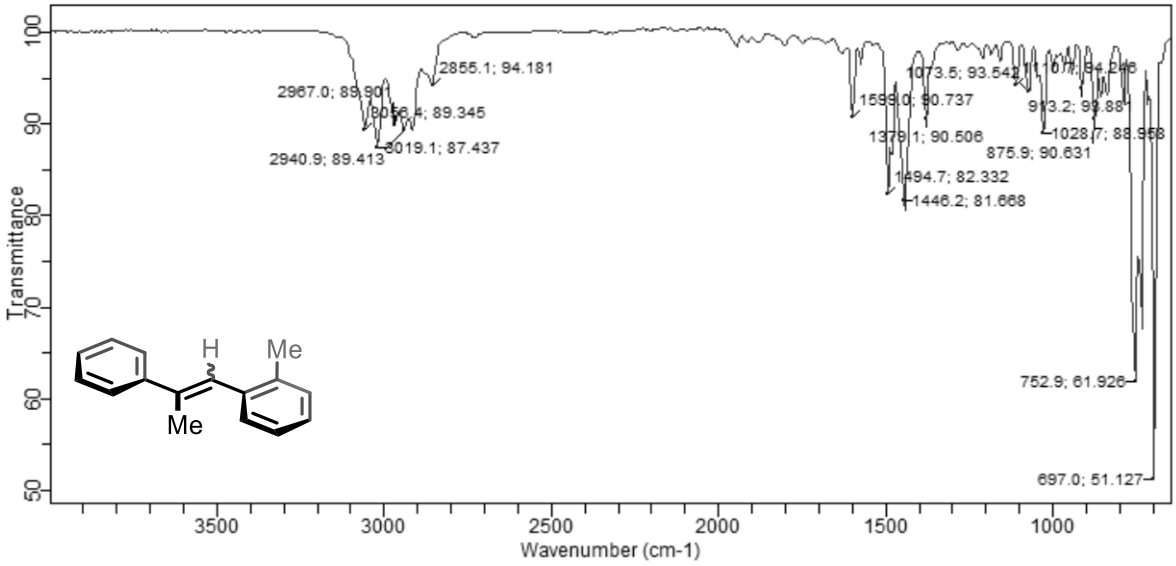

^{1}H NMR (400 MHz, $CDCl_3$) of **1h'** (*E*:*Z* = 90:10)

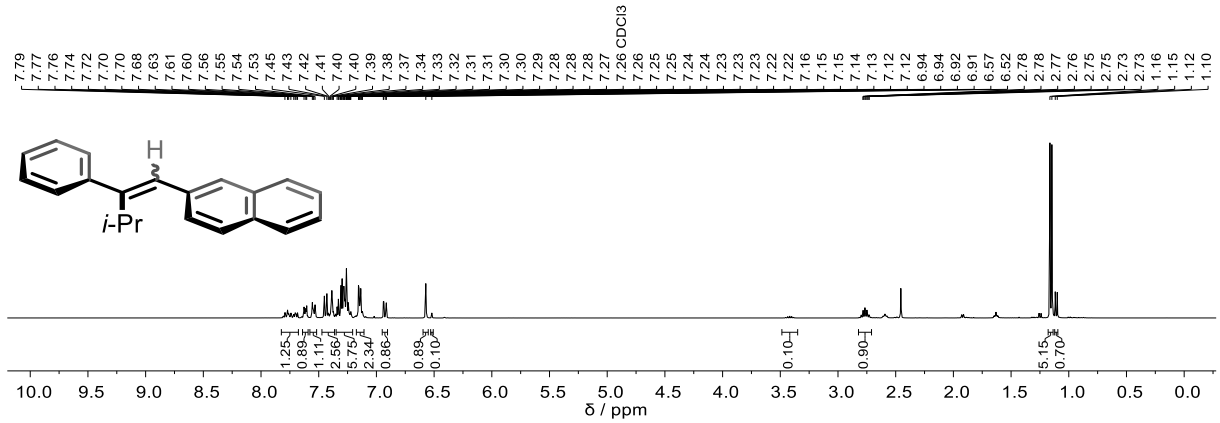

^{13}C{^{1}H} NMR (101 MHz, $CDCl_3$) of **1h'** (*E*:*Z* = 90:10)

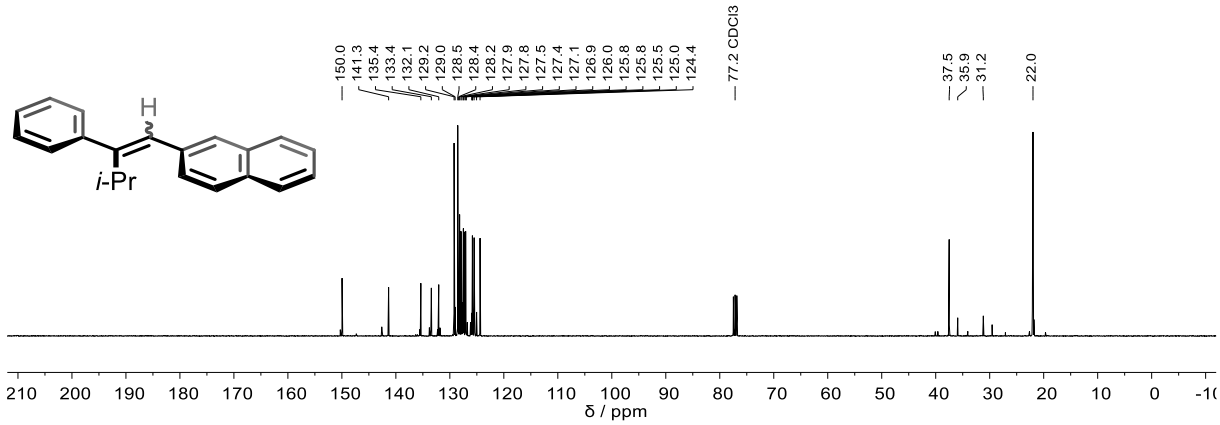

IR (ATR, neat) of **1h'**

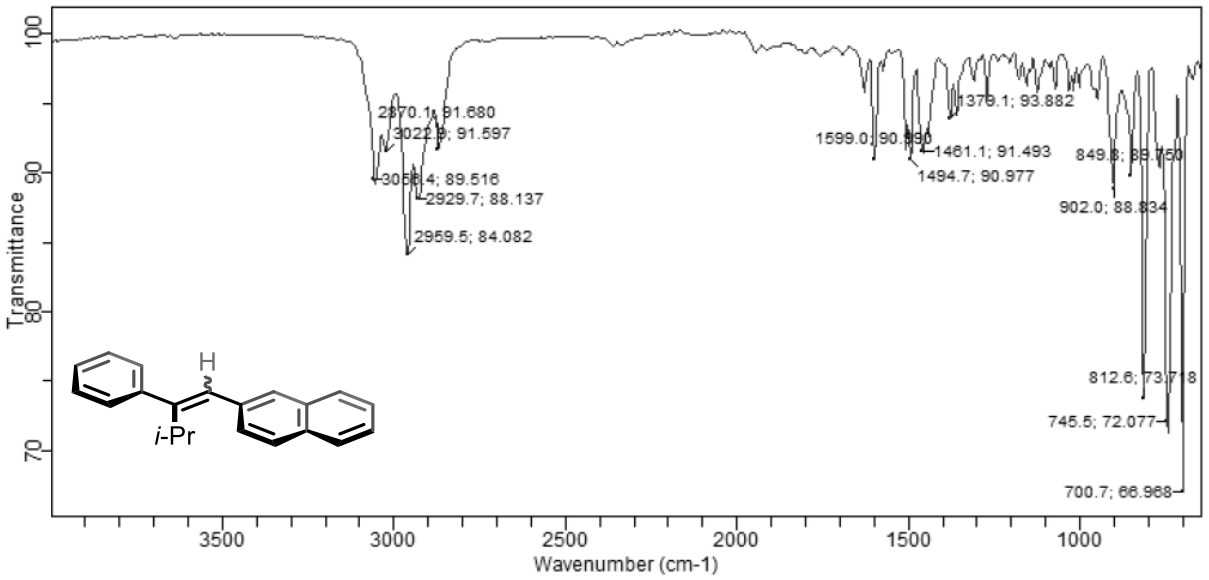

^{1}H NMR (400 MHz, $CDCl_3$) of **1i'** (*E*:*Z* = 50:50)

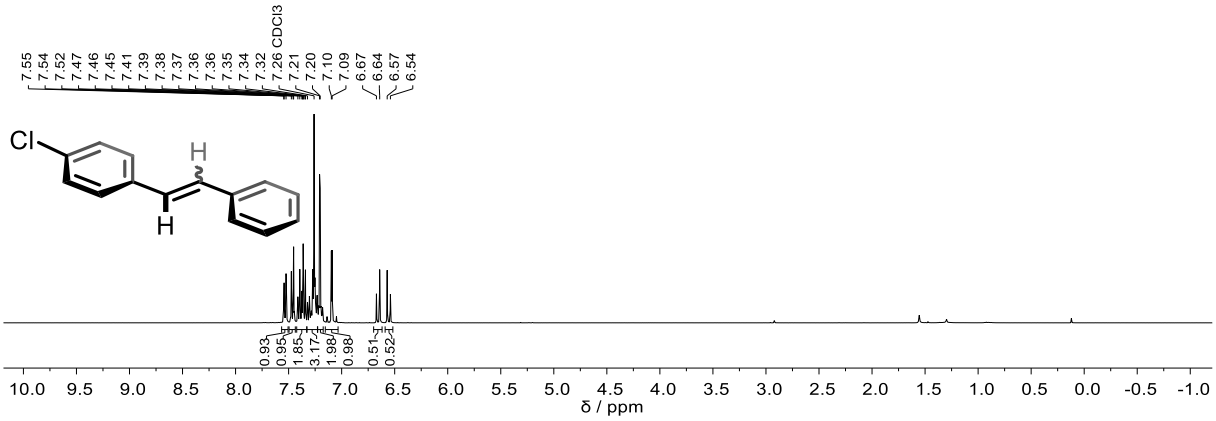

^{13}C{^{1}H} NMR (101 MHz, $CDCl_3$) of **1i'** (*E*:*Z* = 50:50)

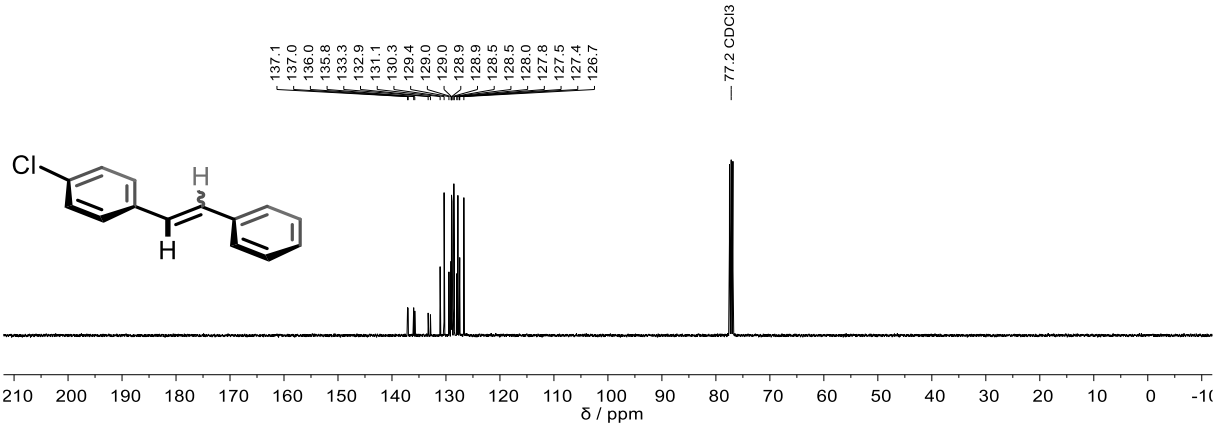

IR (ATR, neat) of **1i'**

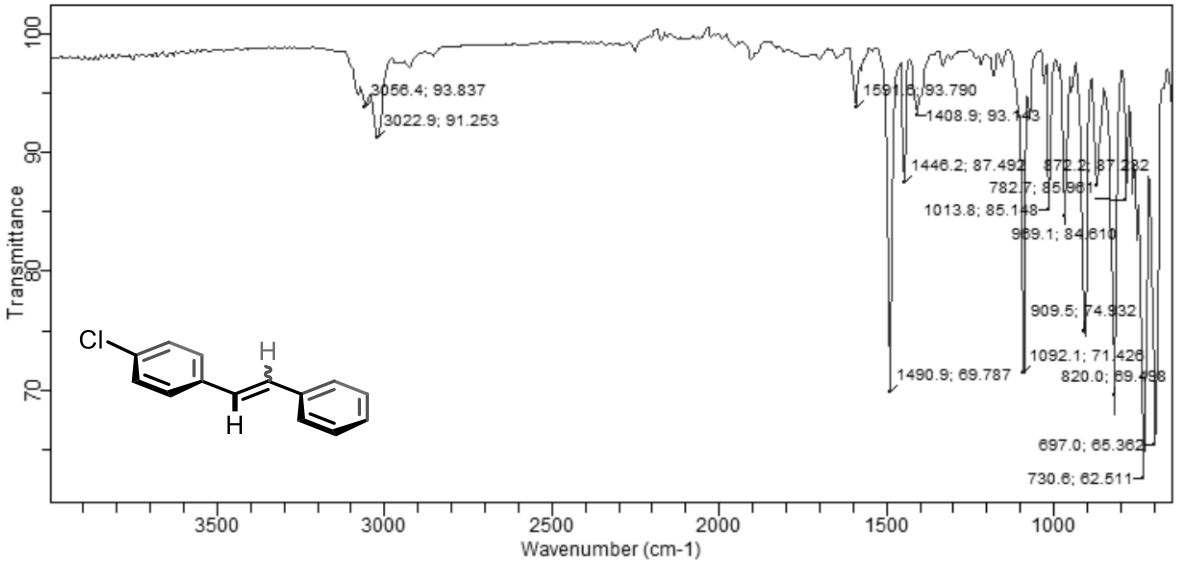

^{1}H NMR (400 MHz, $CDCl_3$) of **1j'** (*E*:*Z* = 97:3)

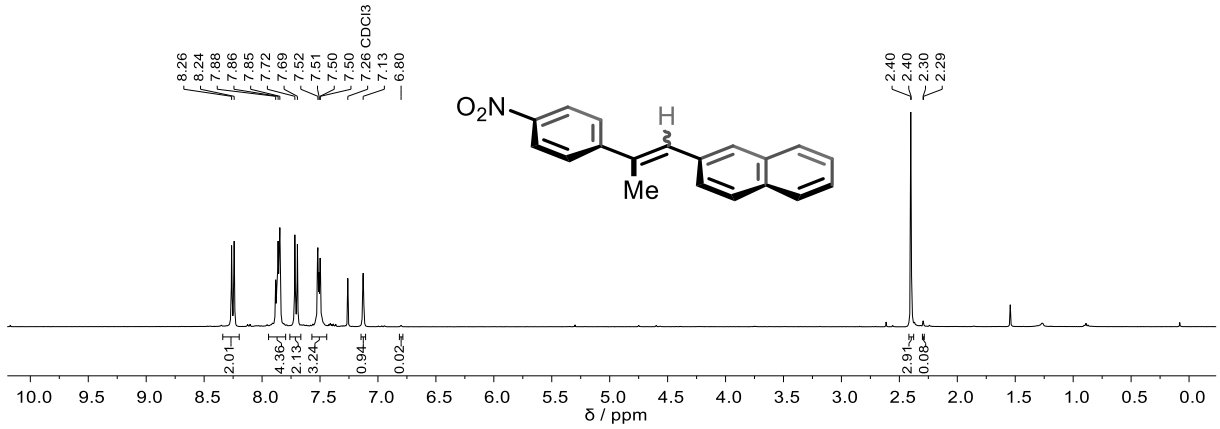

^{13}C{^{1}H} NMR (101 MHz, $CDCl_3$) of **1j'** (*E*:*Z* = 97:3)

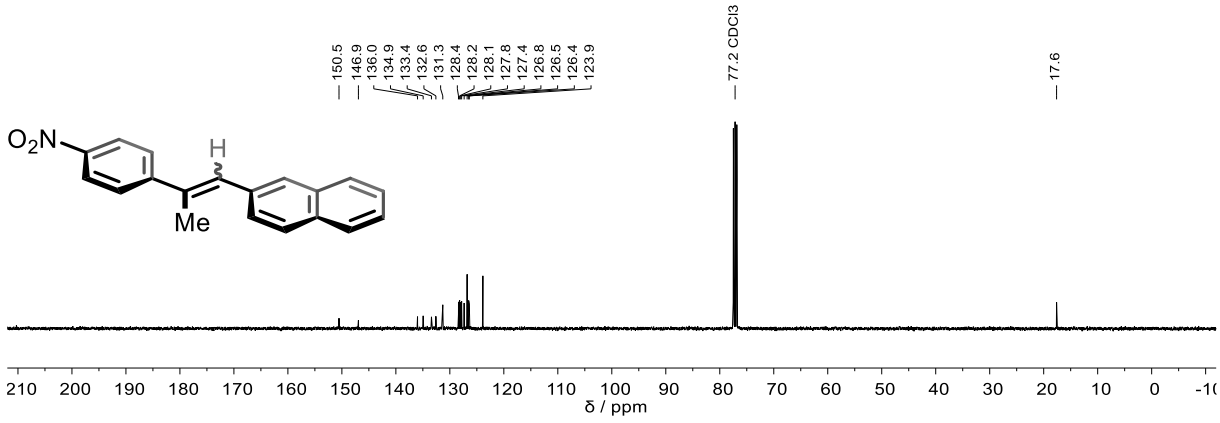

IR (ATR, neat) of **1j'**

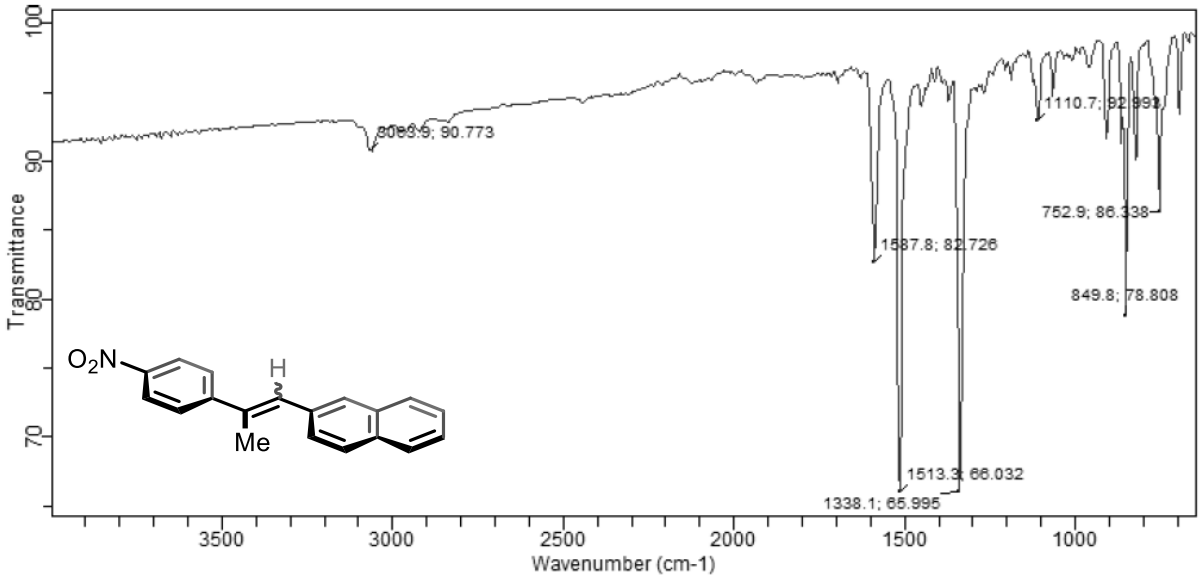

^{1}H NMR (400 MHz, $CDCl_3$) of **1k'** (*E*:*Z* = 53:47)

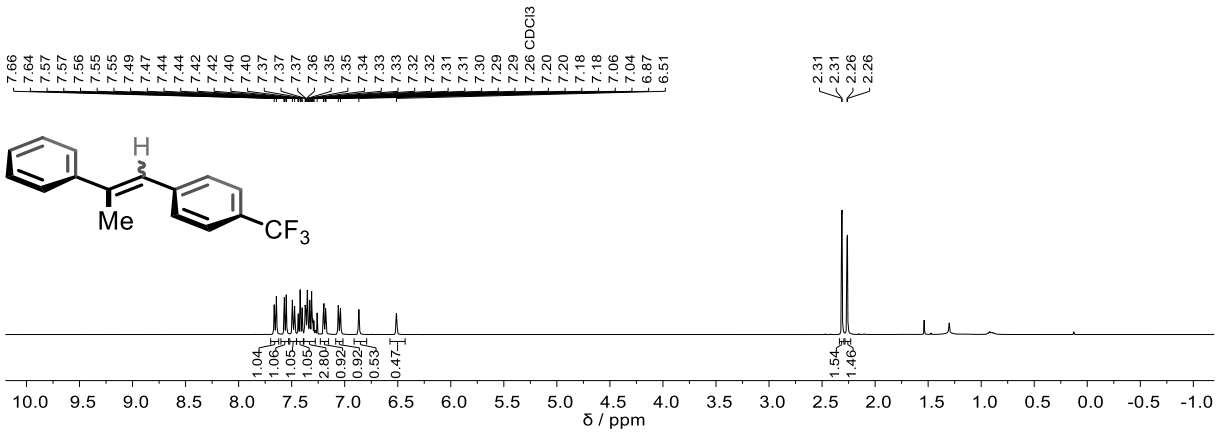

^{13}C{^{1}H} NMR (101 MHz, $CDCl_3$) of **1k'** (*E*:*Z* = 53:47)

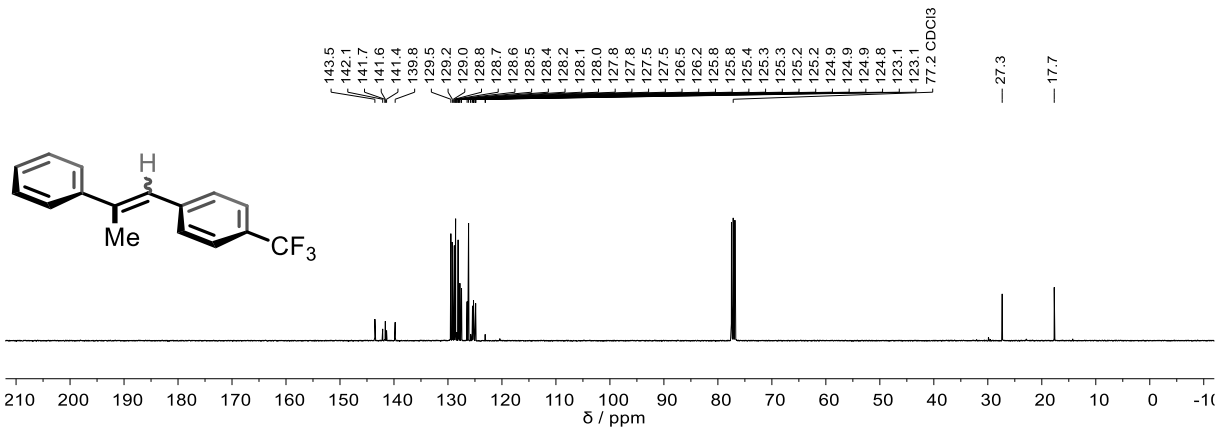

$^{19}F\{^{1}H\}$ NMR (377 MHz, $CDCl_3$) of **1k'** (*E*:*Z* = 53:47)

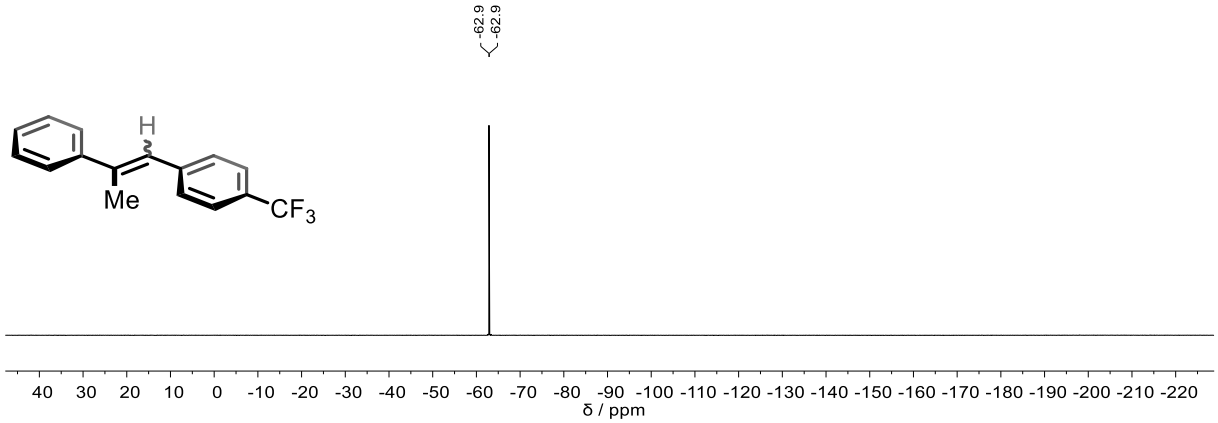

IR (ATR, neat) of **1k'**

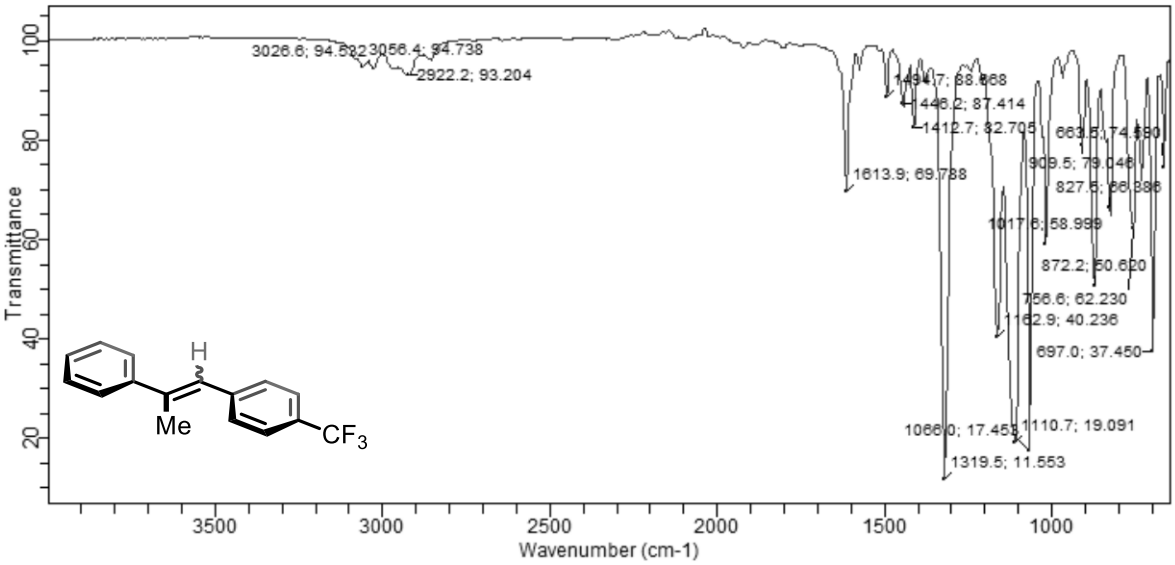

^{1}H NMR (400 MHz, $CDCl_3$) of **1l'** (*E*:*Z* = 57:43)

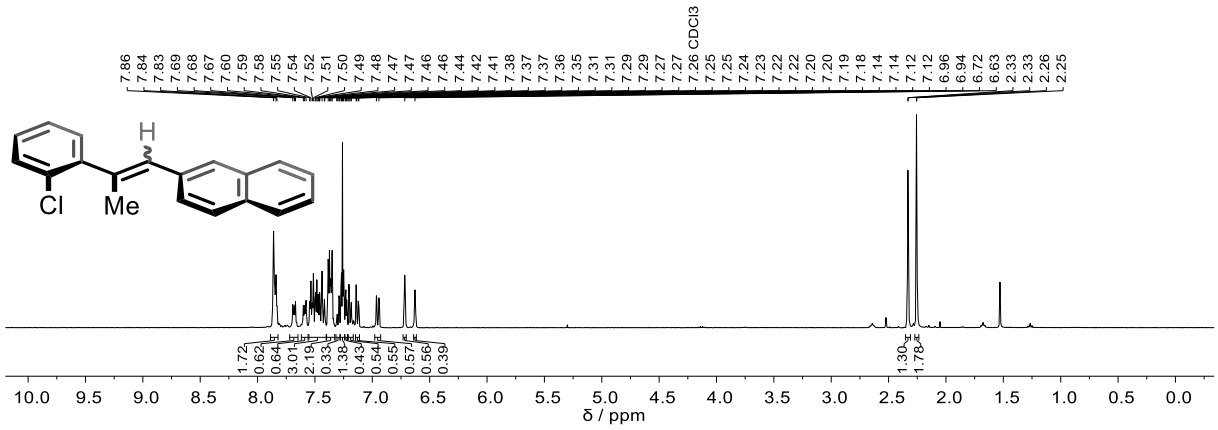

$^{13}C\{^{1}H\}$ NMR (101 MHz, $CDCl_3$) of **1l'** (*E*:*Z* = 57:43)

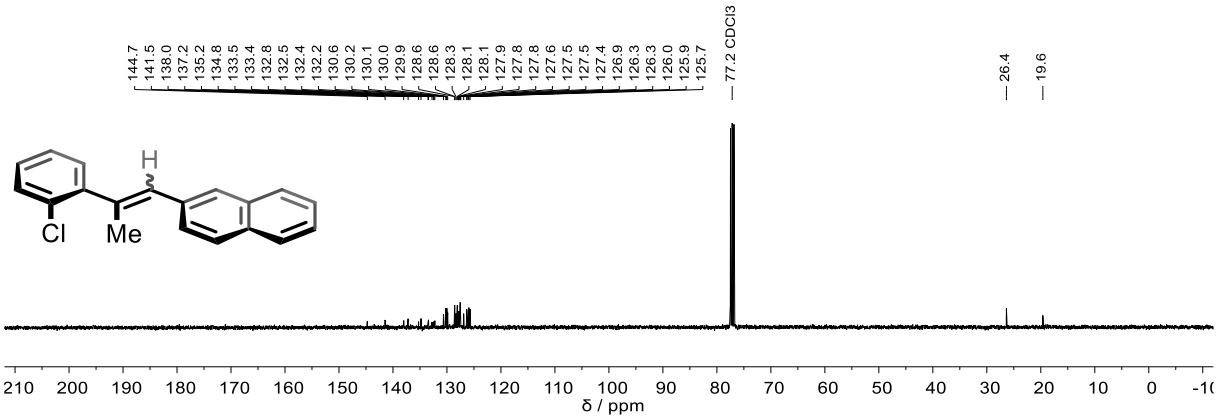

IR (ATR, neat) of **1l'**

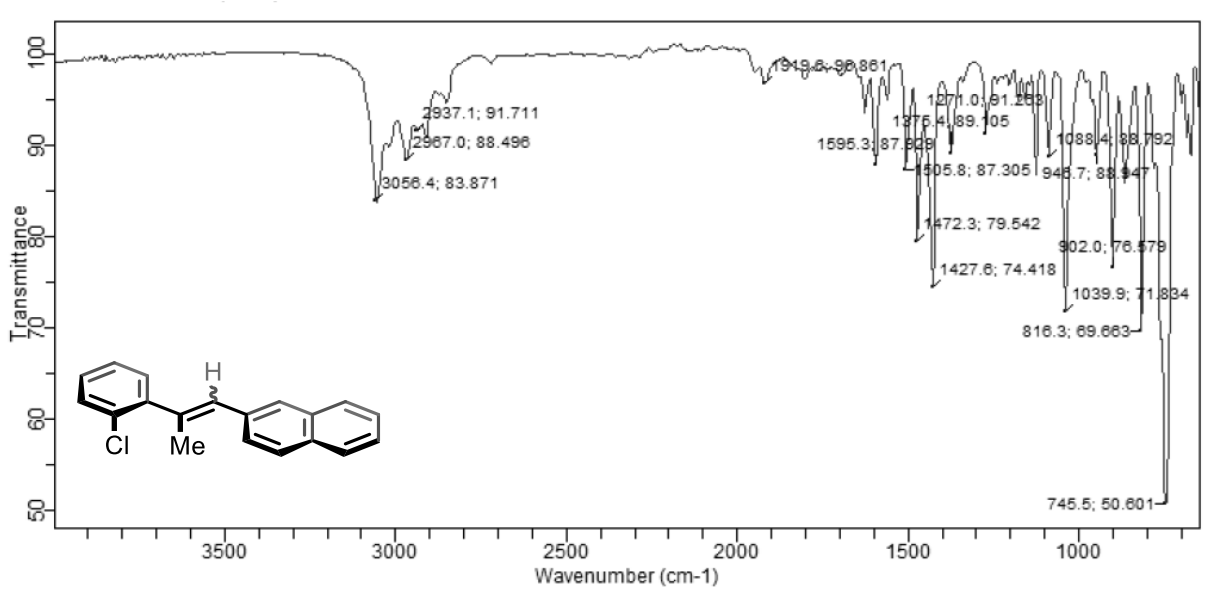

^{1}H NMR (400 MHz, $CDCl_3$) of **1n'** (*E*:*Z* = 95:5)

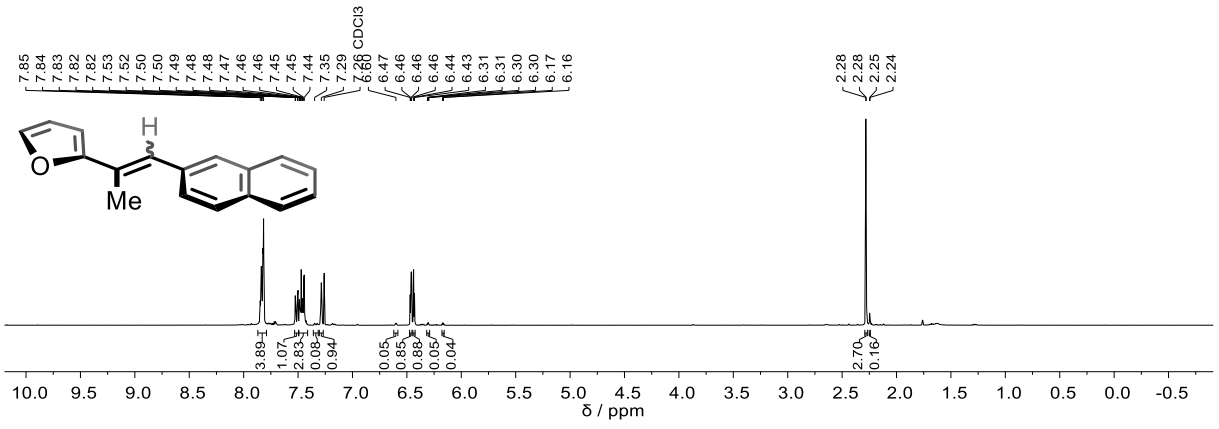

$^{13}C\{^{1}H\}$ NMR (101 MHz, $CDCl_3$) of **1n'** (*E*:*Z* = 95:5)

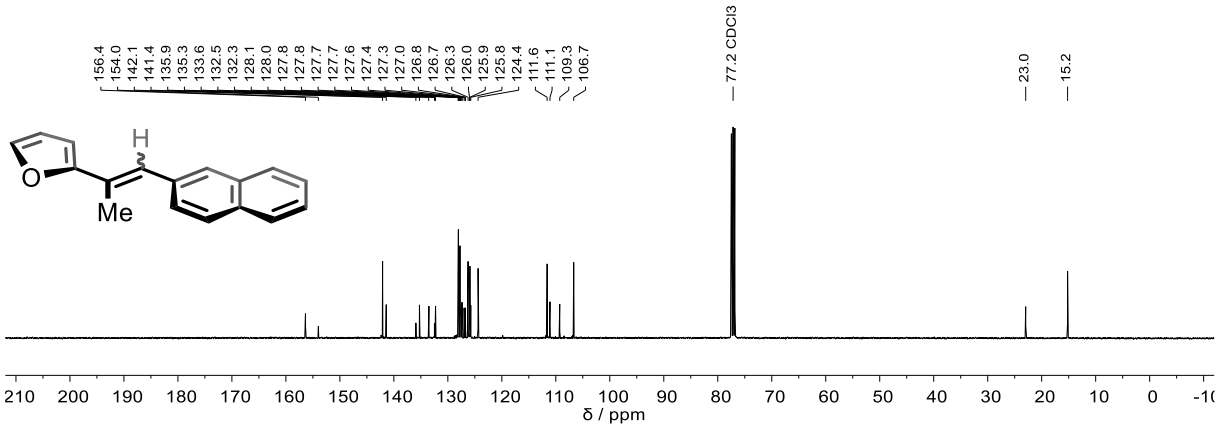

IR (ATR, neat) of **1n'**

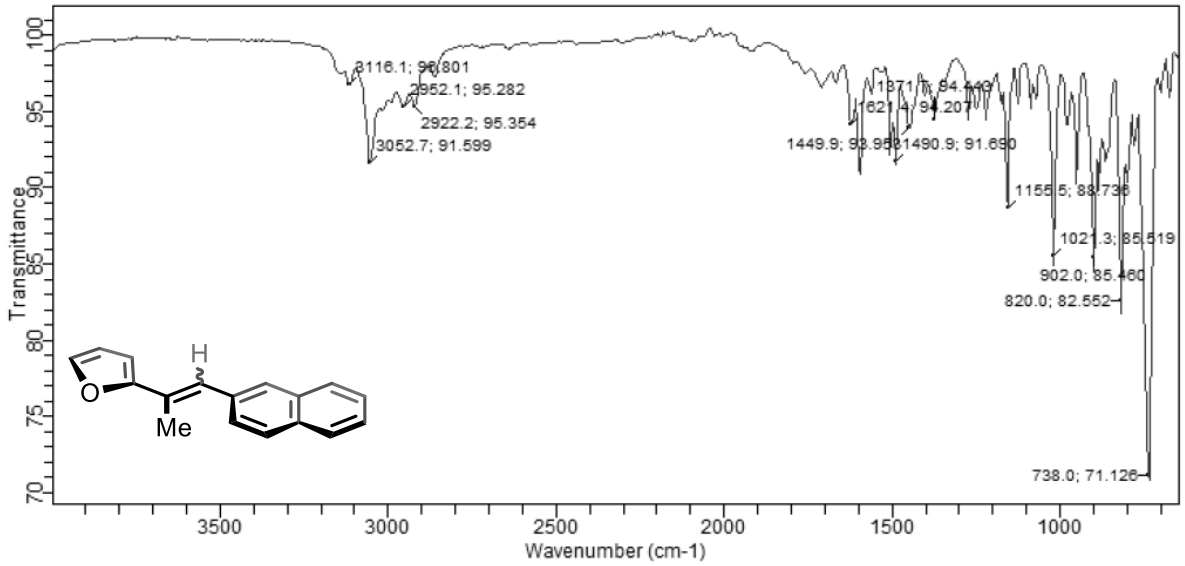

^{1}H NMR (400 MHz, $CDCl_3$) of **1p'** (*E*:*Z* = 50:50)

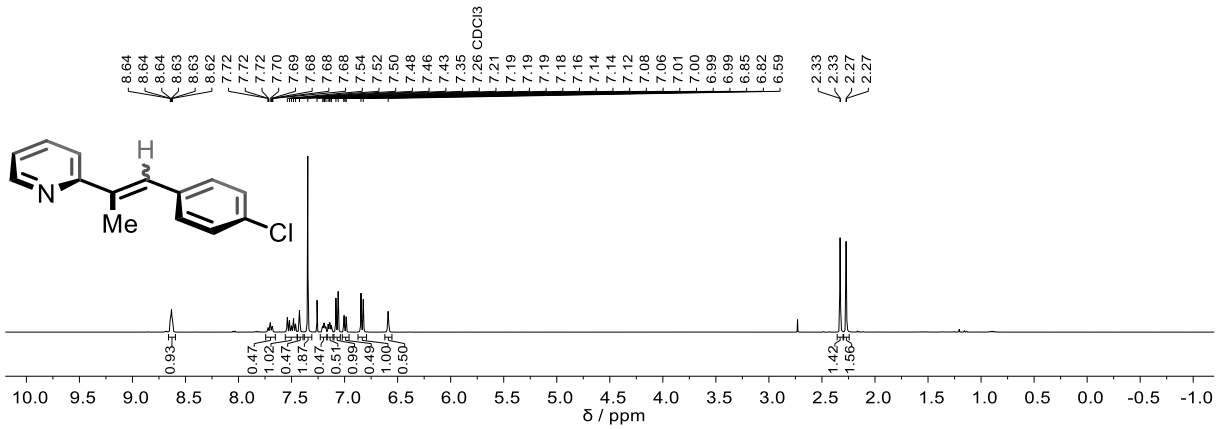

$^{13}C\{^{1}H\}$ NMR (101 MHz, $CDCl_3$) of **1p'** (*E*:*Z* = 50:50)

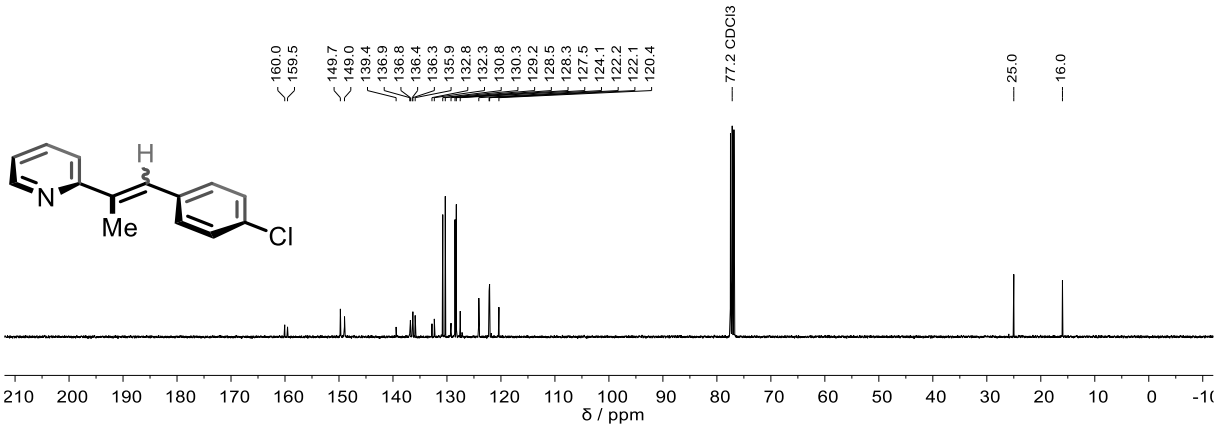

IR (ATR, neat) of **1p'**

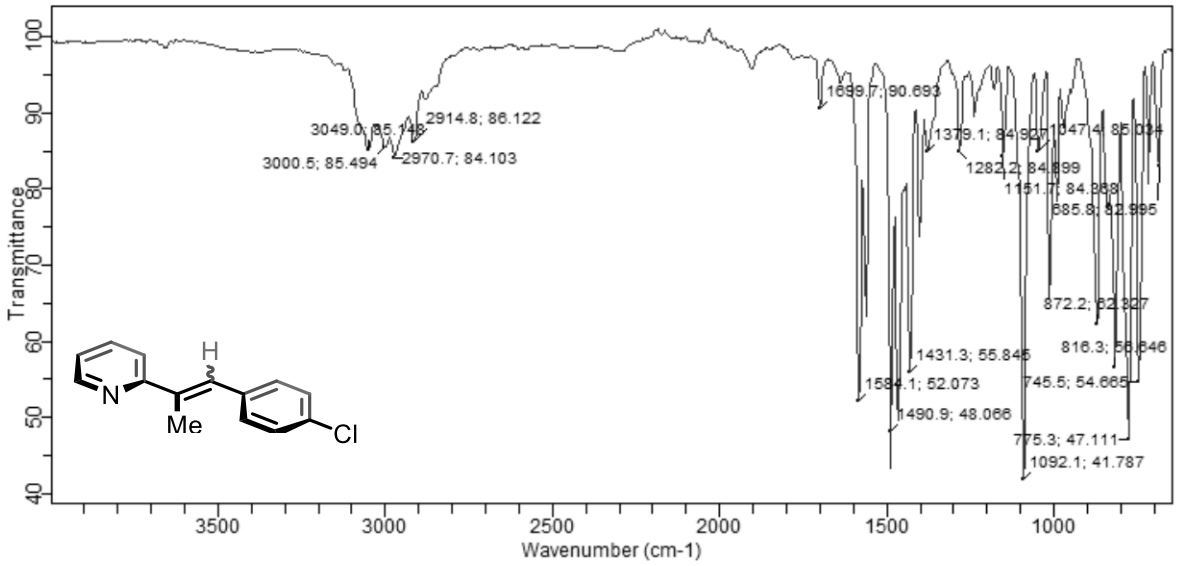

^{1}H NMR (400 MHz, $CDCl_3$) of **1a**^{ci} (*E*:*Z* = 63:37)

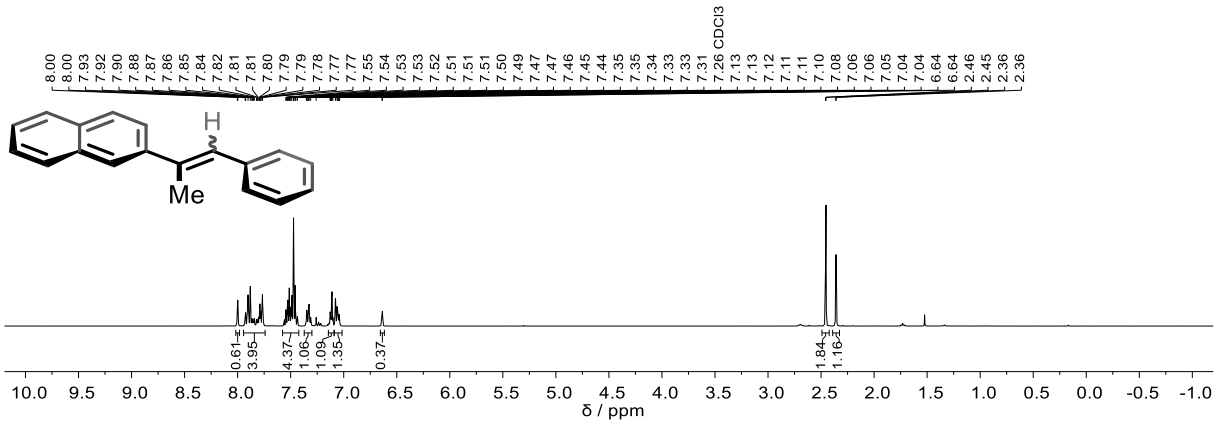

$^{13}C\{^{1}H\}$ NMR (101 MHz, $CDCl_3$) of **1a**^{ci} (*E*:*Z* = 63:37)

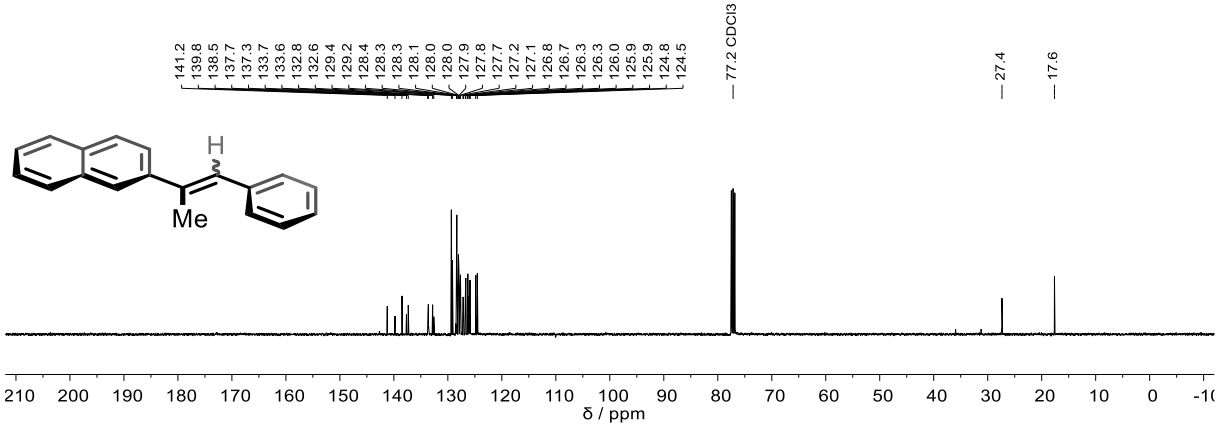

IR (ATR, neat) of **1a**^{ci}

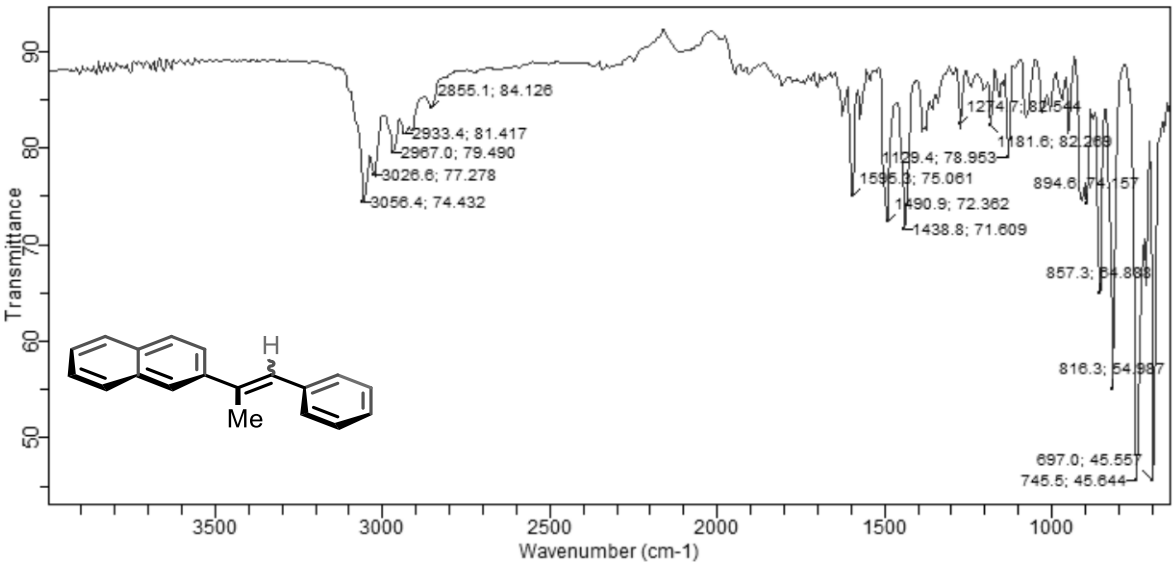

^{1}H NMR (400 MHz, $CDCl_3$) of **1b**^{ci} (*E*:*Z* = 65:35)

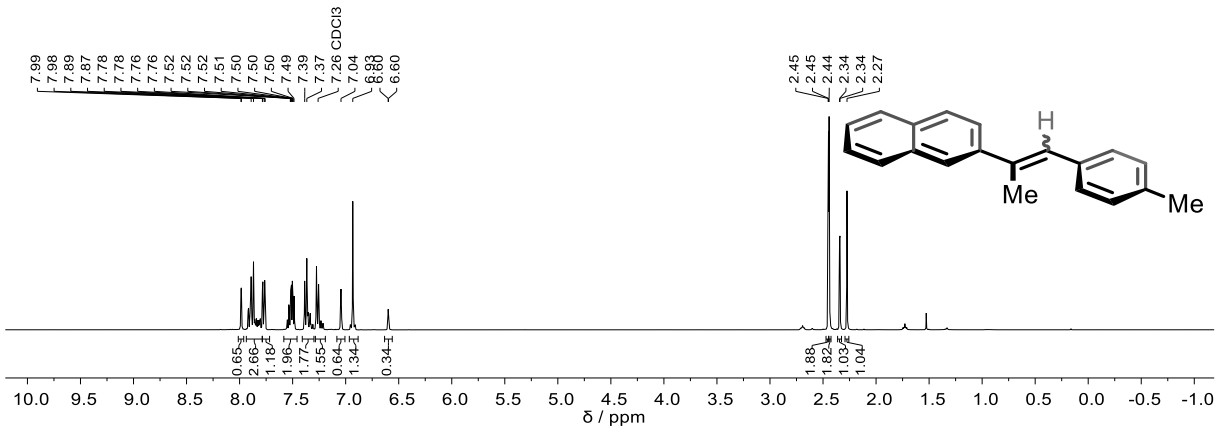

$^{13}C\{^{1}H\}$ NMR (101 MHz, $CDCl_3$) of **1b**^{ci} (*E*:*Z* = 65:35)

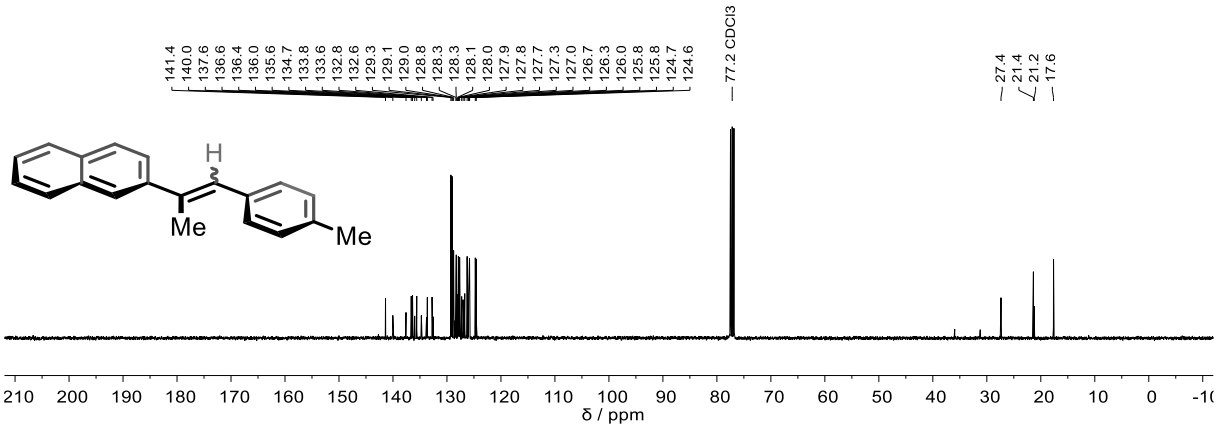

IR (ATR, neat) of **1b**^{ci}

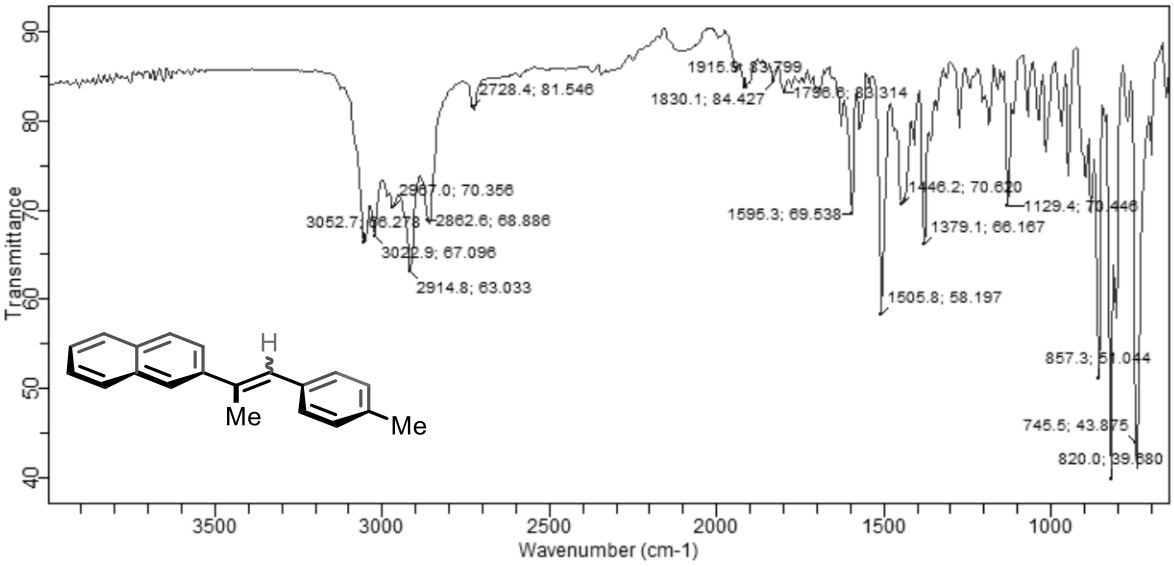

^{1}H NMR (400 MHz, $CDCl_3$) of **1c**^{ci} (*E*:*Z* = 70:30)

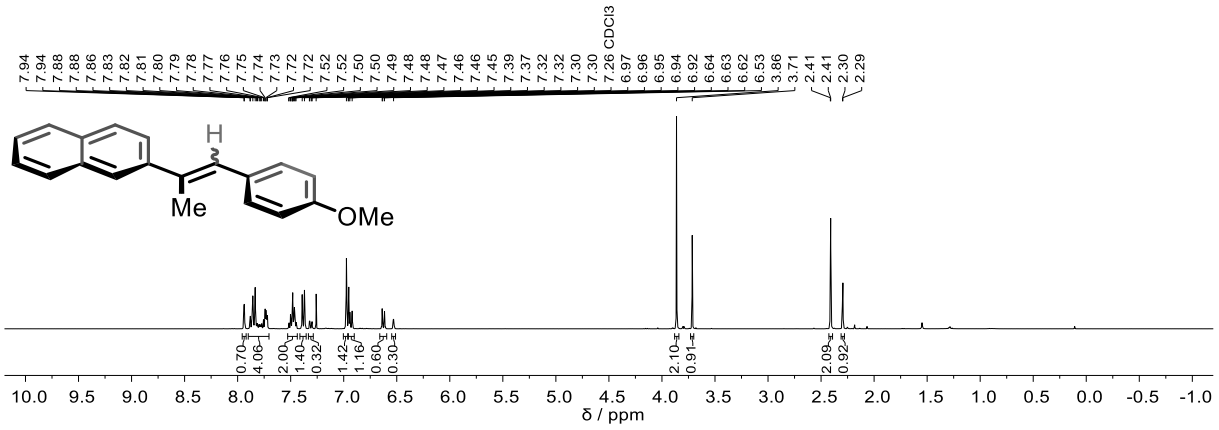

$^{13}C\{^{1}H\}$ NMR (101 MHz, $CDCl_3$) of **1c**^{ci} (*E*:*Z* = 70:30)

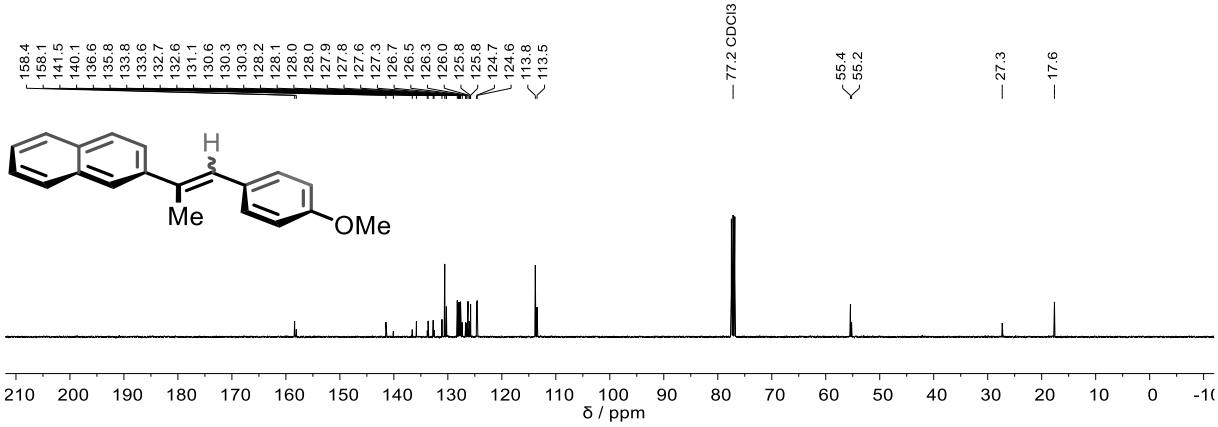

IR (ATR, neat) of **1c**^{ci}

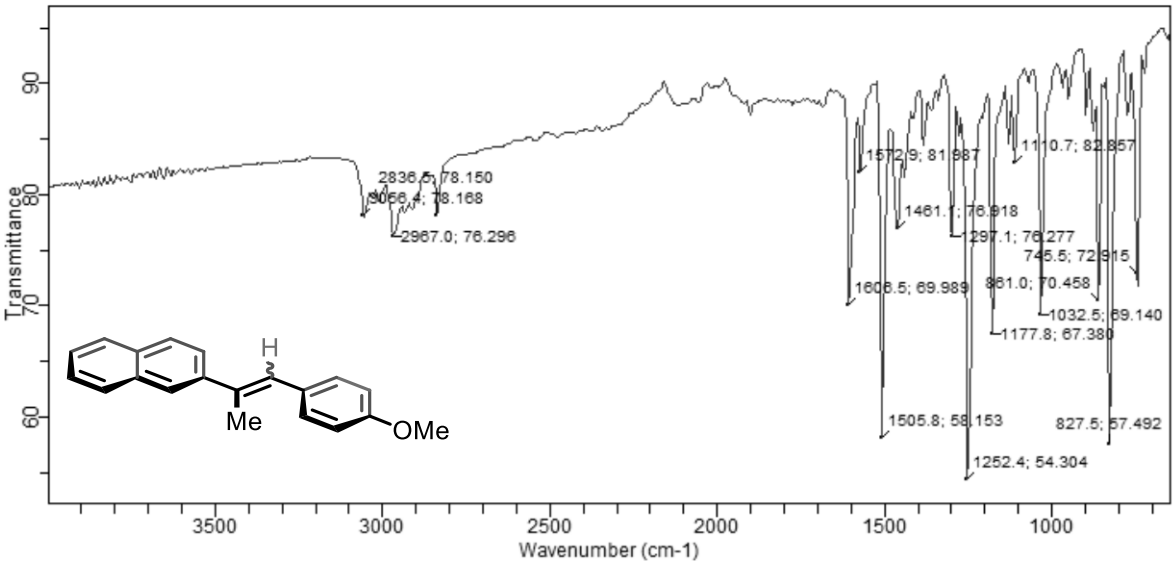

^{1}H NMR (400 MHz, $CDCl_3$) of **1n**^{ci} (*E*:*Z* = 57:43)

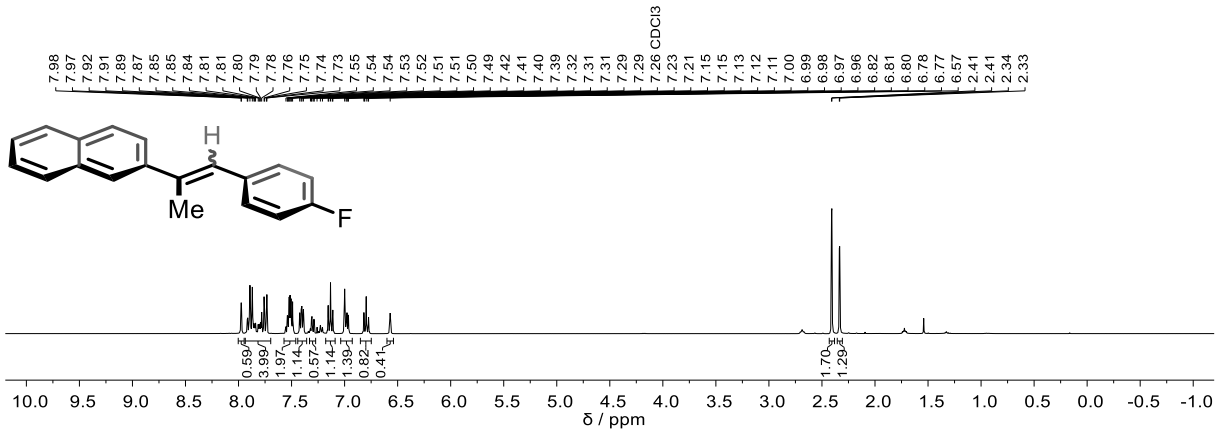

$^{13}C\{^{1}H\}$ NMR (101 MHz, $CDCl_3$) of **1n^{ci}** (*E*:*Z* = 57:43)

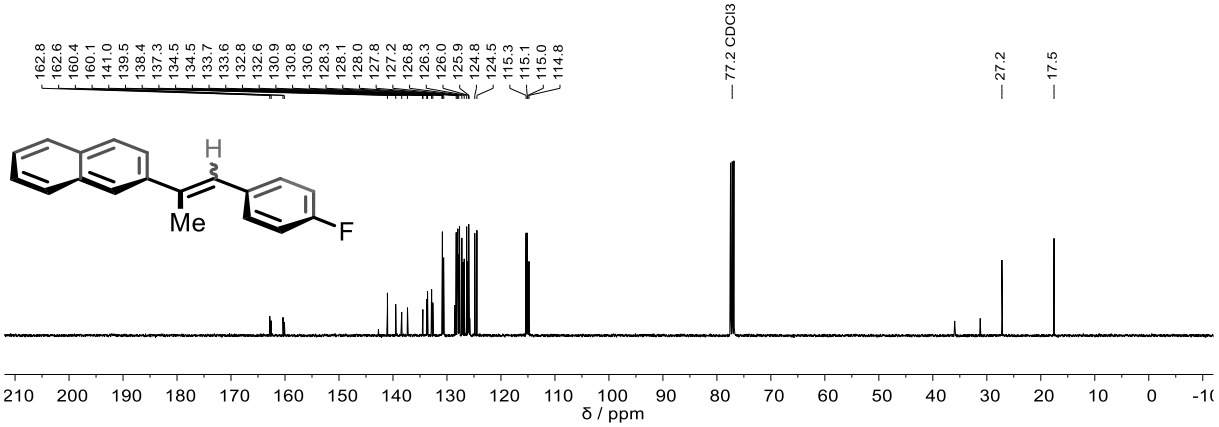

$^{19}F\{^{1}H\}$ NMR (377 MHz, $CDCl_3$) of **1n^{ci}** (*E*:*Z* = 57:43)

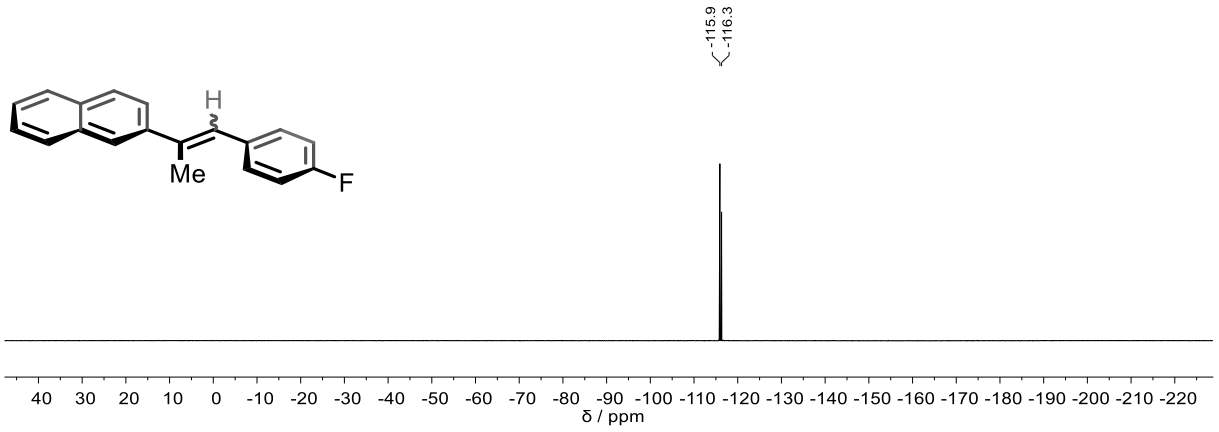

IR (ATR, neat) of **1n^{ci}**

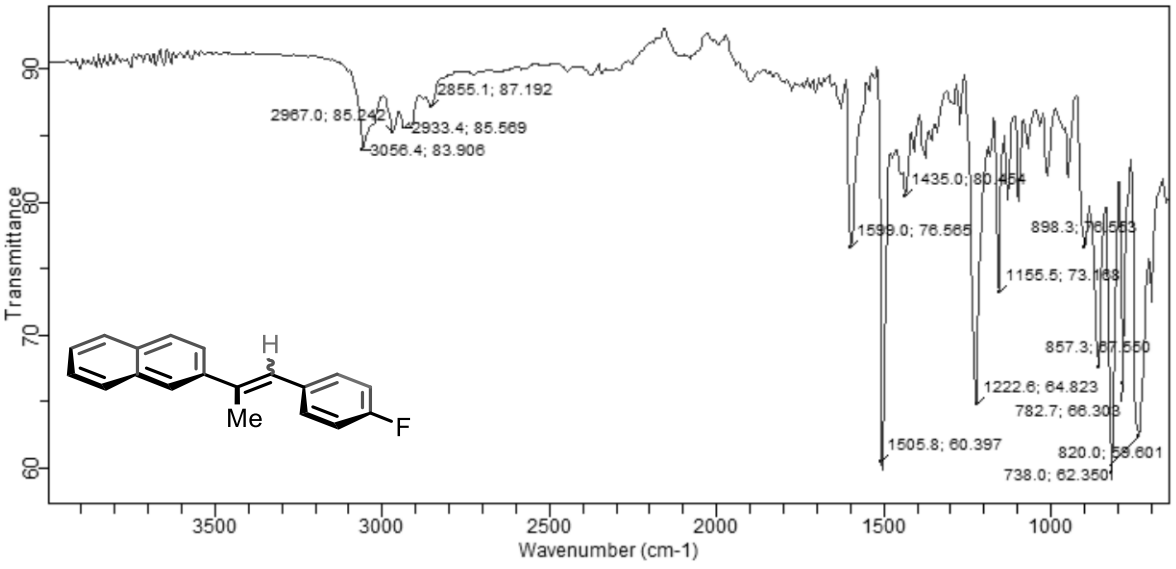

^{1}H NMR (400 MHz, $CDCl_3$) of **1z^{ci}** (*E*:*Z* = 40:60)

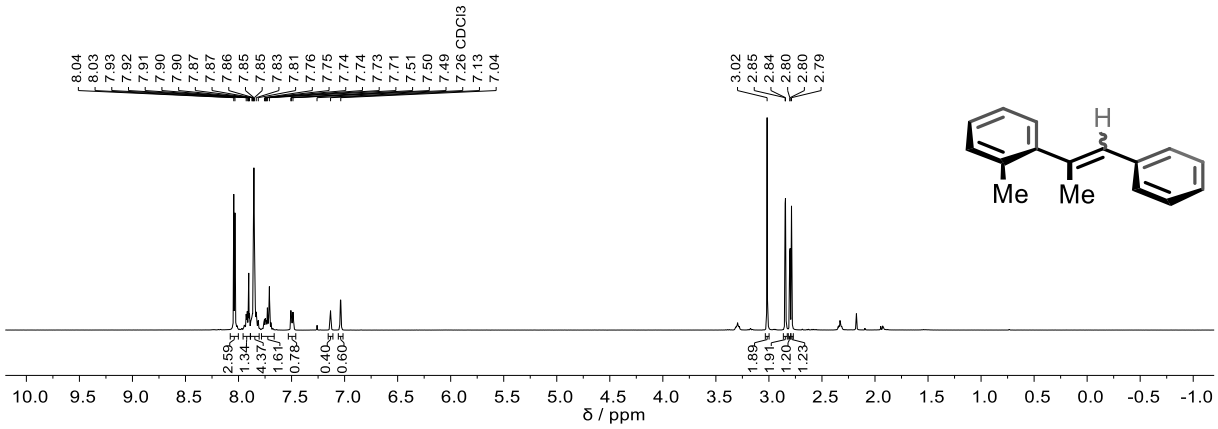

^{13}C{^{1}H} NMR (101 MHz, $CDCl_3$) of **1z^{ci}** (*E*:*Z* = 40:60)

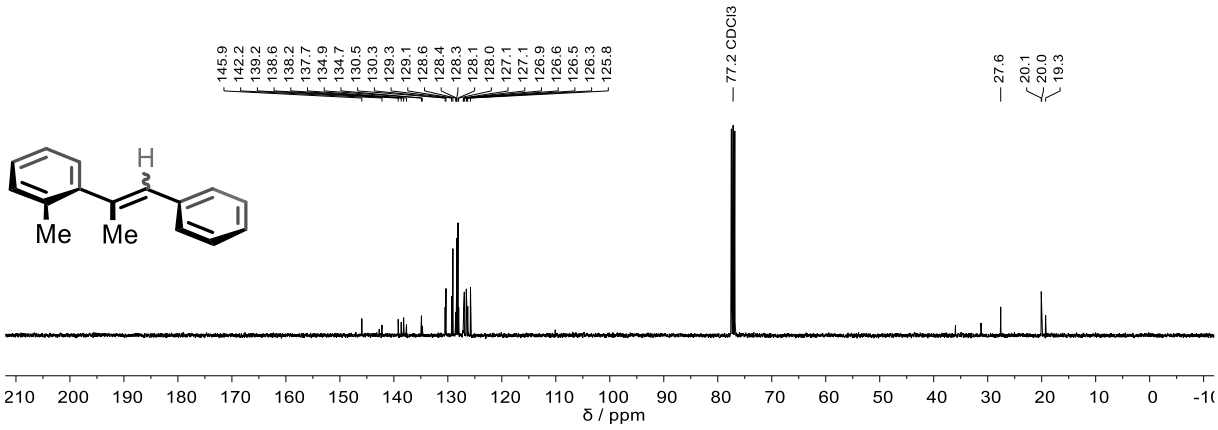

IR (ATR, neat) of **1z^{ci}**

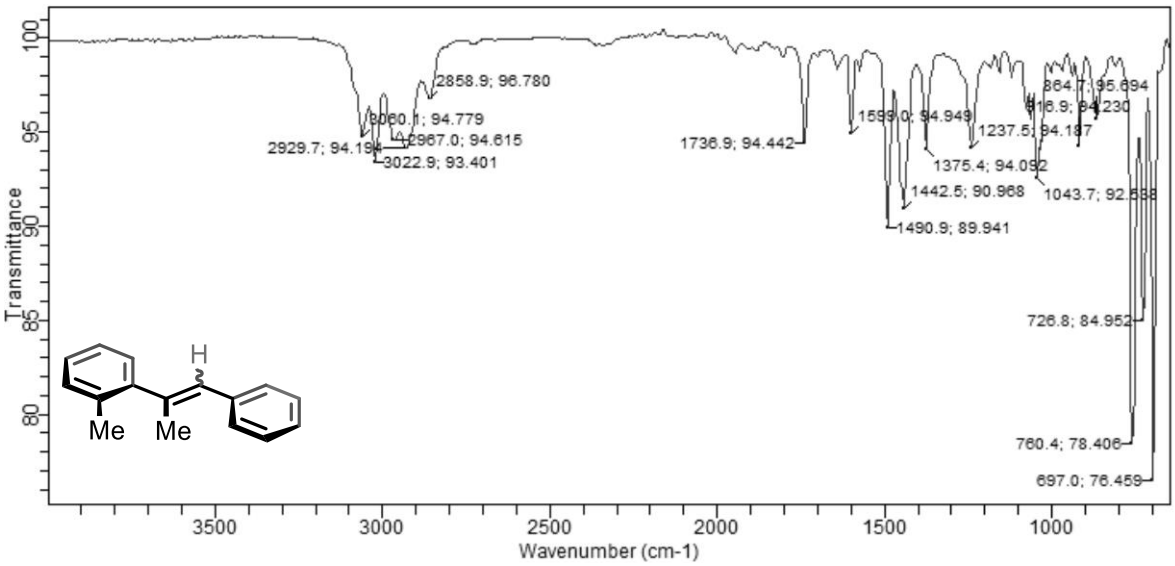

^{1}H NMR (400 MHz, $CDCl_3$) of **1s'** (*E*:*Z* = 57:43)

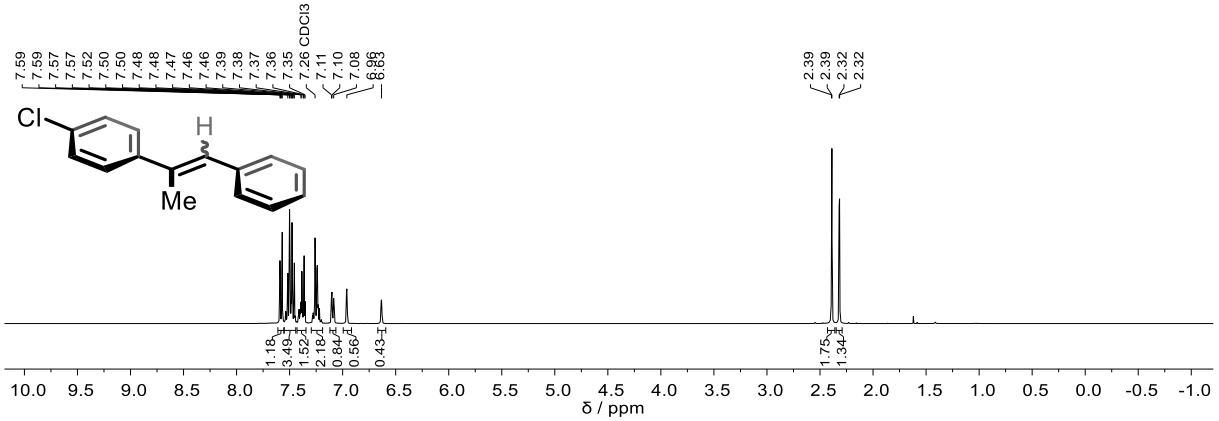

^{13}C{^{1}H} NMR (101 MHz, $CDCl_3$) of **1s'** (*E*:*Z* = 57:43)

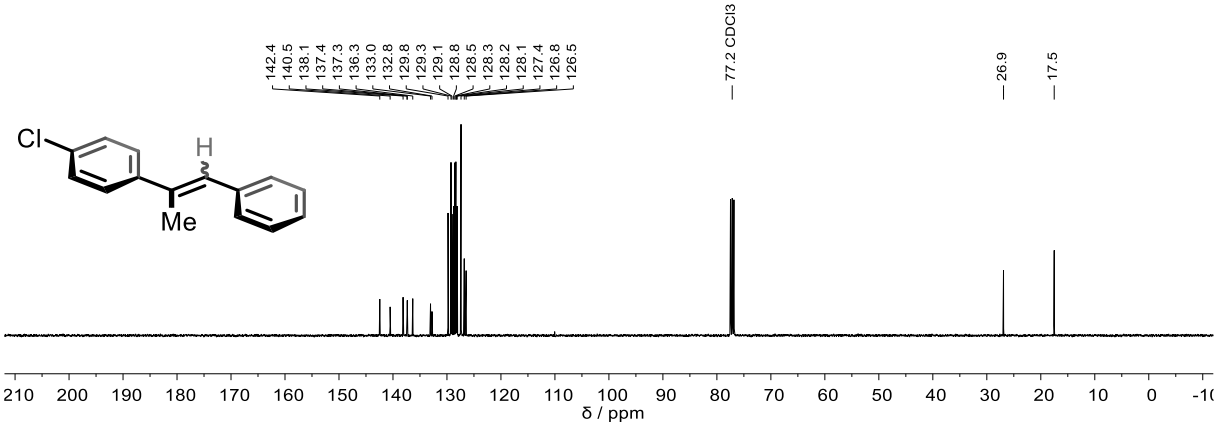

IR (ATR, neat) of **1s'**

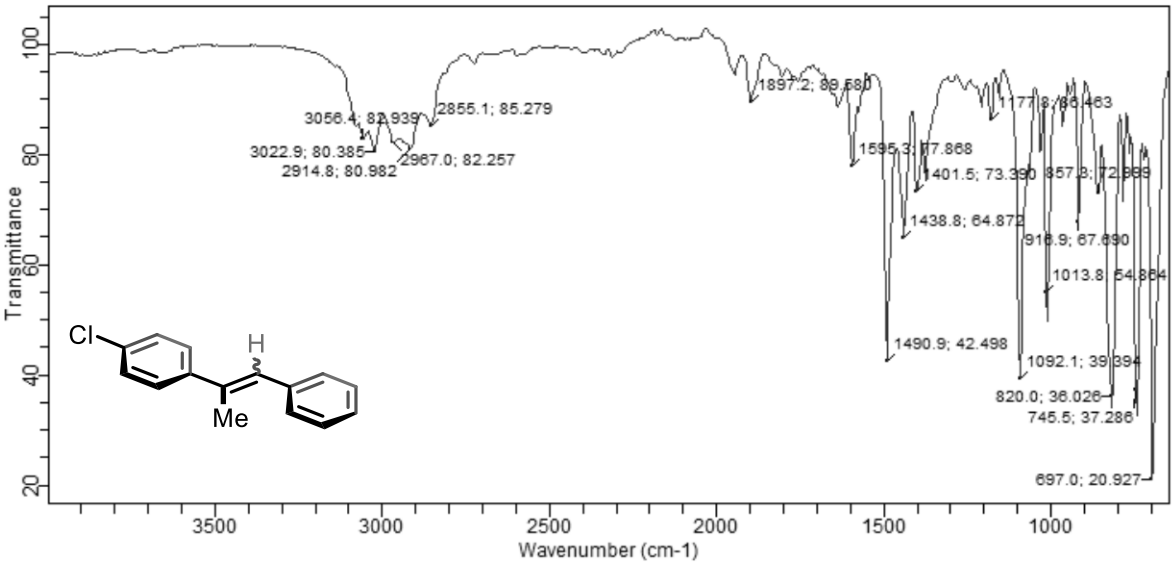

^{1}H NMR (400 MHz, $CDCl_3$) of **2a**

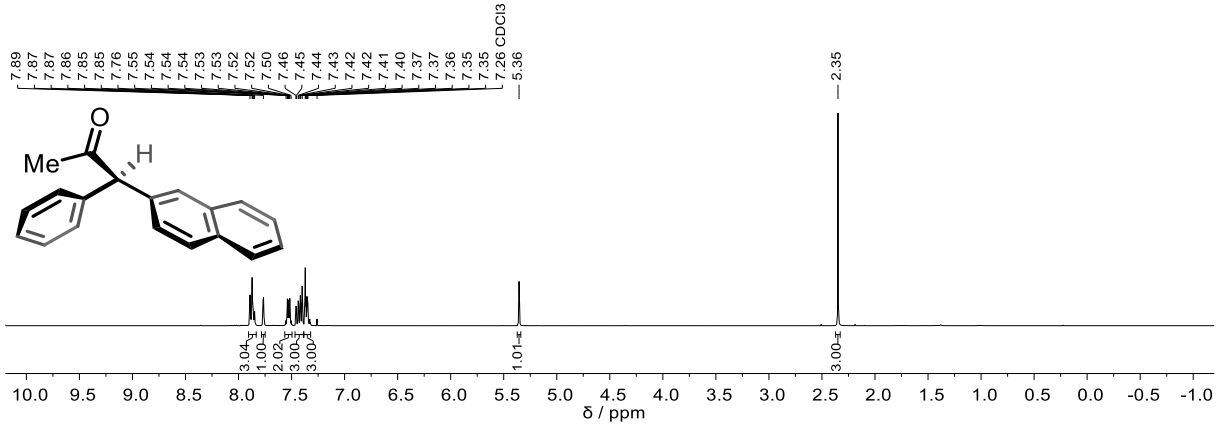

^{13}C{^{1}H} NMR (101 MHz, $CDCl_3$) of **2a**

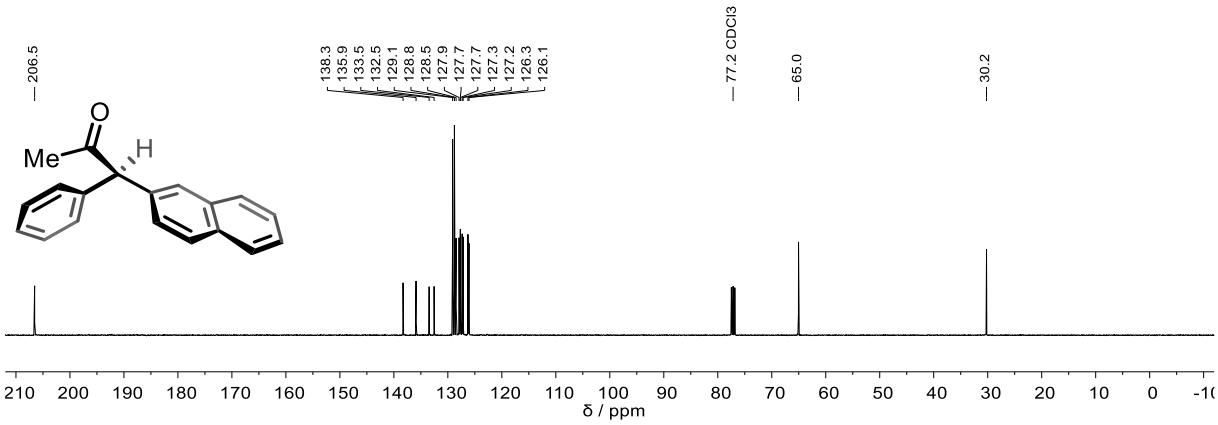

IR (ATR, neat) of **2a**

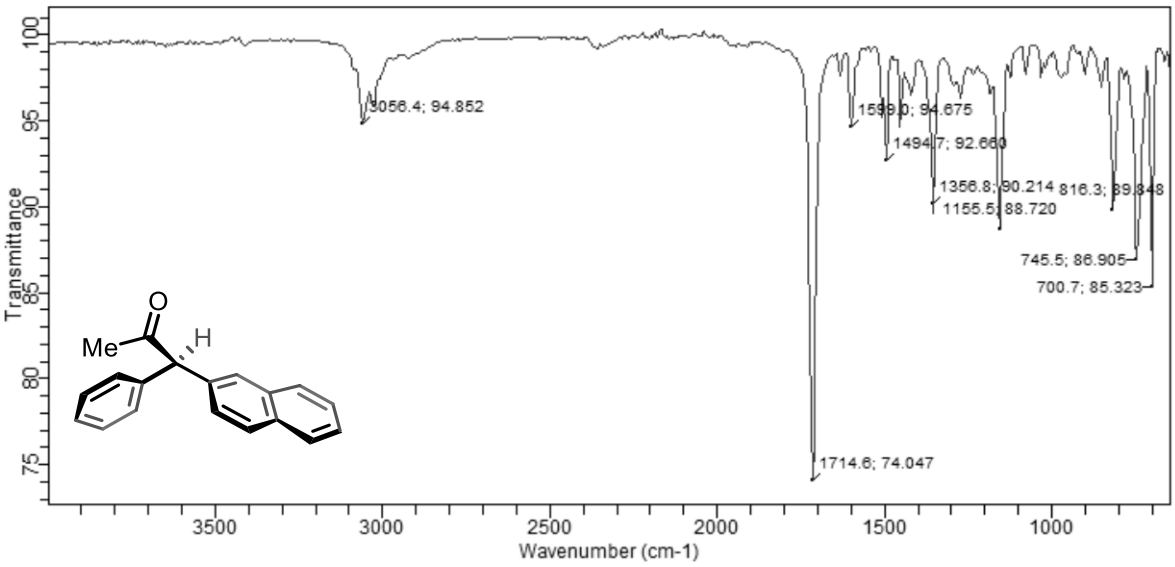

HPLC (IC-3, *n*-hexane:*i*-PrOH 95:5, flow rate 0.8 mL/min, 254 nm, 25 °C) of *rac*-**2a**

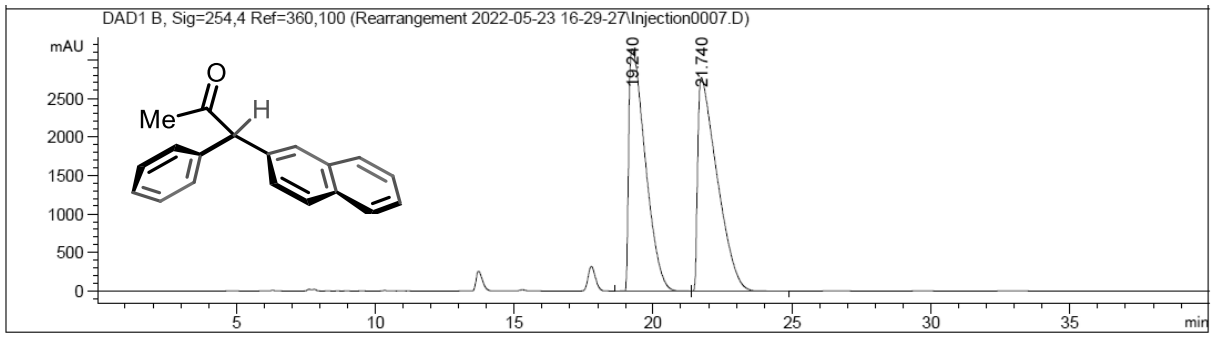


```
Signal 2: DAD1 B, Sig=254,4 Ref=360,100

Peak RetTime Type  Width     Area      Height     Area
  #   [min]        [min]   [mAU*s]     [mAU]       %
----|-------|----|-------|----------|----------|--------|
   1  19.240 BB    0.5416 1.29852e5  3132.66187  49.1638
   2  21.740 BB    0.6401 1.34269e5  2767.11304  50.8362
```

HPLC (IC-3, *n*-hexane:*i*-PrOH 95:5, flow rate 0.8 mL/min, 220 nm, 25 °C) of **2a**

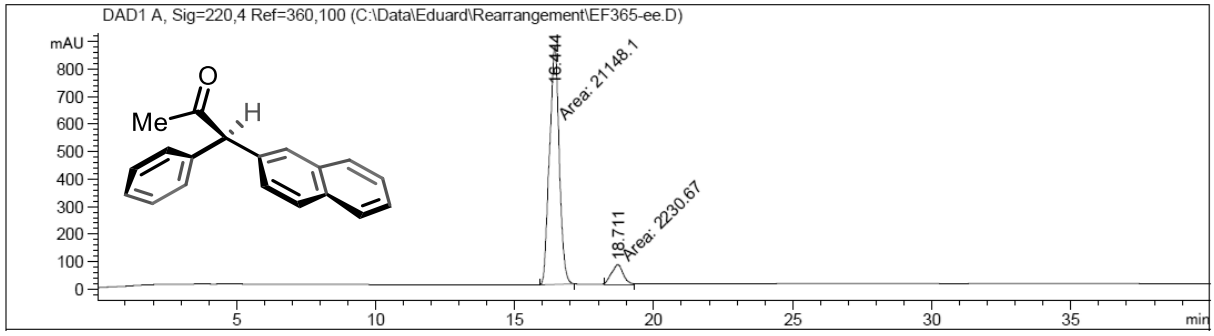


```
Signal 1: DAD1 A, Sig=220,4 Ref=360,100

Peak RetTime Type  Width     Area      Height     Area
  #   [min]        [min]   [mAU*s]     [mAU]       %
----|-------|----|-------|----------|----------|--------|
   1  16.444 MM    0.4063 2.11481e4   867.53387  90.4586
   2  18.711 MM    0.5017 2230.67383   74.10130   9.5414
```

HPLC (IC-3, *n*-hexane:*i*-PrOH 95:5, flow rate 0.8 mL/min, 220 nm, 25 °C) of ***ent*-2a**

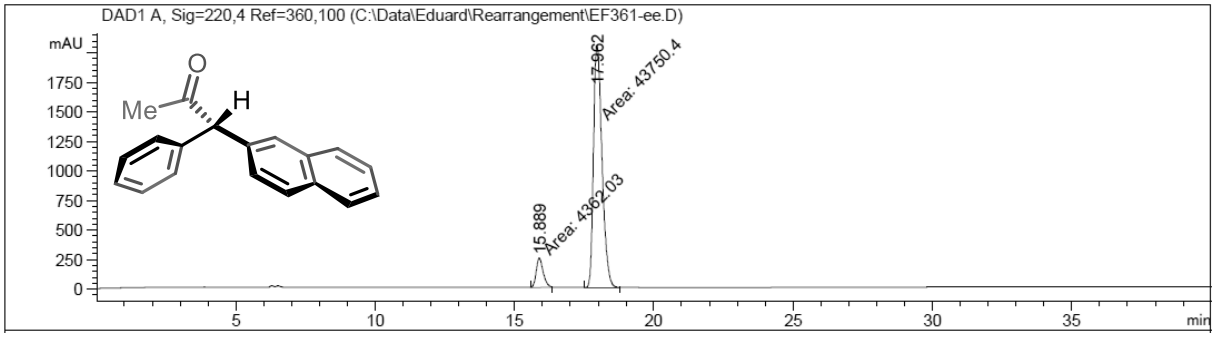


```
Signal 1: DAD1 A, Sig=220,4 Ref=360,100

Peak RetTime Type  Width     Area      Height     Area
  #   [min]        [min]   [mAU*s]     [mAU]       %
----|-------|----|-------|----------|----------|--------|
   1  15.889 MM    0.2917 4362.02783  249.24002   9.0663
   2  17.962 MM    0.3565 4.37504e4  2045.27148  90.9337
```

^{1}H NMR (400 MHz, $CDCl_3$) of ***ent*-2a**

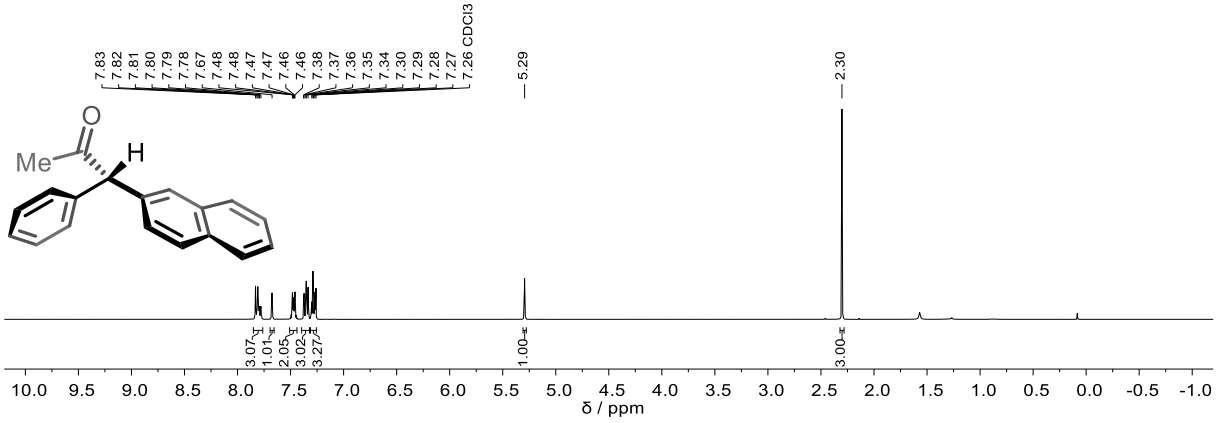

^{13}C{^{1}H} NMR (101 MHz, $CDCl_3$) of ***ent*-2a**

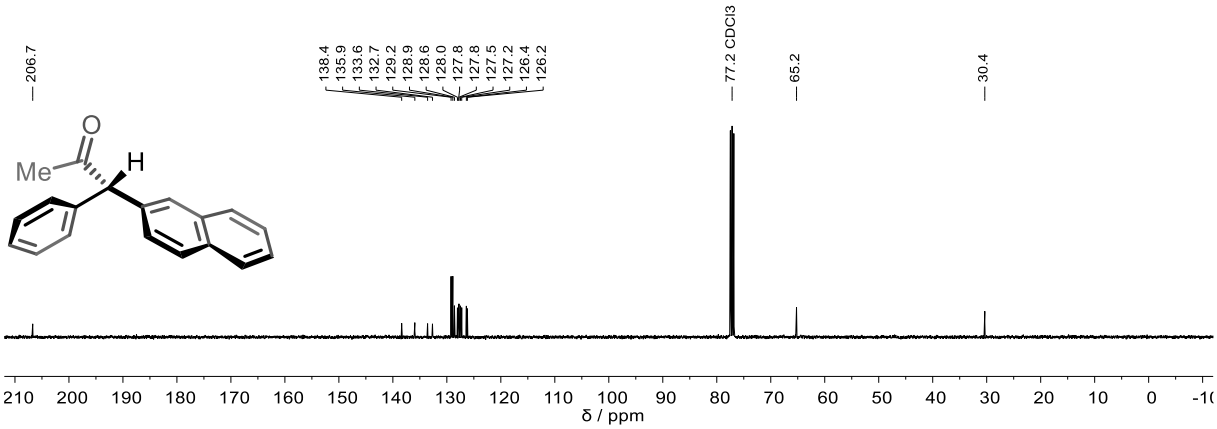

^{1}H NMR (400 MHz, $CDCl_3$) of **2b**

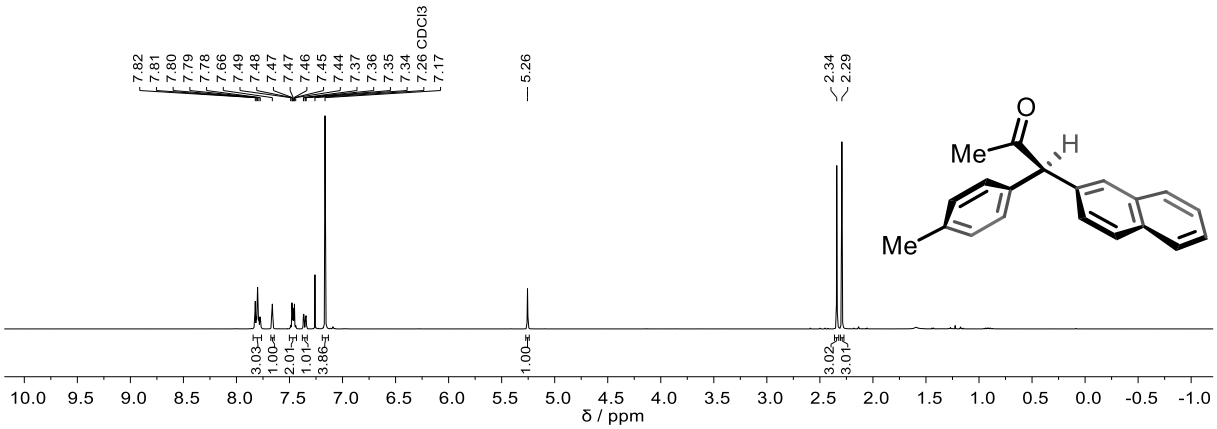

$^{13}C\{^{1}H\}$ NMR (101 MHz, $CDCl_3$) of **2b**

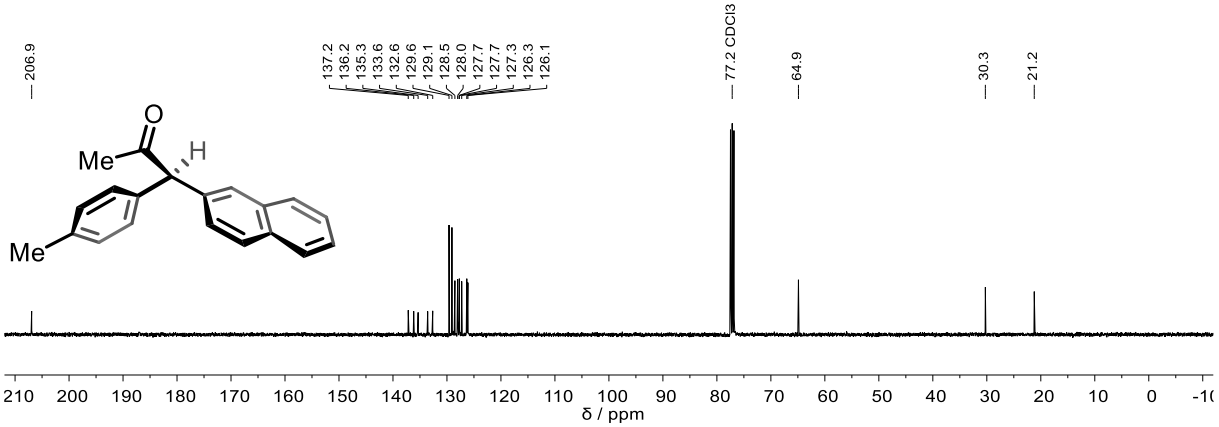

IR (ATR, neat) of **2b**

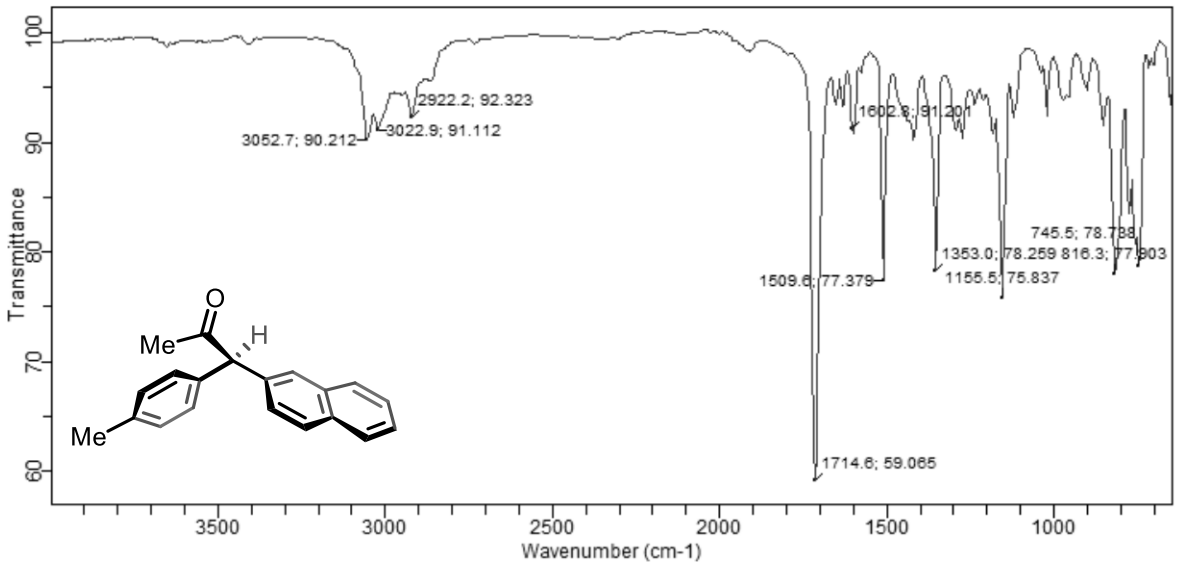

HPLC (ID-3, *n*-hexane:*i*-PrOH 95:5, flow rate 0.8 mL/min, 254 nm, 25 °C) of *rac*-**2b**

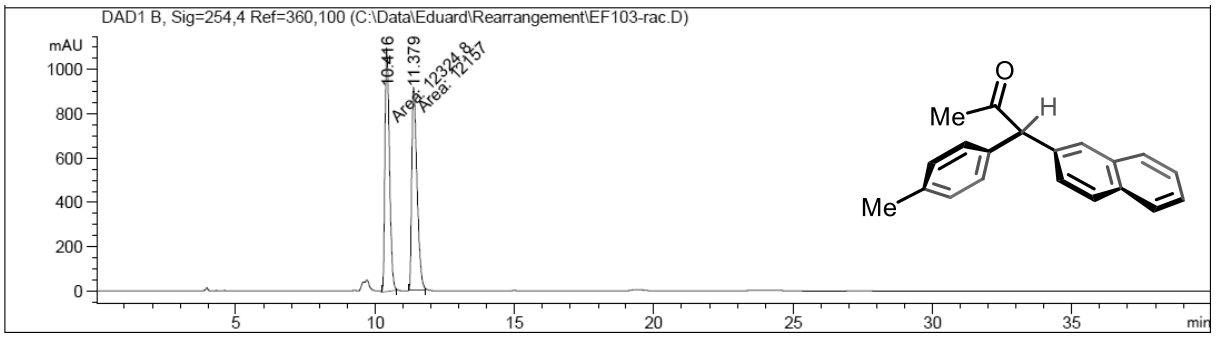

Signal 2: DAD1 B, Sig=254,4 Ref=360,100

Peak #	RetTime [min]	Type	Width [min]	Area [mAU*s]	Height [mAU]	Area %
1	10.416	MM	0.1869	1.23248e4	1099.29309	50.3428
2	11.379	MM	0.2211	1.21570e4	916.59625	49.6572

HPLC (ID-3, *n*-hexane:*i*-PrOH 95:5, flow rate 0.8 mL/min, 254 nm, 25 °C) of **2b**

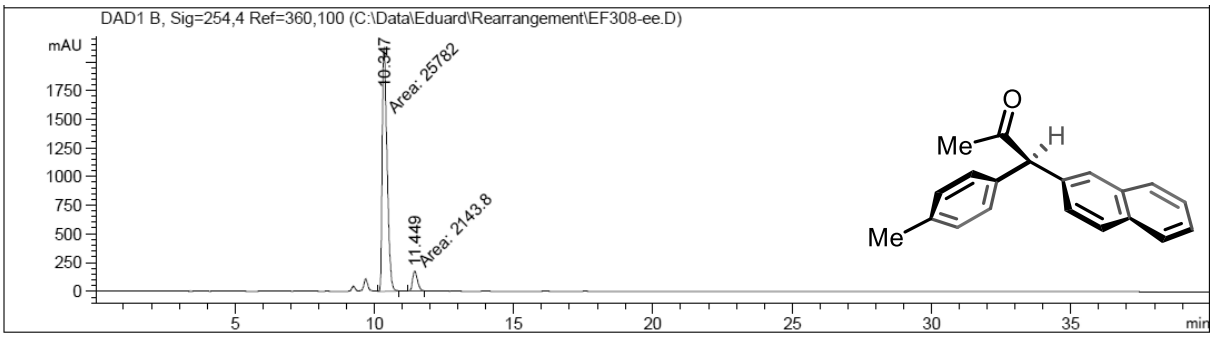

Signal 2: DAD1 B, Sig=254,4 Ref=360,100

Peak #	RetTime [min]	Type	Width [min]	Area [mAU*s]	Height [mAU]	Area %
1	10.347	MM	0.2033	2.57820e4	2113.95313	92.3232
2	11.449	MM	0.2027	2143.80347	176.25803	7.6768

HPLC (ID-3, *n*-hexane:*i*-PrOH 95:5, flow rate 0.8 mL/min, 254 nm, 25 °C) of ***ent*-2b**

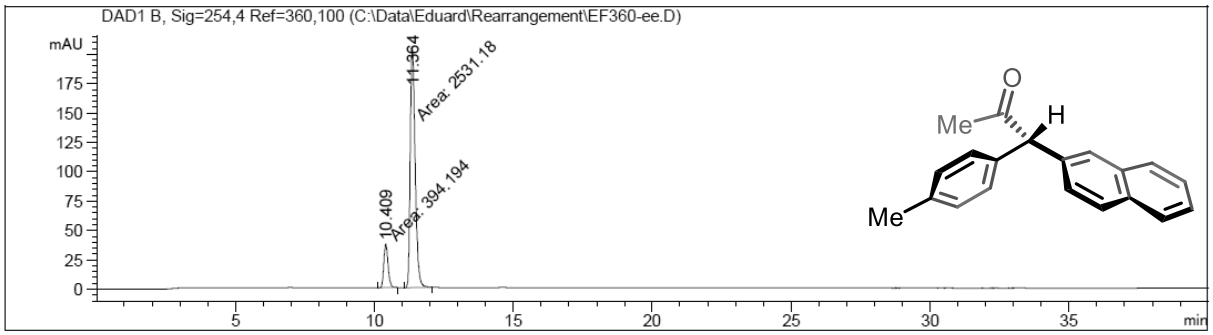

Signal 2: DAD1 B, Sig=254,4 Ref=360,100

Peak #	RetTime [min]	Type	Width [min]	Area [mAU*s]	Height [mAU]	Area %
1	10.409	MM	0.1760	394.19424	37.32212	13.4750
2	11.364	MM	0.2058	2531.17896	204.99701	86.5250

^{1}H NMR (400 MHz, $CDCl_3$) of ***ent*-2b**

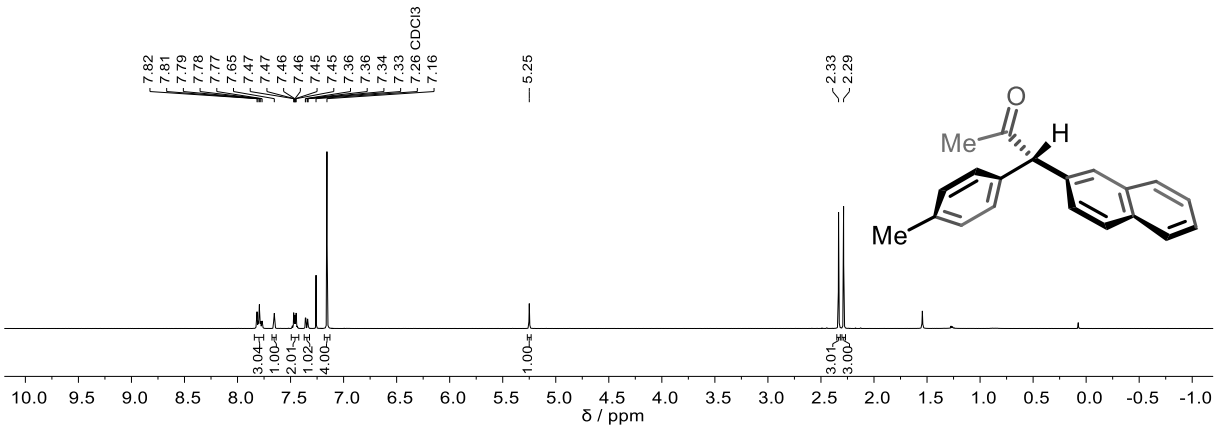

$^{13}C\{^{1}H\}$ NMR (101 MHz, $CDCl_3$) of ***ent*-2b**

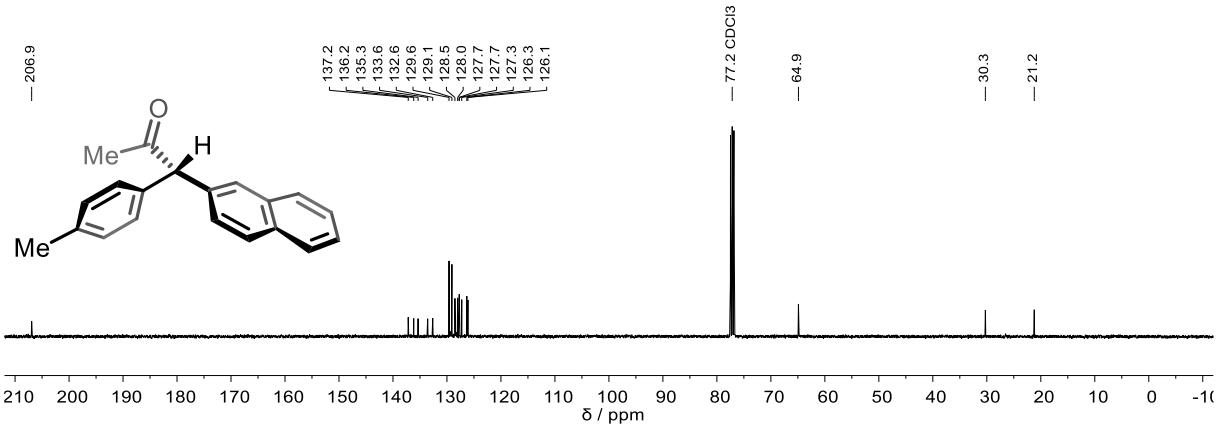

^{1}H NMR (400 MHz, $CDCl_3$) of **2c**

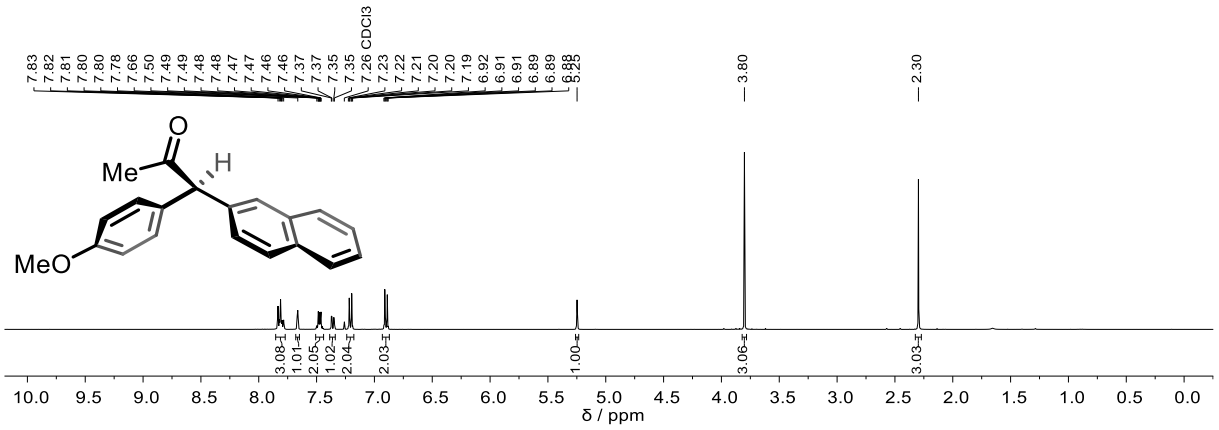

$^{13}C\{^{1}H\}$ NMR (101 MHz, $CDCl_3$) of **2c**

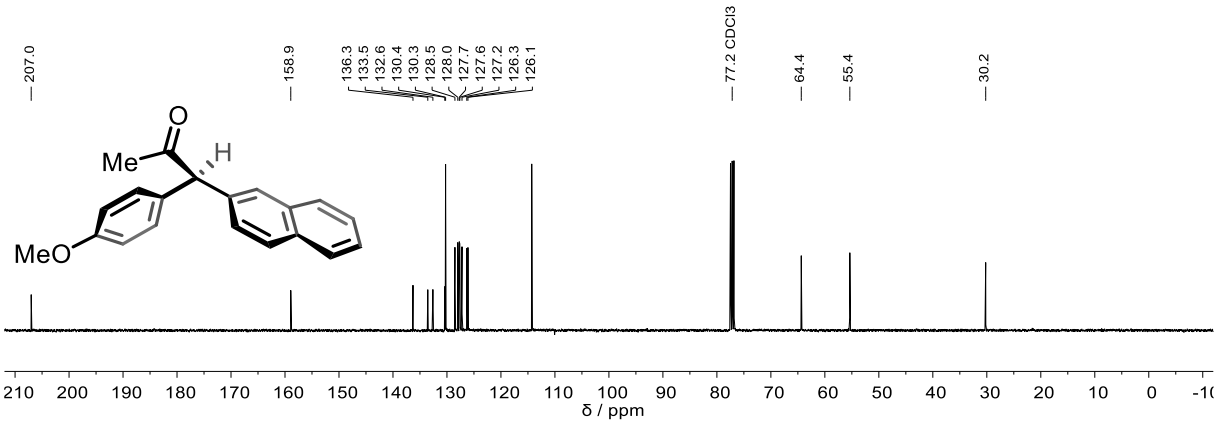

IR (ATR, neat) of **2c**

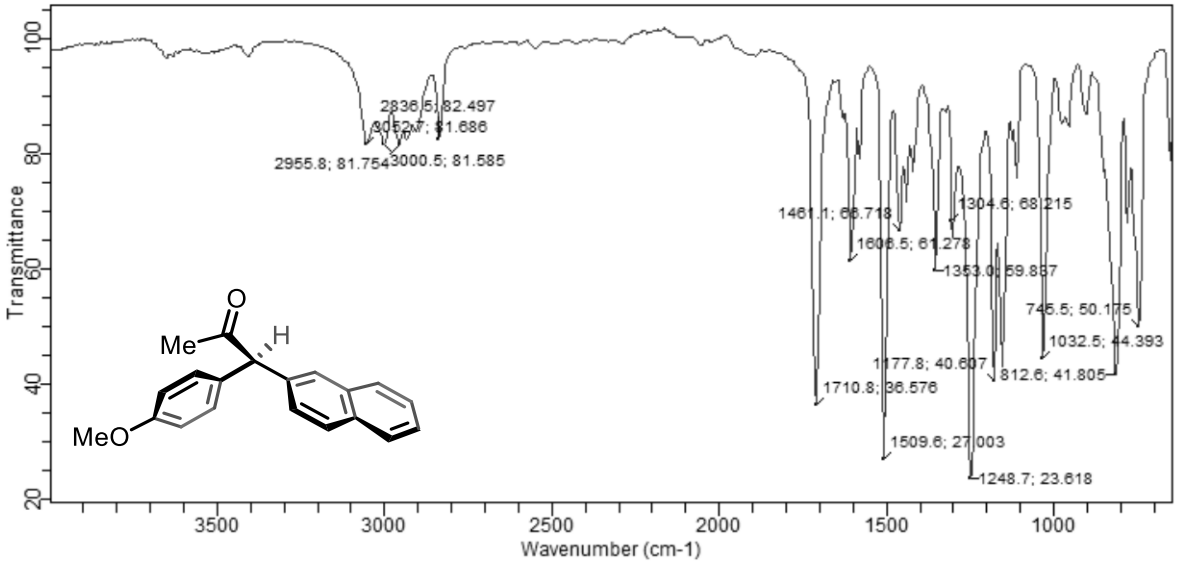

HPLC (IC-3, *n*-hexane:*i*-PrOH 90:10, flow rate 0.8 mL/min, 254 nm, 25 °C) of *rac*-**2c**

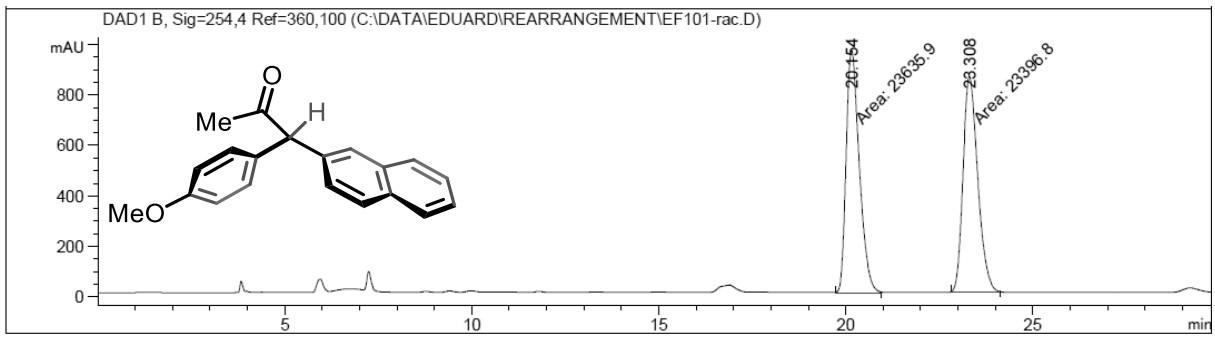


```
Signal 2: DAD1 B, Sig=254,4 Ref=360,100

Peak RetTime Type  Width     Area      Height     Area
  #   [min]        [min]   [mAU*s]     [mAU]       %
----|-------|----|-------|----------|----------|--------|
   1  20.154 MM    0.4091 2.36359e4   962.83221  50.2542
   2  23.308 MM    0.4562 2.33968e4   854.70032  49.7458
```

HPLC (IC-3, *n*-hexane:*i*-PrOH 90:10, flow rate 0.8 mL/min, 254 nm, 25 °C) of **2c**

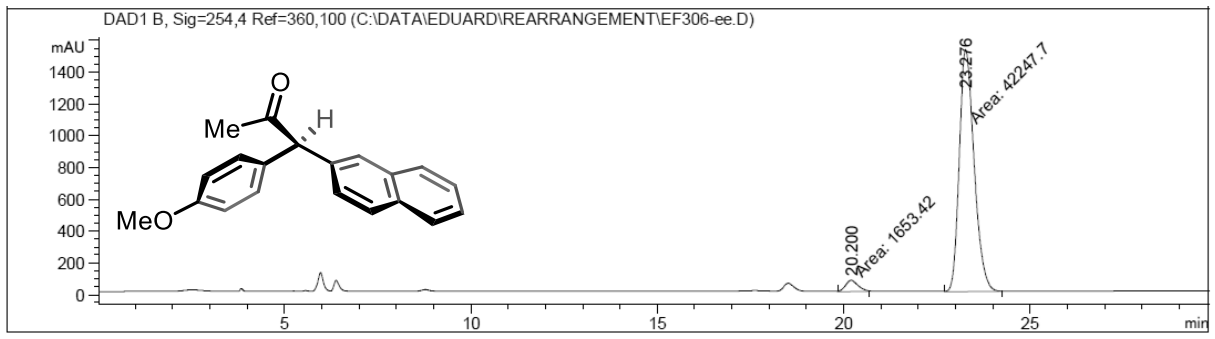


```
Signal 2: DAD1 B, Sig=254,4 Ref=360,100

Peak RetTime Type  Width     Area      Height     Area
  #   [min]        [min]   [mAU*s]     [mAU]       %
----|-------|----|-------|----------|----------|--------|
   1  20.200 MM    0.3881 1653.41882   71.01325   3.7662
   2  23.276 MM    0.4630 4.22477e4  1520.91260  96.2338
```

HPLC (IC-3, *n*-hexane:*i*-PrOH 90:10, flow rate 0.8 mL/min, 254 nm, 25 °C) of ***ent*-2c**

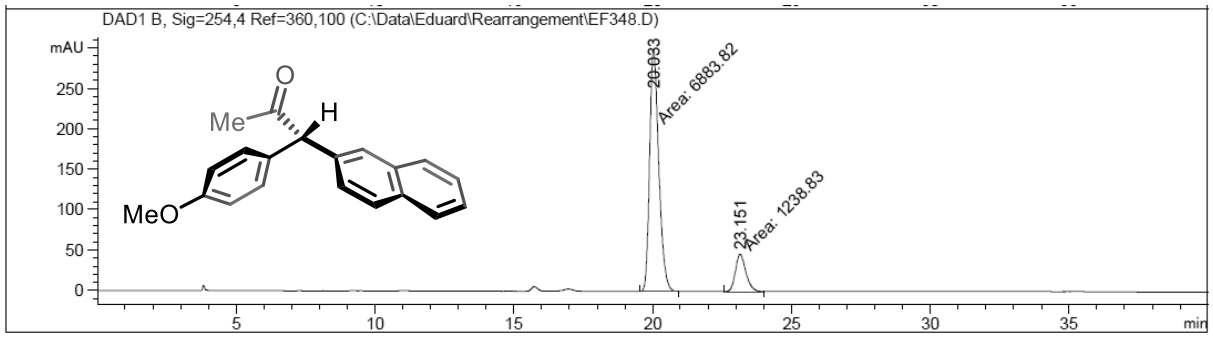

Signal 2: DAD1 B, Sig=254,4 Ref=360,100

Peak #	RetTime [min]	Type	Width [min]	Area [mAU*s]	Height [mAU]	Area %
1	20.033	MM	0.3837	6883.81836	298.99637	84.7484
2	23.151	MM	0.4449	1238.83435	46.40353	15.2516

^{1}H NMR (400 MHz, $CDCl_3$) of ***ent*-2c**

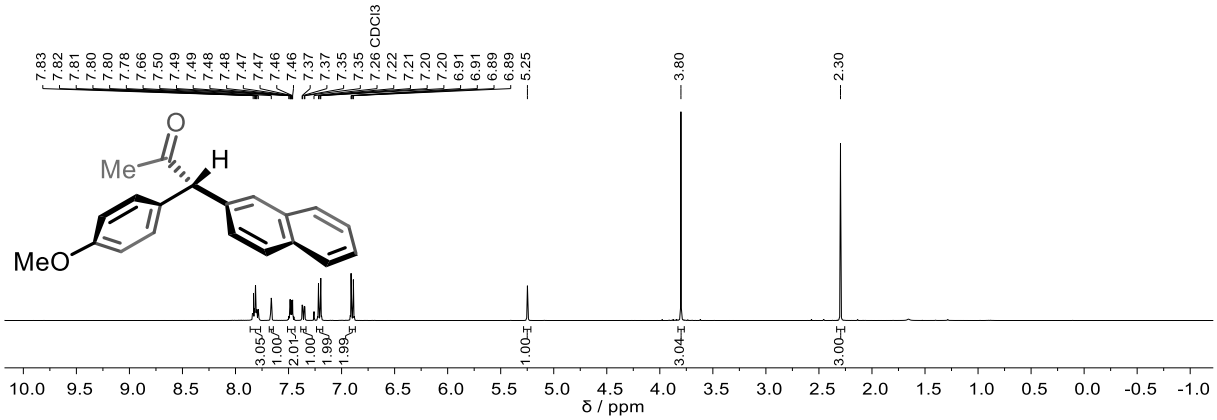

^{13}C{^{1}H} NMR (101 MHz, $CDCl_3$) of ***ent*-2c**

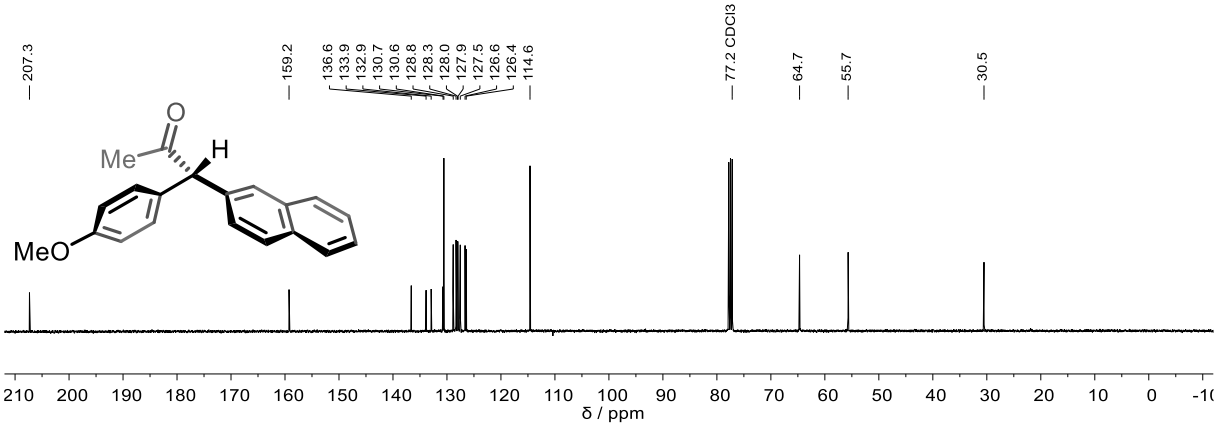

^{1}H NMR (400 MHz, $CDCl_3$) of **2n**

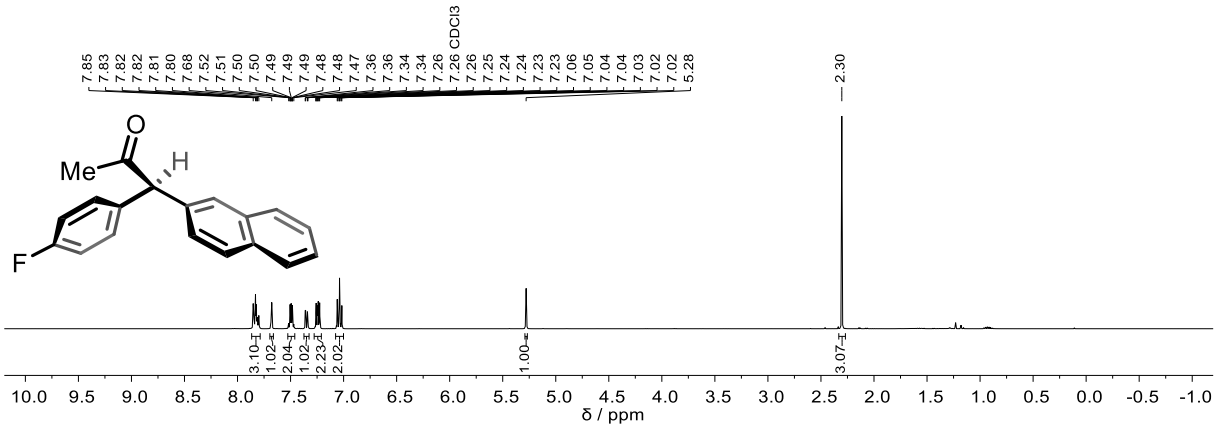

^{13}C{^{1}H} NMR (101 MHz, $CDCl_3$) of **2n**

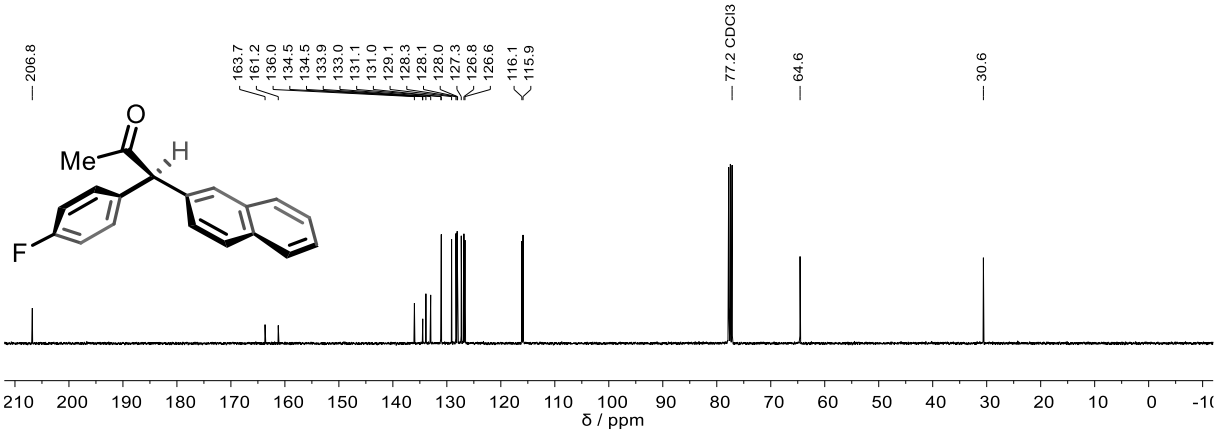

^{19}F{^{1}H} NMR (377 MHz, $CDCl_3$) of **2n**

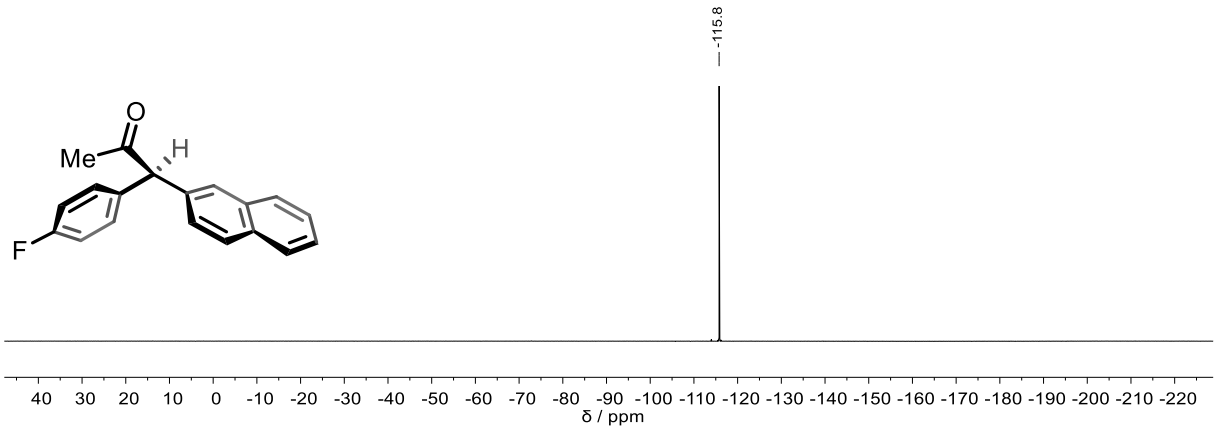

IR (ATR, neat) of **2n**

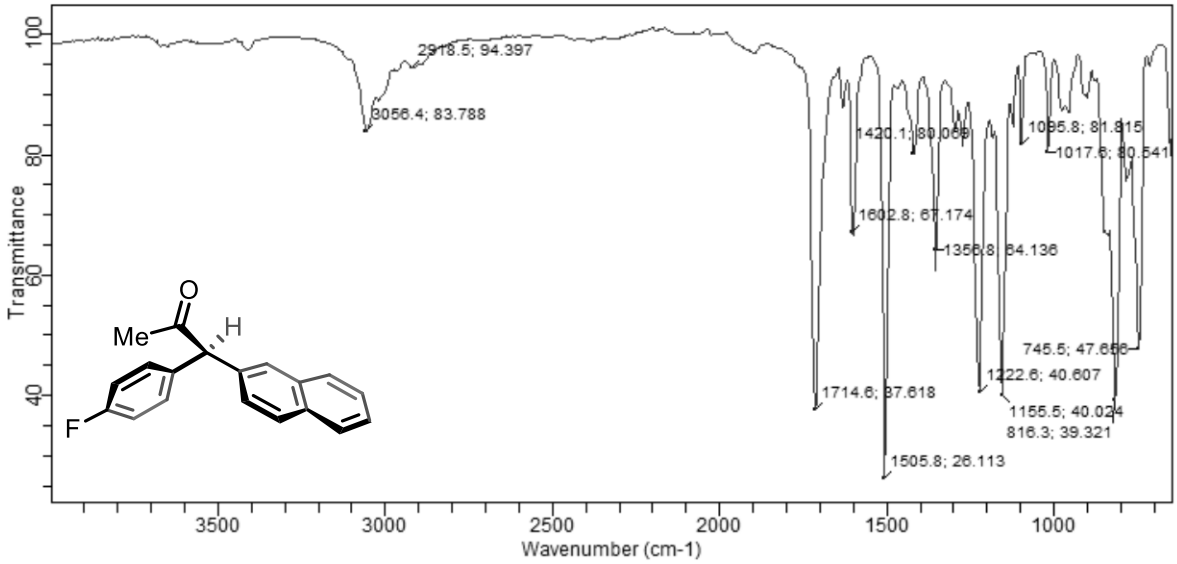

HPLC (ID-3, *n*-hexane:*i*-PrOH 95:5, flow rate 0.6 mL/min, 254 nm, 25 °C) of *rac*-**2n**

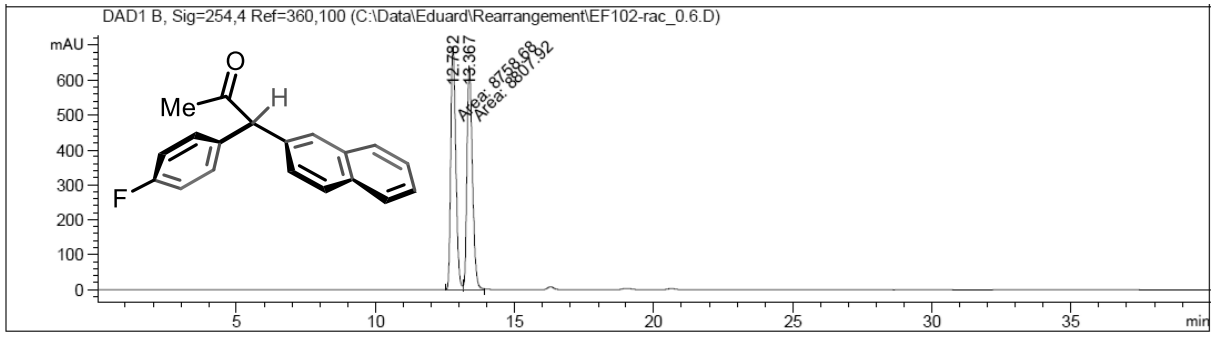


```
Signal 2: DAD1 B, Sig=254,4 Ref=360,100

Peak RetTime Type  Width     Area      Height     Area
  #   [min]        [min]   [mAU*s]     [mAU]       %
----|-------|----|-------|----------|----------|--------|
   1  12.782 MM    0.2102 8758.67773  694.32745  49.8598
   2  13.367 MM    0.2295 8807.92480  639.73535  50.1402
```

HPLC (ID-3, *n*-hexane:*i*-PrOH 95:5, flow rate 0.6 mL/min, 254 nm, 25 °C) of **2n**

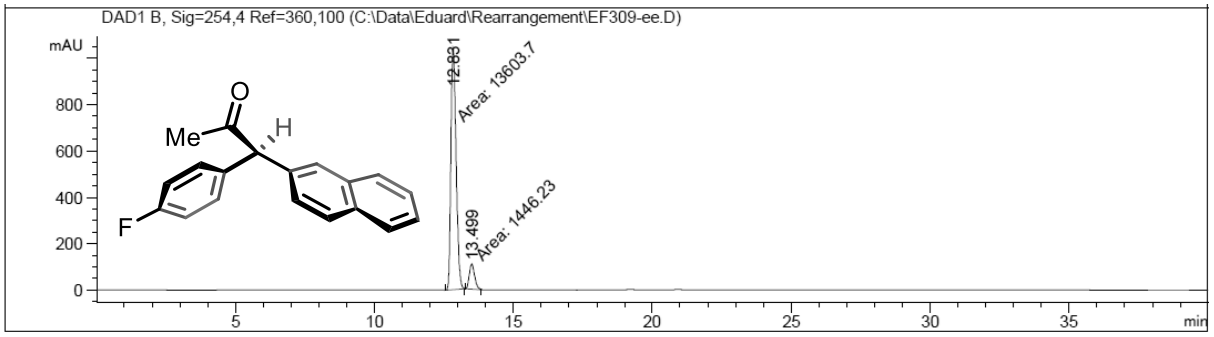


```
Signal 2: DAD1 B, Sig=254,4 Ref=360,100

Peak RetTime Type  Width     Area      Height     Area
  #   [min]        [min]   [mAU*s]     [mAU]       %
----|-------|----|-------|----------|----------|--------|
   1  12.831 MM    0.2175 1.36037e4  1042.53625  90.3905
   2  13.499 MM    0.2230 1446.22522  108.07832   9.6095
```

HPLC (ID-3, *n*-hexane:*i*-PrOH 95:5, flow rate 0.6 mL/min, 254 nm, 25 °C) of ***ent*-2n**

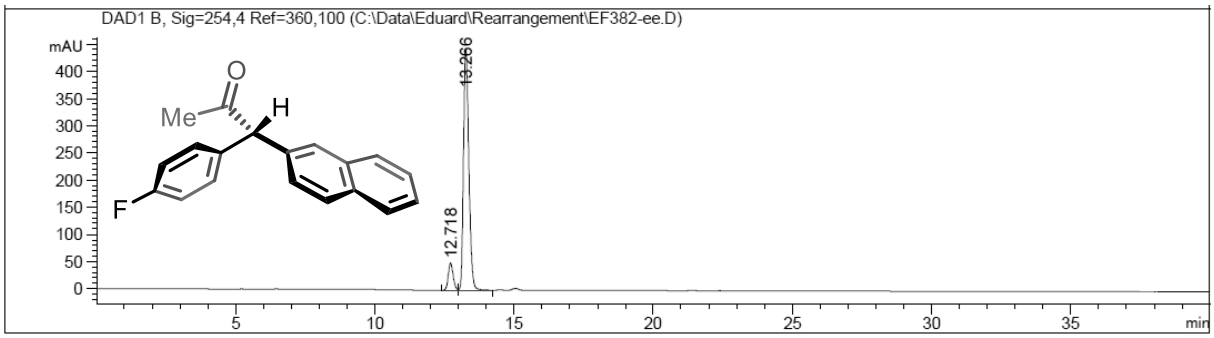

Signal 2: DAD1 B, Sig=254,4 Ref=360,100

Peak #	RetTime [min]	Type	Width [min]	Area [mAU*s]	Height [mAU]	Area %
1	12.718	BV	0.1907	610.38422	49.91346	9.3427
2	13.266	VB	0.2080	5922.86621	442.87628	90.6573

^{1}H NMR (400 MHz, $CDCl_3$) of ***ent*-2n**

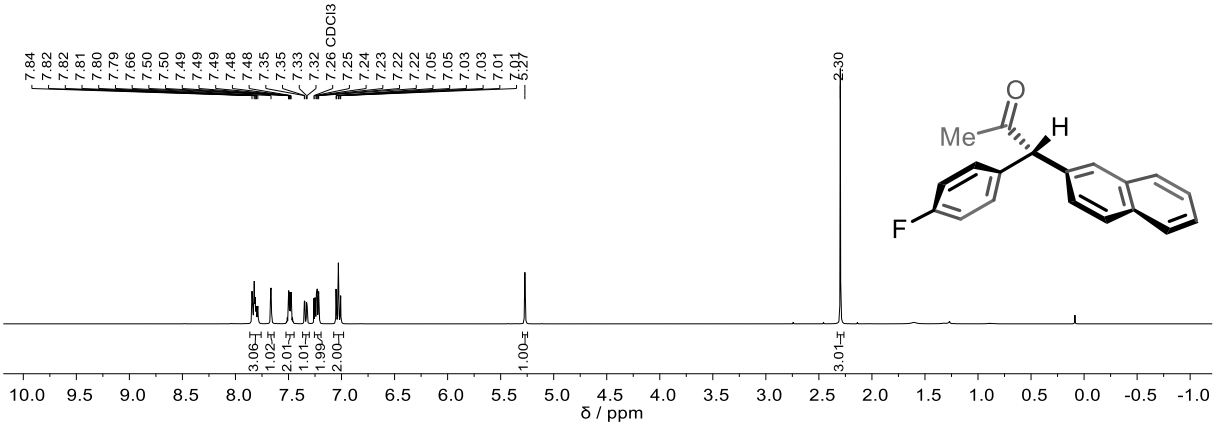

^{13}C{^{1}H} NMR (101 MHz, $CDCl_3$) of ***ent*-2n**

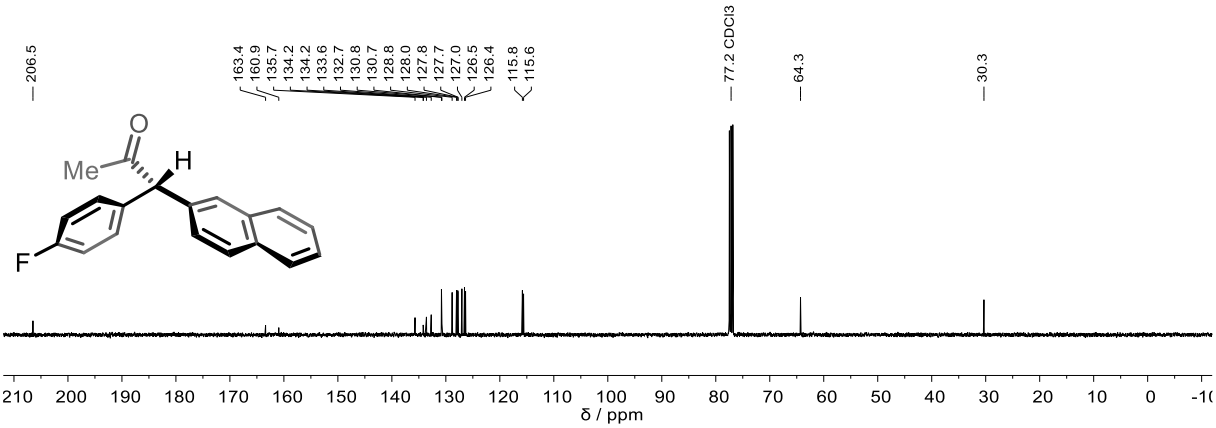

$^{19}F\{^{1}H\}$ NMR (377 MHz, $CDCl_3$) of ***ent*-2n**

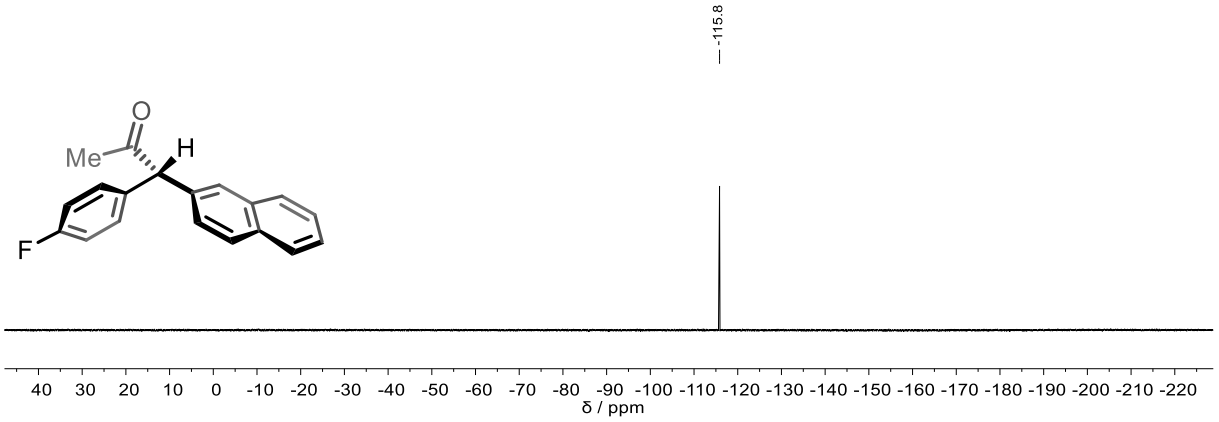

^{1}H NMR (400 MHz, $CDCl_3$) of **2o**

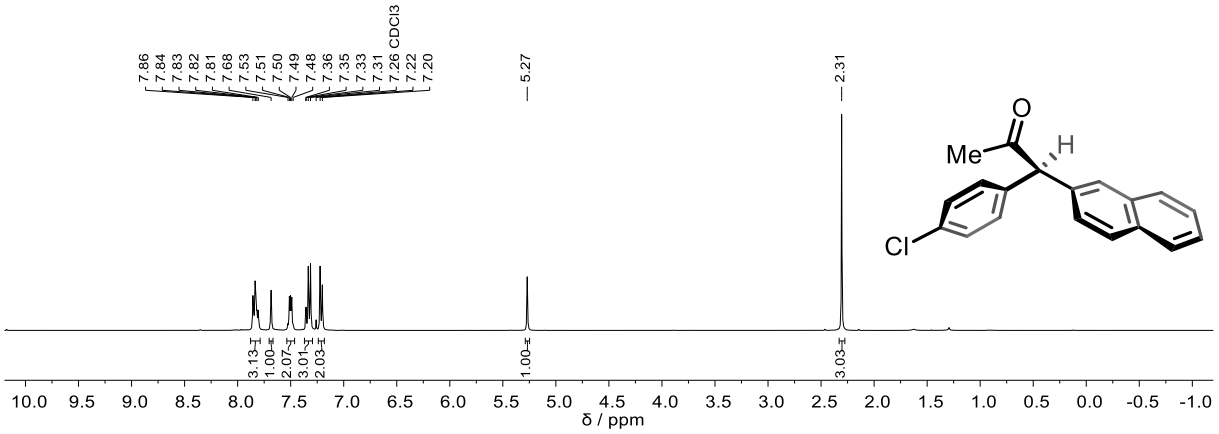

$^{13}C\{^{1}H\}$ NMR (101 MHz, $CDCl_3$) of **2o**

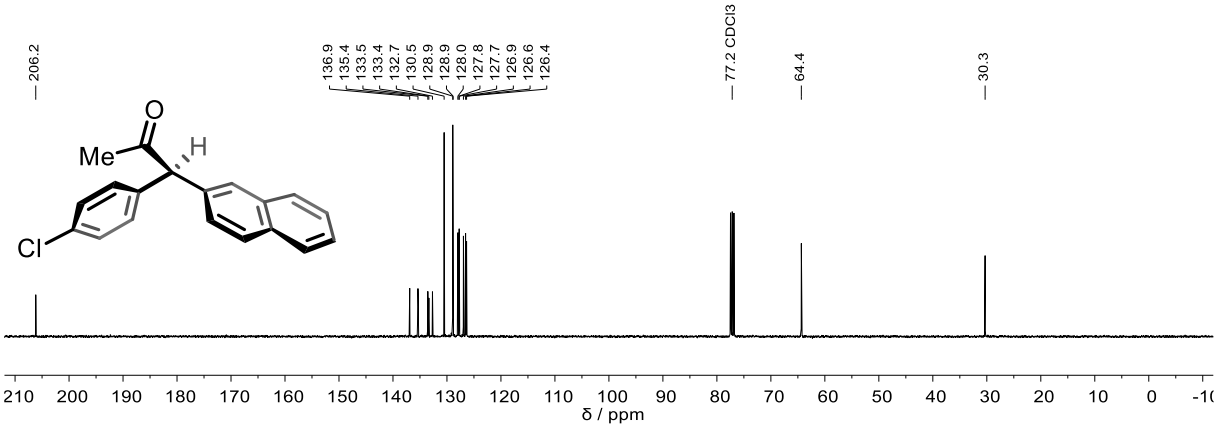

IR (ATR, neat) of **2o**

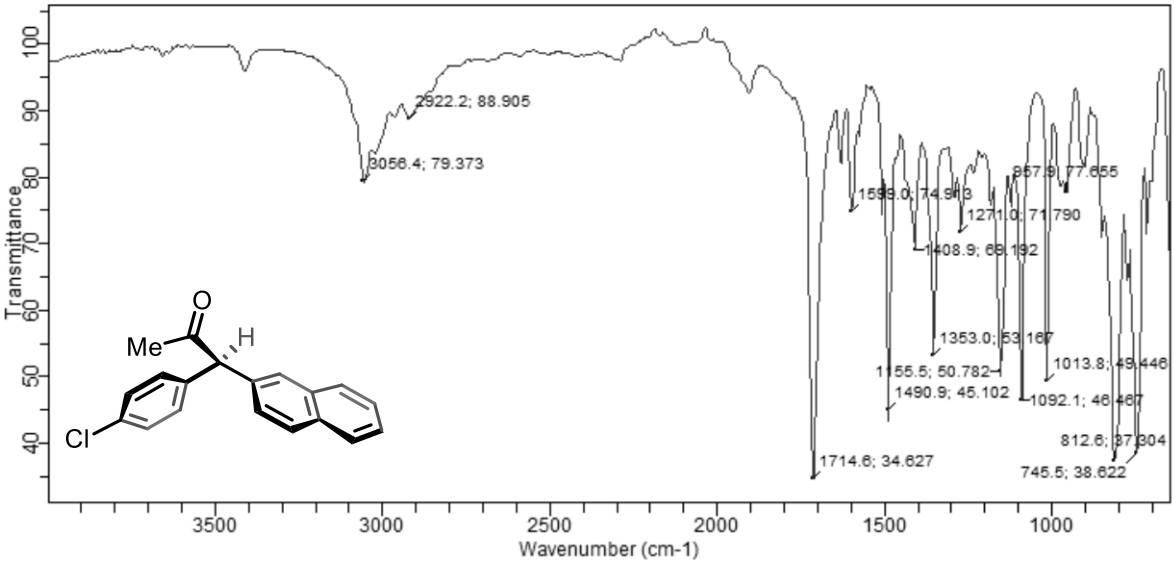

HPLC (ID-3, *n*-hexane:*i*-PrOH 95:5, flow rate 0.8 mL/min, 254 nm, 25 °C) of *rac*-**2o**

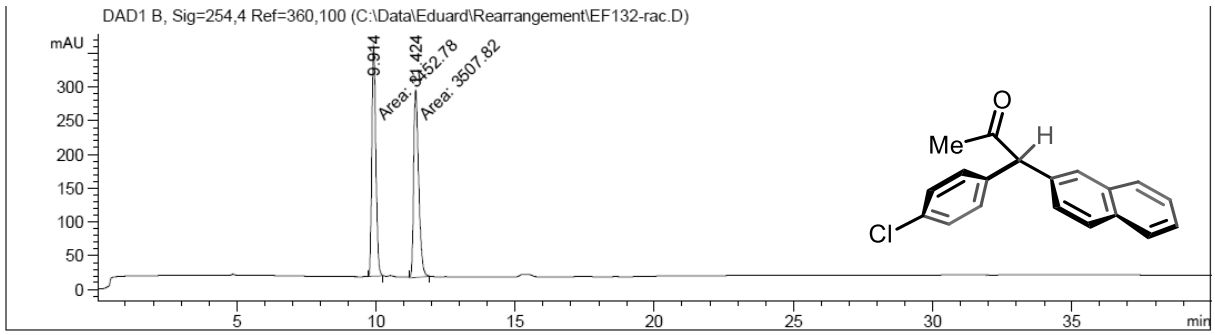


```
Signal 2: DAD1 B, Sig=254,4 Ref=360,100

Peak RetTime Type  Width     Area      Height     Area
  #   [min]        [min]   [mAU*s]     [mAU]       %
----|-------|----|-------|----------|----------|--------|
   1   9.914 MM    0.1685 3452.77979  341.44849  49.6046
   2  11.424 MM    0.2097 3507.81958  278.75873  50.3954
```

HPLC (ID-3, *n*-hexane:*i*-PrOH 95:5, flow rate 0.8 mL/min, 254 nm, 25 °C) of **2o**

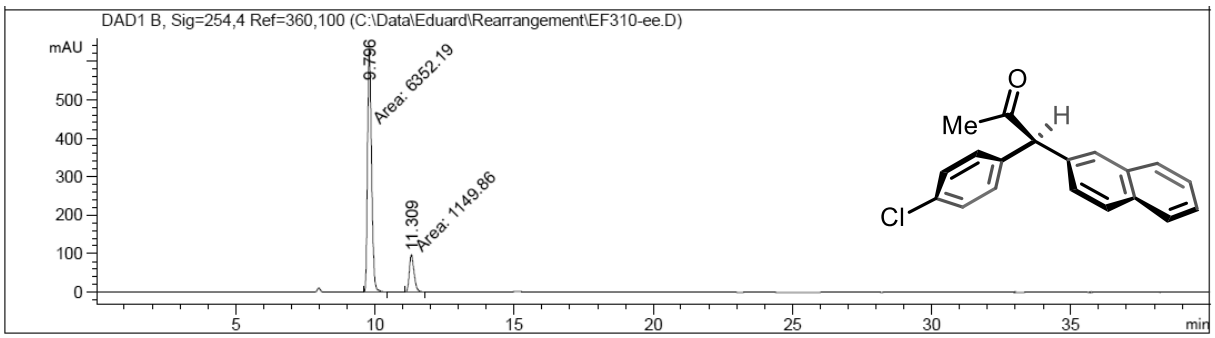


```
Signal 2: DAD1 B, Sig=254,4 Ref=360,100

Peak RetTime Type  Width     Area      Height     Area
  #   [min]        [min]   [mAU*s]     [mAU]       %
----|-------|----|-------|----------|----------|--------|
   1   9.796 MM    0.1690 6352.18896  626.54193  84.6727
   2  11.309 MM    0.1992 1149.86206   96.20136  15.3273
```

^{1}H NMR (400 MHz, $CDCl_3$) of **2z**

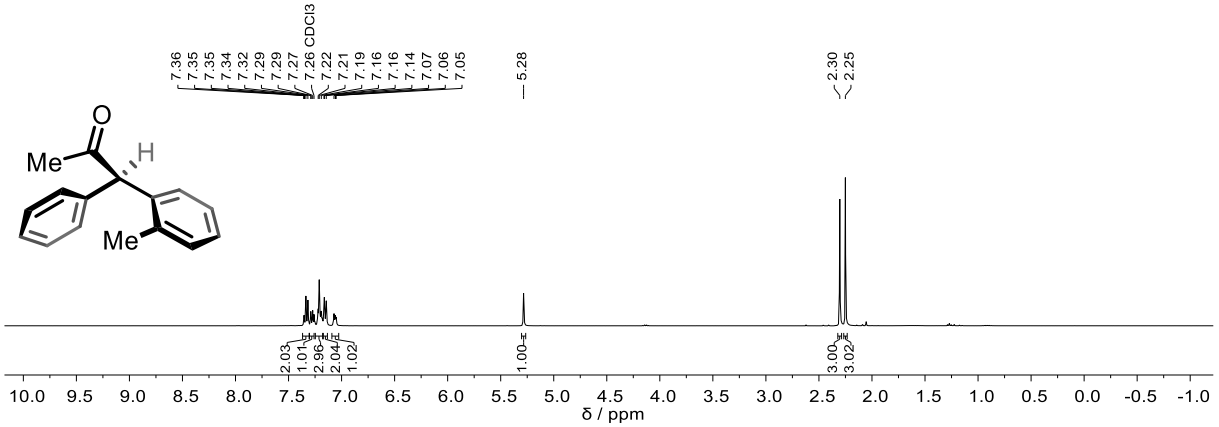

^{13}C{^{1}H} NMR (101 MHz, $CDCl_3$) of **2z**

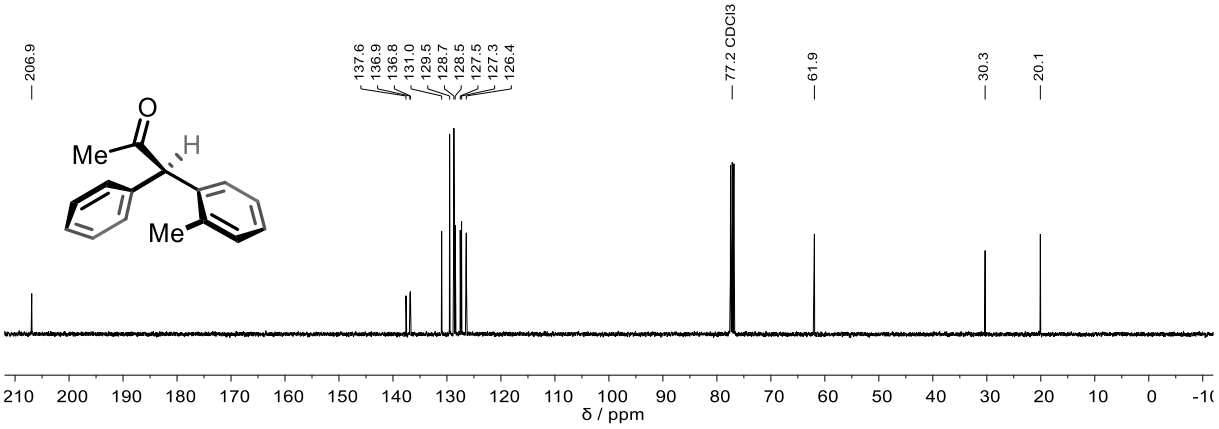

IR (ATR, neat) of **2z**

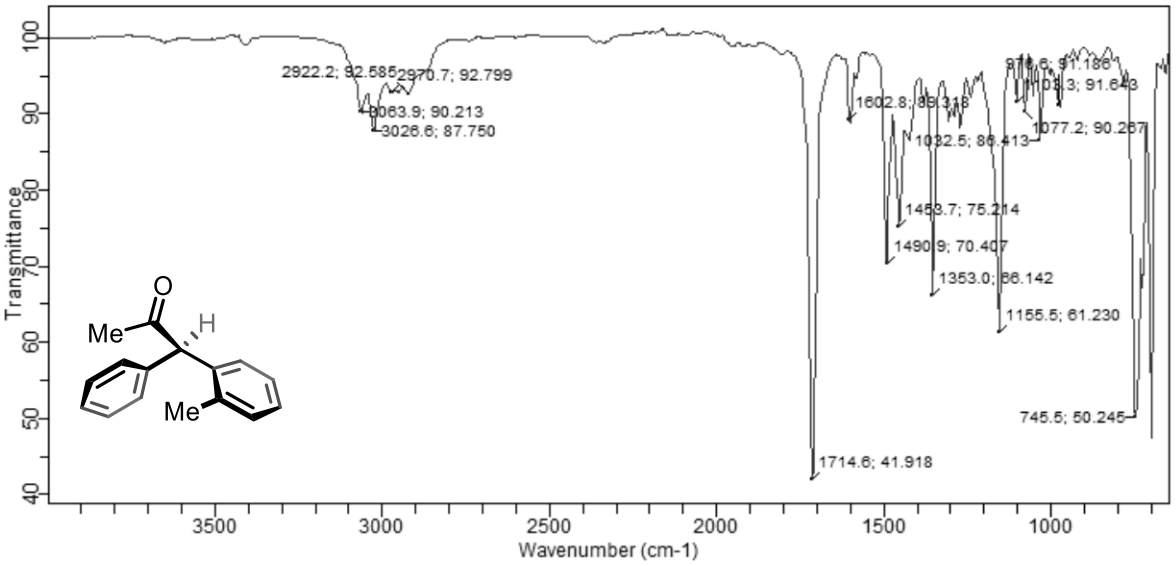

HPLC (IC-3, *n*-hexane:*i*-PrOH 95:5, flow rate 0.8 mL/min, 220 nm, 25 °C) of *rac*-**2z**

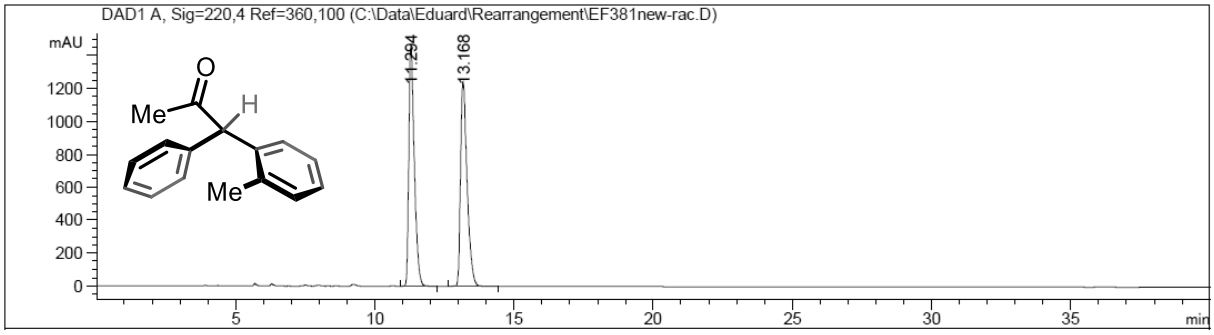

Signal 1: DAD1 A, Sig=220,4 Ref=360,100

Peak #	RetTime [min]	Type	Width [min]	Area [mAU*s]	Height [mAU]	Area %
1	11.294	VB	0.2071	2.02200e4	1463.90662	49.8479
2	13.168	BB	0.2447	2.03434e4	1244.84302	50.1521

HPLC (IC-3, *n*-hexane:*i*-PrOH 95:5, flow rate 0.8 mL/min, 220 nm, 25 °C) of **2z**

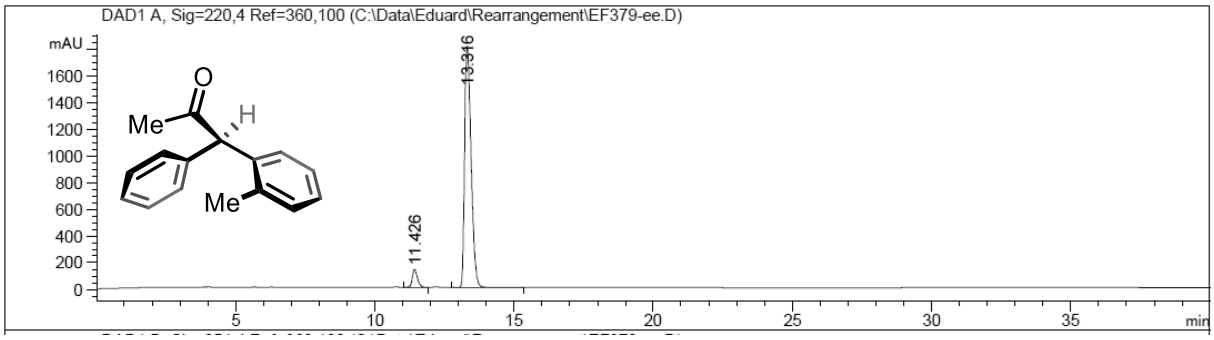

Signal 1: DAD1 A, Sig=220,4 Ref=360,100

Peak #	RetTime [min]	Type	Width [min]	Area [mAU*s]	Height [mAU]	Area %
1	11.426	VB	0.1952	1754.05994	135.34995	5.6476
2	13.316	BB	0.2533	2.93045e4	1805.85168	94.3524

HPLC (IC-3, *n*-hexane:*i*-PrOH 95:5, flow rate 0.8 mL/min, 220 nm, 25 °C) of ***ent*-2z**

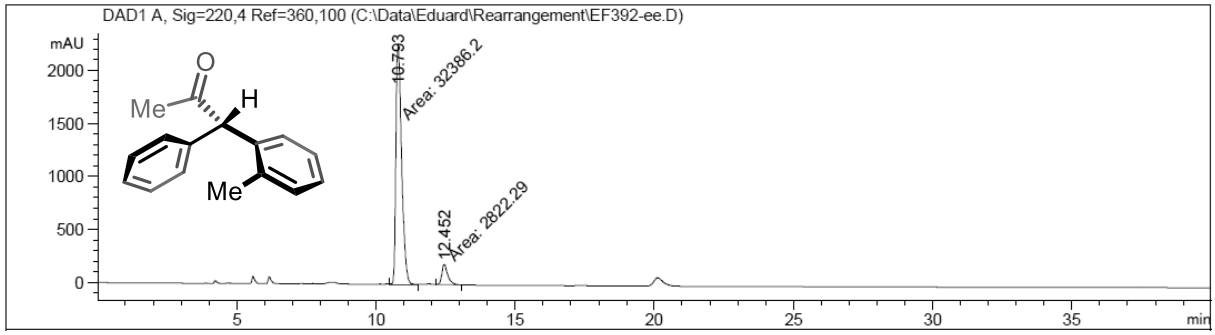

Signal 1: DAD1 A, Sig=220,4 Ref=360,100

Peak #	RetTime [min]	Type	Width [min]	Area [mAU*s]	Height [mAU]	Area %
1	10.793	MM	0.2399	3.23862e4	2249.72241	91.9841
2	12.452	MM	0.2454	2822.28931	191.65350	8.0159

^{1}H NMR (400 MHz, $CDCl_3$) of ***ent*-2z**

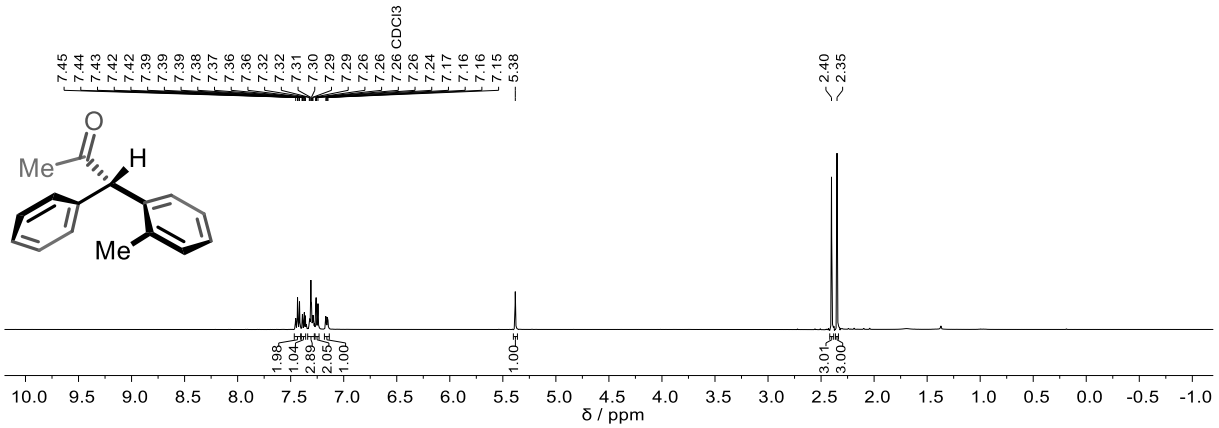

^{13}C{^{1}H} NMR (101 MHz, $CDCl_3$) of ***ent*-2z**

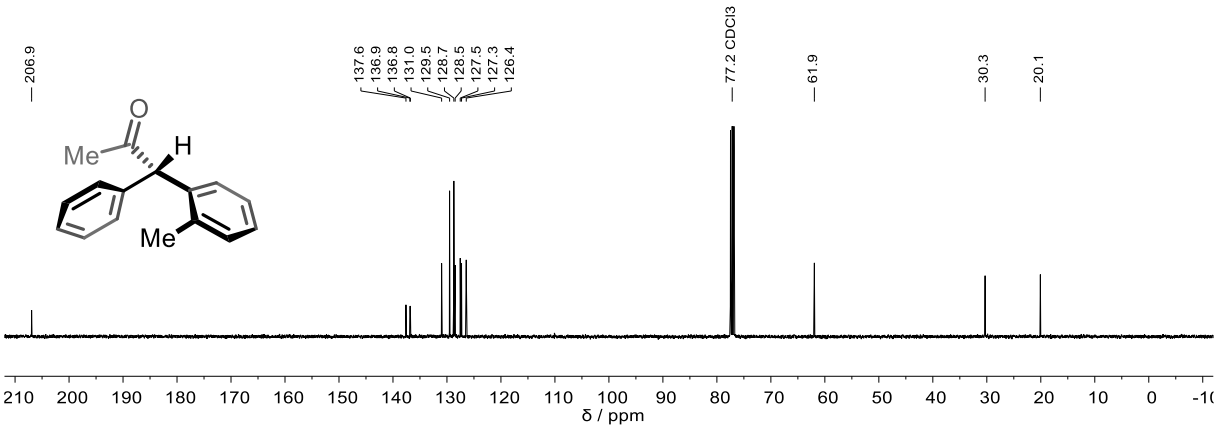

^{1}H NMR (400 MHz, $CDCl_3$) of **2s'**

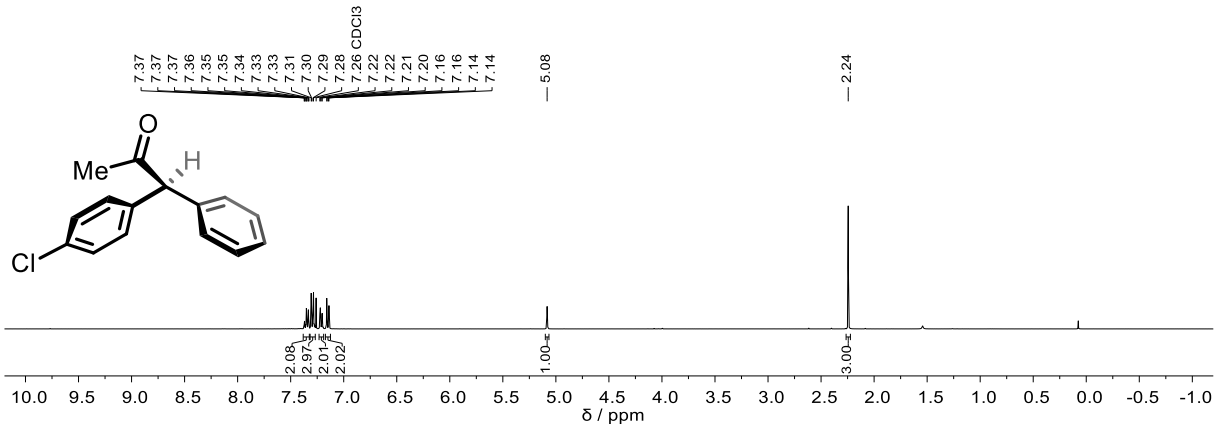

$^{13}C\{^{1}H\}$ NMR (101 MHz, $CDCl_3$) of **2s'**

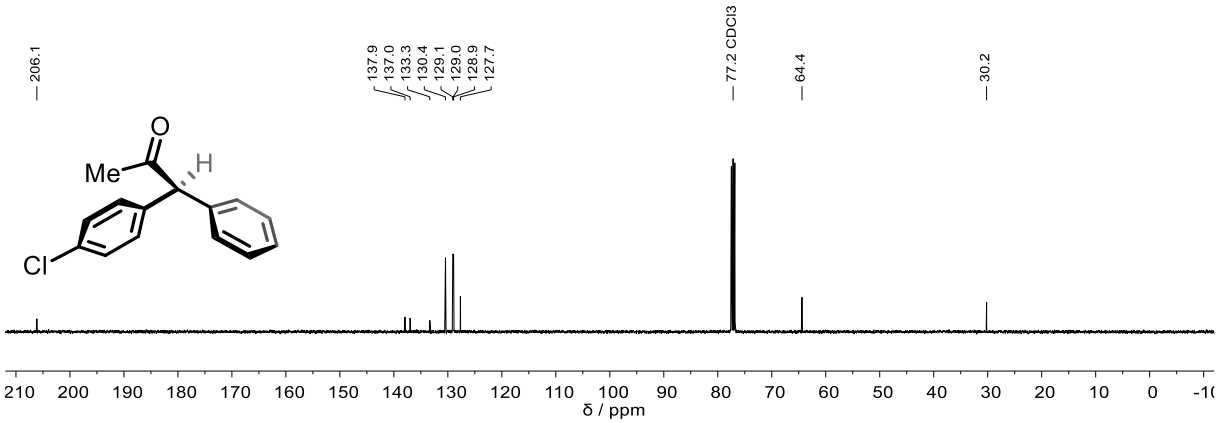

IR (ATR, neat) of **2s'**

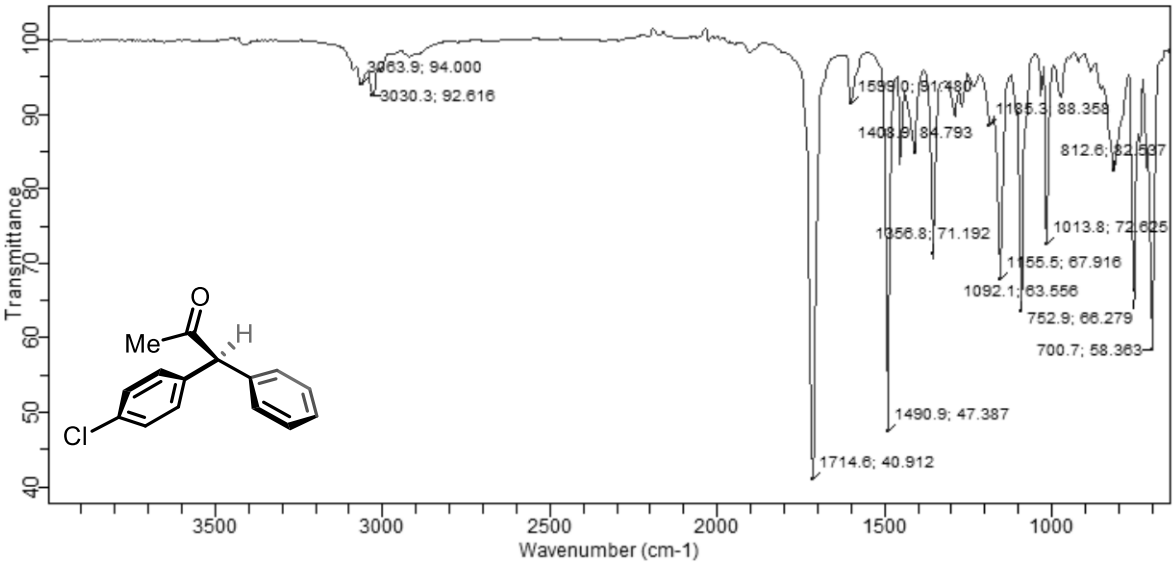

HPLC (ID-3, *n*-hexane:*i*-PrOH 98:2, flow rate 0.8 mL/min, 220 nm, 25 °C) of *rac*-**2s'**

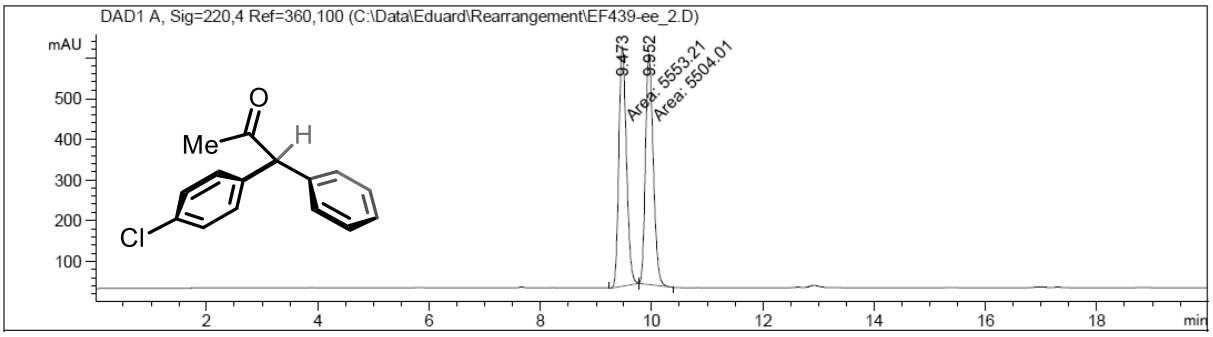

Signal 1: DAD1 A, Sig=220,4 Ref=360,100

Peak #	RetTime [min]	Type	Width [min]	Area [mAU*s]	Height [mAU]	Area %
1	9.473	MM	0.1576	5553.21094	587.12848	50.2225
2	9.952	MM	0.1622	5504.01318	565.57697	49.7775

HPLC (ID-3, *n*-hexane:*i*-PrOH 98:2, flow rate 0.8 mL/min, 220 nm, 25 °C) of **2s'**

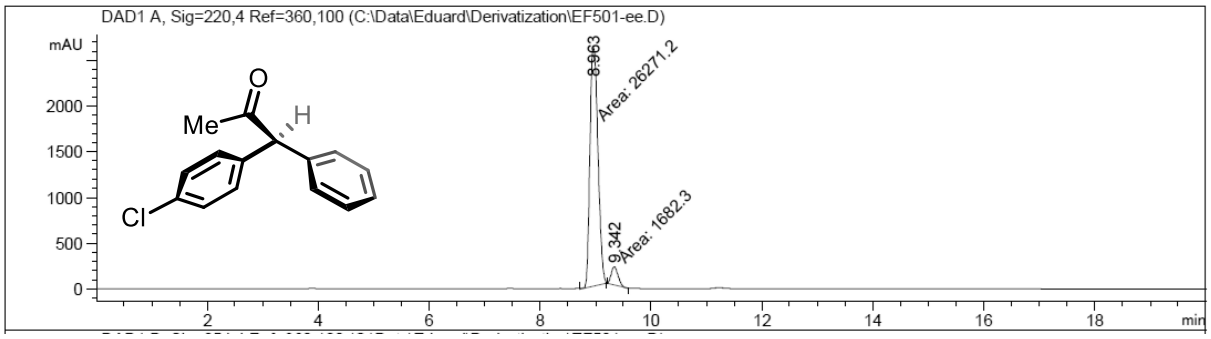


```
Signal 1: DAD1 A, Sig=220,4 Ref=360,100

Peak RetTime Type  Width     Area      Height     Area
  #   [min]        [min]   [mAU*s]     [mAU]       %
----|-------|----|-------|----------|----------|--------|
   1   8.963 MM    0.1672 2.62712e4  2618.66748  93.9818
   2   9.342 MM    0.1426 1682.30493  196.60786   6.0182
```

^{1}H NMR (400 MHz, $CDCl_3$) of **1q'-*d*$_5$** (*E*:*Z* = 53:47)

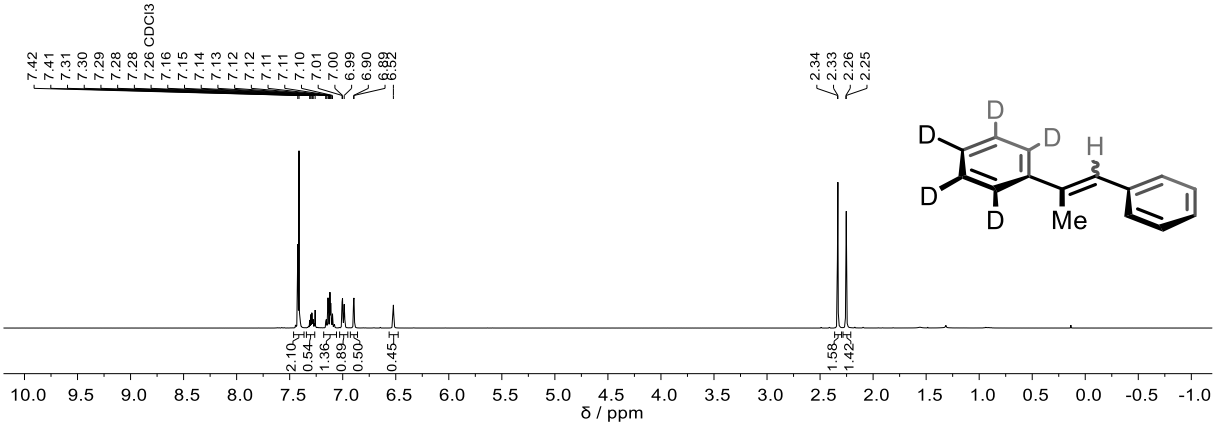

^{13}C{^{1}H} NMR (101 MHz, $CDCl_3$) of **1q'-*d*$_5$** (*E*:*Z* = 53:47)

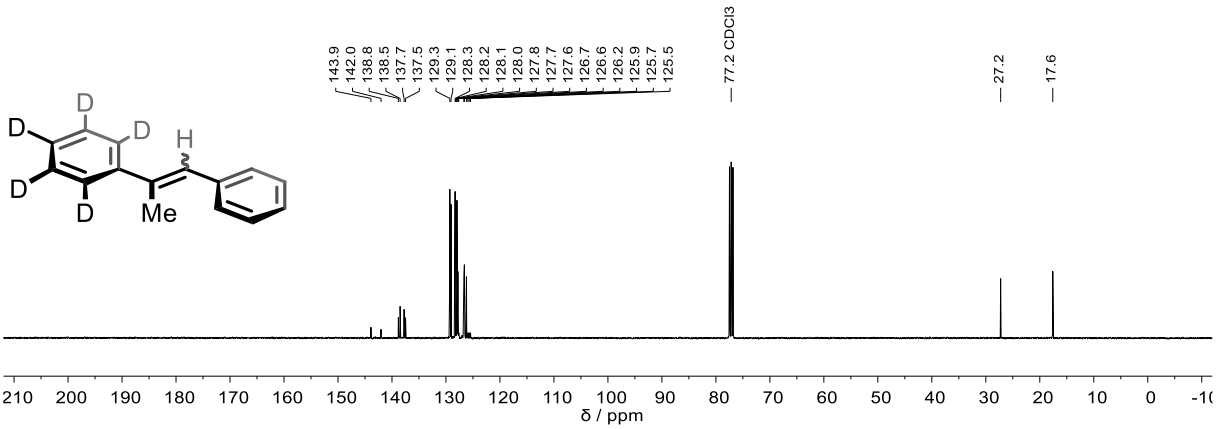

^{2}H NMR (61 MHz, $CHCl_3$) of **1q'-*d*$_5$** (*E*:*Z* = 53:47)

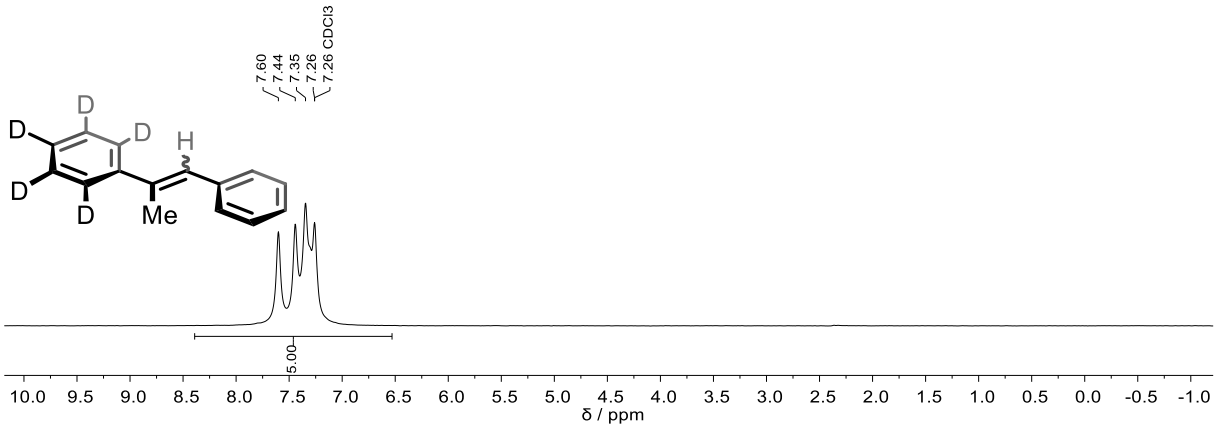

IR (ATR, neat) of **1q'-*d*$_5$**

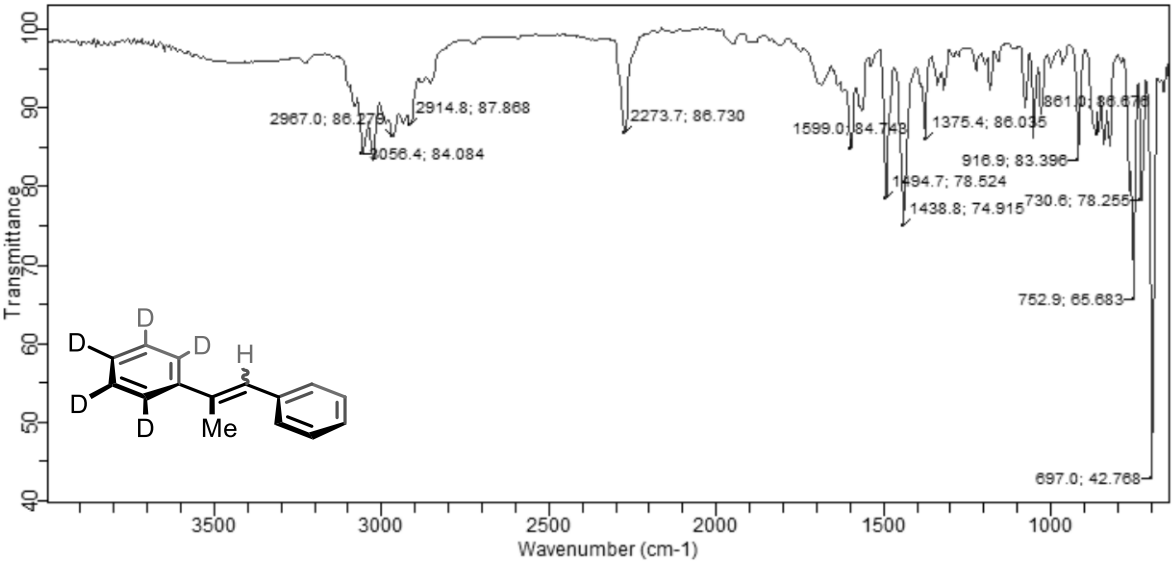

^{1}H NMR (400 MHz, $CDCl_3$) of **2q'-*d*$_5$**

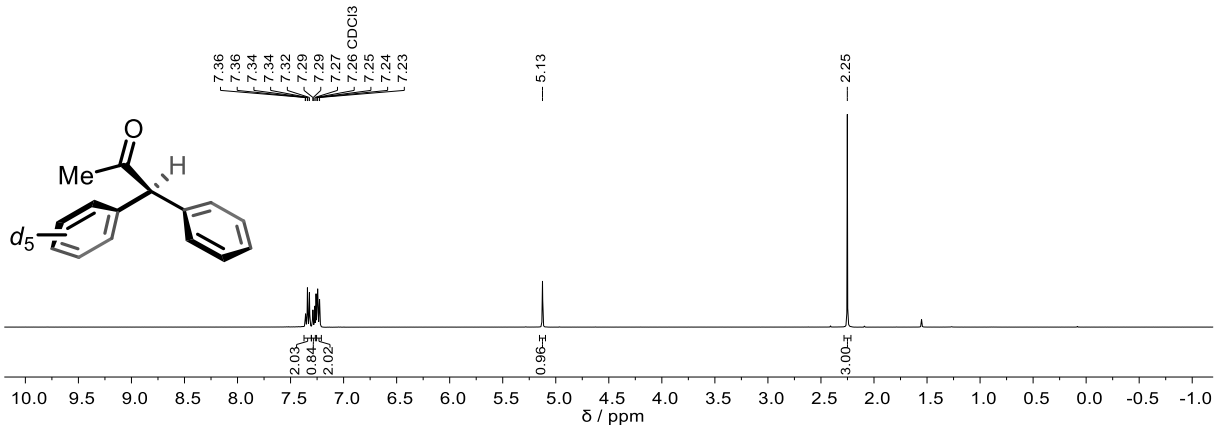

$^{13}C\{^{1}H\}$ NMR (101 MHz, $CDCl_3$) of **2q'-*d*$_5$**

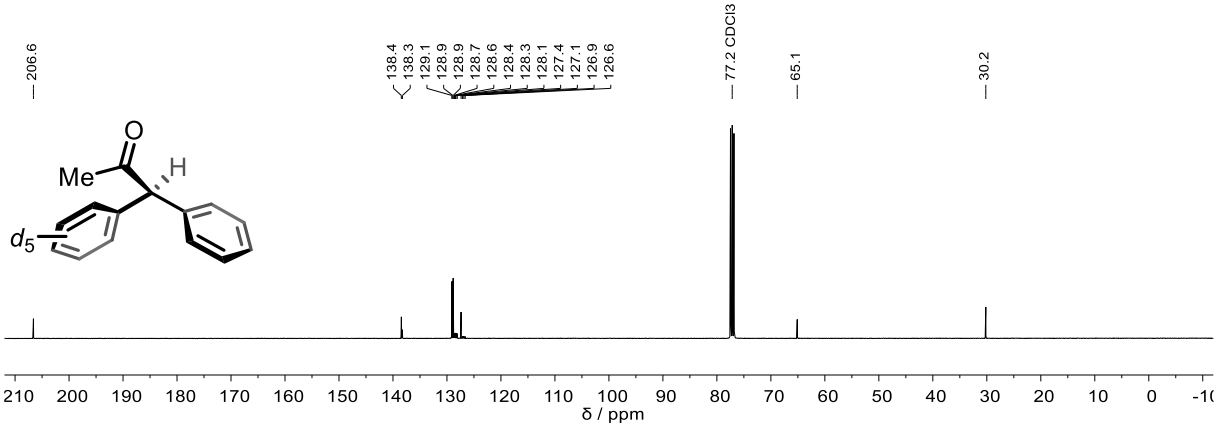

^{2}H NMR (61 MHz, $CHCl_3$) of **2q'-*d*$_5$**

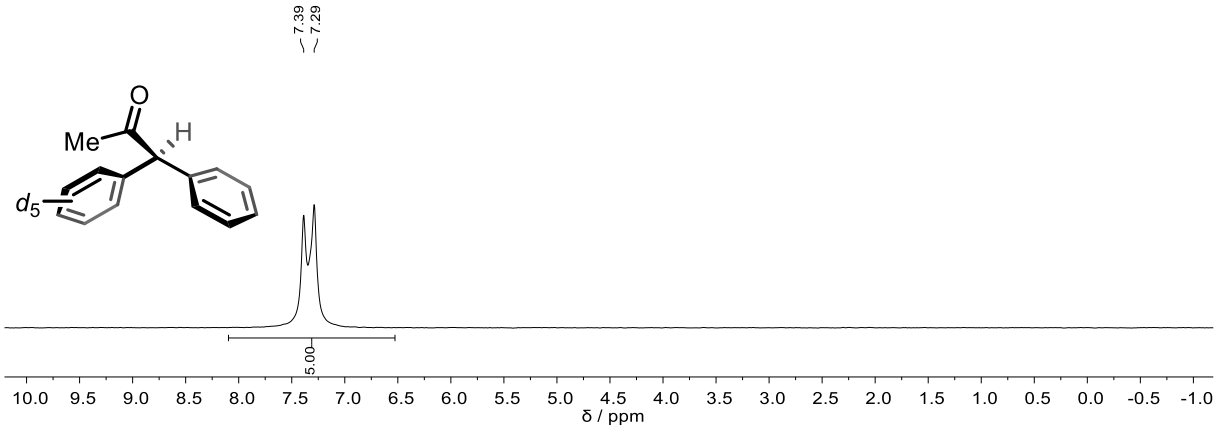

IR (ATR, neat) of **2q'-*d*$_5$**

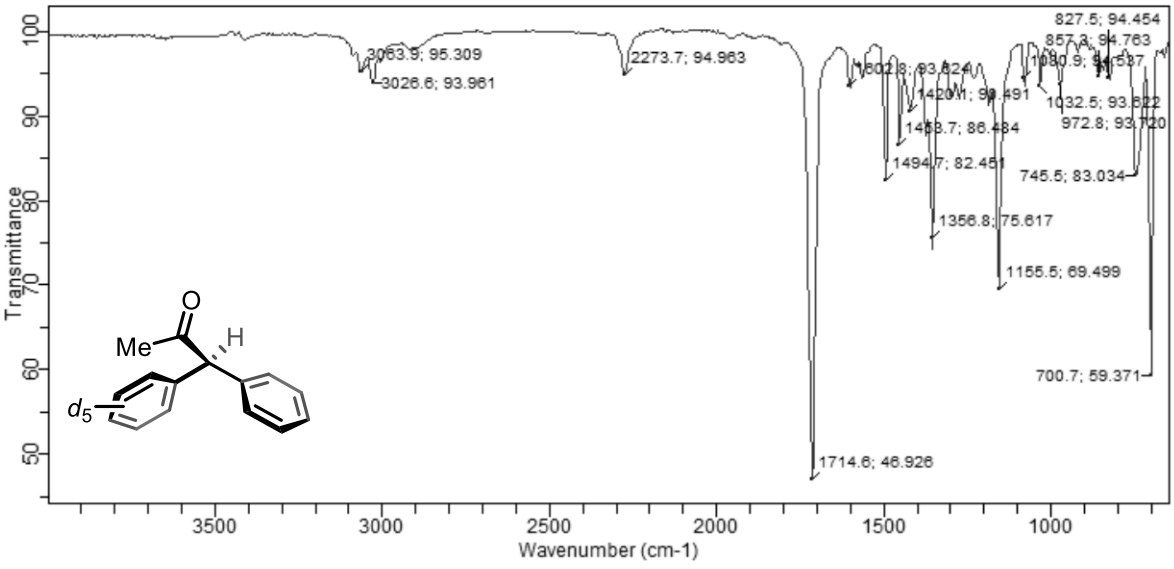

^{1}H NMR (400 MHz, $CDCl_3$) of **5q'-*d*$_5$**

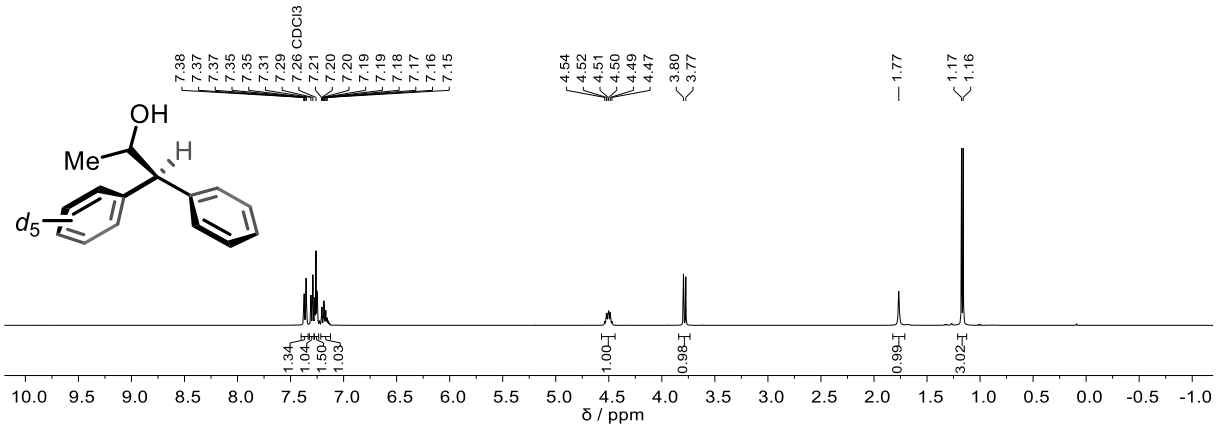

^{13}C{^{1}H} NMR (151 MHz, $CDCl_3$, t_1 = 180 s) of **5q'-*d*$_5$**

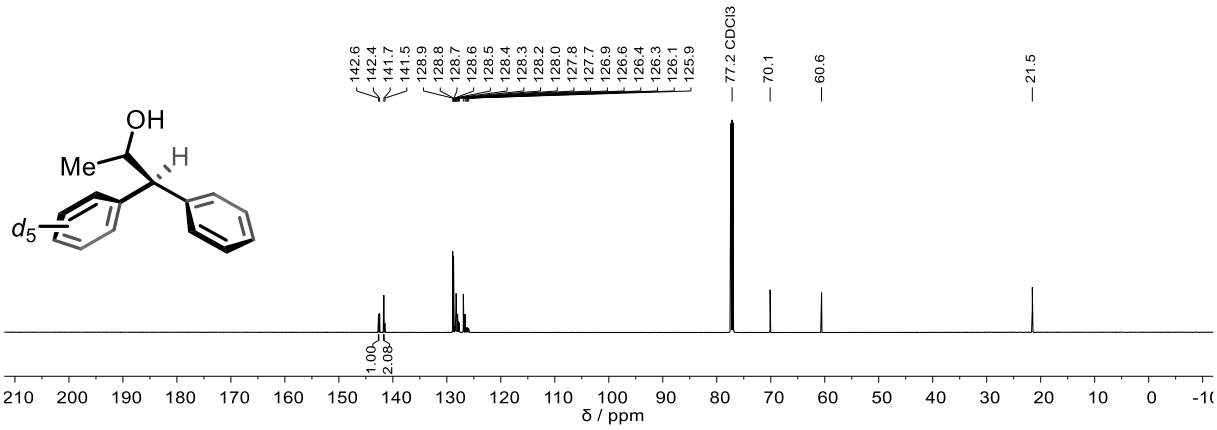

^{2}H NMR (61 MHz, $CHCl_3$) of **5q'-*d*$_5$**

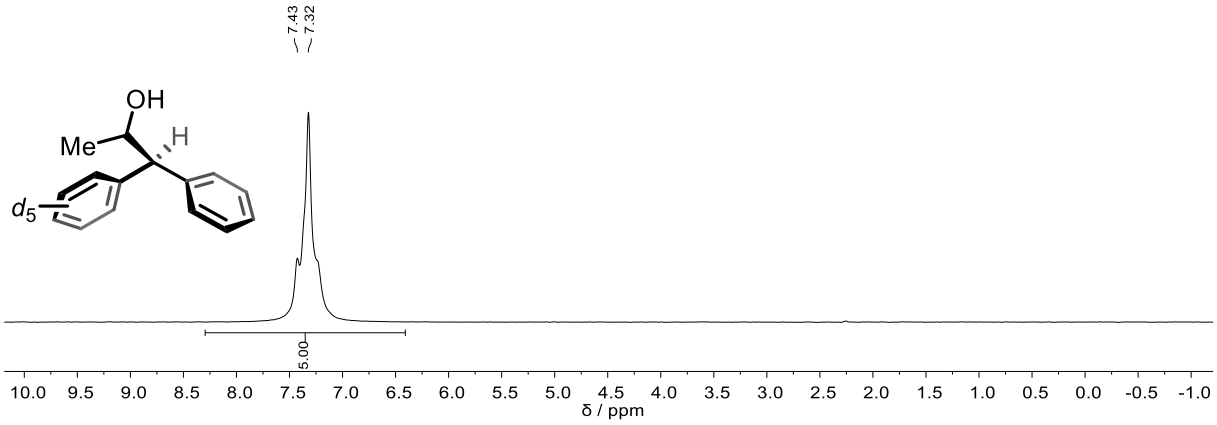

IR (ATR, neat) of **5q'-*d*$_5$**

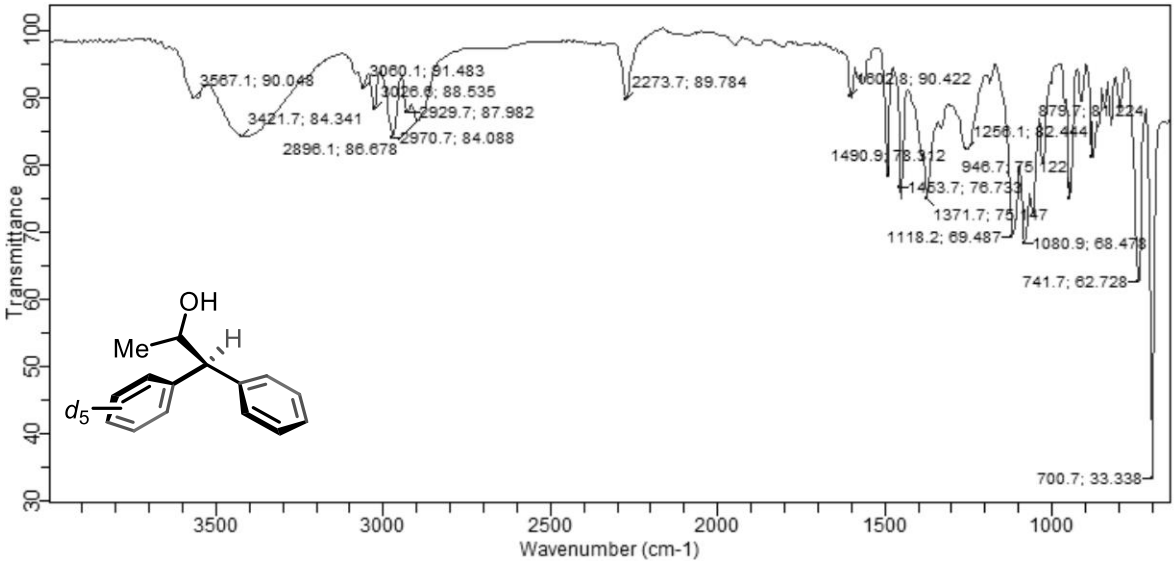

HPLC (OD-3, *n*-hexane:*i*-PrOH 98:2, flow rate 0.5 mL/min, 220 nm, 25 °C) of *rac*-**5q'-*d*$_5$**

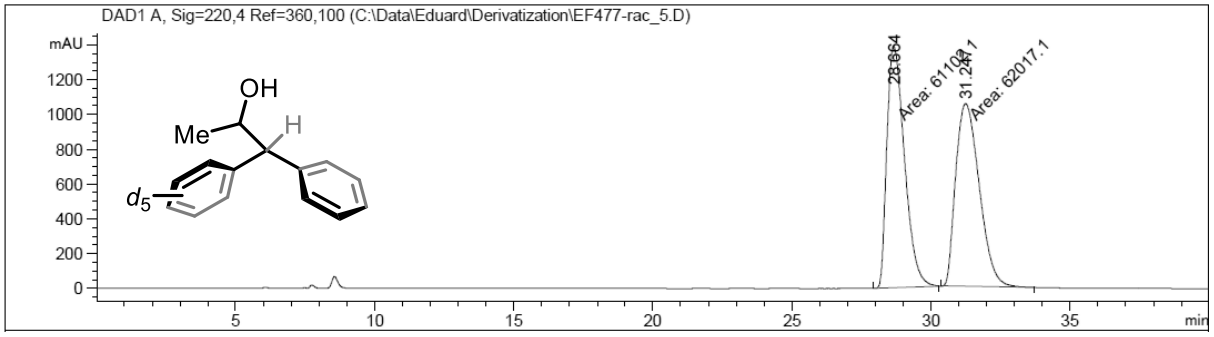

Signal 1: DAD1 A, Sig=220,4 Ref=360,100

Peak #	RetTime [min]	Type	Width [min]	Area [mAU*s]	Height [mAU]	Area %
1	28.664	MM	0.7336	6.11021e4	1388.11450	49.6284
2	31.247	MM	0.9834	6.20171e4	1051.11072	50.3716

HPLC (OD-3, *n*-hexane:*i*-PrOH 98:2, flow rate 0.5 mL/min, 220 nm, 25 °C) of **5q'-*d*$_5$**

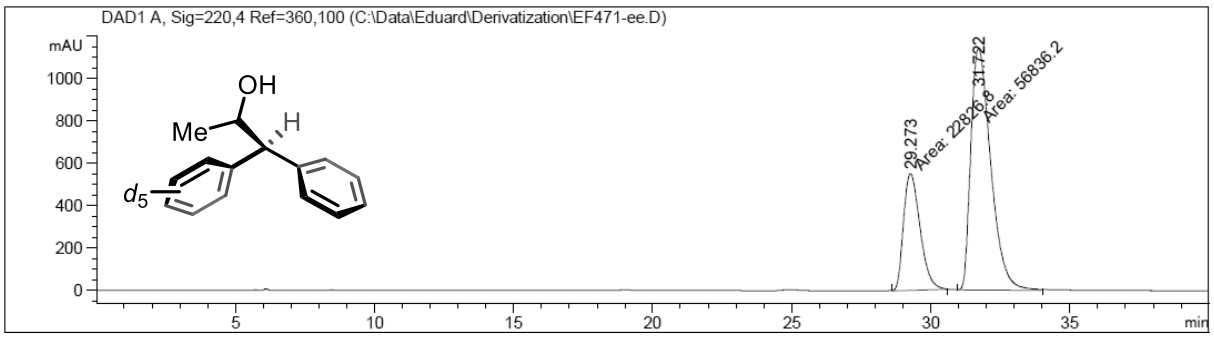

Signal 1: DAD1 A, Sig=220,4 Ref=360,100

Peak #	RetTime [min]	Type	Width [min]	Area [mAU*s]	Height [mAU]	Area %
1	29.273	MM	0.6907	2.28268e4	550.83533	28.6542
2	31.722	MM	0.8299	5.68362e4	1141.38367	71.3458

HPLC (OD-3, *n*-hexane:*i*-PrOH 98:2, flow rate 0.5 mL/min, 220 nm, 25 °C) of **5q'** (control)

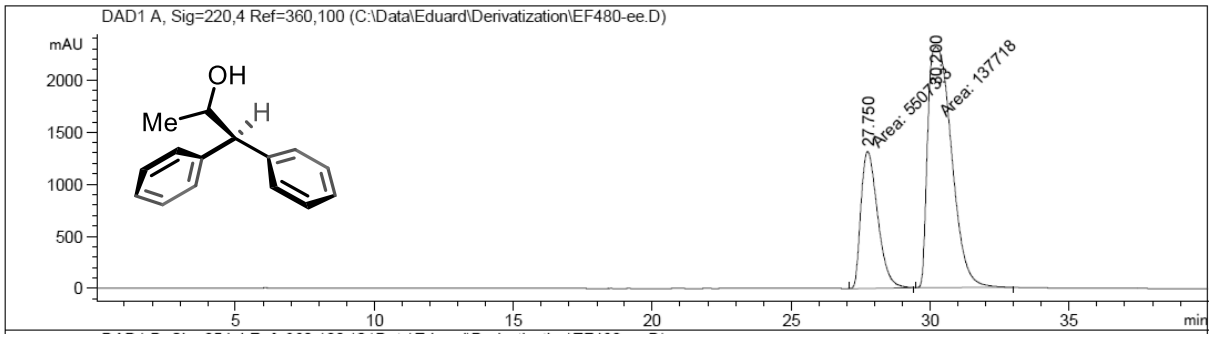

Signal 1: DAD1 A, Sig=220,4 Ref=360,100

Peak #	RetTime [min]	Type	Width [min]	Area [mAU*s]	Height [mAU]	Area %
1	27.750	MM	0.6993	5.50733e4	1312.56213	28.5663
2	30.200	MM	0.9943	1.37718e5	2308.40942	71.4337

^{1}H NMR (400 MHz, $CDCl_3$) of **10r**

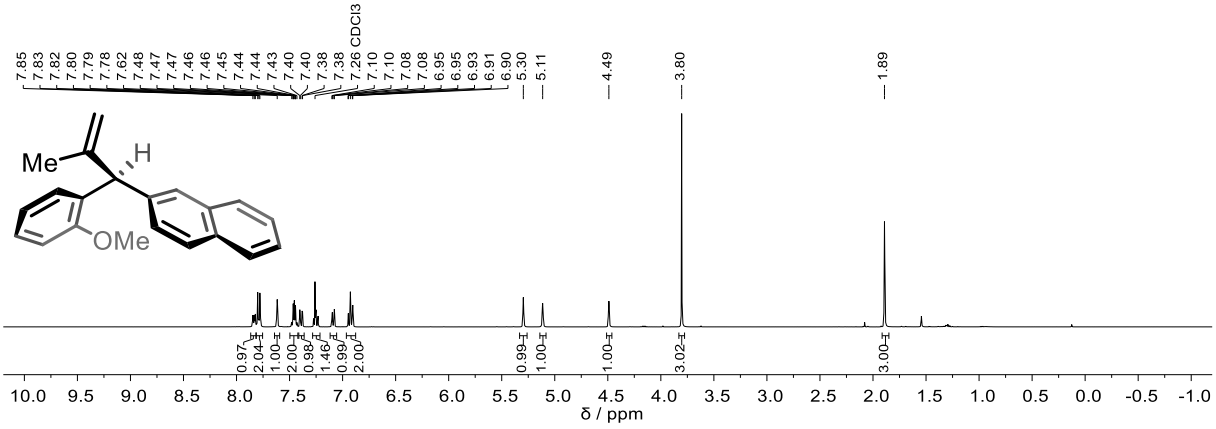

^{13}C{^{1}H} NMR (101 MHz, $CDCl_3$) of **10r**

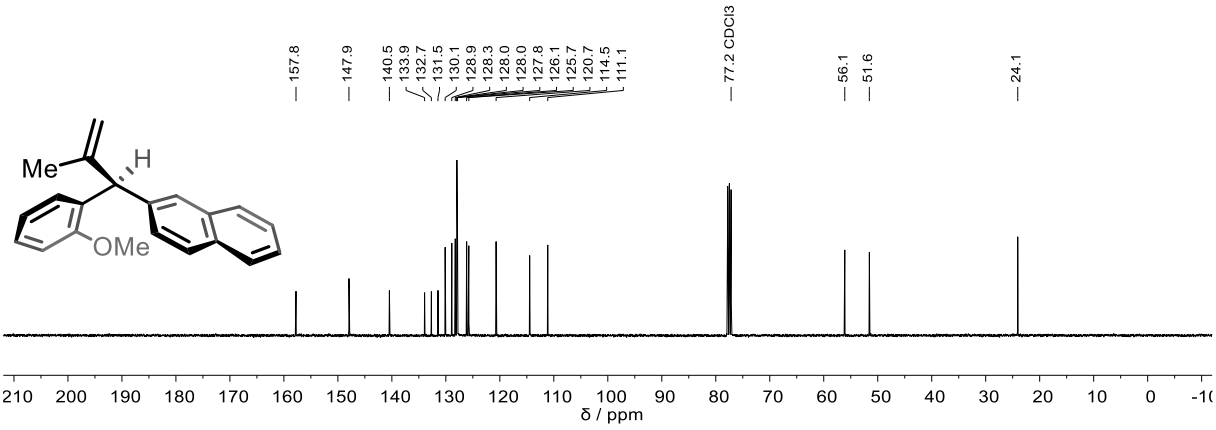

IR (ATR, neat) of **10r**

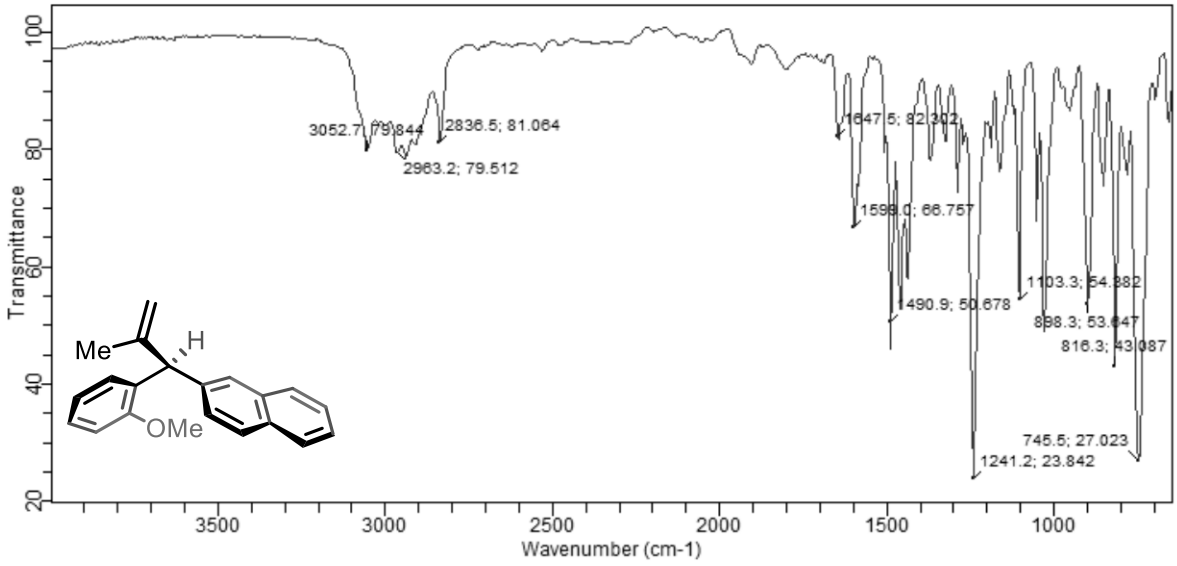

HPLC (IA-3, *n*-hexane:*i*-PrOH 99:1, flow rate 0.6 mL/min, 254 nm, 25 °C) of *rac*-**10r**

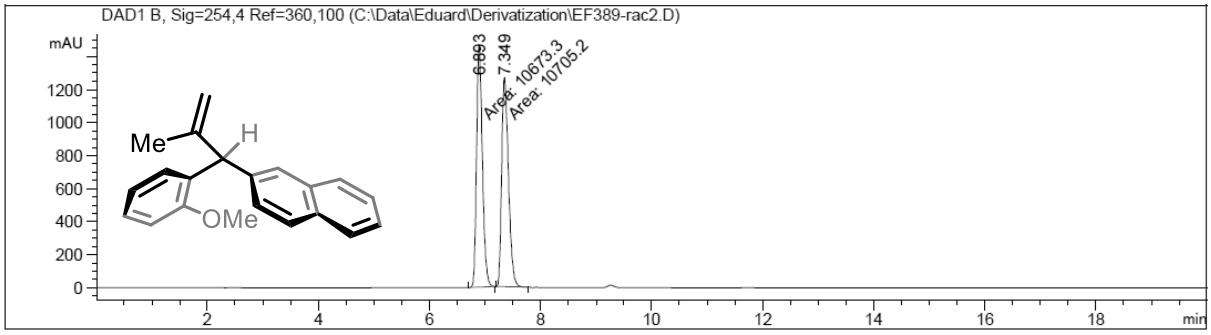


```
Signal 2: DAD1 B, Sig=254,4 Ref=360,100

Peak RetTime Type  Width     Area      Height     Area
  #   [min]        [min]   [mAU*s]     [mAU]       %
----|-------|----|-------|----------|----------|--------|
   1   6.893 MM    0.1217 1.06733e4  1461.47119  49.9253
   2   7.349 MM    0.1409 1.07052e4  1266.44666  50.0747
```

HPLC (IA-3, *n*-hexane:*i*-PrOH 99:1, flow rate 0.6 mL/min, 254 nm, 25 °C) of **10r**

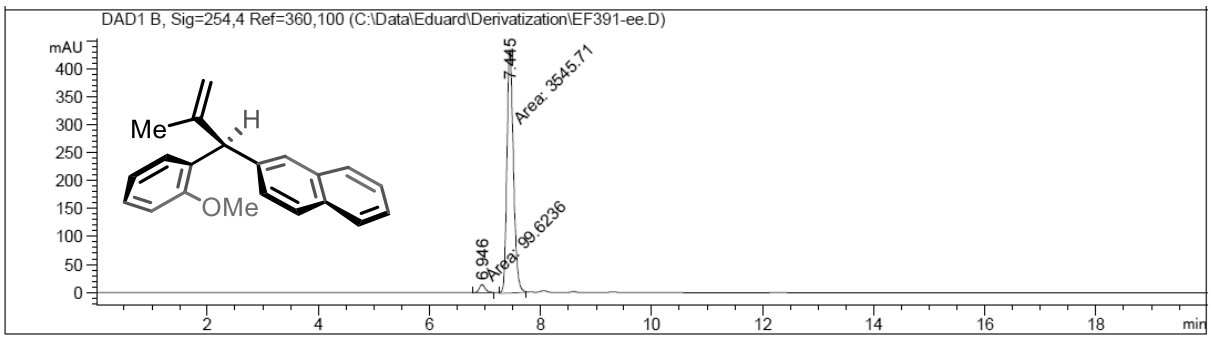


```
Signal 2: DAD1 B, Sig=254,4 Ref=360,100

Peak RetTime Type  Width     Area      Height     Area
  #   [min]        [min]   [mAU*s]     [mAU]       %
----|-------|----|-------|----------|----------|--------|
   1   6.946 MM    0.1193   99.62360   13.91543   2.7329
   2   7.445 MM    0.1363 3545.71143  433.48816  97.2671
```

^{1}H NMR (400 MHz, $CDCl_3$) of **12s'**

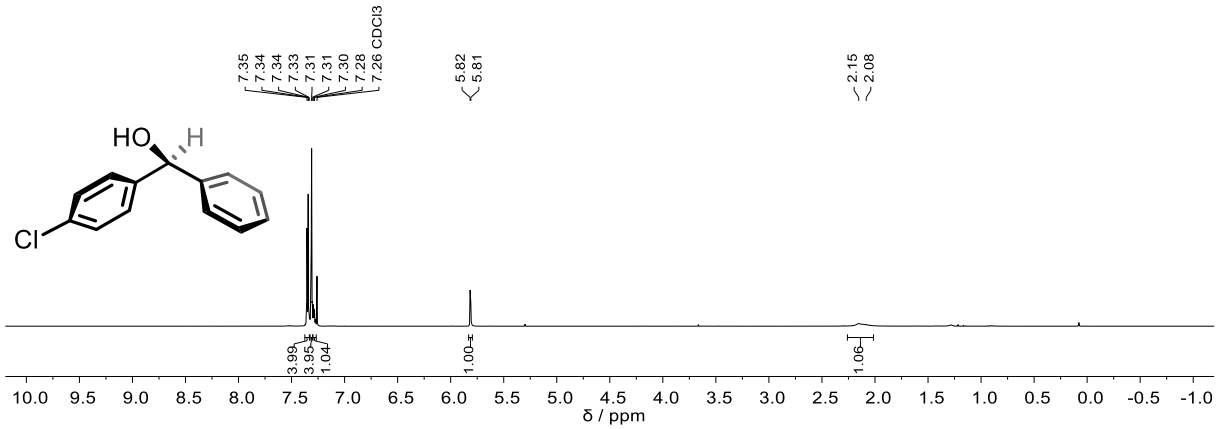

^{13}C{^{1}H} NMR (101 MHz, $CDCl_3$) of **12s'**

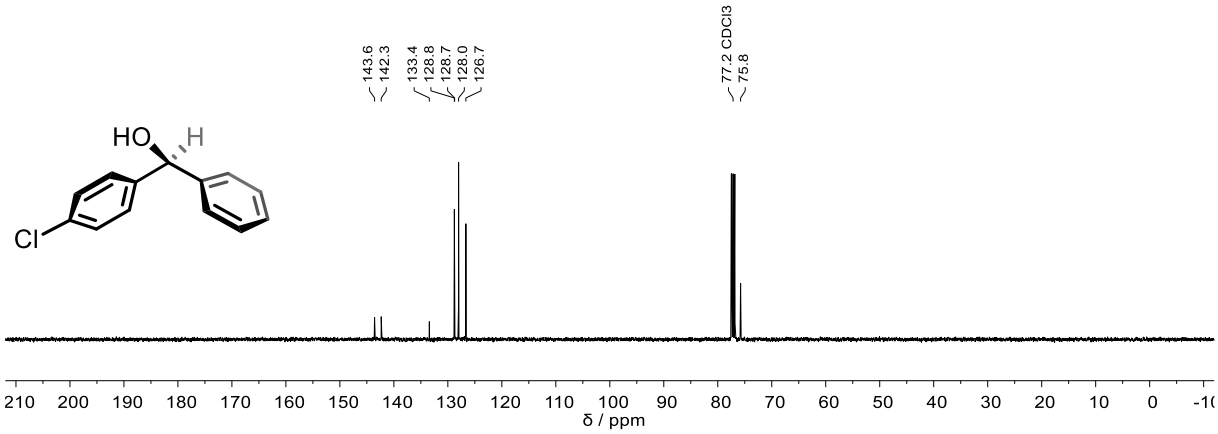

IR (ATR, neat) of **12s'**

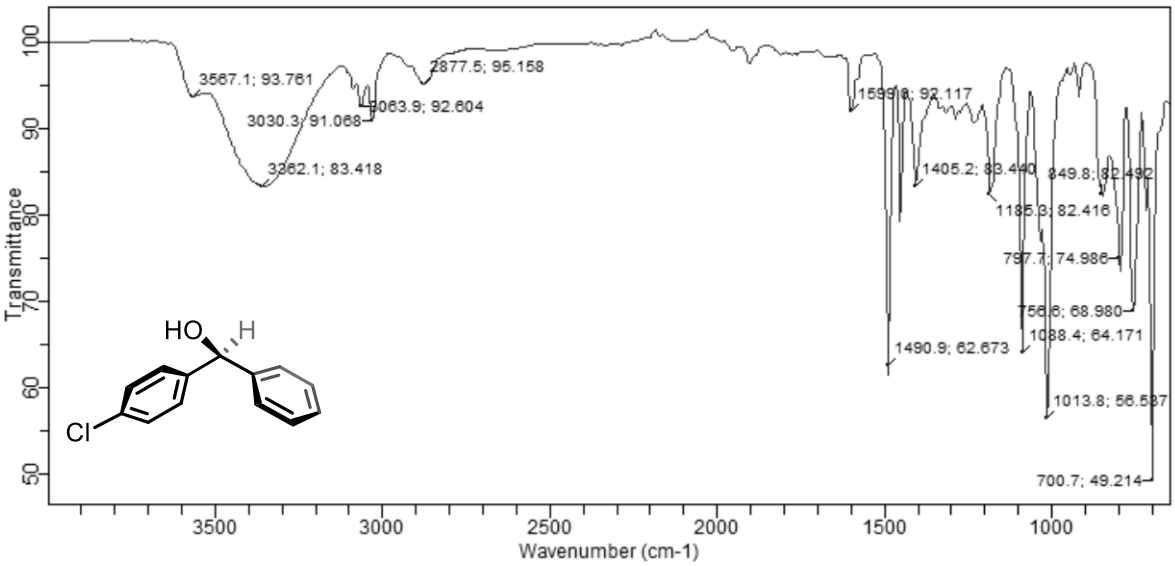

HPLC (IA-3, *n*-hexane:*i*-PrOH 98:2, flow rate 0.8 mL/min, 220 nm, 25 °C) of *rac*-**12s'**

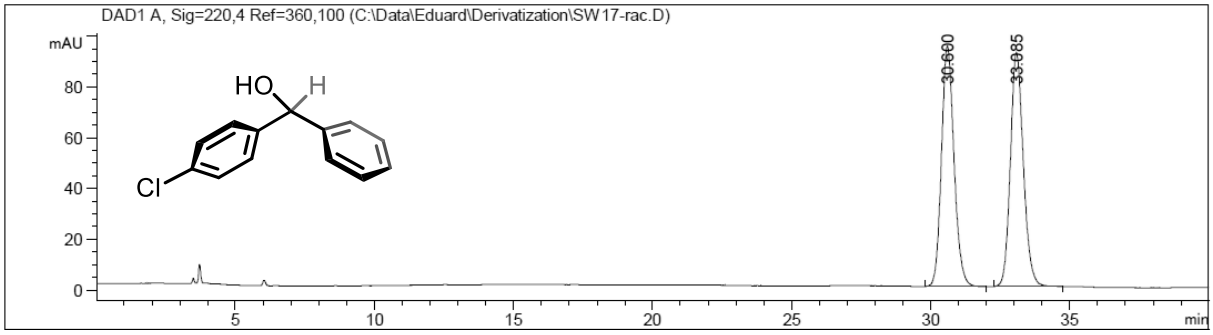

Signal 1: DAD1 A, Sig=220,4 Ref=360,100

Peak #	RetTime [min]	Type	Width [min]	Area [mAU*s]	Height [mAU]	Area %
1	30.600	BB	0.4796	2968.19824	94.72411	49.8857
2	33.085	BB	0.4936	2981.80029	92.13029	50.1143

HPLC (IA-3, *n*-hexane:*i*-PrOH 98:2, flow rate 0.8 mL/min, 220 nm, 25 °C) of **12s'**

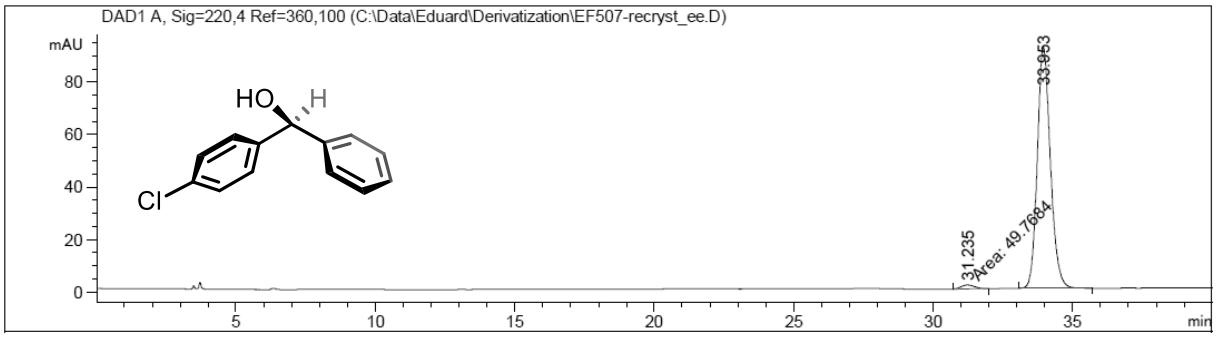

Signal 1: DAD1 A, Sig=220,4 Ref=360,100

Peak #	RetTime [min]	Type	Width [min]	Area [mAU*s]	Height [mAU]	Area %
1	31.235	MM	0.5389	49.76836	1.53915	1.6302
2	33.953	BB	0.4988	3003.09180	92.00826	98.3698

^{1}H NMR (400 MHz, $CDCl_3$) of **12q'-*d*$_5$**

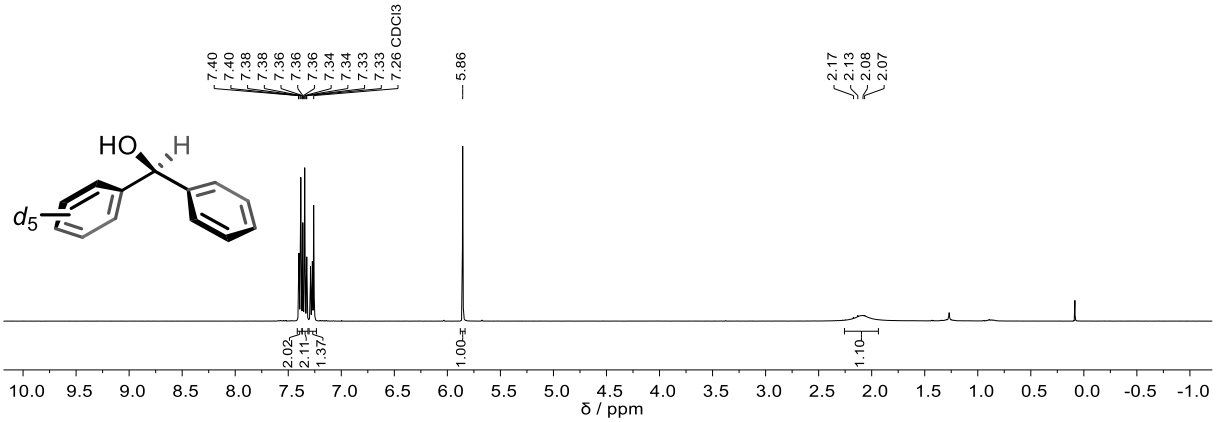

$^{13}C\{^{1}H\}$ NMR (126 MHz, $CDCl_3$) of **12q'-*d*$_5$**

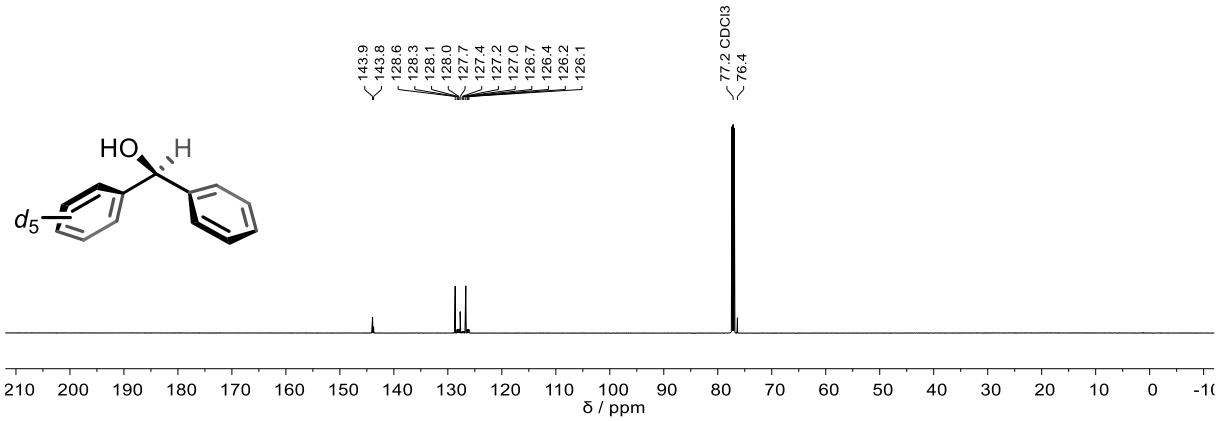

^{2}H NMR (92 MHz, $CHCl_3$) of **12q'-*d*$_5$**

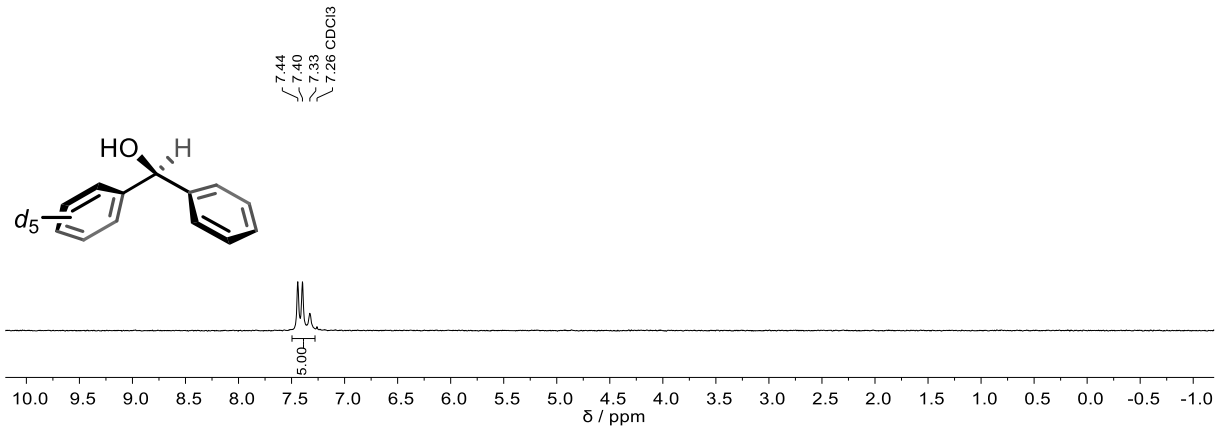

IR (ATR, neat) of **12q'-*d*$_5$**

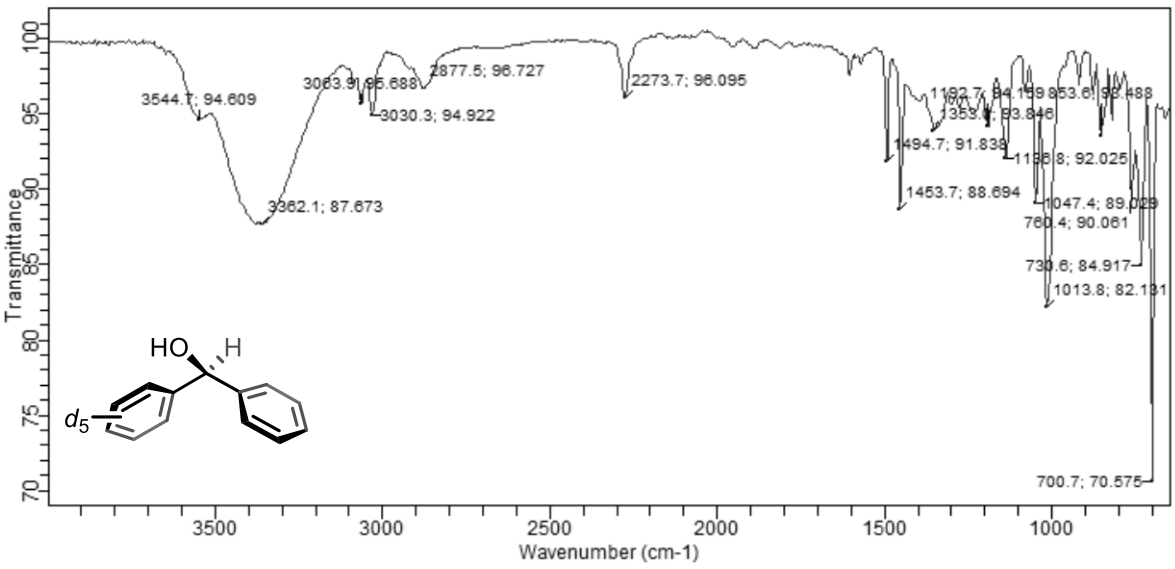

^{1}H NMR (400 MHz, $CDCl_3$) of **17**

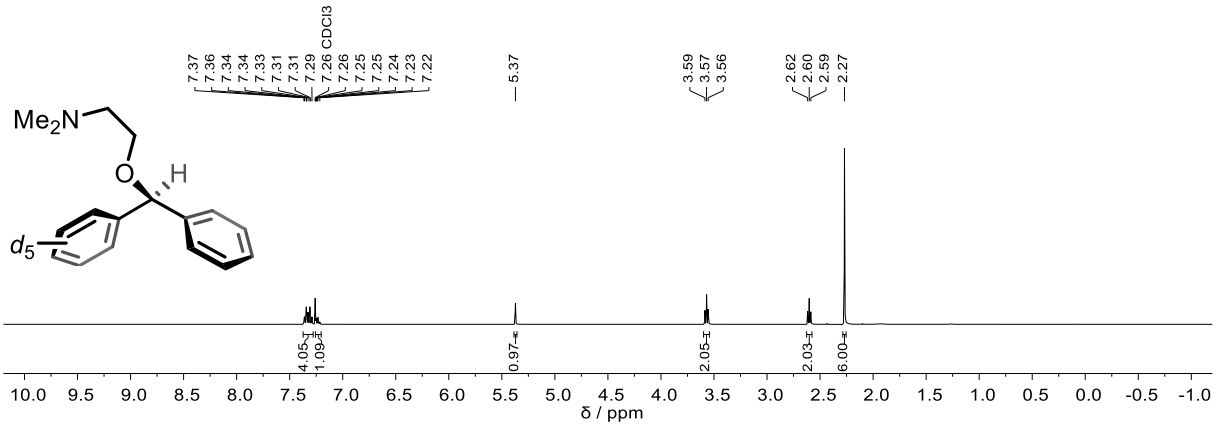

^{13}C{^{1}H} NMR (126 MHz, $CDCl_3$) of **17**

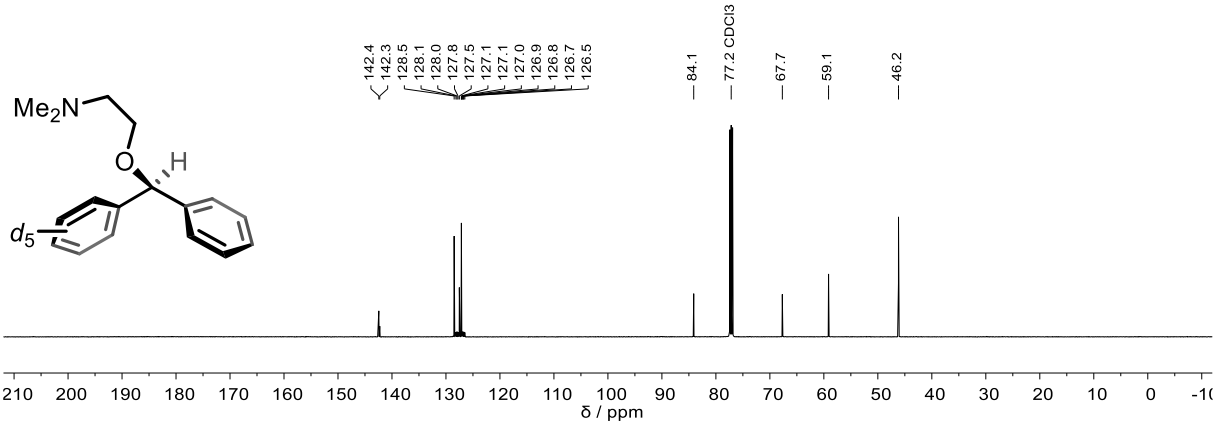

^{2}H NMR (61 MHz, $CHCl_3$) of **17**

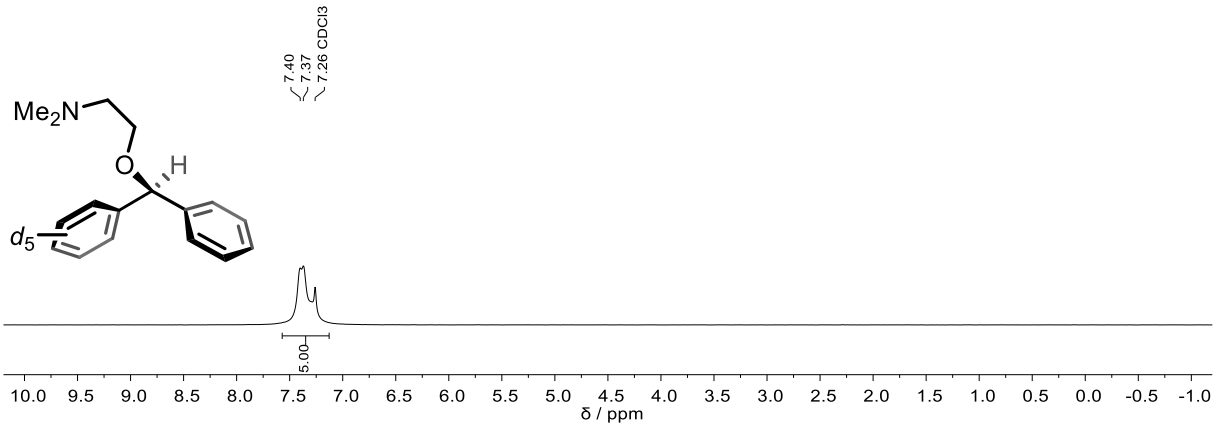

IR (ATR, neat) of **17**

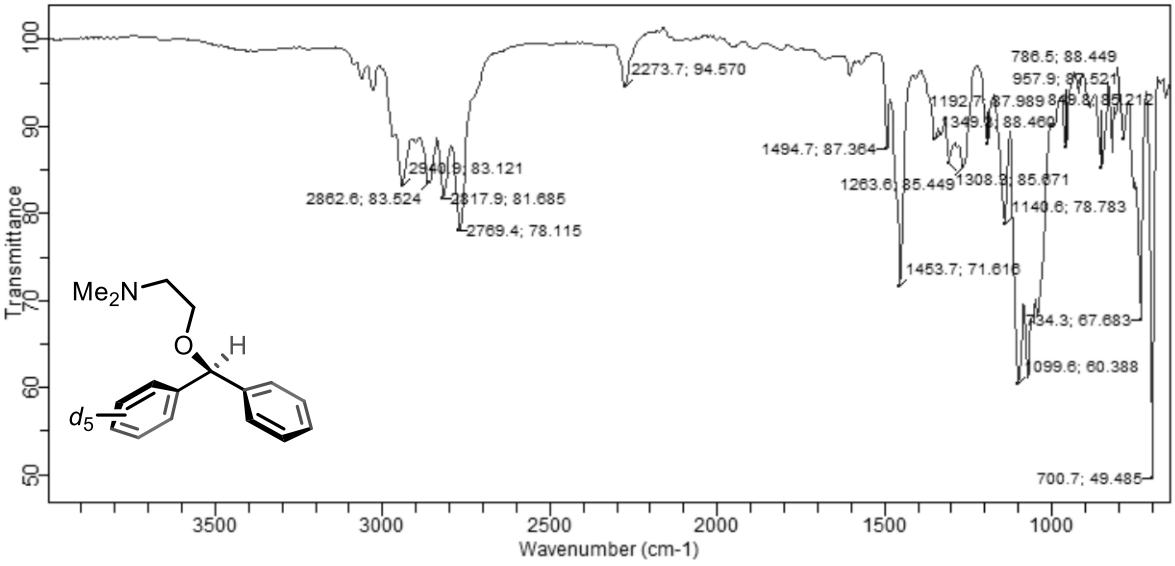

^{1}H NMR (400 MHz, $CDCl_3$) of **20s'**

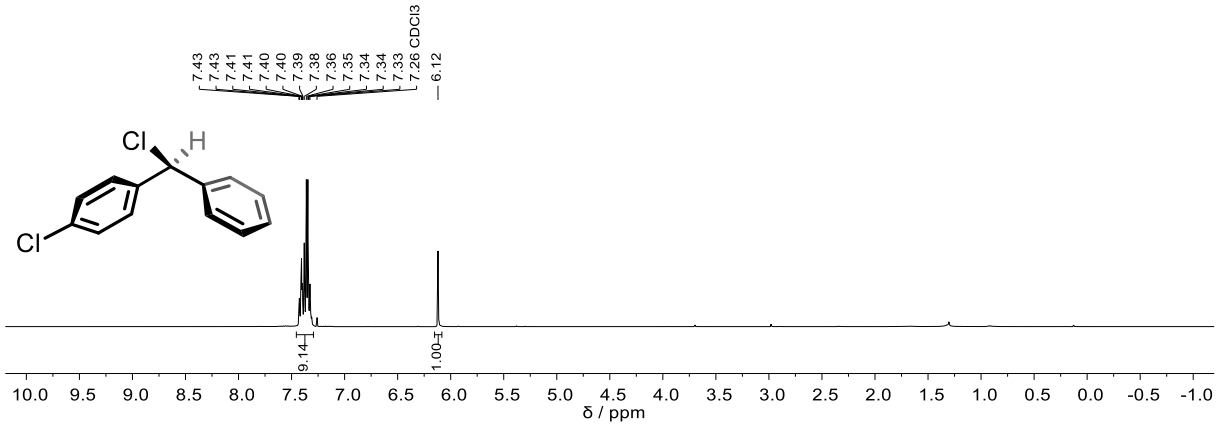

^{13}C{^{1}H} NMR (101 MHz, $CDCl_3$) of **20s'**

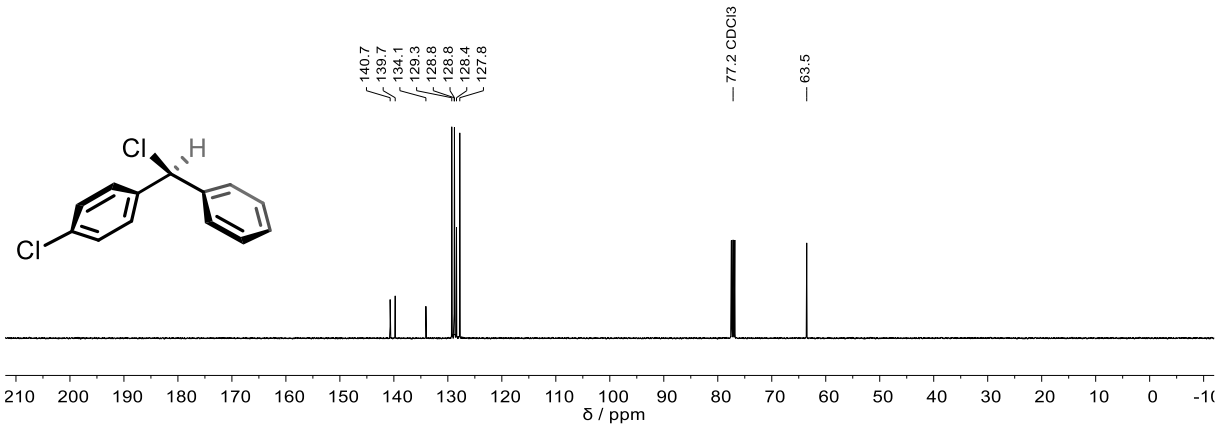

IR (ATR, neat) of **20s'**

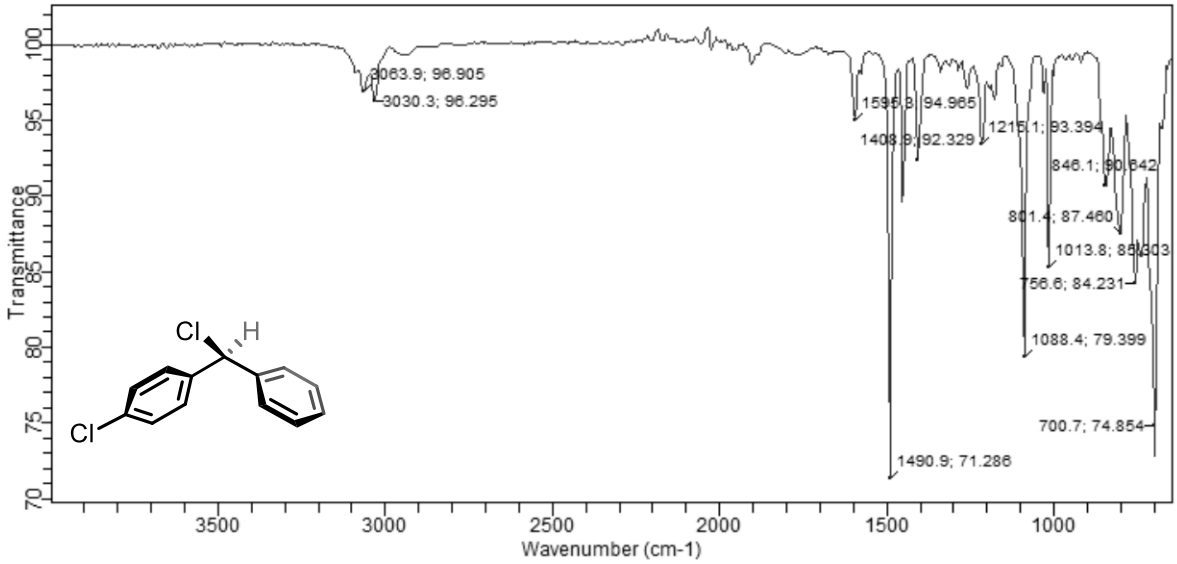

HPLC (OD-3, *n*-hexane:*i*-PrOH 99.9:0.1, flow rate 0.6 mL/min, 220 nm, 25 °C) of *rac*-**20s'**

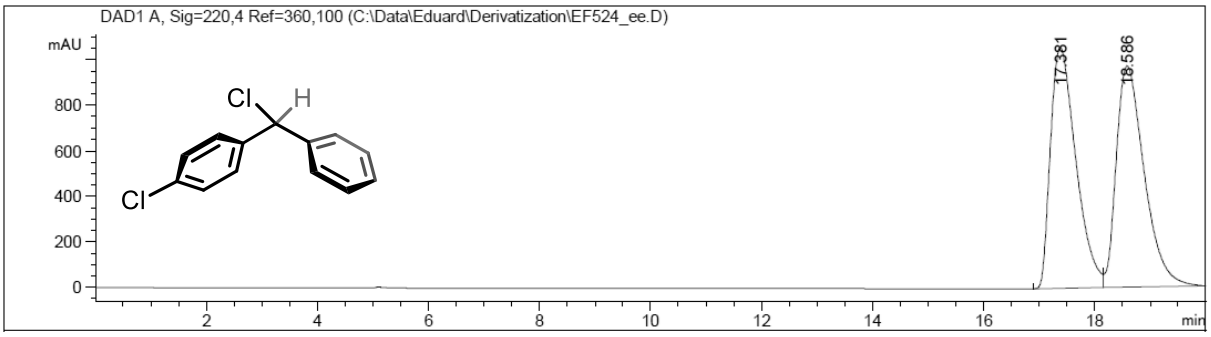


```
Signal 1: DAD1 A, Sig=220,4 Ref=360,100

Peak RetTime Type  Width     Area      Height     Area
  #   [min]        [min]   [mAU*s]     [mAU]       %
----|-------|----|-------|----------|----------|--------|
   1  17.381 BV    0.4946 3.36686e4  1059.83923  49.6918
   2  18.586 VBA   0.5410 3.40862e4   972.40503  50.3082
```

HPLC (OD-3, *n*-hexane:*i*-PrOH 99.9:0.1, flow rate 0.6 mL/min, 220 nm, 25 °C) of **20s'**

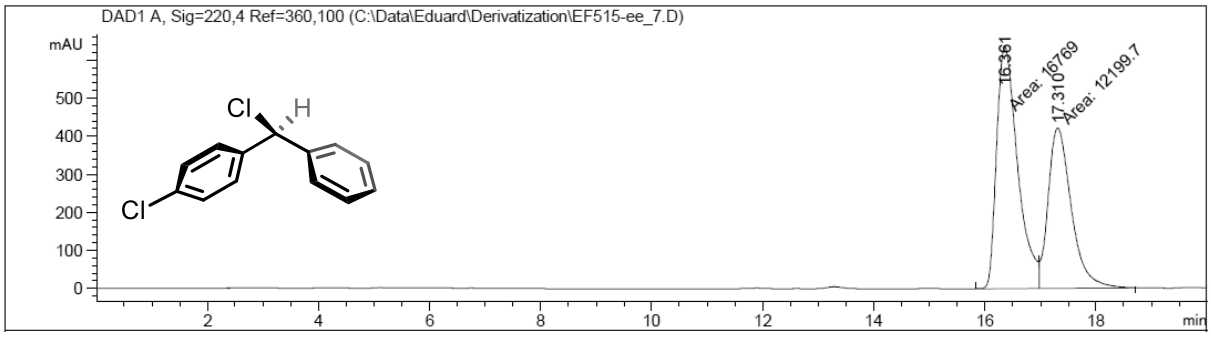


```
Signal 1: DAD1 A, Sig=220,4 Ref=360,100

Peak RetTime Type  Width     Area      Height     Area
  #   [min]        [min]   [mAU*s]     [mAU]       %
----|-------|----|-------|----------|----------|--------|
   1  16.361 MF    0.4401 1.67690e4   634.97919  57.8867
   2  17.310 FM    0.4826 1.21997e4   421.31967  42.1133
```

^{1}H NMR (400 MHz, $CDCl_3$) of **19**

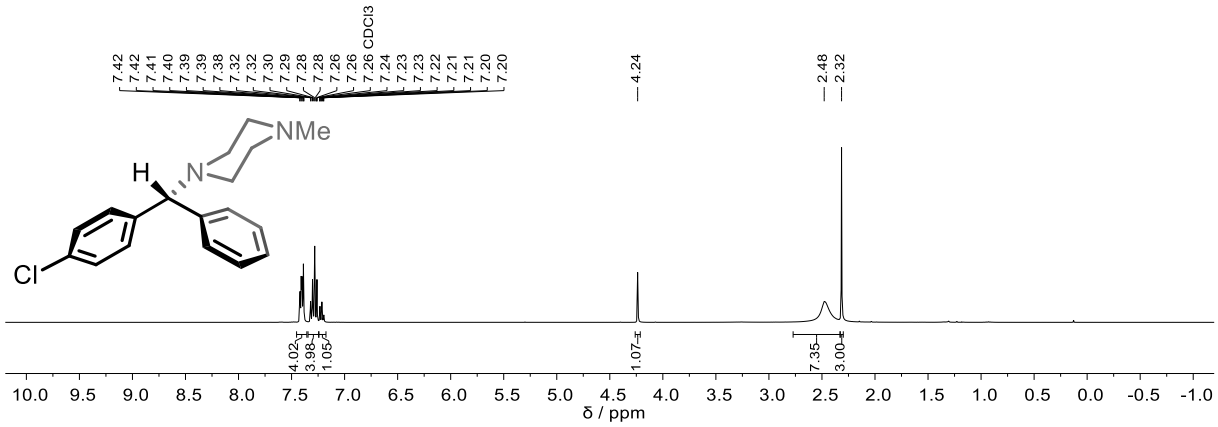

^{13}C{^{1}H} NMR (101 MHz, $CDCl_3$) of **19**

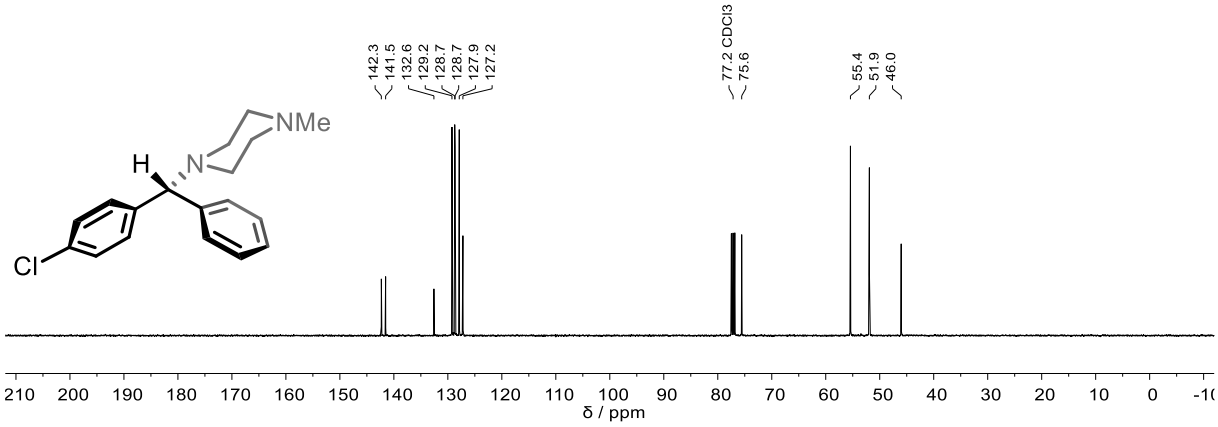

IR (ATR, neat) of **19**

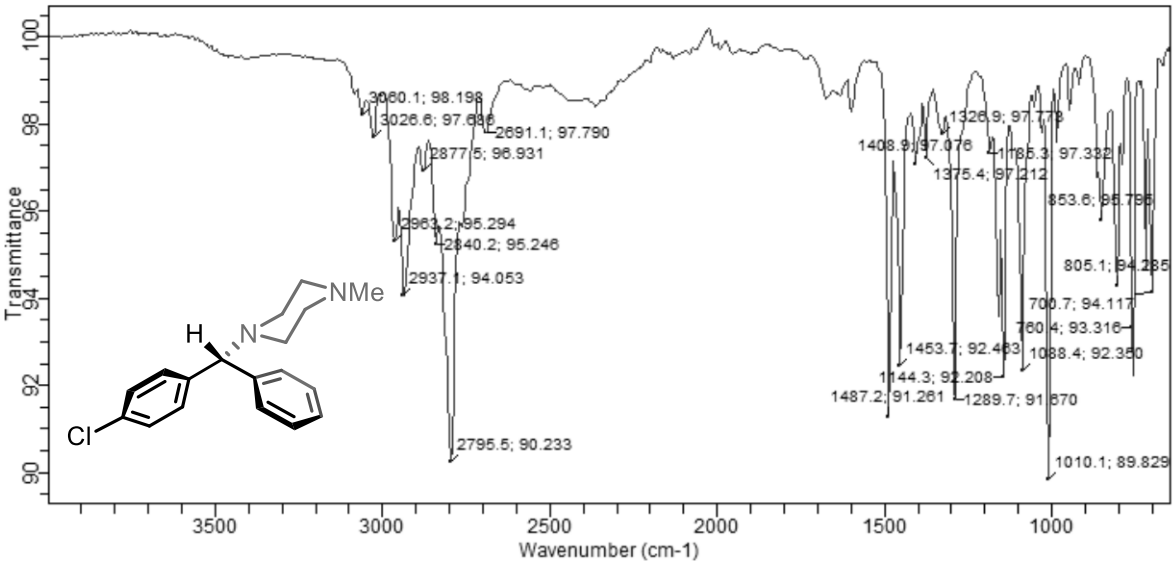

HPLC (OD-3, *n*-hexane:(*i*-PrOH + 1% (*v*/*v*) Et_2NH) 98:2, flow rate 0.8 mL/min, 220 nm, 25 °C) of *rac*-**19**

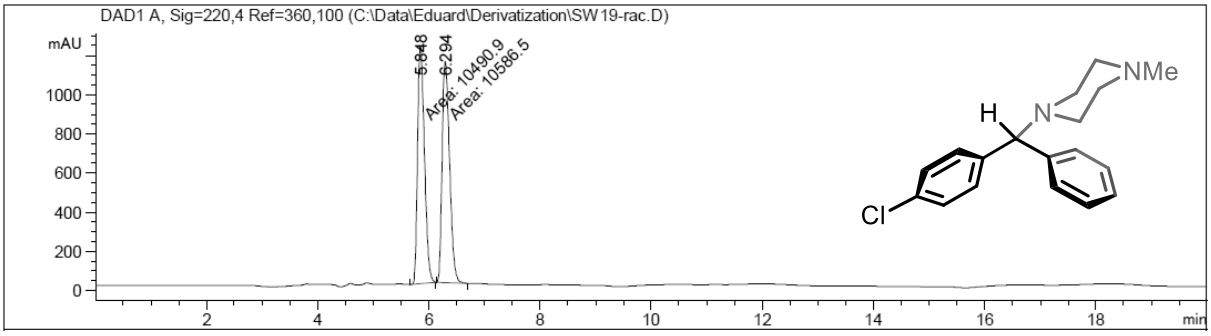


```
Signal 1: DAD1 A, Sig=220,4 Ref=360,100

Peak RetTime Type  Width     Area      Height     Area
  #   [min]        [min]   [mAU*s]     [mAU]       %
----|-------|----|-------|----------|----------|--------|
   1   5.848 MM    0.1441 1.04909e4  1213.60779  49.7732
   2   6.294 MM    0.1562 1.05865e4  1129.91858  50.2268
```

HPLC (OD-3, *n*-hexane:(*i*-PrOH + 1% (*v*/*v*) Et_2NH) 98:2, flow rate 0.8 mL/min, 220 nm, 25 °C) of **19**

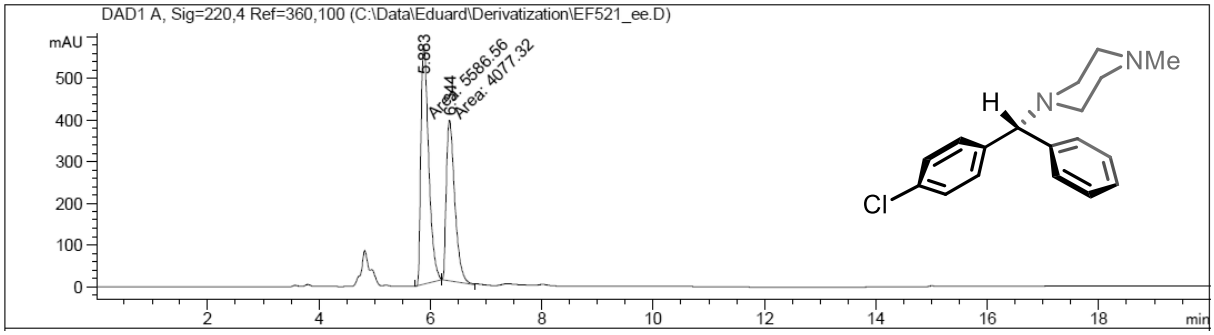


```
Signal 1: DAD1 A, Sig=220,4 Ref=360,100

Peak RetTime Type  Width     Area      Height     Area
  #   [min]        [min]   [mAU*s]     [mAU]       %
----|-------|----|-------|----------|----------|--------|
   1   5.883 MM    0.1619 5586.56006  575.12598  57.8087
   2   6.344 MM    0.1758 4077.31836  386.50586  42.1913
```

^{1}H NMR (400 MHz, $CDCl_3$) of **S8**

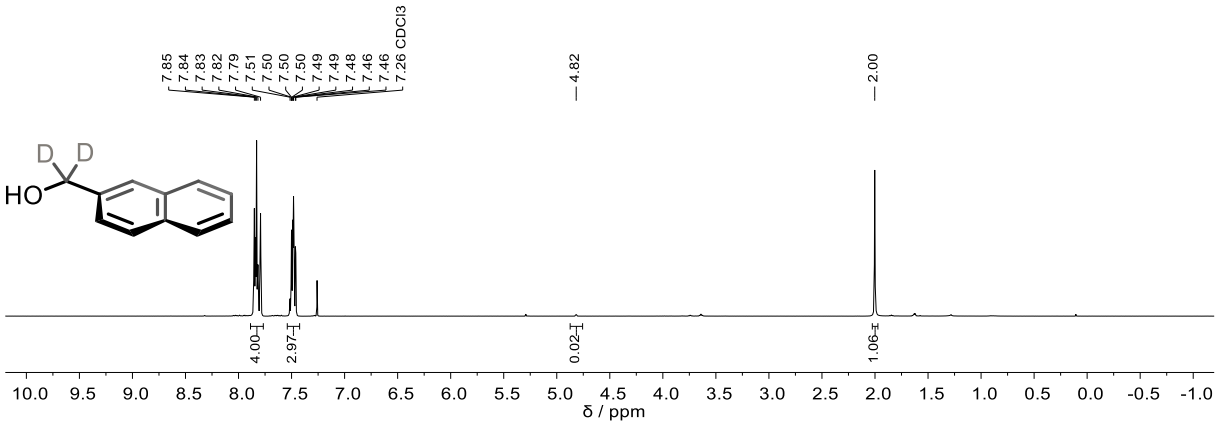

^{13}C{^{1}H} NMR (101 MHz, $CDCl_3$) of **S8**

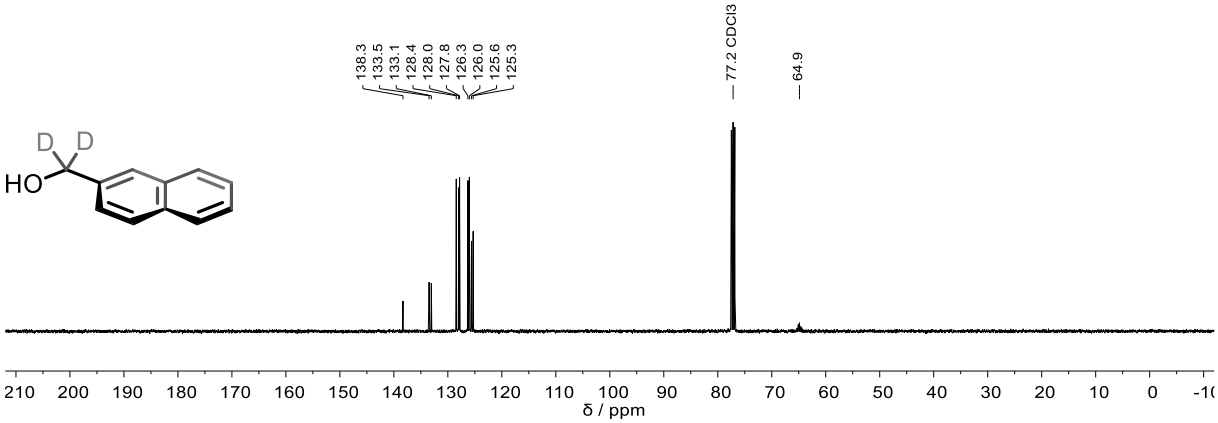

^{2}H NMR (61 MHz, $CDCl_3$) of **S8**

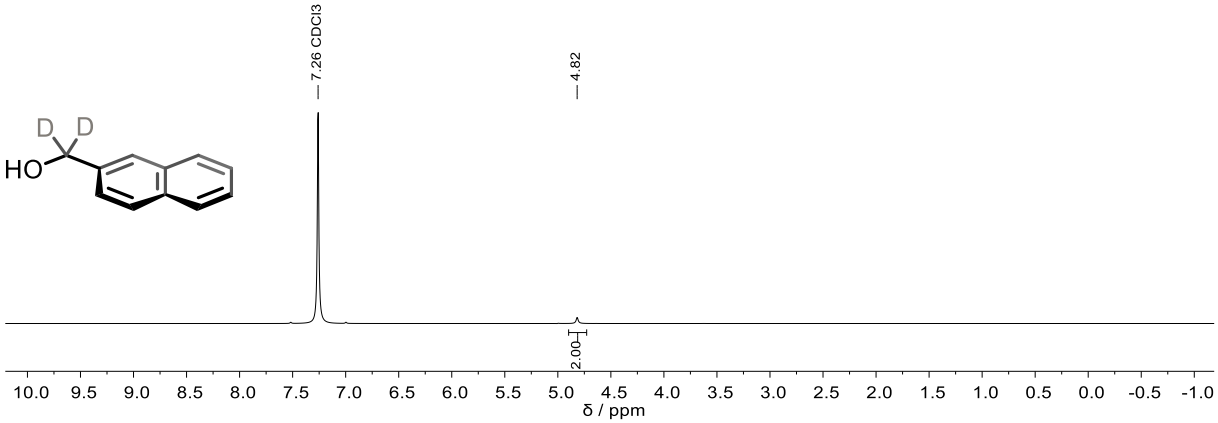

IR (ATR, neat) of **S8**

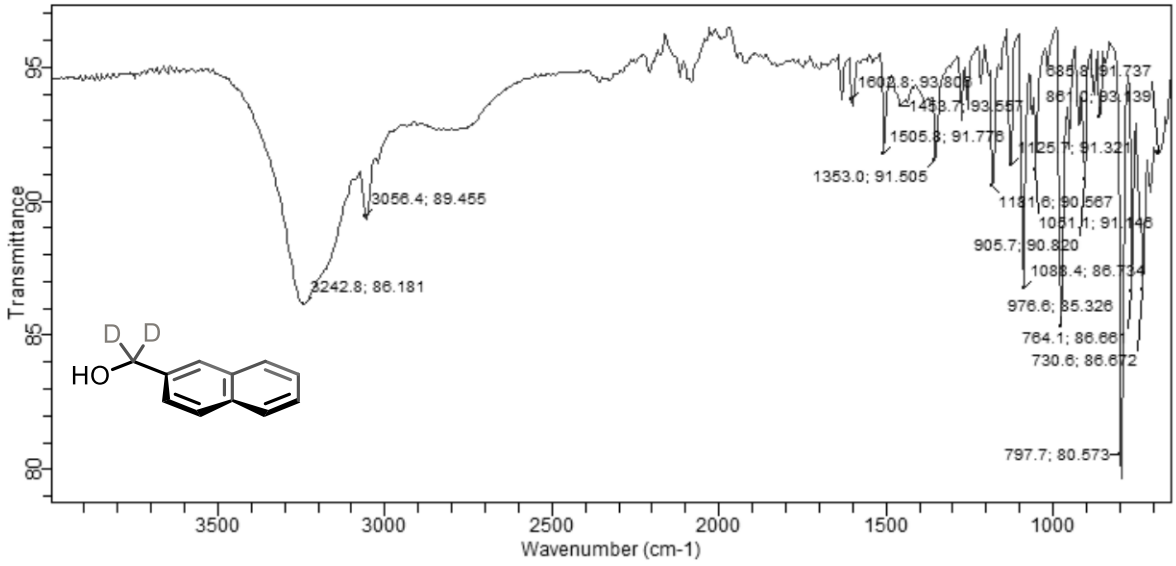

^{1}H NMR (400 MHz, $CDCl_3$) of **S9**

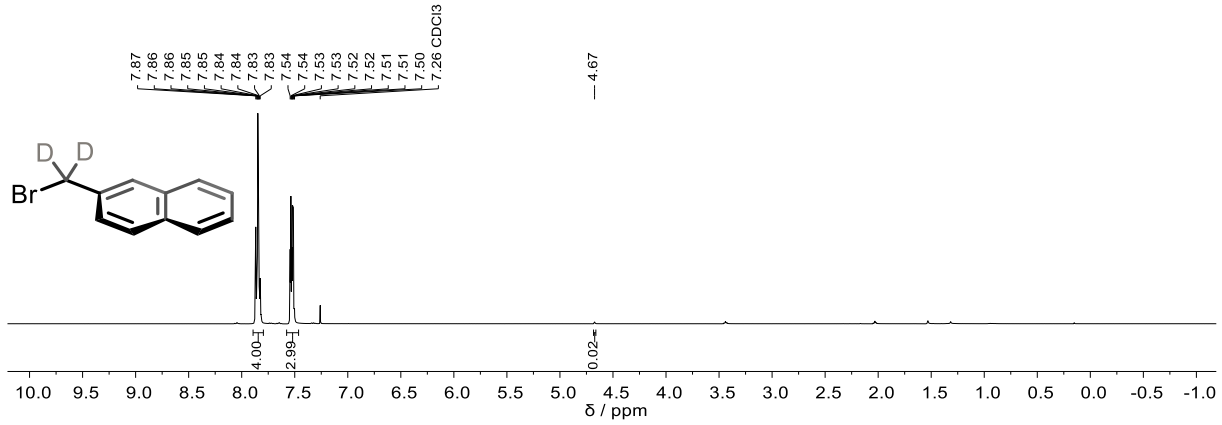

^{13}C{^{1}H} NMR (101 MHz, $CDCl_3$) of **S9**

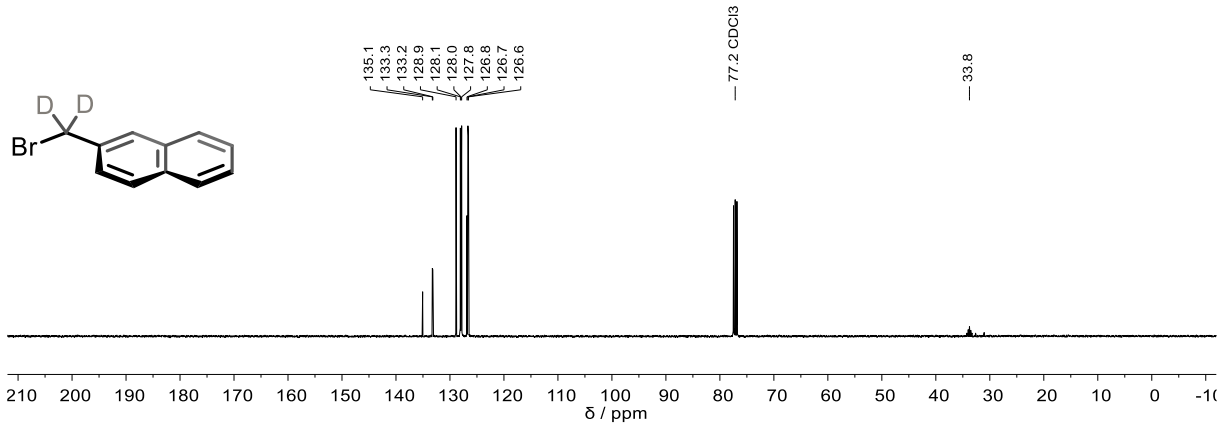

^{2}H NMR (61 MHz, $CDCl_3$) of **S9**

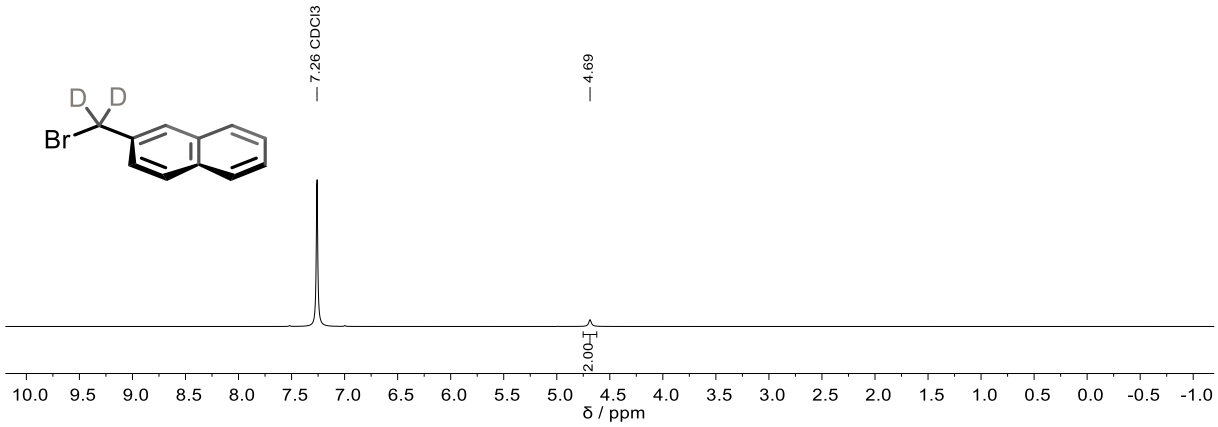

IR (ATR, neat) of **S9**

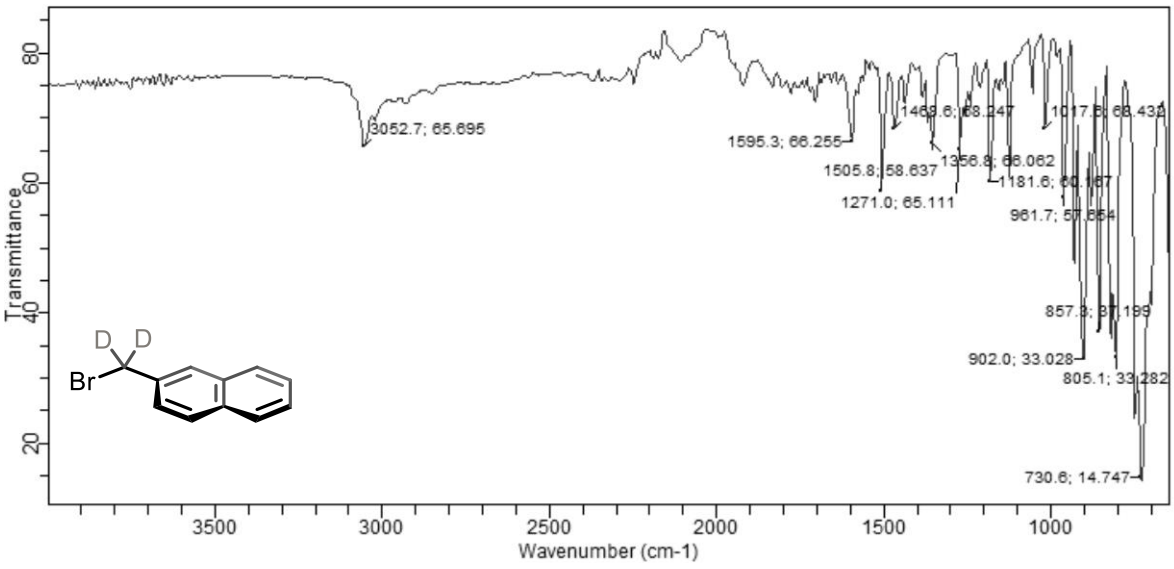

^{1}H NMR (400 MHz, $CDCl_3$) of **S1-*d*$_2$**

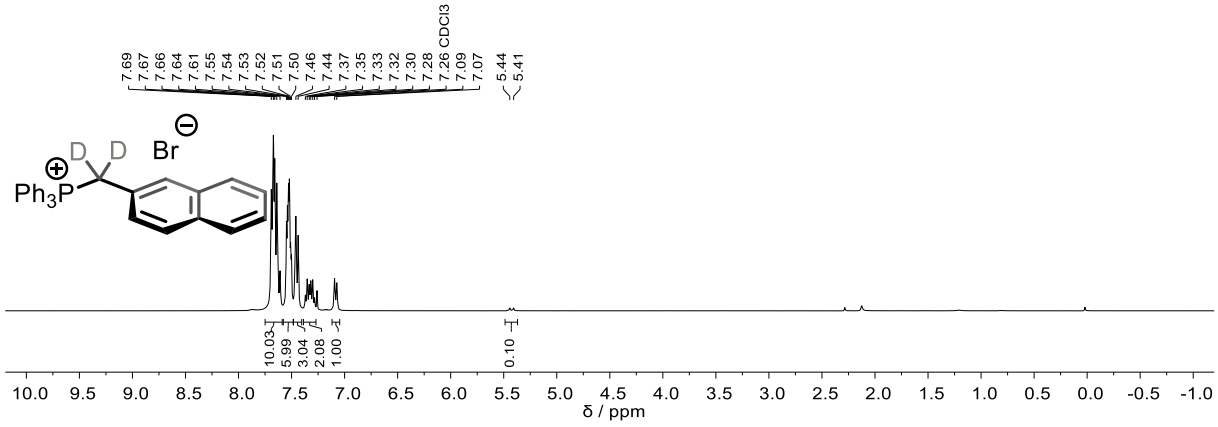

$^{13}C\{^{1}H\}$ NMR (101 MHz, $CDCl_3$) of **S1-*d*$_2$**

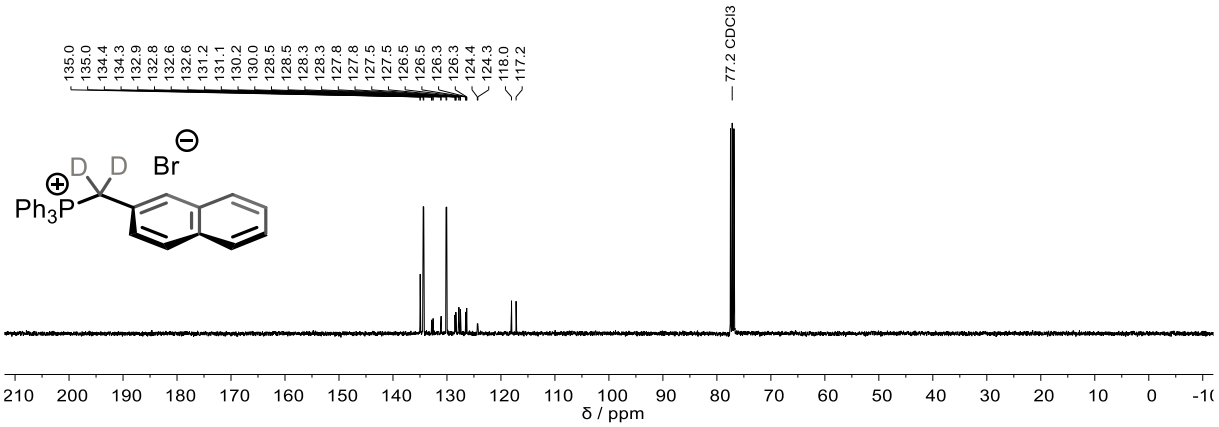

$^{31}P\{^{1}H\}$ NMR (162 MHz, $CDCl_3$) of **S1-*d*$_2$**

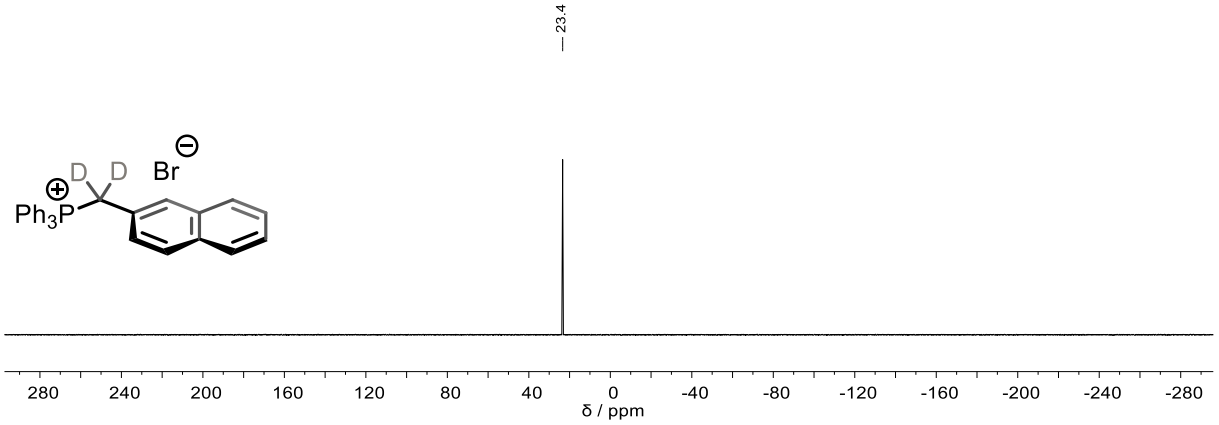

^{2}H NMR (61 MHz, $CHCl_3$) of **S1-*d*$_2$**

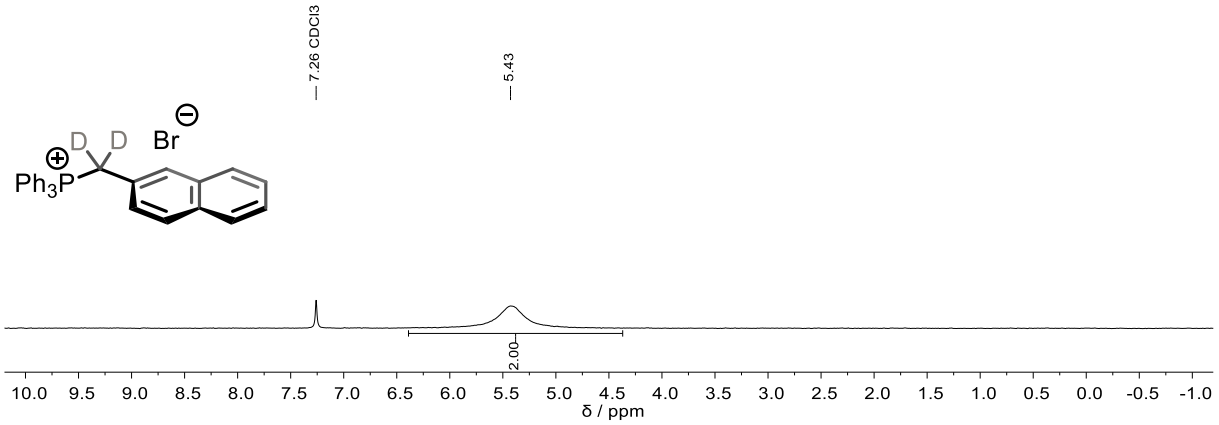

IR (ATR, neat) of **S1-*d*$_2$**

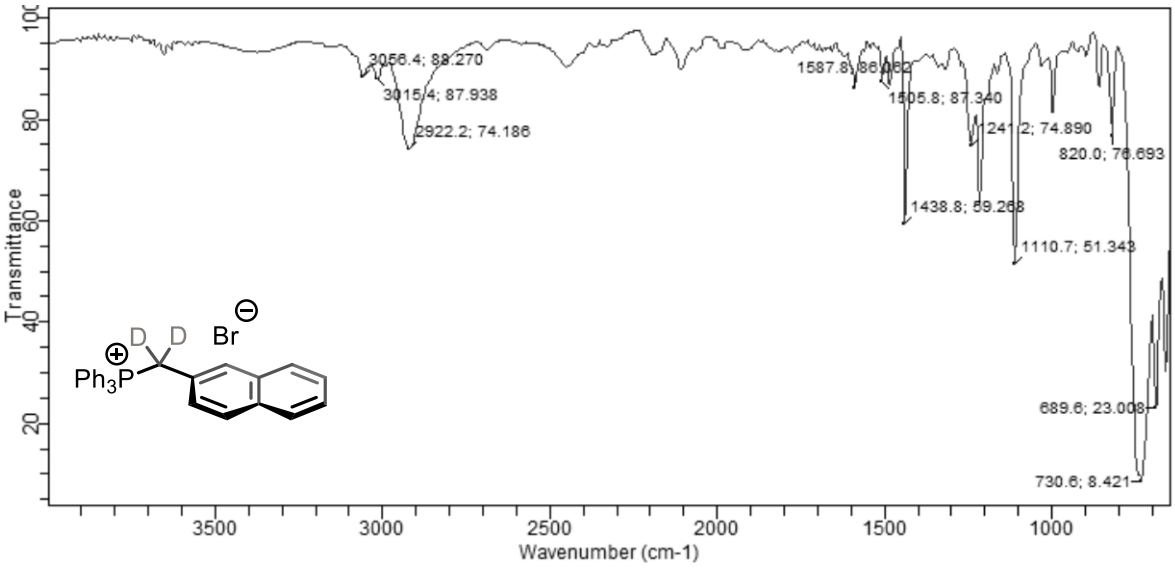

^{1}H NMR (400 MHz, $CDCl_3$) of **1a-*d*$_4$** (*E*:*Z* = 55:45, 98% deuteration)

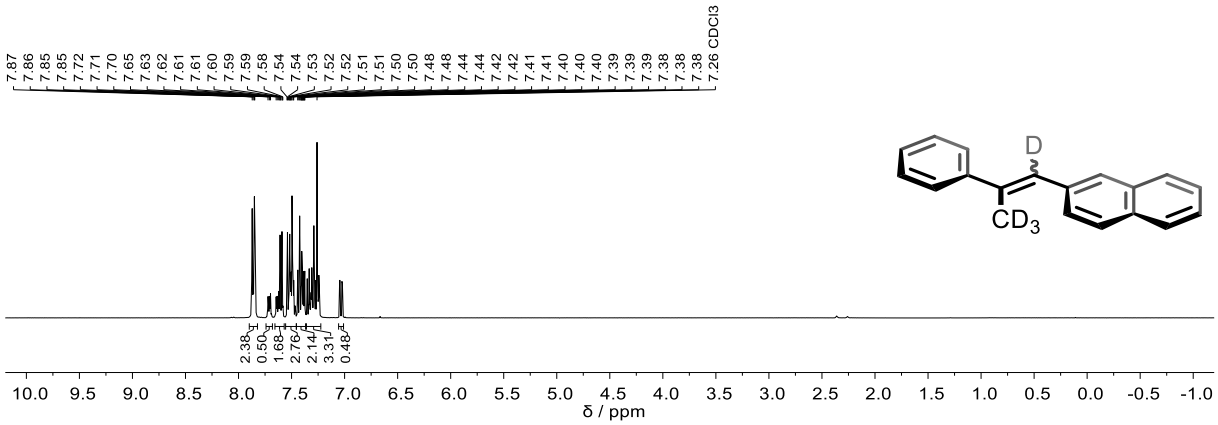

^{13}C{^{1}H} NMR (101 MHz, $CDCl_3$) of **1a-*d*$_4$** (*E*:*Z* = 55:45, 98% deuteration)

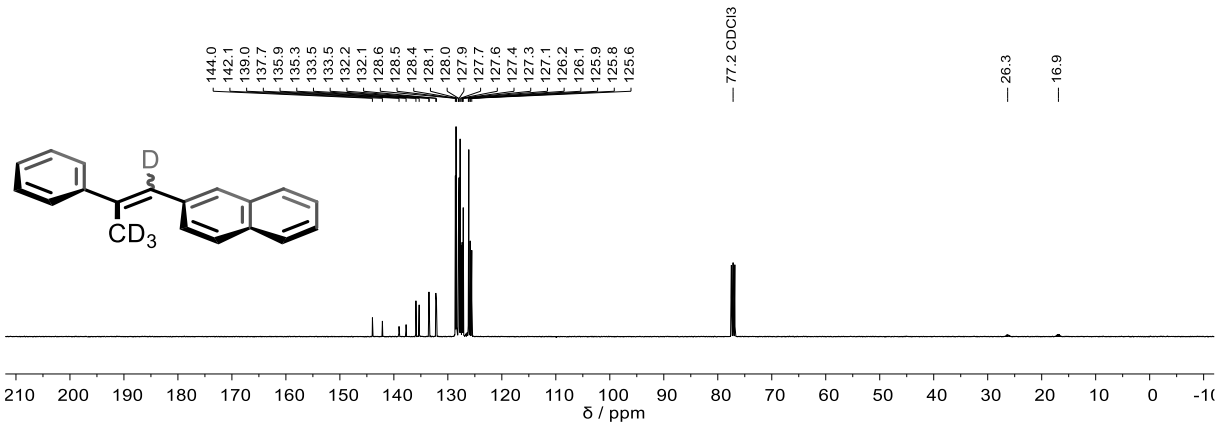

^{2}H NMR (61 MHz, $CHCl_3$) of **1a-*d*$_4$** (*E*:*Z* = 55:45, 98% deuteration)

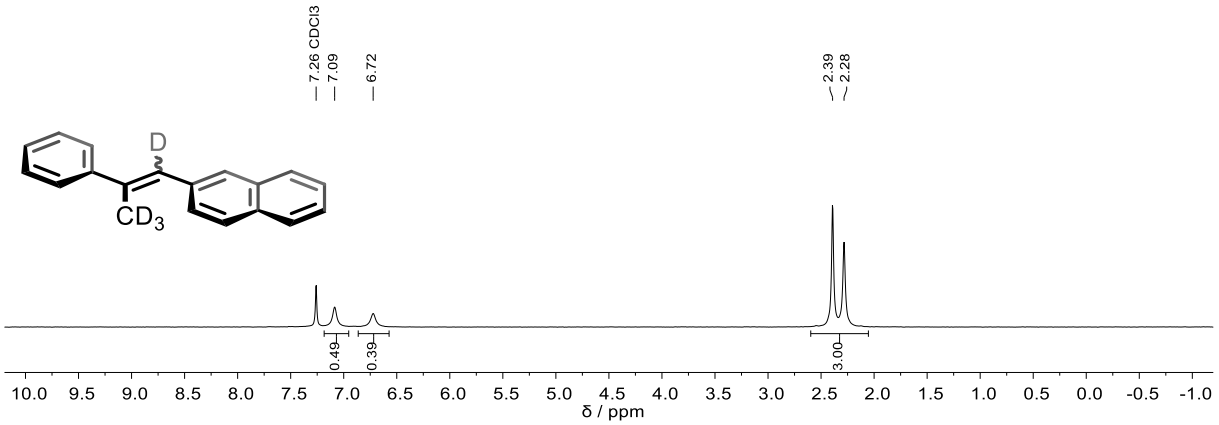

IR (ATR, neat) of **1a-*d*$_4$**

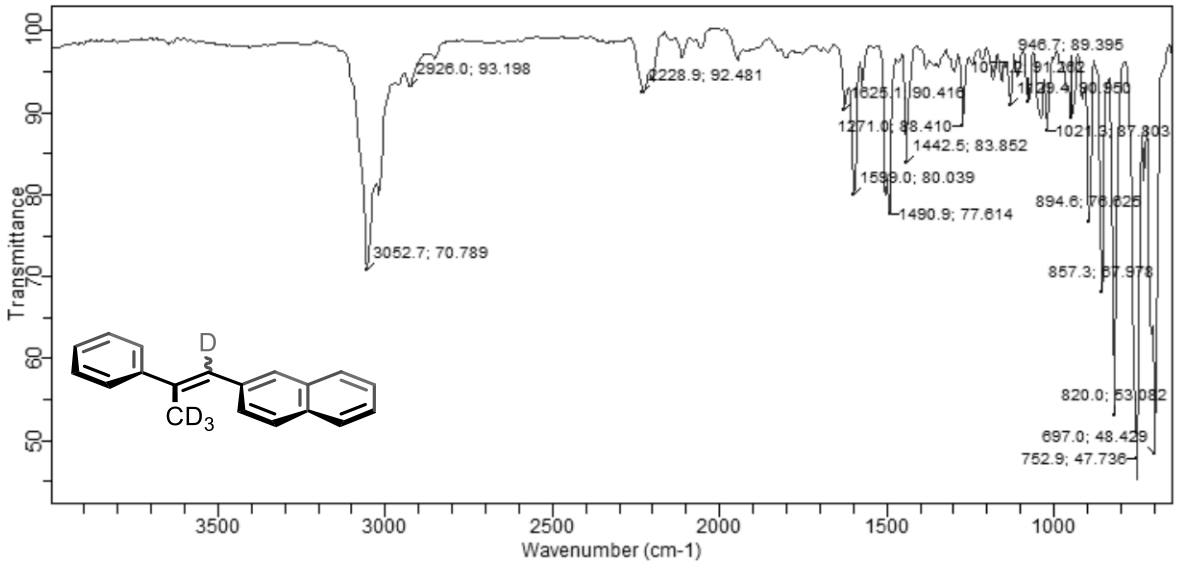

^{2}H NMRs (92 MHz, THF) of **1a-*d*$_4$** (*E*:*Z* = 55:45) <u>before</u> KIE experiment

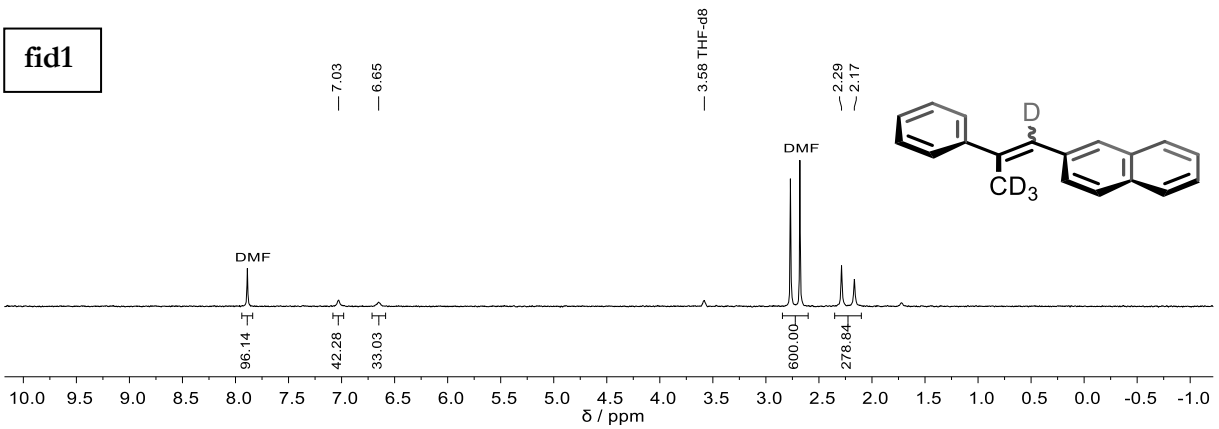

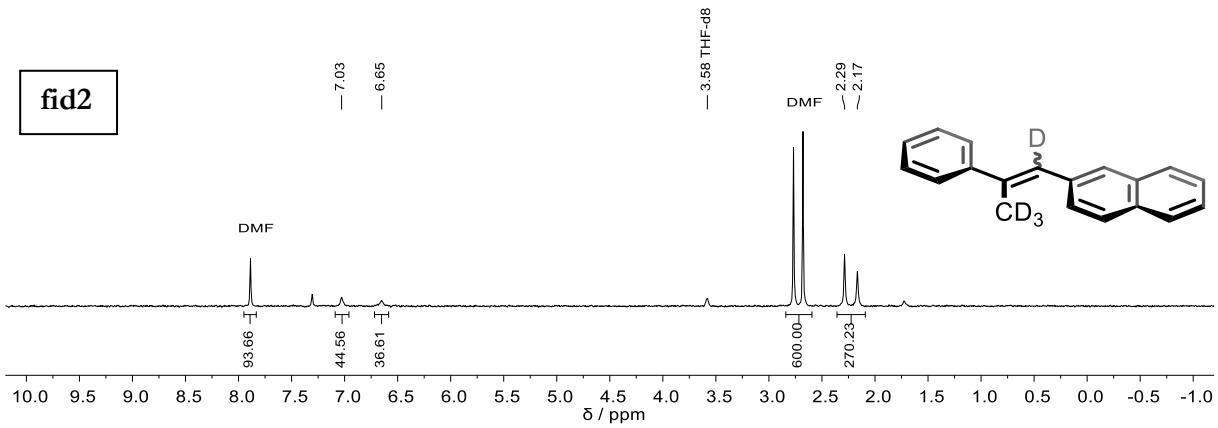

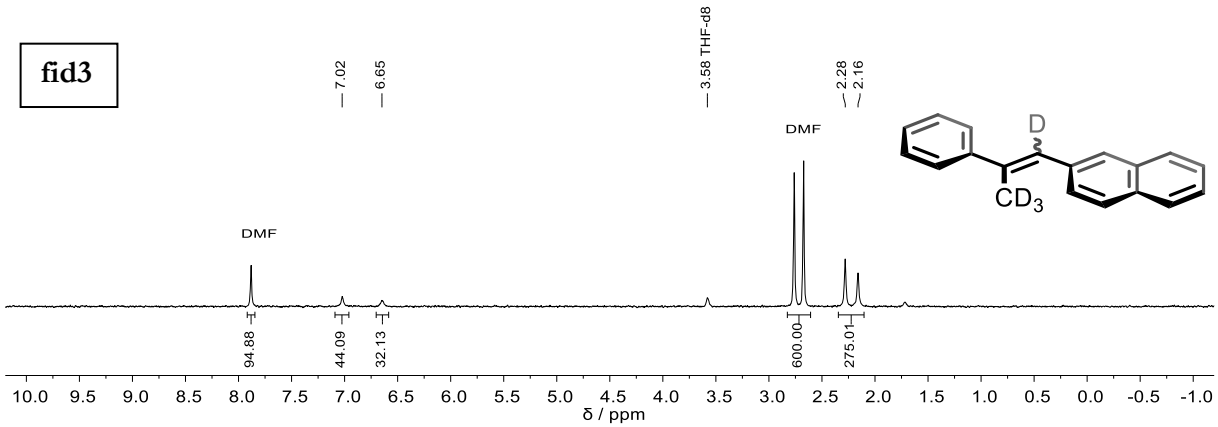

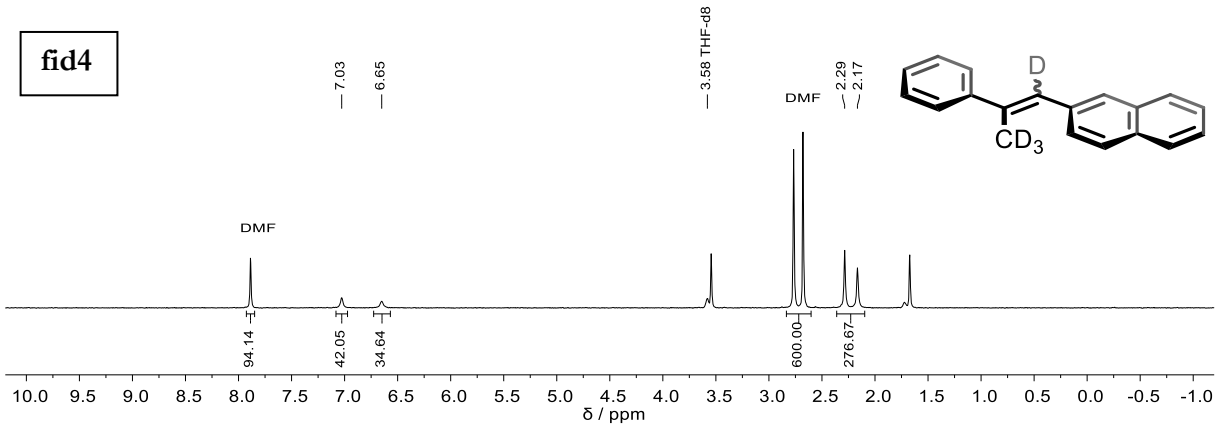

^{2}H NMRs (92 MHz, THF) of recovered **1a-*d*$_4$** after KIE experiment

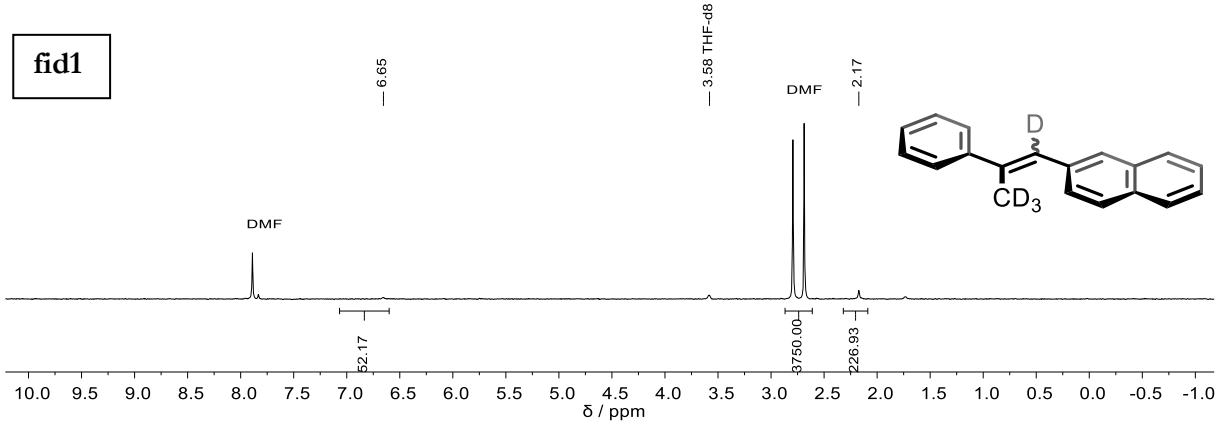

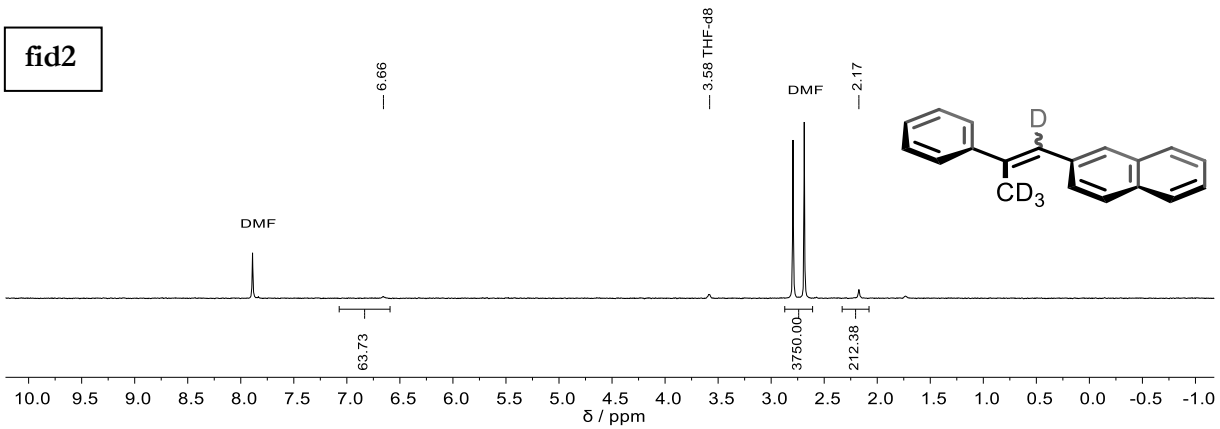

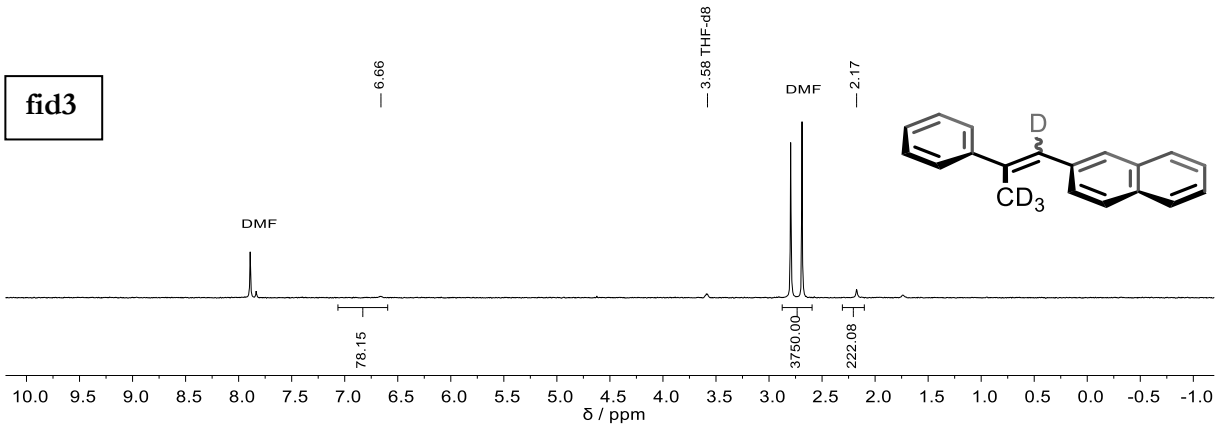

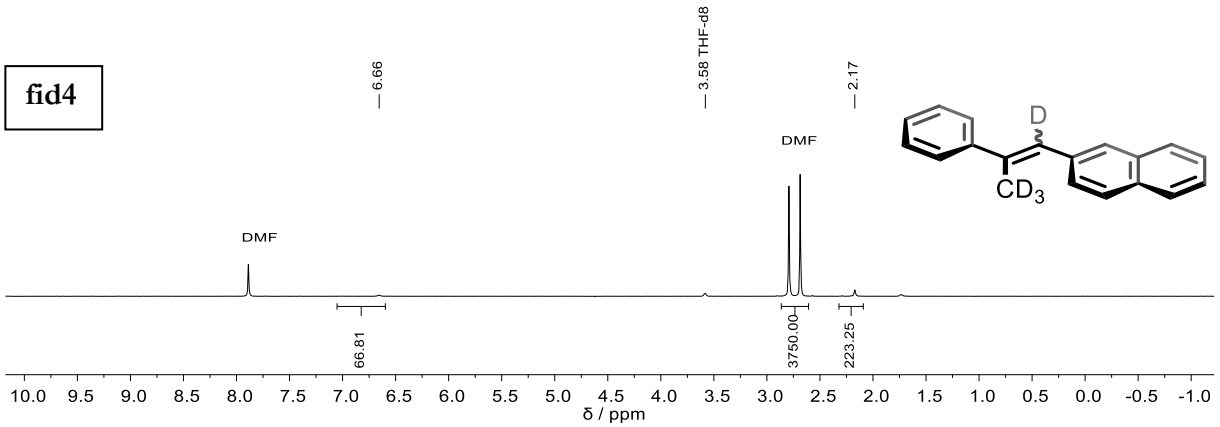

^{1}H NMRs (400 MHz, $CDCl_3$) of crude reaction mixture for KIE (83.3 ± 0.1% conversion)

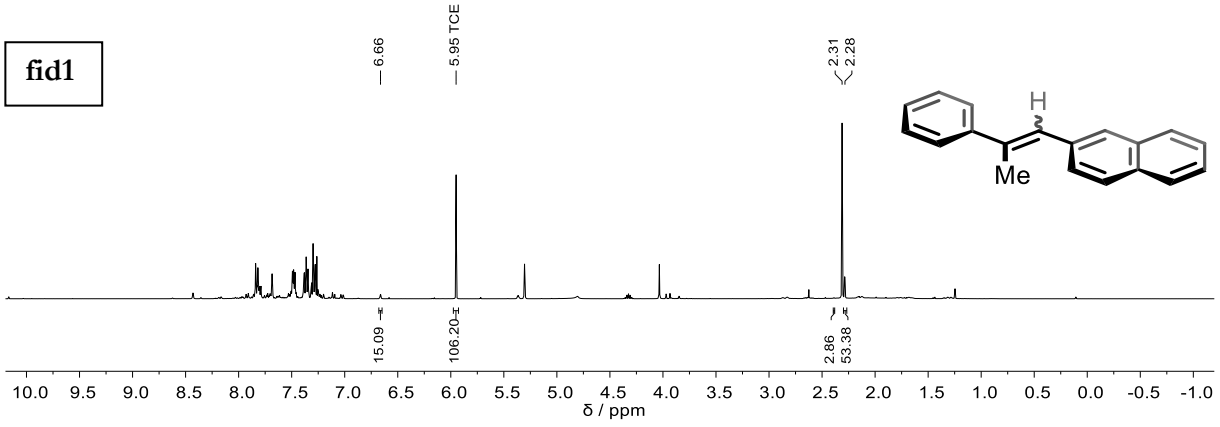

fid2

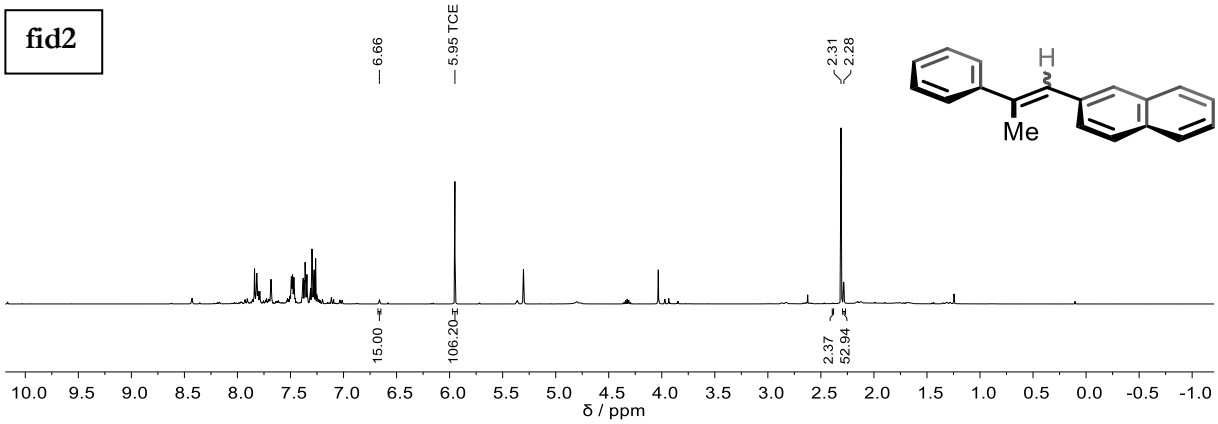

fid3

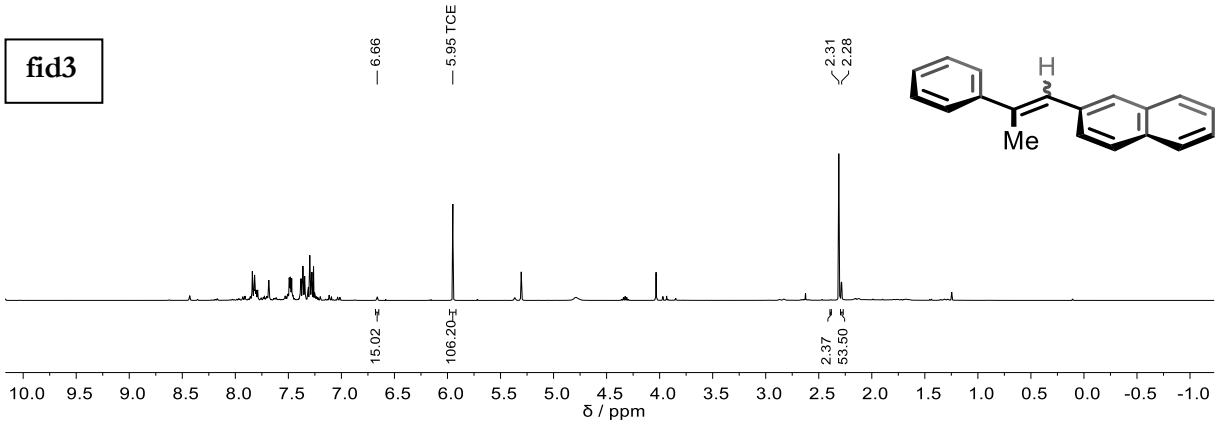

fid4

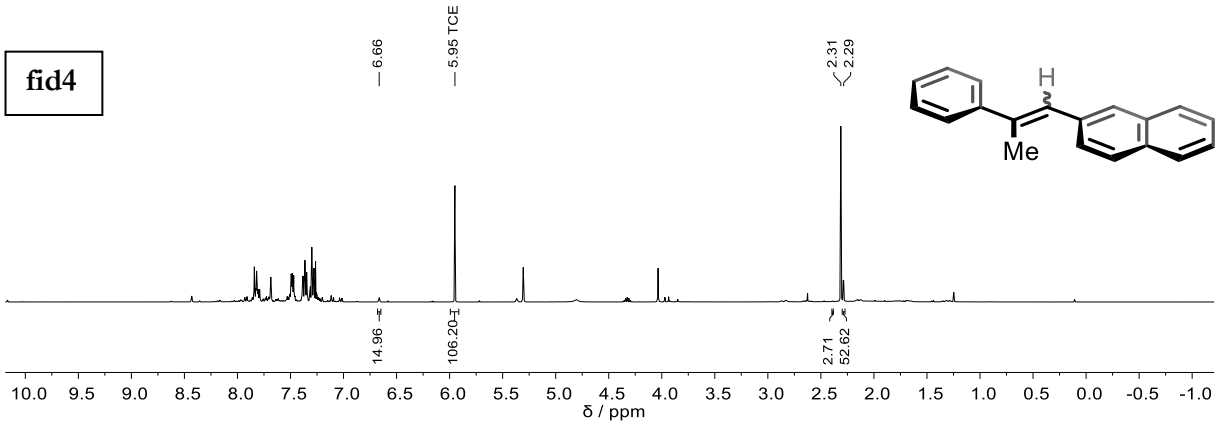

8 Danksagung

Diese Arbeit ist das Resultat von jahrelanger harter Arbeit und wäre ohne das Mitwirken vieler besonderer Menschen in dieser Form nicht möglich gewesen. Diesen Menschen möchte ich hiermit meinen Dank für ihre großartige Unterstützung aussprechen.

Mein größter Dank gilt allen aktiven und ehemaligen Mitgliedern des AK Breder für die gemeinsame Zeit innerhalb und außerhalb des Labors. Ihr habt meine Promotion zu einer einzigartigen Reise gemacht. Ganz besonders danke ich Anna und Caro, denn durch euch hat es jeden Morgen Spaß gemacht, ins Labor zu kommen. Ich hätte mir keine besseren Laborkolleginnen wünschen können. Anna, ich wünsche dir, dass du eines Tages Professorin werden kannst!

Ich möchte mich auch bei Anja und Michaela bedanken. Ihr beide haltet den Laden am Laufen und sorgt immer für großartige Unterstützung in jeglicher Hinsicht.

Außerdem danke ich Elias, Jana, Julia, Marcel und Sooyoung für die tolle Zusammenarbeit bei unseren Projekten und Johannes, Kajetan, Lukas, Nick und Sophie für eure Zeit und Motivation, bei mir eine Bachelorarbeit oder ein Forschungspraktikum zu machen. Es hat mir sehr viel Spaß gemacht mit euch zusammenzuarbeiten, euch etwas beizubringen und von euch zu lernen.

I would also like to thank Ooi sensei and his entire group, who welcomed me warmly in Nagoya and made my research internship an unforgettable experience. **お招きいただきありがとうございます。** Big thanks also to the Winter/Spring Spirit Crew Anuphon, Bene, Elli, Jana, Joey, Nils, Tobi, and Yufeng. I deeply enjoyed every second with you.

Danke nochmal an Anna und Elias für das Korrekturlesen meiner Arbeit.

Alex, ich möchte mich bei dir für die Möglichkeit in deiner Gruppe zu promovieren herzlich bedanken, ebenso für die Unterstützung und die Betreuung in den letzten Jahren, sowie für den fachlichen Austausch. Ich habe viel von dir über Chemie gelernt.

Ich danke auch dem gesamten Prüfungsausschuss für Ihre Zeit, die Sie in diese Arbeit und die Verteidigung investiert haben. Ich hoffe, ich konnte eine gute Geschichte erzählen.

Schlussendlich danke ich meiner Familie und Daniela für eure bedingungslose Liebe und Unterstützung, die mich auch in schweren Zeiten weitermachen lässt.

9 Eidesstattliche Erklärung

(1) Ich erkläre hiermit an Eides statt, dass ich die vorliegende Arbeit ohne unzulässige Hilfe Dritter und ohne Benutzung anderer als der angegebenen Hilfsmittel angefertigt habe. Die aus anderen Quellen direkt oder indirekt übernommenen Daten und Konzepte sind unter Angabe des Literaturzitats gekennzeichnet.

(2) Bei der Auswahl und Auswertung folgenden Materials haben mir die nachstehend aufgeführten Personen in der jeweils beschriebenen Weise unentgeltlich geholfen:

1. Dr. Sooyoung Park – Entwicklung der dualen Reaktionsbedingungen, Synthese der Photokatalysatoren, der chiralen Selenkatalysatoren **3d–i**, der Ketone **2d–m**, **2p–y**, **2a'–g'**, **2m'**, **2o'**, ***ent*-2r**, ***ent*-2s**, ***ent*-2y** inkl. deren Vorläufer und der Derivate **9r**, **11r** und **12r**.

2. Jana L. Flügel – Synthese der Ketone **2r'**, **2t'**, ***ent*-2t'** inkl. deren Vorläufer, sowie deren weitere Umsetzung zu den Wirkstoffen **13**–**16**, **18** und *ent*-**18**.

3. Elias Harrer – Durchführung der computerchemischen Rechnungen inkl. Visualisierung.

4. Marcel Fischer – Durchführung der STERN–VOLMER Messungen inkl. Visualisierung.

5. Ludwig d'Heureuse & Christopher Schöll – Synthese der Katalysatoren **3b–c**.

(3) Weitere Personen waren an der inhaltlich-materiellen Herstellung der vorliegenden Arbeit nicht beteiligt. Insbesondere habe ich hierfür nicht die entgeltliche Hilfe eines Promotionsberaters oder anderer Personen in Anspruch genommen. Niemand hat von mir weder unmittelbar noch mittelbar geldwerte Leistungen für Arbeiten erhalten, die im Zusammenhang mit dem Inhalt der vorgelegten Dissertation stehen.

(4) Die Arbeit wurde bisher weder im In- noch im Ausland in gleicher oder ähnlicher Form einer anderen Prüfungsbehörde vorgelegt.

Regensburg, den 16.12.2025 Eduard Frank